J P 9-1-1-2

E-444

COO-3072-102

Princeton University
Elementary Particles Laboratory
Department of Physics

PRODUCTION OF HIGH MASS MUON PAIRS BY 225 GeV/c HADRON BEAMS AND A DETERMINATION OF THE PION STRUCTURE FUNCTION

Gary Elliott Hogan

Contract EY-76-02-3072

PRODUCTION OF HIGH MASS MUON PAIRS BY 225 GeV/c HADRON BEAMS AND A DETERMINATION OF THE PION STRUCTURE FUNCTION

by

Gary Elliott Hogan

A DISSERTATION

PRESENTED TO THE

FACULTY OF PRINCETON UNIVERSITY

IN CANDIDACY FOR THE DEGREE

OF DOCTOR OF PHILOSOPHY

RECOMMENDED FOR ACCEPTANCE BY THE

DEPARTMENT OF

PHYSICS

JUNE, 1979

AAB1815

Table Of Contents

ABSTRACT

Results are presented from an experiment with a large acceptance spectrometer that measured the production cross section of high mass muon pairs from the collision of 225 GeV/c hadron beams with a nuclear target, including, for the first time, measurements using positive and negative pion beams. Various features of the data, such as the helicity angle of the muon pairs and the ratio of the cross sections for positive and negative pions provide conclusive evidence for the quark-antiquark annihilation model for the production of muon pairs. This model is then used to determine the momentum distribution for valence quarks in the pion. Our best fit to the distribution, $\bar{u}(x) = (.73 \pm .11)\ x^{-1/2}[1-x]^{(1.28 \pm .15)}$, shows that the pion's structure is clearly different from the proton's structure.

Chapter I Introduction

In recent years, many different types of experiments have been undertaken to probe the structure of hadrons. The first indications of a non-point like structure for hadrons came with the electron-proton elastic scattering experiments of Hofstadter and his collaborators[1] in 1961, at Stanford, which showed that the proton was not a simple point particle. Later, the deep-inelastic electron-proton experiments[2] in 1968, at SLAC, showed that the proton seemed to be constructed of many point-like constituents which Feynman called 'partons'.

These partons were immediately identified with the quarks in the theory of Gell-Mann and Ne'emann.[3] This theory built up various families of hadrons from three different types (flavors) of particles (quarks). (Experimental evidence now exists for at least five flavors of quarks.) In its simplest form, the theory had baryons (such as protons and neutrons) composed of 3 quarks and mesons (such as pions) composed of a quark and an antiquark. Table 1-I shows the properties of the "known" quarks, including the b quark that (along with a $\bar{b}$) may be the main constituent of the upsilon particle (9.5 GeV/c^2) discovered[4] just before this experiment started. Also included in the table are the compositions of some of the hadrons in the simple quark model.

Table 1-I

Quark Quantum Numbers

Flavor	u	d	s	c	b
Spin	1/2	1/2	1/2	1/2	1/2
Charge	2/3	-1/3	-1/3	2/3	-1/3
Baryon Number	1/3	1/3	1/3	1/3	1/3
Isospin	1/2	1/2	0	0	0
Strangeness	0	0	1	0	0
Charm	0	0	0	1	0
Beauty	0	0	0	0	1

Hadron Compositions

Proton	uud
Neutron	udd
Pi^+	$u\bar{d}$
Pi^-	$\bar{u}d$
J/Ψ	$c\bar{c}$
Upsilon	$b\bar{b}$

The successful predictions of the theory are numerous, the most spectacular being the prediction of various new particles such as the Omega-minus baryon and, in later unification theories, the J/Ψ vector meson.

One of the other consequences of the model, worked on by Drell and Yan[5] in 1970, involved the production of lepton pairs in the reaction:

$$A + B \rightarrow L^- L^+ + X \qquad (1\text{-}1)$$

where A and B are hadrons and X means any other particles.

Their theory visualized the underlying reaction to be the electromagnetic annihilation of a quark and antiquark into a virtual photon which then decays into a pair of leptons. See Figure 1-1. They showed that this was a valid way to picture the reaction when the photon's rest mass was sufficiently greater than the quark rest mass. When this condition is valid, the quarks in a hadron can then be taken to be point-like particles which are momentarily free of interactions with the rest of the hadrons (the impulse approximation). The quark structure of nucleons measured in deep-inelastic electron-proton scattering experiments can then be used to predict cross sections for the reaction:

$$p + p \rightarrow \mu^{+} \mu^{-} + X \qquad (1\text{-}2)$$

Their simple result was that the cross section should go as:

$$A + B \rightarrow L^{+} L^{-} + X \qquad (1\text{-}3)$$

$$d^2\sigma/(dM^2 dx_f) = (4\pi\alpha^2/[3M^4]) \sum_i \{[e_i^2/(x_A+x_B)]$$

$$[x_A f_i^A(x_A) x_B f_{\bar{i}}^B(x_B) + x_A f_{\bar{i}}^A(x_A) x_B f_i^B(x_B)]\}$$

(The sum is over quark flavors.)

$$M^2 = x_A x_B s$$

$$x_f = x_A - x_B$$

Where:

x_A = Fraction of momentum of the parent hadron A carried by the quark.

i = Quark flavor.

$\bar{i}$ = Antiquark of flavor i.

$s^{1/2}$ = Center of mass energy of the hadron-hadron collision.

e_i = Quark charge in units of the electron's charge.

M = Invariant rest mass of the lepton pair.

x_f = Feynman-x of the lepton pair $\equiv 2p_{||}/s^{1/2}$.

$p_{||}$ = The lepton pair's momentum in the collision's center of mass.

$f_i^A(x_A)$ = Probability that a quark of flavor i in hadron A will have momentum x_A.

The quarks and leptons are assumed to be massless.

The quark compositions listed in Table 1-I show an antiquark in the pion, but not in the proton. The most naive quark model would then have a zero cross section for proton-proton production of dileptons by this mechanism. The necessary antiquarks in the protons appear when a more formal approach is made to the quark theory. This theory, QCD (Quantum Chromodynamics), is modeled after QED (Quantum Electrodynamics). In QED, one of the important corrections to the simple theory is the existence of virtual electron-positron pairs which are responsible for the vacuum polarization effect. QCD shows a similar effect involving virtual quark-antiquark pairs. These quark pairs are called 'sea' quarks. The quarks of the simple Gell-Mann model are called 'valence' quarks. The valence quarks are expected to dominate the probability distribution function at large x, the sea quark probability falling steeply for x greater than zero.

Drell and Yan showed that the probability ("structure") function $f_i^A(x_A)$ can be simply related to the deep-inelastic results:

$$x_A f_i^A(x_A) = \nu W_2^{Ai}(x_A) \qquad (1-4)$$

The pair production cross section turns out to be just the cross section for the timelike annihilation diagram (see Figure 1-2) times the probability that the two quarks have the given momentum x_A and x_B. In defining x_A and x_B, the Drell-Yan formula ignores the possibility that the virtual photon may have some transverse momentum (p_T) relative to the hadron collision axis.

The formula also ignores the effect that "color" would have on the cross section. Color (the C of QCD) is another quantum number that quarks may have. A quark can have any one of three colors, so that if quarks must have matching colors (ie, red and $\overline{\text{red}}$) to annihilate, the probability of a matched pair of quark and antiquark meeting is reduced by 1/3 compared to the νW_2 measurements from ep scattering, which average over the color of the quarks involved in the collision. This is one of the few cases where the increase of quark types by the addition of the color quantum number decreases a cross section. Including color then results in the cross section:

$$d^2\sigma/(dM^2 dx_f) = (4\pi\alpha^2/[9M^4]) \sum_i \{[e_i^2/(x_A+x_B)] \quad (1\text{-}5)$$

$$[x_A f_i^A(x_A) x_B f_{\bar{i}}^B(x_B) + x_A f_{\bar{i}}^A(x_A) x_B f_i^B(x_B)]\}$$

or alternatively:

$$d^2\sigma/(dx_A dx_B) = (4\pi\alpha^2 s/(9M^4)) \sum_i \{e_i^2 \quad (1\text{-}6)$$

$$[x_A f_i^A(x_A) x_B f_{\bar{i}}^B(x_B) + x_A f_{\bar{i}}^A(x_A) x_B f_i^B(x_B)]\}$$

Drell and Yan stated that this mechanism would dominate the production of massive lepton pairs. In considering nucleon-nucleon scattering, where the antiquark must come from a sea distribution that falls steeply with x_A and x_B, the formula says that dilepton production will fall quickly with mass. This has in fact been seen in a recent dilepton experiment.[4] If, however, the nucleon A in the reaction is replaced by a pion, which has a valence antiquark that can appear at large x_A, then the cross section should fall much more slowly and become much larger than the nucleon-nucleon cross section. Thus at high mass, the spectrum is dominated by the reaction where the antiquark comes from the pion. Indeed, by carefully measuring the mass and x_f spectrum of pion-induced dileptons, one can reverse the above equations and measure the pion structure function.

The mechanism considered here is basically an electromagnetic interaction, and it is of interest to find any differences it might have with some hypothetical strong interaction that would also produce a dilepton. The isospin symmetery of the strong interaction demands that when an isospin 1 particle such as a pion interacts with an isospin 0 object, the cross section should be independent of the third isospin component of the incident particle because the reaction can only occur via one isospin channel. For example, as Carbon-12 is an isoscalar nucleus, the cross section for the reactions:

$$pi^{\pm} + Carbon_{12} \rightarrow \mu^+\mu^- + X \qquad (1-7)$$

should be the same and the ratio of the cross sections should be 1. That is, the ratio:

$$R = \sigma\ (pi^+ C \rightarrow \mu^+\mu^- + X)/\sigma(pi^- C \rightarrow \mu^+\mu^- + X) \qquad (1-8)$$

$$= 1 \text{ for strong interactions.}$$

Any deviation from 1 in this ratio would indicate a non-strong interaction at work. The Drell-Yan mechanism predicts just such an asymmetry in the cross section for the production of high mass muon pairs where only the valence quarks contribute. When a pion collides with an isoscalar nuclear target, which has equal numbers of u and d quarks, and forms a massive pair, the relative size of the cross sections depends only on the charge of the antiquark in the pion (-2/3 for the $\bar{u}$ in the pi^- and 1/3 for the $\bar{d}$ in the pi^+). Thus the Drell-Yan mechanism predicts that the cross section ratio R should be the ratio of the square of the charges (1/4) at large masses.

The Drell-Yan mechanism involves the decay of a virtual photon. As Drell and Yan pointed out, if one assumes that the quarks and leptons are (relatively) massless, and that they are spin 1/2 fermions, then the spin of the photon is aligned with its direction of travel. Hence the decay directions of the final state leptons should show a correlation with the polar angle of the decay (the angle, in the absence of any p_T, of the direction of travel of one of the muons relative to the direction of the target in the photon rest frame). See Figure 1-3. In the simple model shown here, one expects a $1 + \cos^2\theta^*$ distribution.

As Figure 1-4 shows, both of these effects, the polar angle dependence and the pion charge dependence, have been hinted at in an earlier experiment (known as E331 at FNAL) by our experimental group.[6] It was to pin these effects down and ultimately to measure the pion structure function that we performed an upgraded version of our experiment in the Fall of 1977 at Fermilab.

The Experiment

Our experiment used a large acceptance, high resolution spectrometer to measure inclusive muon pair production. A variety of different incident particles and targets were used:

$$
\begin{aligned}
\pi^{+} + C &\rightarrow \mu^{+}\mu^{-} + X \\
\pi^{-} + C &\rightarrow \mu^{+}\mu^{-} + X \\
\pi^{-} + Cu &\rightarrow \mu^{+}\mu^{-} + X \\
\pi^{-} + W &\rightarrow \mu^{+}\mu^{-} + X \\
p + C &\rightarrow \mu^{+}\mu^{-} + X \\
K^{+} + C &\rightarrow \mu^{+}\mu^{-} + X \\
\bar{p} + C &\rightarrow \mu^{+}\mu^{-} + X
\end{aligned}
\qquad (1\text{-}9)
$$

with $s = 416\ GeV^2$.

An isoscalar target (carbon) was used for both positive and negative beams to measure the π^{+}/π^{-} production ratio. For the high intensity negative beam runs that measured the pion structure function, two different short, metal targets (copper and tungsten) were used. The reasons for switching to the metal targets are given in the next chapter.

The acceptance of the apparatus was usefully large for:

$$2m_{\mu} < M_{\mu\mu} < 12 \text{ GeV}/c^2 \qquad (1\text{-}8)$$
$$0 < x_f < 1$$
$$p_T < 5 \text{ GeV}/c$$
$$|\cos\theta^*| < 0.9$$

where θ^* is the polar angle.

Because we were interested only in high mass dimuons (3 GeV/c^2 and above), a special mass dependent trigger logic was developed for the experiment which greatly suppressed the trigger rate of events with mass less than 2.5 GeV/c^2.

This thesis will deal mainly with the production of dimuons in the framework of the Drell-Yan mechanism. Other features of this experiment will appear in the theses of Catherine Newman and Kari Karhi (both of the University of Chicago).

In this report, it will prove convenient at times to break up the experiment into the five different periods listed in Table 1-II, depending on target type and beam conditions.

Table 1-II Different Run Periods
and Average Intensities

(1) The first positive beam run with a carbon target ($+C_I$). Average beam intensity = 4.2×10^6 particles per pulse. Pions and kaons not separated.

(2) The second run of positive beam on carbon ($+C_{II}$). Beam = 6.1×10^6 particles per pulse. Pions and kaons separated.

(3) The negative beam on carbon (-C). Beam = 7.5×10^6 particles per pulse.

(4) The negative beam on copper (-Cu). Beam = 14×10^6 particles per pulse.

(5) The negative beam on tungsten (-W). Beam = 20×10^6 particles per pulse. At this point, we used about half of all the primary protons available from the accelerator.

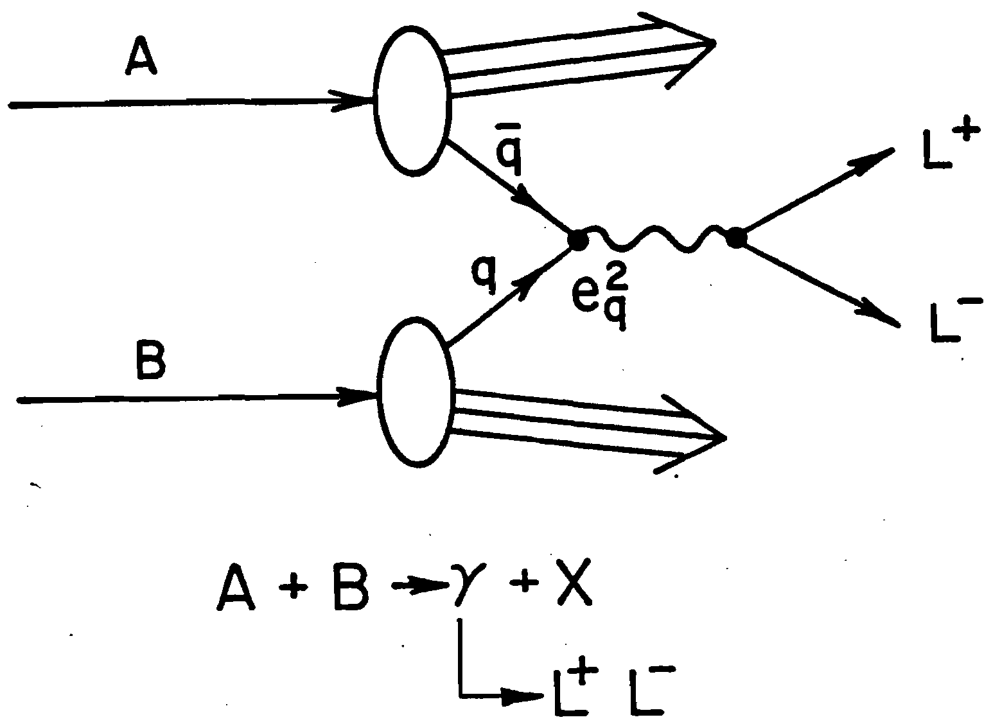

Figure 1-1. Drell-Yan mechanism for dilepton production.

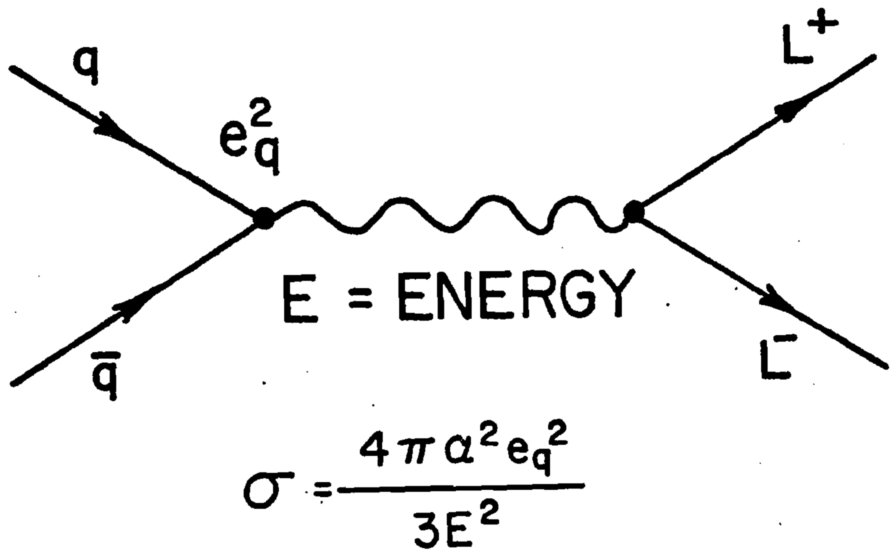

Figure 1-2. Quark annihilation into two leptons.

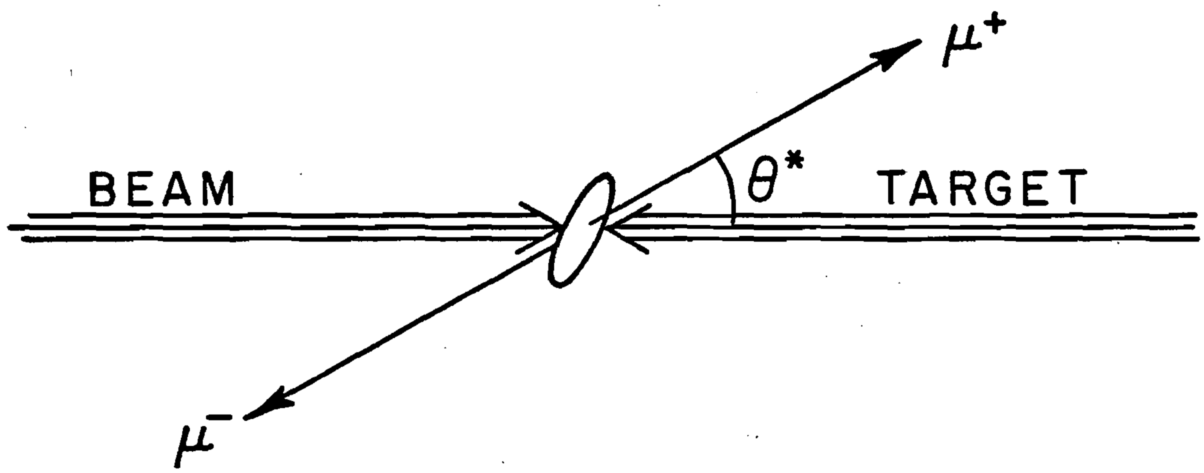

Figure 1-3. Polar angle definition. The figure corresponds to the u-channel defined in Chapter V.

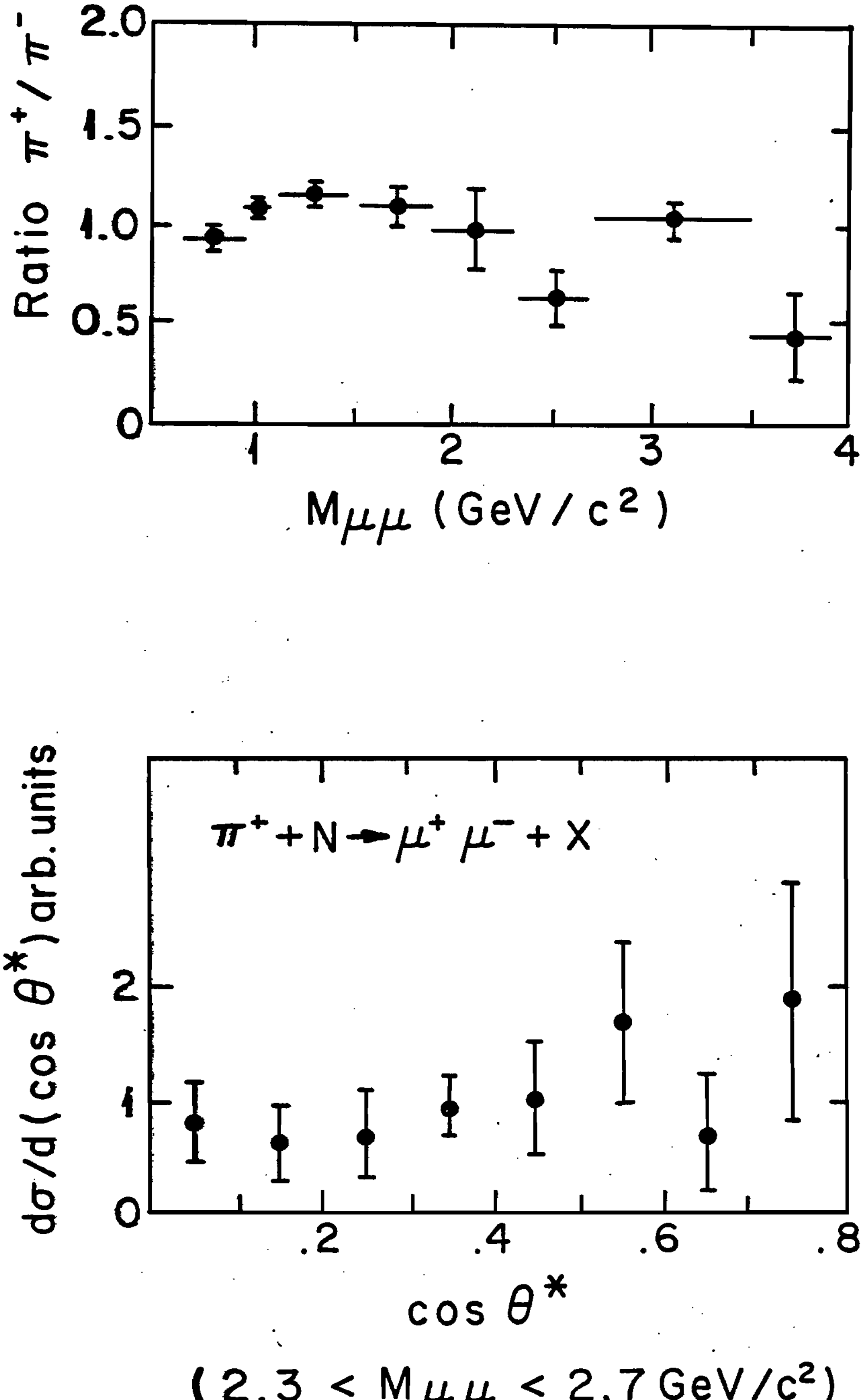

Figure 1-4. Results of Branson et al, showing the change in the pi^+/pi^- ratio with mass and the $\cos^*\theta$ distribution.

Chapter II The Equipment

INTRODUCTION

This experiment took place at the Fermi National Accelerator Laboratory in Batavia, Illinois during the Fall of 1977. Figure 2-1 shows the general layout of the accelerator, which produced 400 GeV/c protons at intensities of up to 2.5×10^{13} protons per pulse. These protons were transported to the experimental areas in two forms, a slow spill of 1.25 seconds, followed immediately by a fast spill about 1 msec long for the neutrino experiments.

Our experiment used the slow spill. The protons allotted to us struck the aluminum neutrino target, producing the secondary particles (pions, kaons, and protons) used in our experiment. The N0 and N1 beam lines carried this secondary beam to the Muon Spectrometer Laboratory. Three small scintillator counters defined the size and arrival time of the beam. Four threshold gas Cerenkov counters analyzed the beam composition.

Our apparatus, shown in Figure 2-2, was built around the former Chicago Cyclotron Magnet (the CCM) which was located in the upstream end of the muon lab.

At the point that the beam entered the muon lab, a scintillator hodoscope (V_M, the 'Halo Veto' in Figure 2-2) vetoed the halo of muons surrounding the beam. This counter array had a 2 by 2 inch hole in the center to let the beam through. (The last beam counter, placed just before the target, covered this hole.) To veto muons in the beam, a small scintillator counter (V_{muon}) was placed just behind the F bank at the position of the non-interacting muon "beam".

Three different targets, carbon, copper, and tungsten, were used during the experiment. Each target was one pion absorption length long.

Downstream of the target, there was first a 1.7 meter drift space followed by a 3 meter thick iron shield (including 8 inches of Borax for increased shielding against slow neutrons) covering the aperture of the spectrometer. The Borax was placed in the gap shown in the shield in Figure 2-2. The drift space was needed to separate events produced in the target from those produced in the shield. The shield protected the spectrometer from the flood of hadrons coming from the target before most of them could decay into muons and so give a false signal, and before the hadrons could reach and overload the wire chambers.

Three major scintillator hodoscopes were used to select quickly high-mass dimuon candidates. The first of these, the J hodoscope, which directly followed the iron shield, measured the opening angle of the pairs. The F hodoscope bank, placed 10 meters downstream of the CCM, was used in coincidence with the J to measure roughly the muons' momenta. In addition, the trigger required that these hodoscopes, along with the P hodoscope mounted 15 meters downstream of the CCM, contain hits from two or more well separated particles. The additional iron in front of the P bank, formerly the Rochester Cyclotron Magnet, improved our hadron rejection. The additional range requirement imposed by the iron also helped in rejecting low mass dimuon events.

To measure track positions, we had 14 planes of multiwire proportional chambers (MWPC) in front of the CCM and 12 planes of spark chambers after the magnet. A CERN-Heidelberg group loaned us two large MWPC's.[7] The other large chambers were part of the spectrometer facility which was bulit for a Chicago-Harvard-Illinois-Oxford collaboration (Fermilab experiment #98).[8]

Much of the electronics was provided by Fermilab's Physics Research Equipment Pool (PREP). These included standard fast logic modules (NIM, Nuclear Instrument Modules) and computer interface logic (CAMAC).

The Beam

This experiment used the N1 secondary beam line. See Figure 2-3. The 400 GeV/c primary protons incident on a 15 inch Al target during the slow spill produced the secondaries. The quadrupole triplet magnet train in the N0 beam line focused the secondaries into the neutrino decay pipe. These magnets were set to maximize the negative beam flux into the neutrino decay pipe for the neutrino experiments. After the decay pipe, the 1W0 dipole magnet in enclosure 100 bent the beam into the N1 beam line.

Because the N1 beam line closely paralleled the neutrino beam, some of the N1 magnets could bend muons in the fast (neutrino) spill into the neutrino experimental areas, causing background problems for the experiments located there. The solution to this problem was to prevent any muons from reaching the N1 line during the fast spill by turning off the N0 magnet 1W0 .25 seconds before the end of the slow spill. It took this long for the magnet to reach zero field. So we were able to use only the first second of the 1.25 second slow spill.

The radio frequency (rf) of the accelerator resulted in a beam structure of bunches ("buckets") less than 2 nsec wide every 18.83 nsec during the spill.

The choice of beam momentum was a compromise between maximizing detector acceptance and production cross section by running at the highest possible momentum, and maximizing the number of pions in the beam (both positive and negative) for a given flux of primary protons by running at lower momentum. We adjusted the magnets to accept 225 Gev/c momentum particles, with a momentum spread of $\pm$ 5%. We used both positive and negative beams.

During the positive running, the accelerator provided more beam then we could handle. Since a major goal of the experiment was to measure pion induced muon pairs, we put polyethylene into the secondary beam (in enclosure 100) to enrich the pion to proton ratio at the cost of decreasing the total flux. Because the proton absorption cross section is 40% larger than the pion cross section, the percentage of pions in the beam increased as the beam passed through the absorber. The amount of absorber could be varied from zero to 8 feet (3 interaction lengths) from our control console. The percentage of positive pions could be varied from 14% to 35% of the beam. We adjusted the absorber to keep the event rate at about 10 events per pulse. We did not use any absorber in the negative runs where we wanted all of the antiprotons we could get. With the negative beam, we obtained a yield of 2 x 10^{-5} particles per primary proton. Due to the use of a variable length absorber in the positive beam, the actual positive yield varied at the muon lab. A typical yield was 1 x 10^{-6} particles per proton.

The aperture and timing of the beam was defined by the three beam scintillator counters shown in Figure 2-4. T_1's size was 3"x3", T_2 was 2"x2", and T_4 was 2"x1.5". T_1 came before and T_2 after the last set of dipole magnets in enclosure 104. T_4 came just before the target. The beam counters constrained the defined beam to an angular spread of about 1 mrad. The beam was focused to a 2 cm by 3 cm spot at the target.

Accompanying the hadron beam was a small contamination of muons. The muons came from the decay of pions and kaons in flight along the beam line (914 m). About 7% of the pions and 27% of the kaons produced in the neutrino target decayed into muons, most of which were swept out of the beam.

For the purposes of the trigger logic the muons were divided into two categories, 'beam' muons which arrived at the lab within the beam spot definition, and 'halo' muons which were outside the defined beam aperture. Our measurements indicate that the beam muons represented about

2% of the negative beam and about 6% of the positive beam. It was higher for the positive beam because the polyethylene absorber reduced the hadron flux without affecting the muons. The halo muon component was of similar size.

Because of the high penetrating power of muons, the halo muons did not need to stay within the beam line proper in order to get through the shielding surrounding the beam line. The result was that the halo of muons extended outward from the beam to cover the entire aperture of the experiment (1mx2m). We kept the halo out ot the beam definition by using a 1mx2m halo veto counter array (V_M) around the beam at the target. To further veto halo contamination, at the downstream end of each of the three dipoles in enclosure 104, the beam passed through a four inch diameter hole in a jaw counter (V_{jaw}). Each jaw counter had two scintillators with semicircular pieces removed from their ends. A veto counter (V_{muon}, 10cm x 20cm) placed in the beam path, but downstream of the 3 meter hadron shield and the CCM, detected the beam muons. Any one of these three vetos, V_M, V_{muon}, or V_{jaw}, would inhibit the trigger.

We determined the beam composition using 4 threshold gas Cerenkov counters (labelled C_2, C_3, C_4, and C_5). The counters used the beam pipe between the magnet enclosures as pressure vessels for the helium radiators (115m, 49m, 69m, and 26m in length). As shown in Figure 2-5, a spherical mirror focused the Cerenkov light on a RCA C31000M photomultiplier tube. We lined up the mirrors by placing a small light bulb at one end of the beam pipe and adjusting the image to be at the center of the quartz window. The quartz window had a quarter wave coating of magnesium floride to improve its transmission. Figure 2-6 shows a typical pressure curve for the positive beam. For the first positive beam run and for all of the negative runs, the counters were set just below the proton threshold to separate (anti)protons from pions and kaons. (In the first positive beam run only three counters were working.) For the second positive run, when all of the counters were working, we set C_3 and C_5 to detect pions and kaons, and C_2 and C_4 to detect only pions. I will discuss the use of the counter information later in the analysis section. Table 2-I gives the average beam composition. The positive compositions are our own measurements, the negative compositions are an earlier measurement (in the same beam line) by Aubert, et al.[9] These beam compositions do not include the muon contamination.

Table 2-I Average Beam Compositions

Positive Beam	Pions	.31
	Kaons	.013
	Protons	.68
Negative Beam	Pions & Kaons	.995
	Antiprotons	.005

The Target

To measure the cross section ratio of pi^+ to pi^- induced pairs, we used an isoscalar nucleus for the target. A long carbon target was used, consisting of three 4 inch cubes of high density carbon (2.2 gm/cm^3). See Figure 2-7. We placed scintillator counters (T_{I2} and T_{I3}) between the target segments so we could tell in which block the interaction occurred. The target was followed with a final interaction counter (T_{I6}) placed 4 inches downstream of the last segment. The high multiplicity of charged particles from interactions created large pulses in the counters following the block containing the interaction. Thus, by looking at the pulse height from the counters, we could tell in which block the interaction occurred.

However, the interaction counters could not handle the rate of the high intensity negative beam runs. In these runs, we used short ($\leq$ 6 inches) metal targets to localize the interaction point.

The metal targets had another advantage due to their high atomic weight. As shown in our previous experiment, the reaction cross sections that we were interested in went as A^1 whereas the absorption of the beam in the target due to all processes went as only $A^{2/3}$. Thus the ratio of interesting reactions to beam flux as a function of the target type goes as $A^{1/3}$ for the same number of absorption lengths. Thus copper (tungsten) with an atomic mass number of 63.5 (183.9) has a 74% (148%) higher event rate than carbon for the same amount of beam. Unfortunately, the higher atomic number material also induced more multiple scattering in the muon tracks, and so degraded the spectrometer's resolution. We first ran with a copper target before we decided that rate was more important then resolution and switched to tungsten. The use of different targets also provided us with information on the atcmic mass number dependence of the reactions of interest.

The copper target (density 8.96 gm/cm^3) was 6 inches long, the tungsten (density 17.08 gm/cm^3) was 4 inches long. The tungsten was actually an alloy, Mallory 1000, which contains 90% W, 6% Ni, and 4% Cu.

The Multiwire Proportional Chambers

Fourteen planes of MWPC's measured the position of the muon tracks before the CCM. Eight of the planes were 1 meter by 1 meter chambers with one sense plane each, built by the E-98 collaboration.[10] These chambers had a 1.5mm wire spacing. They were operated at about 3.7kV using the gas mixture: 80% Argon, 20% CO_2, and .4% Freon.

The other planes (numbered 1,2,3 and 8,9,10 in Figure 2-8) were contained in two large chambers (1m by 2m in area, with 2mm wire spacing) built by a CERN-Heildelberg group. They were operated at about 3.7kV using a gas mixture of 60% Argon and 40% Isobutane bubbled through cold methylal. Each chamber had an x measuring plane and a y measuring plane. The y-plane was split half way across the acceptance of the spectrometer. This resulted in a 2cm wide dead area in the middle of the y-plane.

Figure 2-8 shows in more detail the arrangement of the chambers. Two items of note: (1) the chamber setup divided into left and right halves. Furthermore, the trigger only accepted pairs with this same left-right division in their geometry, greatly reducing the possibility of confusing hits from different tracks. (2) We tilted four of the 1 by 1 meter chambers at a 45 degree angle to form u and v planes to resolve ambiguities. This arrangement also covered the dead area in the y-planes of the CERN chambers, thus increasing the probability of finding a track going down the middle of the apparatus.

It was important to survey the chambers accurately. The final check of the relative alignment used actual tracks through the chambers. First, we defined the coordinate system so that the the z axis went through the center of the two CERN chambers. Then we projected tracks formed from hits in these chambers into the other chambers. The distance of the nearest spark to this line was measured for a large sample of tracks as a function of the plane's measured coordinate and the perpendicular coordinate. A correlation of the spark distance with the measured coordinate represented an error in the z position of the chamber being tested. Correlation with the perpendicular coordinate represented an error in the assumed rotation angle around the z axis between the chamber's coordinate system and the experiment's system. We then adjusted, in the off-line analysis, the parameters of the chambers to get rid of these errors. The first attempt revealed a tilt in one of the CERN chambers, which was also removed in the off-line analysis. These off-line measurements could detect a rotation of about .25 mrad and a z displacement of about .25 cm. In the coordinate that each chamber measured, the alignment was good to .25mm.

Chamber efficiencies were determined by projecting confirmed muon tracks (tracks with hits in both upstream and downstream chambers that pointed at struck counters in all three triggering hodoscope banks) through a chamber and looking for a hit at the projection point within a small (about 3 mm) window. This calculation assumed that the efficiences of different planes were uncorrelated. It also made the (valid) assumption that the track reconstruction program was redundant enough not to be badly affected by any chamber having a low efficiency. Table 2-II shows the alignment and efficiency parameters of the chambers. The listed resolution is calculated from the wire spacing.

The two types of chambers had different readout systems. On the CERN chambers, the sense amplifiers fed into 200ns-long delay cables which went into gated latch circuits.[11] The latch gate was 60ns long. The 200ns delay allowed only a preliminary decision to be made on the trigger before the signals had to be latched. If an event did not satisfy the full trigger logic, the latches were reset within 1 microsecond.* If the full trigger was satisfied, the latch information was transferred to shift registers for read out to the computer.

On the 1 by 1 meter chambers a signal from the sense amplifier would fire a one-shot with a 500ns long output. An external latch signal would transfer the one-shot outputs into shift registers. However, the shift registers lacked a fast reset and could only be reset by reading them out (a several millisecond long process). So to prevent this from causing an unacceptable amount of dead time, the latch signal had to come from the master trigger. Thus the one-shot's memory time set the ultimate time constraint on the trigger logic.

For both chamber systems, a computer/chamber interface system[12] converted the information in the shift registers into wire locations which were then passed along to the on-line computer.

---

* Unfortunately, the rf noise from the spark chambers could fire this reset. To prevent this, the reset circuit required a pulse greater than 1 microsecond long. This requirement determined the dead time due to the reset.

Table 2-II Upstream MWPC

Plane	Type	Res (mm)	Z Position (Meters To CCM)	Tilt (Degrees)	Efficiency
1	Y	.58	4.908	90.00	.97
2	Y	.58	4.908	90.00	.97
3	X	.58	4.883	0.00	.96
4	U	.46	4.603	-44.95	.96
5	U	.46	4.413	-45.17	.96
6	V	.46	4.155	44.89	.94
7	V	.46	3.988	44.96	.97
8	X	.58	3.620	0.15	.94
9	Y	.58	3.595	90.15	.96
10	Y	.58	3.595	90.15	.96
11	X	.46	3.065	0.05	.86
12	X	.46	2.900	0.06	.96
13	Y	.46	2.658	90.15	.86
14	Y	.46	2.478	90.02	.95

<u>The Chicago Cyclotron Magnet</u>

The CCM had an effective diameter of 5.18 meters and a gap of 1.29 meters. We approximated the magnetic field as a hard edge cylinder with a field of 6.96 kilogauss.

<u>The Spark Chambers</u>

We had 12 planes of spark chambers[13] after the CCM. Measuring 2 meters by 4 meters, each chamber frame had two spark gaps. The gaps were formed from an x measuring wire sense plane (the cathode) and a tilted sense plane (the anode). The two planes formed a narrow angle (7.1 degrees) stereoscopic pair. When the spark gap fired, capacitors attached to the struck sense wires would be charged up. The presence or absence of the charge would then be recorded in a shift register. The shift registers were read by the same type of system used with the MWPC's.

Because we expected a higher event rate than the original designers (E-98 again), we made new high voltage supplies for the chambers, one for each gap. The spark voltage was set at about 7kV. In another step to improve the rate capabilities of the chambers, we used a high flow rate gas system that cleaned the gas mixture (90% Ne, 10% He, bubbled through 1-propanol) as it recycled the gas.

The planes common to a given spark obviously had correlated efficiences. Thus the efficiencies listed in Table 2-III give the probability that both planes of a gap with their associated readout electronics worked, that the first worked and not the second, that the second worked and not the first, and that both did not work. The table lists the measured resolution of the chambers for beam particles, as well as their positions, tilts, and efficiences. We checked these parameters in the same manner as the MWPC's.

Table 2-III Downstream Spark Chambers

Plane	Type	Res (mm)	Z Position	Tilt	Efficiency ab	Efficiency $a\bar{b}$	Efficiency $\bar{a}b$	Efficiency $\bar{a}\bar{b}$
15	U	.25	3.91	-7.1	.944	.006	.021	.029
16	X	.35	3.92	0.0				
17	X	.38	4.03	0.0	.821	.062	.005	.112
18	V	.28	4.04	+7.1				
19	U	.43	5.74	-7.1	.955	.004	.015	.026
20	X	.33	5.75	0.0				
21	X	.38	5.87	0.0	.975	.012	.007	.006
22	V	.45	5.88	+7.3				
23	U	.25	7.56	-7.1	.884	.013	.020	.083
24	X	.30	7.57	0.0				
25	X	.33	7.68	0.0	.748	.212	.006	.033
26	V	.28	7.69	+7.1				

The Triggering Hodoscopes

The three large scintillator arrays (the J, F, and P) formed the central element of the trigger. Figures 2-9 and 2-10 show the arrangement of the individual counters in the arrays. The J counters varied from 1.75 inches to 8 inches wide, the F counters were either 7.25 or 7.5 inches wide, and the P counters varied from 6 inches to 13 inches wide. All of the arrays were divided into up and down halves so that we could insist on one muon in the upper part of the apparatus and one in the lower part. I will discuss this feature and others in the section on the trigger. The counters had adiabatic light pipes leading to RCA 8575 phototubes. The high voltage and timing of the counters was set using muons produced in the target. Fast (RG-8) cables (foam dielectric with v = .8c) brought the phototube signals to the discriminators for the J and F banks at the main electronics rack. Discriminators and logic for the P hodoscope were located next to the P bank.

The output of the discriminators, with a width set at 17ns, were fed into CAMAC latches. Since a particle track in the chambers had to point at struck counters (as defined by the CAMAC latch bits) in all three hodoscopes to be called a muon, the counter latch information provided a timing check on the tracks.

The Trigger

The trigger can be divided into two parts: the dimuon logic, which required that two or more muons be produced in an event, and the mass logic, which actually estimated the invariant mass of the pair.

Because of the large size of the experiment (25 meters from the target to the P hodoscope) and the tight time constraints (we needed a final trigger decision in less than 500ns), the main electronics rack had to be placed in a central location, next to the spark chambers, despite the rf noise these chambers gave off when fired. Of this 500ns (the memory time of the one-shots in the 1x1 meter MWPC electronics), about 200ns was used in the travel time of the muons from the 1 by 1 meter MWPC's to the P hodoscope and in the travel time of a trigger signal back to the MWPC's, leaving less than 300ns to do the complete logic.

In this 300ns, the dimuon logic checked for the following items:

Table 2-IV, The Dimuon Logic

(a) The presence and arrival time of the beam particle,

(b) That the beam particle was not a muon and that no other particles entered off the beam axis,

(c) That only one beam particle entered in a given bucket,

(d) That the particle interacted in the target,

(e) That two or more muons traveled all the way through the spectrometer.

Not all of these elements were in the trigger at all times; in particular, parts (c) and (d) were not in the trigger during the high intensity runs on the metal targets. Figure 2-11 shows the overall flow of the trigger logic and Table 2-V defines the symbols used.

Table 2-V

Definition Of Logic Elements Used In Figure 2-11

T_1, T_2, T_4 = The beam defining counters. T_4, which is just before the target, defines the arrival time of the beam. The signals from the other two counters must come within 6 nsec of T_4 for a valid beam particle.

T_I => Pulse height of the target counter T_{I6} indicates an interaction in the target.

T_4>2 => Pulse height of the counter T_4 indicates 2 or more particles in a single beam bucket.

V_{jaws}, V_M => Vetos which indicate off axis halo particles.

V_{muon} = Indicates a muon in the beam.

$J_{xU(D)}$ => A hit in the upper (lower) J_x counters.

$J_{yR(L)}$ => A hit in the right (left) side of the J_y counters.

$F_{T(B)}$ => A hit in the top (bottom) half of the F bank.

ULDR => A complete set of hits in diagonally opposite quadrants of the J hodoscope (upper left and lower right quadrants in both the x and y J counters).

URDL => Hits in the upper right and lower left J counters.

J => Hits in diagonally opposite quadrants (ULDR or URDL) with some combination of hits in either x or y separated by at least one counter.

F => Hits in both the top and bottom F counters with some combination of hits separated by at least one counter.

P => Same as F, but applied to P bank.

$\overline{Run}$ = Computer controlled switch to turn data taking on or off.

Beam Gate = Defines the beam spill length.

J<n => Less than n J counter hits.

The trigger made the five dimuon checks at three levels of sophistication. The first level (pretrigger 1 as defined in Figure 2-11) was a quick check of items (a), (d), and (e) and was used to latch the signals from the CERN chambers (at a rate of about 450 triggers per million B).

Pretrigger 2 included a more careful check for the presence of two muons by making a more detailed examination of the geometry of the hits in the J hodoscope. This pretrigger (the rate was approximately 350 per million B) set the CAMAC latches for the various counters and started the mass calculation logic by providing a clock/latch signal for the mass logic's internal latches. The mass logic accepted three different clock signals, one for the F bank and one for each allowed pair of J quadrants.

Because the runs with metal targets had no check that there was an interaction in the target (item d), it was possible for a beam particle which interacted after penetrating deep into the iron shield to produce a flood of particles at the J hodoscope. To eliminate these events, a maximum limit was placed on the number of hits allowed in the J hodoscope at the Pretrigger 2 level in the logic during the metal target runs. The limit was 15 for copper and 10 for tungsten. A clean dimuon event would have only 4

J counters on. On the basis of our reconstruction efficiency checks, (see Chapter III), we estimate that this cut lost less than 2% of the real events.

The third level in the dimuon logic used all available information. The five items in the dimuon trigger were defined as (a) all the beam counters hit within 6ns of each other, (b) no hits in halo or muon vetos, (c) the pulse height in T_4 consistent with only one particle in the beam, (d) the pulse height in T_{I6} consistent with two or more particles leaving the target, and (e) two or more separated hits in all three counter banks, the J, F, and P. The dimuon trigger rate was 5 events per million B.

The mass logic, the second part of the trigger, used the J and F bank signals to estimate the dimuon mass. Basically, the logic used coincidences between the J_x and F counters to calculate the logarithms of the muon momenta, and coincidences between J counters to calculate the logarithm of the opening angle. The sum of these three numbers is proportional to the log of the mass. The logic then checked that the sum was greater than some selected value. Appendix A gives a full description of the logic. It performed the calculation in 100ns and estimated the mass correctly to within a factor of two about 95% of the time.

At the highest mass setting used, the trigger rate was 0.4 events per million B.

The result of the dimuon logic was combined with the result of the mass logic to form the master trigger.

The master trigger sent the latch signal to the 1x1 meter MWPC's and fired the spark chambers. After waiting 5 microseconds to allow the rf noise from the spark chambers to subside, the on-line computer started reading in the data. It took about 12ms to read in the data and 10 to 20ms for the spark chamber power supplies to recover, during which the experiment was gated off.

Two live time gates were defined in the logic. Gate 1 was controlled by the computer's on/off switch ($\overline{\text{Run}}$), the definition of the spill interval (the Beam Gate), and the dead time due to the spark chamber rf noise. Gate 2, the actual live time of the trigger, included the effects of the dead time which came from the 20msec needed to read in an event and the 1 microsecond reset time of the CERN chamber latches.

In order to normalize our final cross sections, the number and type of particles incident on the target were needed. The beam flux was determined by counting the number of occurences of various coincidences between the Cerenkov counters and the beam signal (B in Figure 2-11). For example, a B signal with no Cerenkov counters on represented a proton. (See Chapter IV for more information on particle identification.) The counting was done using CAMAC scalers that were active when Gate 2 was on.

The pulse heights of the target interaction counters and of the Cerenkov counters were recorded using CAMAC analog to digital converters (ADC's).

Data Aquisition

We used a Xerox Data System Sigma III as the on-line computer. A custom-made high speed CAMAC interface for the Sigma transfered the data directly into the computer's core memory. The computer wrote the data on magnetic tape, and monitored the status of the experiment. The monitor functions included keeping track of scaler sums, scaler ratios, readout errors, etc. A number of on-line displays showed counter and chamber hit distributions and multiplicity distributions, counter pulse height distributions, and pictures of individual events. The computer also ran the mass box logic checker about once every 10000 events.

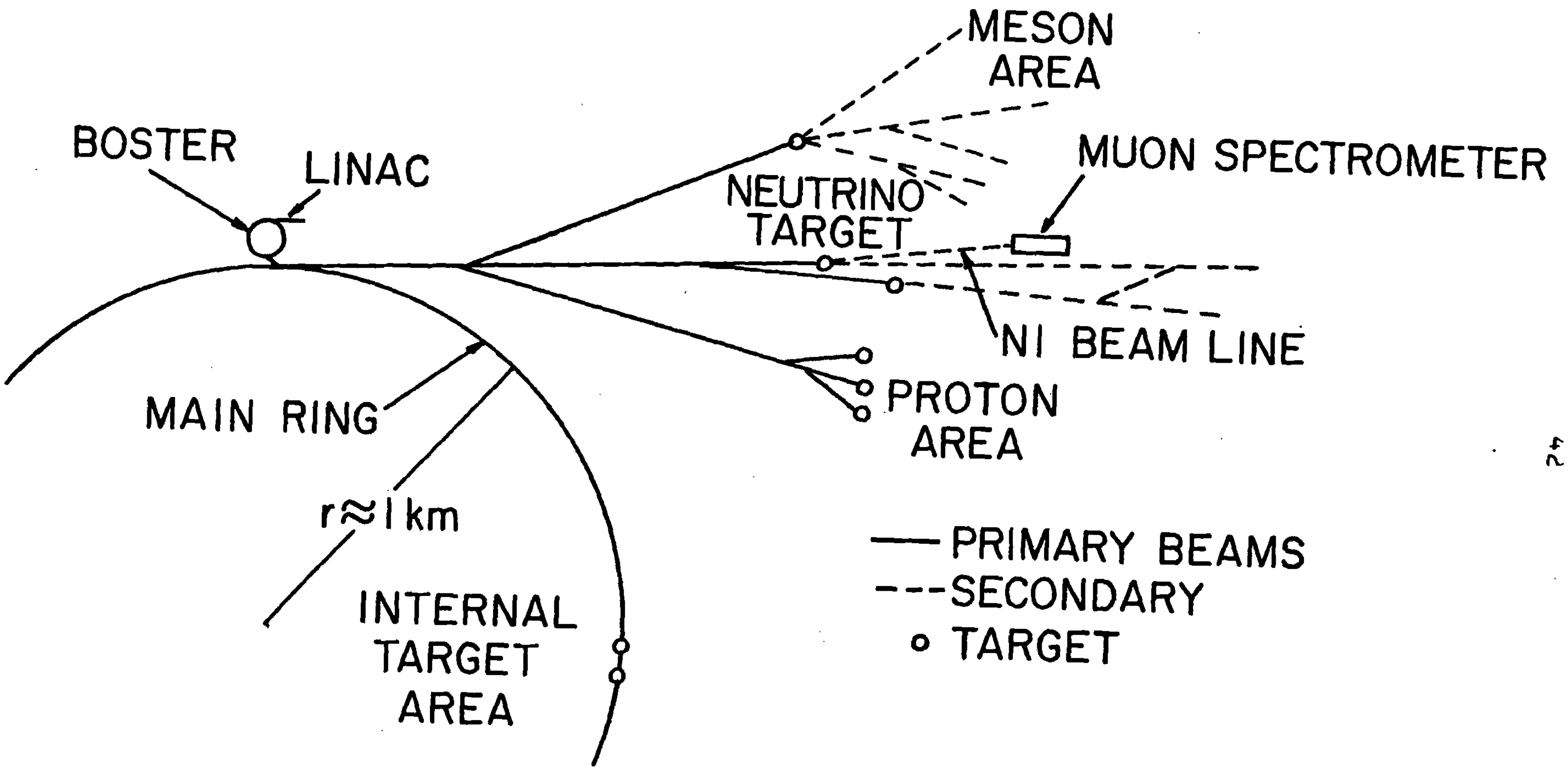

Figure 2-1. Diagram of the accelerator.

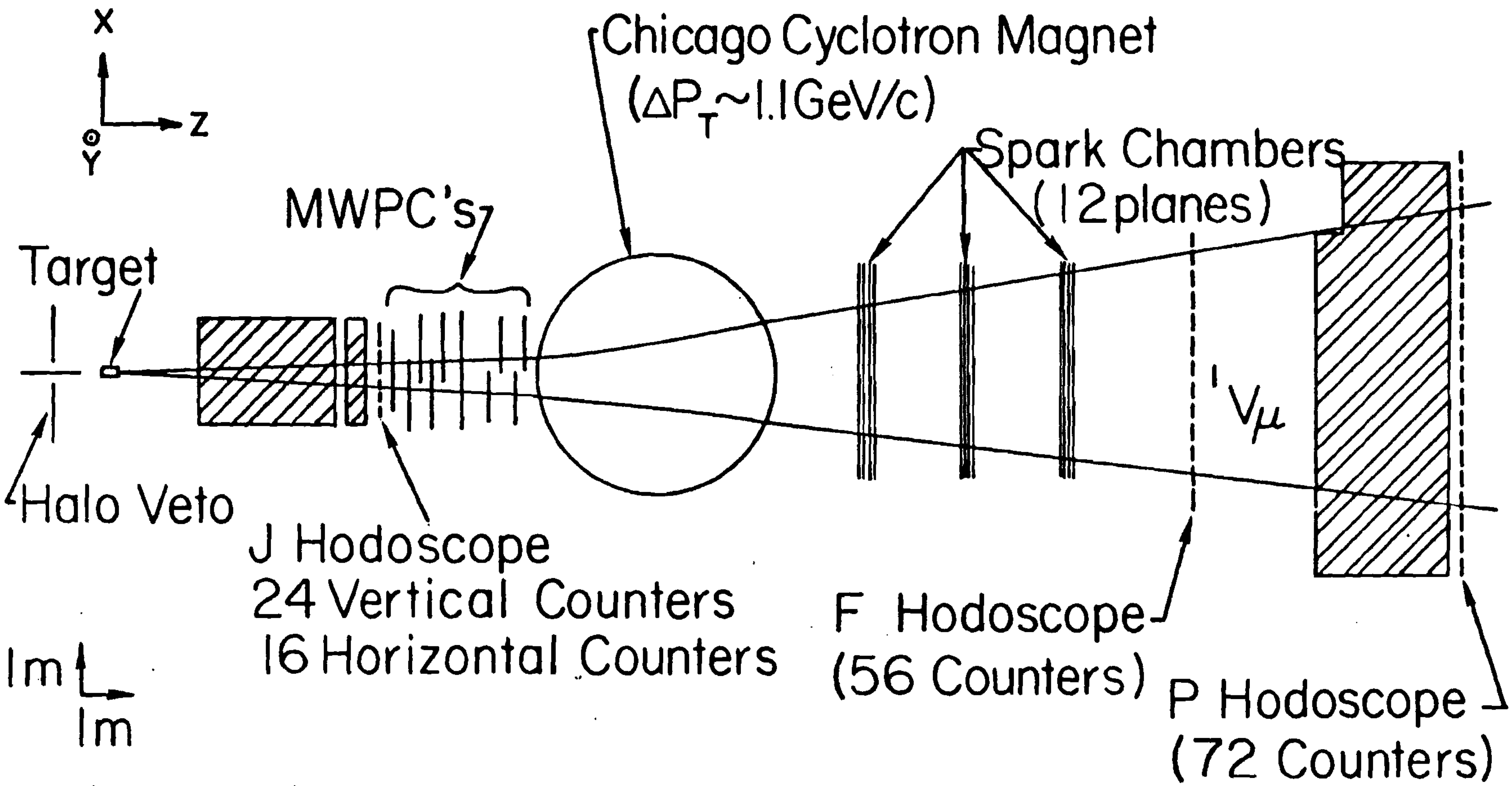

Figure 2-2. Diagram of the apparatus.

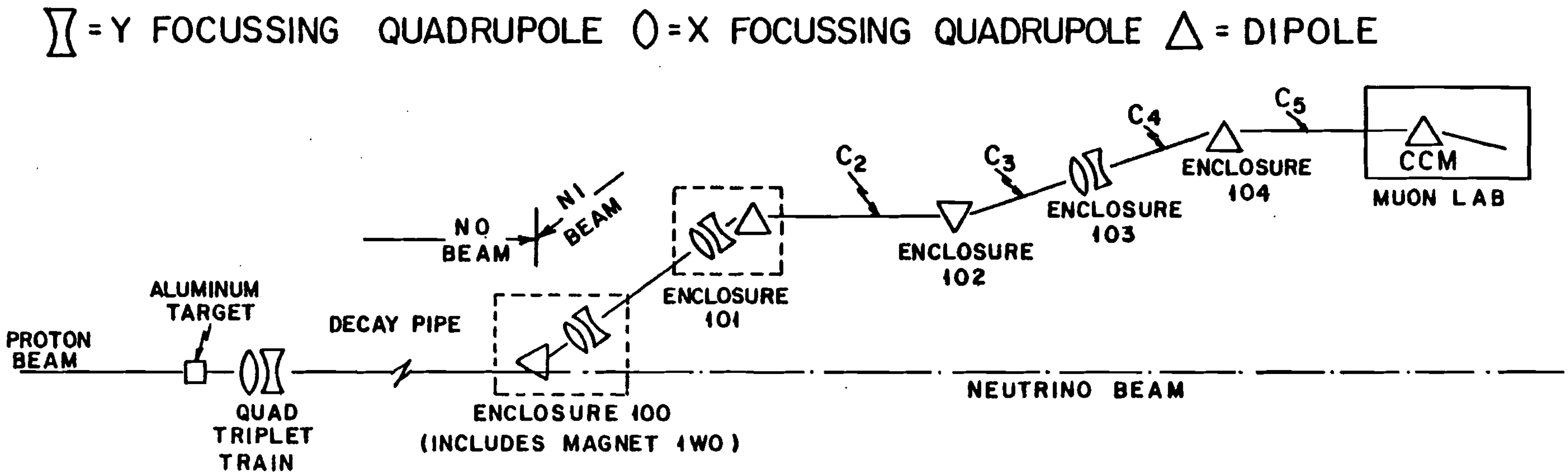

Figure 2-3. Diagram of the neutrino beam line.

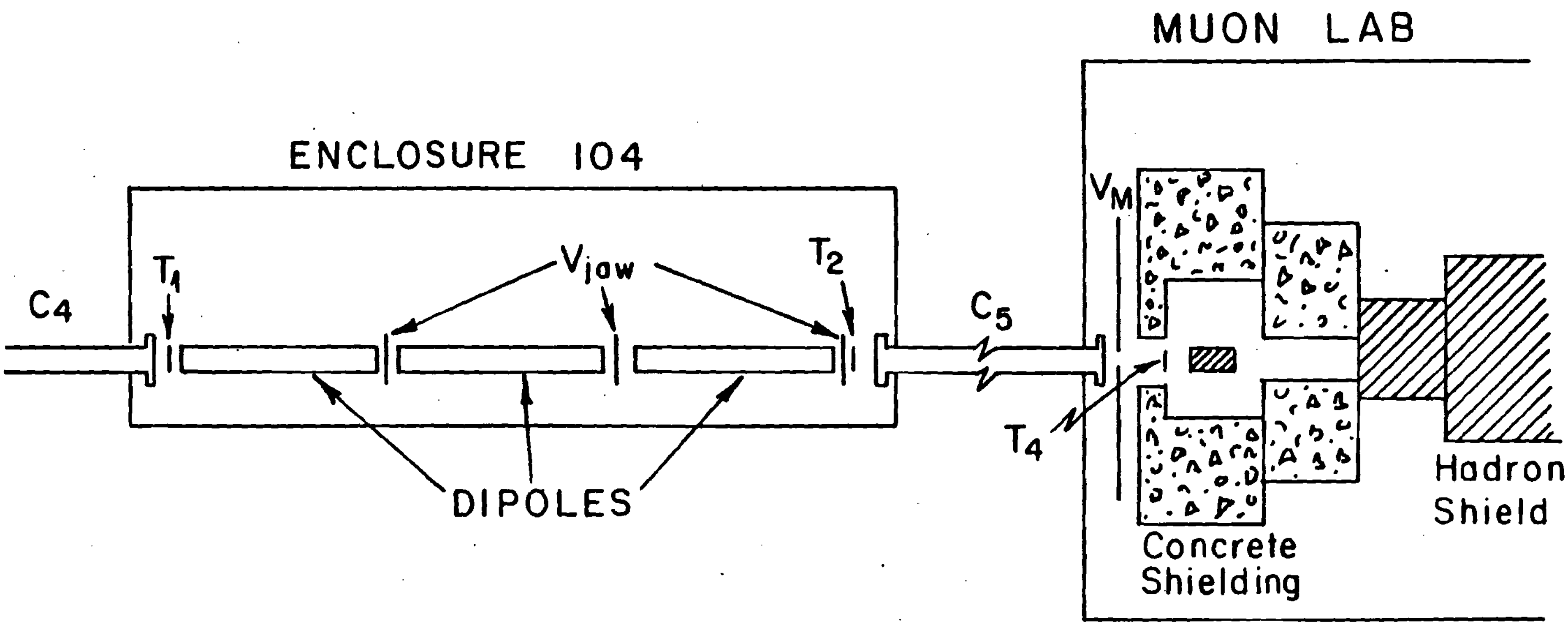

Figure 2-4. Diagram showing the locations of the beam defining counters.

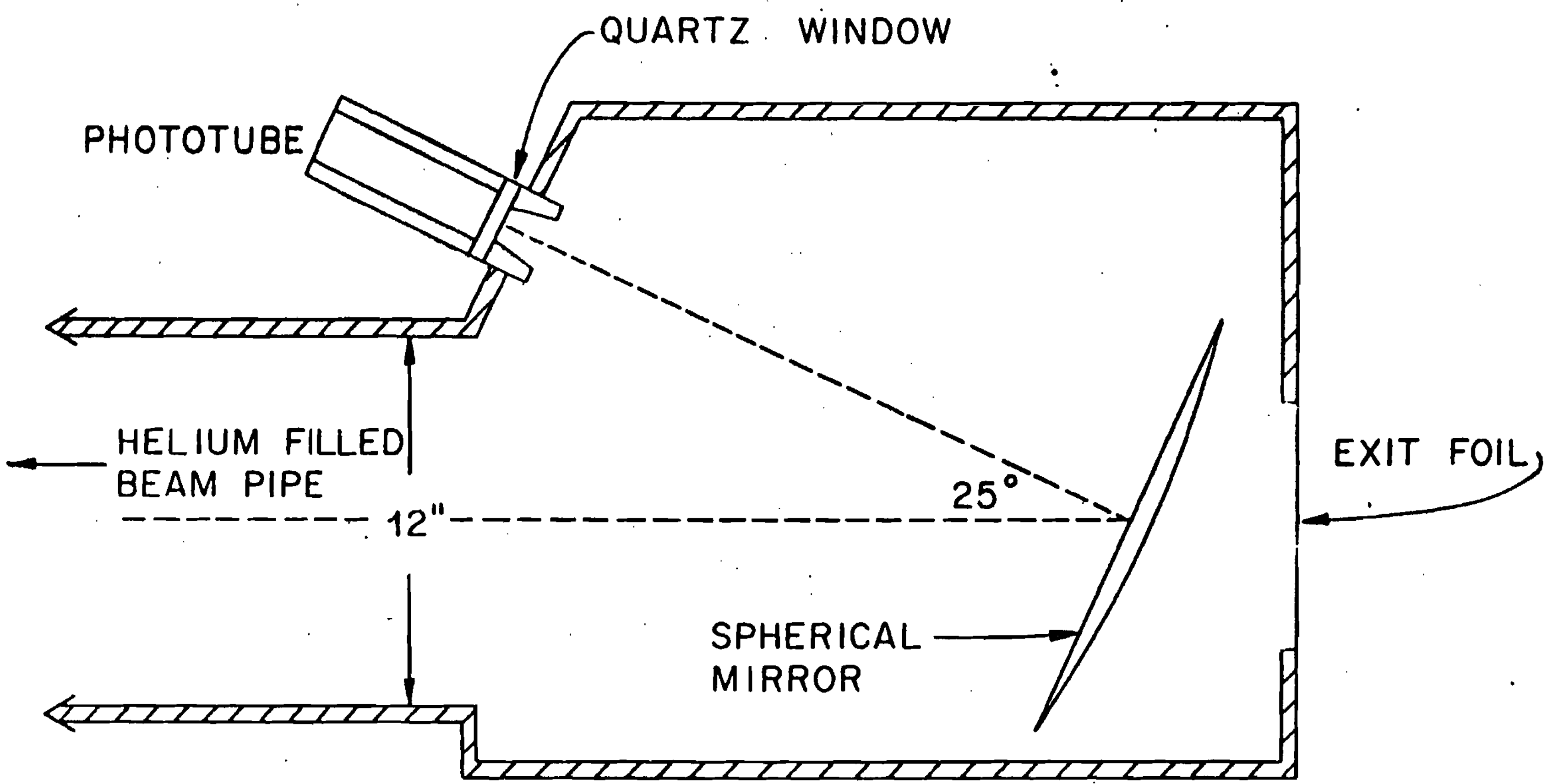

Figure 2-5. Simplified drawing of a beam Cerenkov counter.

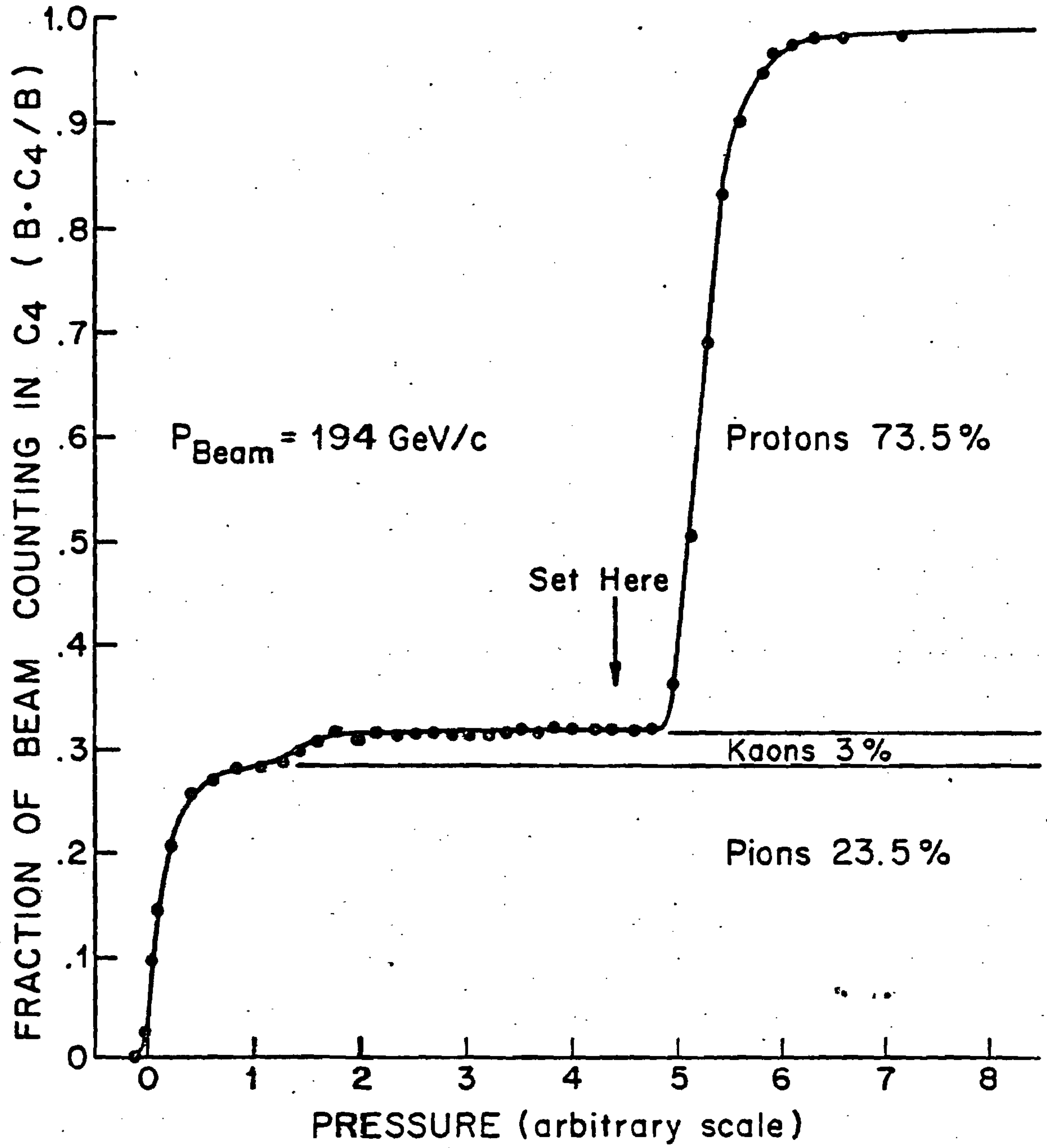

Figure 2-6. Typical pressure curve for C_4.

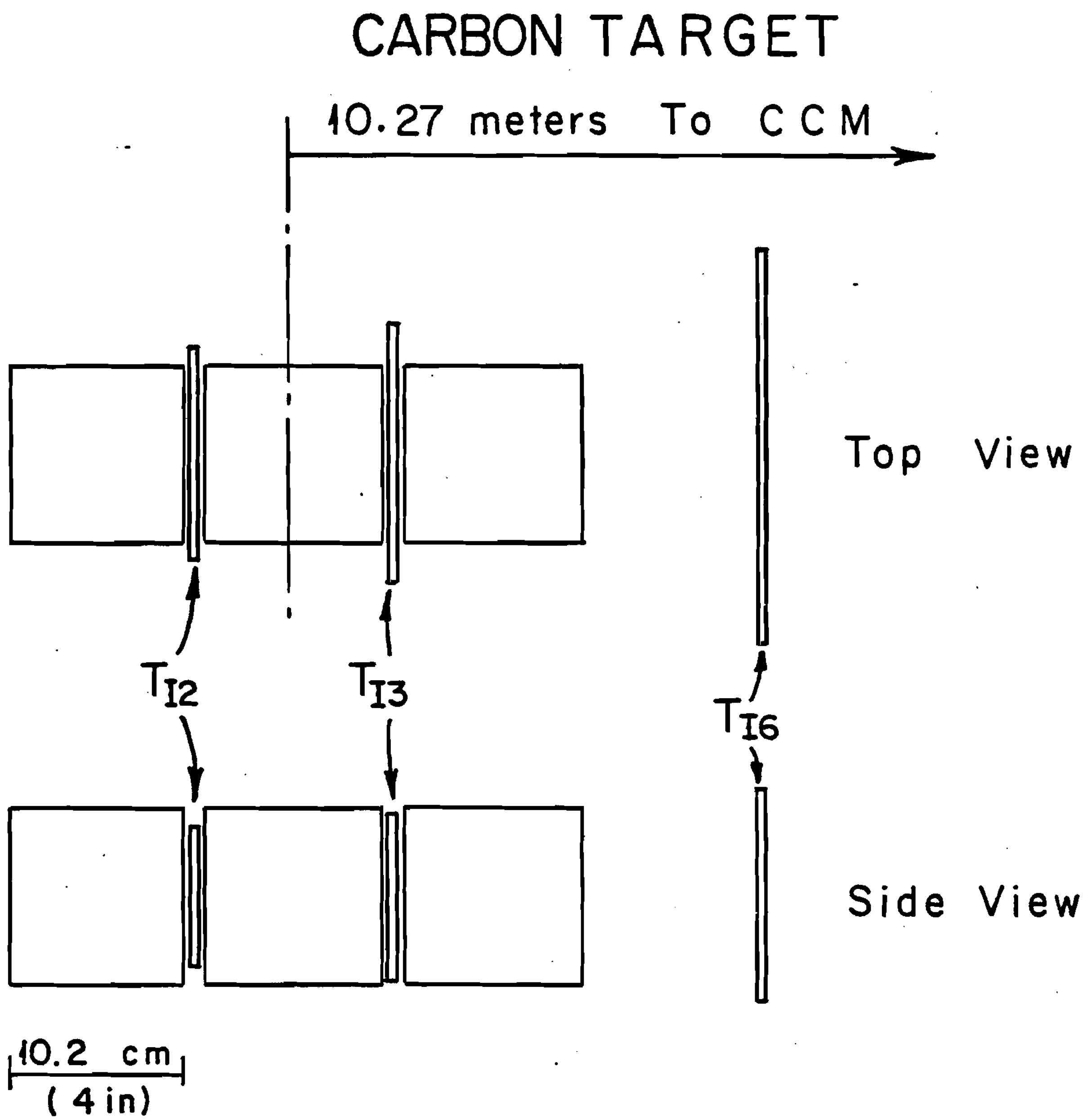

Figure 2-7. Diagram showing the relation of the carbon target blocks to the target counters.

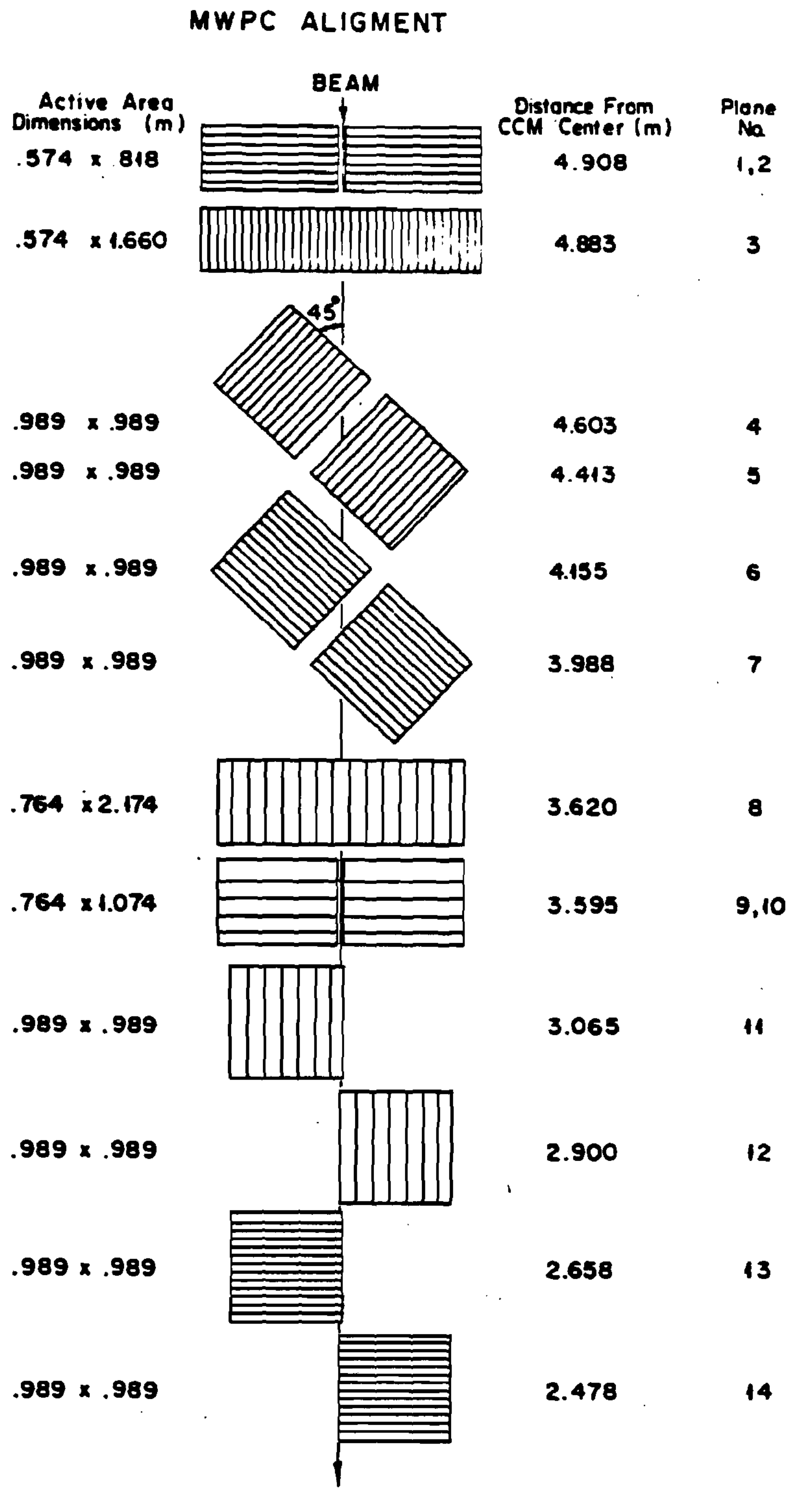

Figure 2-8. Diagram showing the position and sizes of the MWPC's active area. The lines inside the box are only to guide the eye and do not represent the actual wire spacing.

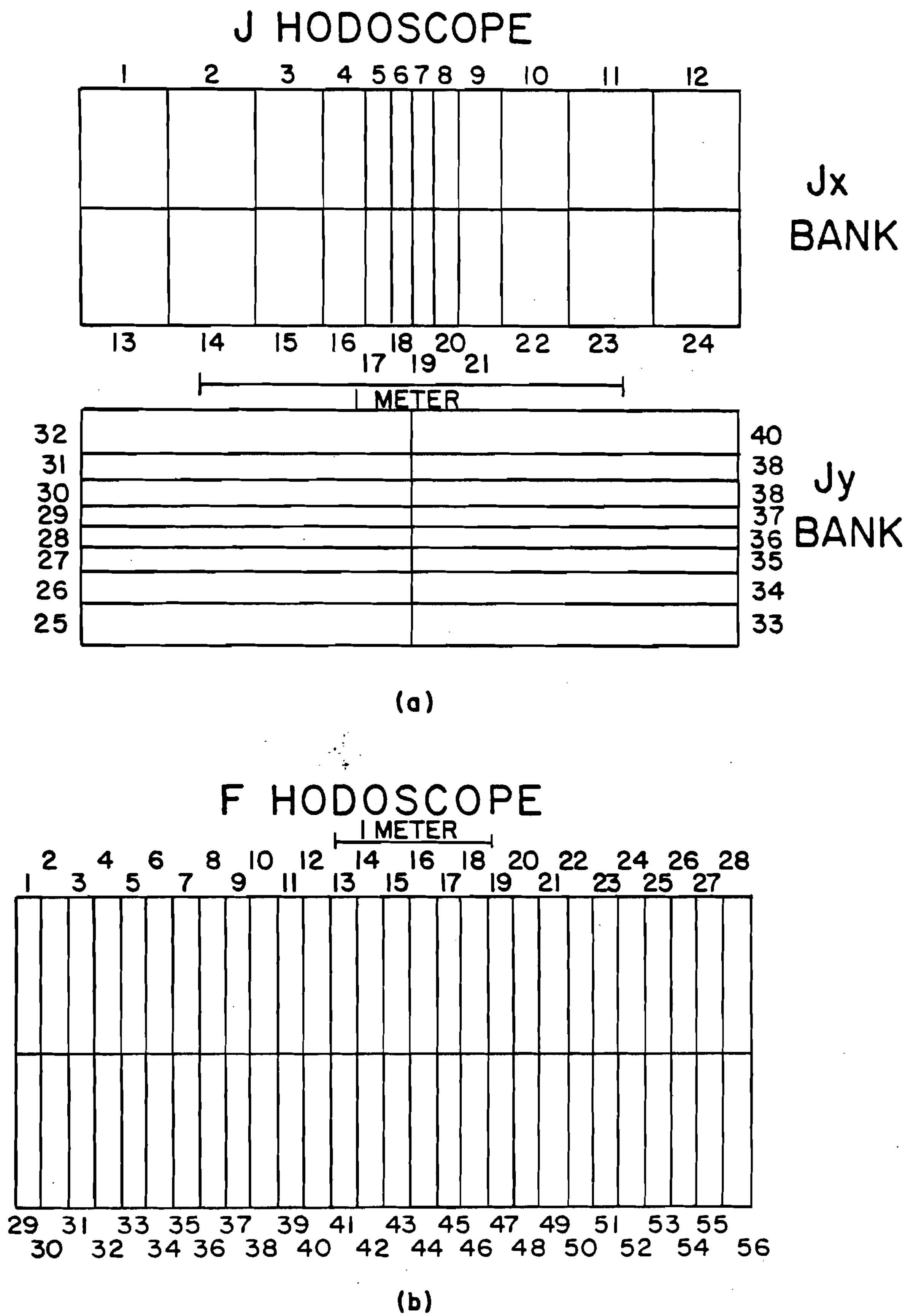

Figure 2-9. Diagram of the J and F hodoscopes.

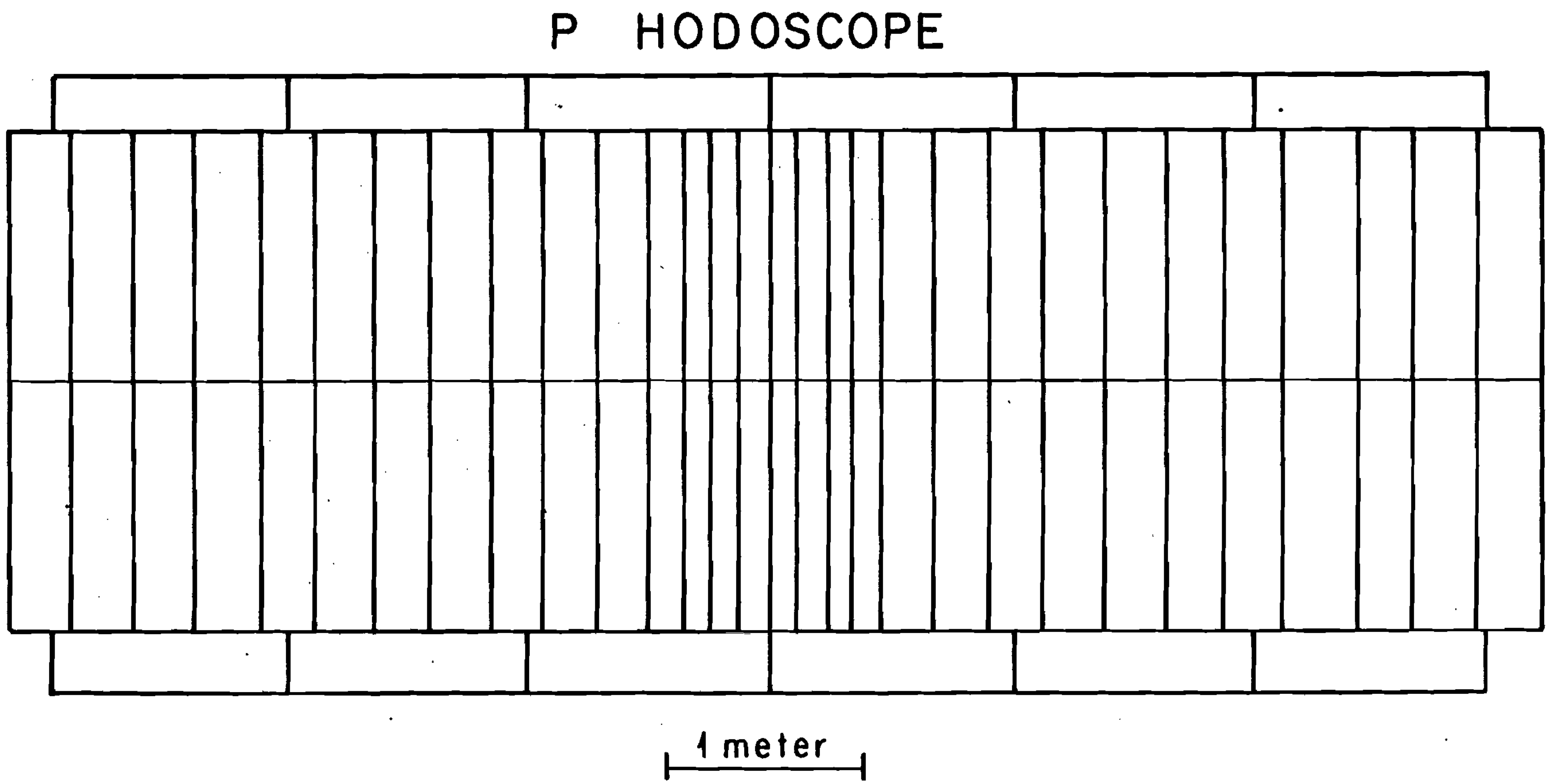

Figure 2-10. Diagram of the P hodoscope.

TRIGGER LOGIC DIAGRAM

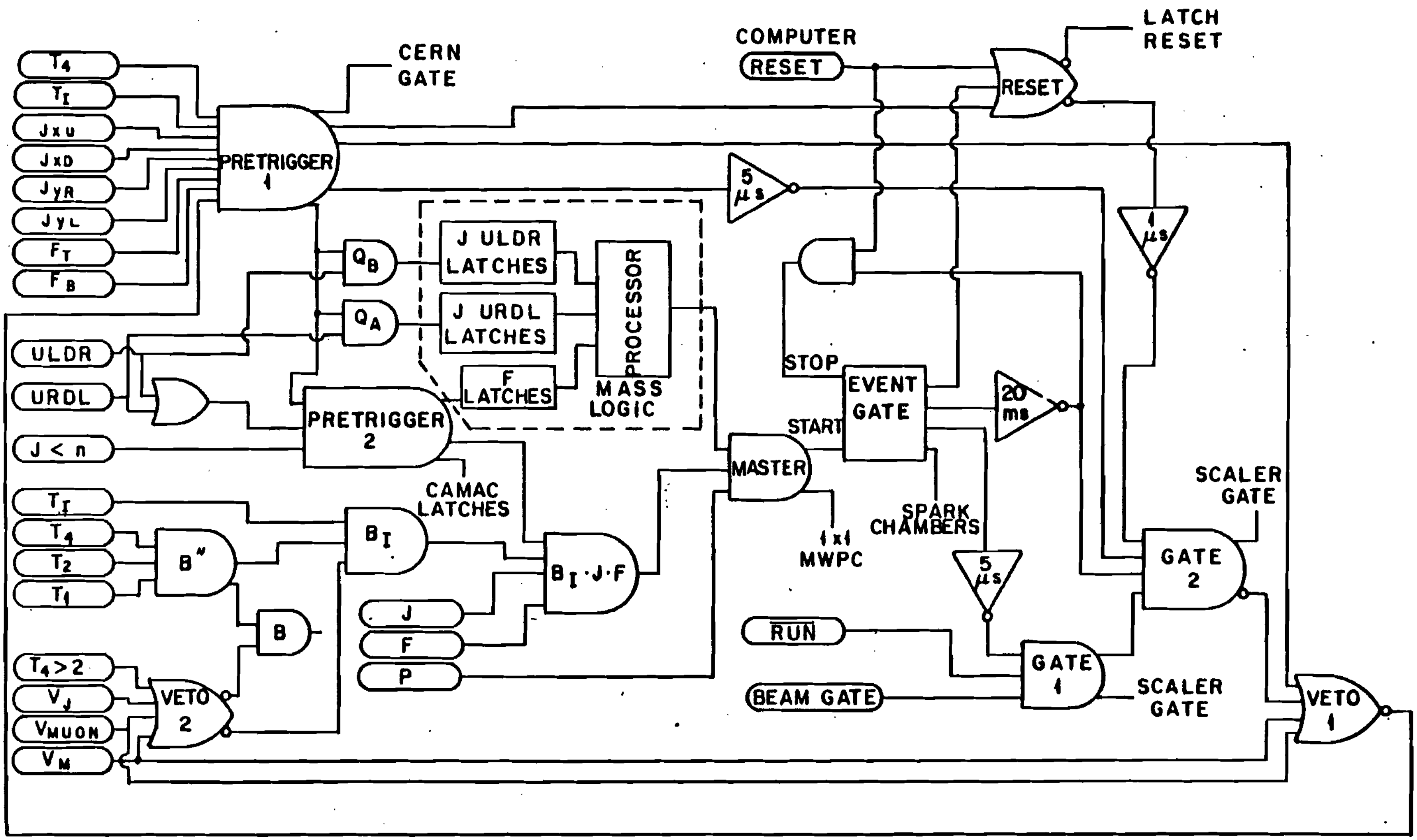

Figure 2-11. Trigger logic diagram.

Chapter III The Reconstruction Program

INTRODUCTION

This chapter describes the reconstruction program used to transform the data from a set of chamber sparks into particle tracks with slopes and intercepts. The program first found tracks in the upstream chambers. Those upstream tracks that pointed at the target and at struck counters in the J hodoscope were used as a starting point for a track search in the 2 by 4 meter spark chambers. To become muon tracks, candidate tracks had to have linked upstream and downstream track segments and point at all three hodoscope arrays. Track parameters were then saved on a secondary tape.

The Coordinate System

The program used a right-handed coordinate system centered on the CCM, with positive z coordinate in the direction of the beam, positive y upward, and positive x to the west. The centers of the two CERN chambers defined the z axis. Chapter II described the method used to locate the other chambers. Position distributions of tracks at the hodoscopes in the vicinity of a hit counter provided the final locations for the counter banks. Figure 3-1 shows an example for the F hodoscope. In this coordinate system the beam came into the lab with an angle of 3.0 mrad in x and -6.25 mrad in y. The center of the target was positioned off the z axis by -24mm in x and +34mm in y.

The Upstream Track Finder

The upstream track finder used an exhaustive approach. As Figure 2-3 shows, the upstream x and y planes could measure four types of track segments: x-left, x-right, y-left, and y-right. Three planes measured each of these track types with little of no overlap between left and right. The program started with a search for three-point tracks of a given type by simply taking all pairs of sparks in two planes and, forming a line between them, searching for a third spark in the remaining plane within 7.5 mm of this line. If a third spark was located, the program did a least squares fit to a line using the sparks and calculated a chi square based on the chamber resolution. Lines with a probability of the chi square (confidence level) less than .001 were rejected. As a timing check on particle tracks, lines also had to intersect the J hodoscope within 12.5 mm of a hit counter. Finally, the line had to pierce an imaginary box surrounding the target as shown in Figure 3-2. The program searched the y planes first, then the x planes. Good track segments were then inserted into a track buffer along with a label giving the track type.

After all possible 3 point tracks were tried, all possible 2 point tracks were formed from the remaining unused sparks for each track type. To cover the dead area in the CERN y chambers, the program also searched for 2 point y tracks in the small overlap area between the last two y measuring 1 by 1 meter chambers. This last type of two-point track entered the upstream track buffer twice, once as a right-side track and once as a left-side track. Like the 3 point tracks, the two-point tracks had to point at J counters and at the target.

The program then tried to pair the x and y tracks segments that were on the same side into global tracks using the information from the u and v chambers. All possible x and y track pairs were projected into the uv chambers, which were searched for sparks within 3.25 mm of this line. Any such sparks were combined with the x and y sparks to form a global track. To be kept, a global line had to point at a <u>pair</u> of overlapping struck J counters (one x and one y in the same quadrant) and have a chi square of less than 8 per degree of freedom. If, after all xy pairs had been tried, some x or y tracks appeared in more than one global track, the program kept the global track with the greatest number of sparks, or, if the two (or more) global tracks had the same number of sparks, the program chose the lowest chi square.

The next step combined any unpaired x or y track that still existed with all possible pairs of unused u and v sparks. If one or more additional sparks were found along the resulting line, and the line pointed at the J hodoscope, and if the line had a chi square per degree of freedom of less than 8, the program kept the line. The line did not need to point at the target. Finally, the upstream track finder formed all possible 4 point uv tracks from the unused u and v sparks, and if it could find one more spark on the line, etc, the program saved the line.

The program had room for 21 x and y tracks and 30 global tracks. The redundancy of this track finder gave the program a theoretical efficiency of greater than 99.5% even if one of the 1 by 1 chambers failed completely. The actual efficiency for finding two track pairs was closer to 98% according to the reconstruction efficiency check described at the end of this chapter.

The Downstream Track Finder

The downstream track finder tried to find a track in x and y at the same time. The track finder started with a list of all stereo spark pairs (from the two sense planes of a given spark gap) which, when converted to x and y coordinates, lay within the 2 by 4 meter area of the chambers. Unpaired sparks were discarded.

The program then started down the list of x upstream tracks, globally paired tracks first, looking for a matching downstream track using the fact that when in a cylindrical magnetic field, the impact parameter (the distance of closest approach to the magnet center) of the track before and after the magnet stays the same. Test lines were formed from the impact parameter of an upstream track and with each spark in the pair list as shown in Figure 3-3. (The spark displacement from the track has been increased for clarity.) The intersection of each test line with a projection plane in the middle of the sparks chambers (5.8 meters from the CCM) was calculated. If a group of x sparks formed part of a track, these projection points would cluster togther. Hence the method consisted of searching for a cluster of sparks in the projection plane. A cluster was defined as 3 or more points within 5mm of each other.

The stereo spark pairs found in an x cluster were then projected in y to find a y cluster with a width of less than 25mm. When the reference upstream x track was part of a global track, several different assumptions about the y component of the downstream track were tried in attempting to find a y cluster. The first assumption was that the y downstream track had the same y intercept at the CCM as the reference upstream global track. The second was that the track had the same y slope. If both of these failed or if the upstream track was not a global track, the program tried to find a y track that pointed at the target.

The spark pairs found in a double (x and y) cluster were used in a least squares fit to form a candidate track. Each plane was searched for the closest spark (if any) within 13.75mm of this candidate track. If this new set of sparks contained at least 3 x sparks, 1 u spark, and 1 v spark and the resulting track could link with some permitted combination of x and y upstream tracks, the spark set was fit to a line which then became the new candidate track. The test was then repeated on the candidate track with a 3.75mm window. Should the track fail, several different variations on the initial track parameters were tried in the spark search in an attempt to find a good downstream track.

Once the program had a good candidate track, it checked that the track pointed at a hit F counter within 37.5mm in x and 75mm in y. If two tracks had more than 2 sparks in common, the track with the greater number of sparks was kept. Given equal number of sparks, the track with the smallest chi square was picked. Finally, a track had to point within 400mm of a hit P hodoscope counter, loose because of the scattering in the Rochester iron. The range requirement so imposed assured us that the downstream tracks were muons. The hodoscope checks also served as timing checks on the tracks.

Linking

The resulting set of upstream and downstream track segments then needed to be linked together. Linked track segments had three parameters in common: the x impact parameters, the y intercepts at the CCM, and the y slopes at the CCM.

The program first tried linking the downstream tracks to global upstream tracks using as a chi square for linking:

$$\chi^2 = (\Delta x/\delta_x)^2 + (\Delta y/\delta_y)^2 + (\Delta s_y/\delta_s)^2 \qquad (3\text{-}1)$$

where:

$\delta_x = 3.75\text{mm}$

$\delta_y = 35.4\text{mm}$

$\delta_s = 5$ milliradians

Links must have had a chi square less than 30. Each downstream track was allowed to link with only one upstream track. If the links could be made in more than one way, the program tried first to maximize the number of links and then, if it still had a choice, to minimize the link chi square. If a downstream track would not link to an upstream global track, the program tried to link it to the unused separate x and y upstream tracks, including the individual x and y pieces of unused global tracks. When doing x and y links separately, an x link required that $\triangle x$ be less than 27.5mm and the y link required that the y portion of the link chi square be less than 20. The resulting x and y upstream tracks had to point at a overlapping pair of J counters. Again, the number of links was maximized when options existed. Figures 3-4, 3-5, and 3-6 show distributions of the linking quantities for both beam muons and all muons. The multiple scattering in air and in the chamber material caused the increased widths in the all muon curves.

<u>Momentum</u>

A muon's momentum was calculated from the well known formula for a particle in a cylindrical field:

(3-2)

$$p_0 = (x + \cot(\triangle s_x/2) * [r*r - x*x]^{1/2}) * B * 2.9974E-4$$

p_0 = momentum in GeV/c

Δs_x = difference in x slopes

r = magnetic field radius

x = impact parameter (in cm)

B = field strength (in kilogauss)

The last two x upstream chambers were inside the fringe field of the magnet. So, once the approximate momentum of the muon was known, the spark positions inside these chambers were corrected to where they would have been if there had been no field and the line refit. In this refit, the entire track, upstream and downstream, was fit at the same time, doubling the lever arm of the fit. This fit forced the x impact parmeters of the upstream and downstream track segments to be the same. After a search added any missed sparks and threw out any sparks that were too far off this line, the line was fit yet again. The program then recalculated the momentum. Figure 3-7 shows the reconstructed momentum spectrum for beam muons. The width agrees with that expected from the chambers' resolution. Finally, the momentum was corrected for the energy loss in the iron and in the target based on the momentum dependent calculations of Therict.[14]

Reconstruction Efficiency

Figure 3-8 shows the percentage of triggers in which the program found two or more muons as a function of run number (approximately 10000 triggers per run). These numbers represent the minimum reconstruction efficiency of the program because some of the events actually had only one muon. A few runs had a low percentage of reconstructed triggers. The problem was generally caused by malfunctioning equipment which was quickly fixed. These runs represent only a very small fraction of the data.

Of the events with two muons in them (as determined by scanning a large sample of events by hand) that were not reconstructed, Table 3-I lists the main reasons why the program seemed to fail. Table 3-II gives the average reconstruction efficiencies for the different targets and beam based on the scans.

The manual scanning defined a muon as a line of sparks in the downstream chambers that appeared to point at struck F and P hodoscopes. Because the program would find a downstream track only if it had already found a matching upstream track, the manual scan could pick up those events in which the upstream track finder had failed (usually due to too many or too few sparks) or in which the program failed to find an upstream-downstream link. Two physicists separately scanned 8500 events taken during various parts of the experiment.

Table 3-I Reconstruction Failures

Reason	% Of Failed Events
Blasted Event (too many tracks)	10 to 35%
Plane Inefficiencies	10 to 35%
Linking Failures	30 to 50%

Table 3-II Reconstruction Efficiency

Beam/target	Efficiency
+C	.94
-C	.94
-Cu	.90
-W	.92
All	.92

Obviously the high reconstruction efficiencies leave little room for any serious problems.

Data Handling

We carried out the reconstruction and data preparation in several steps. First the raw data and reconstructed tracks were written out to secondary tapes. Next, tertiary tapes were created by writing out only the reconstruction information for events with two or more muons. Finally, the data were compacted still further by creating tapes containing only good events (see chapter IV). We used this last set of tapes for the final analysis.

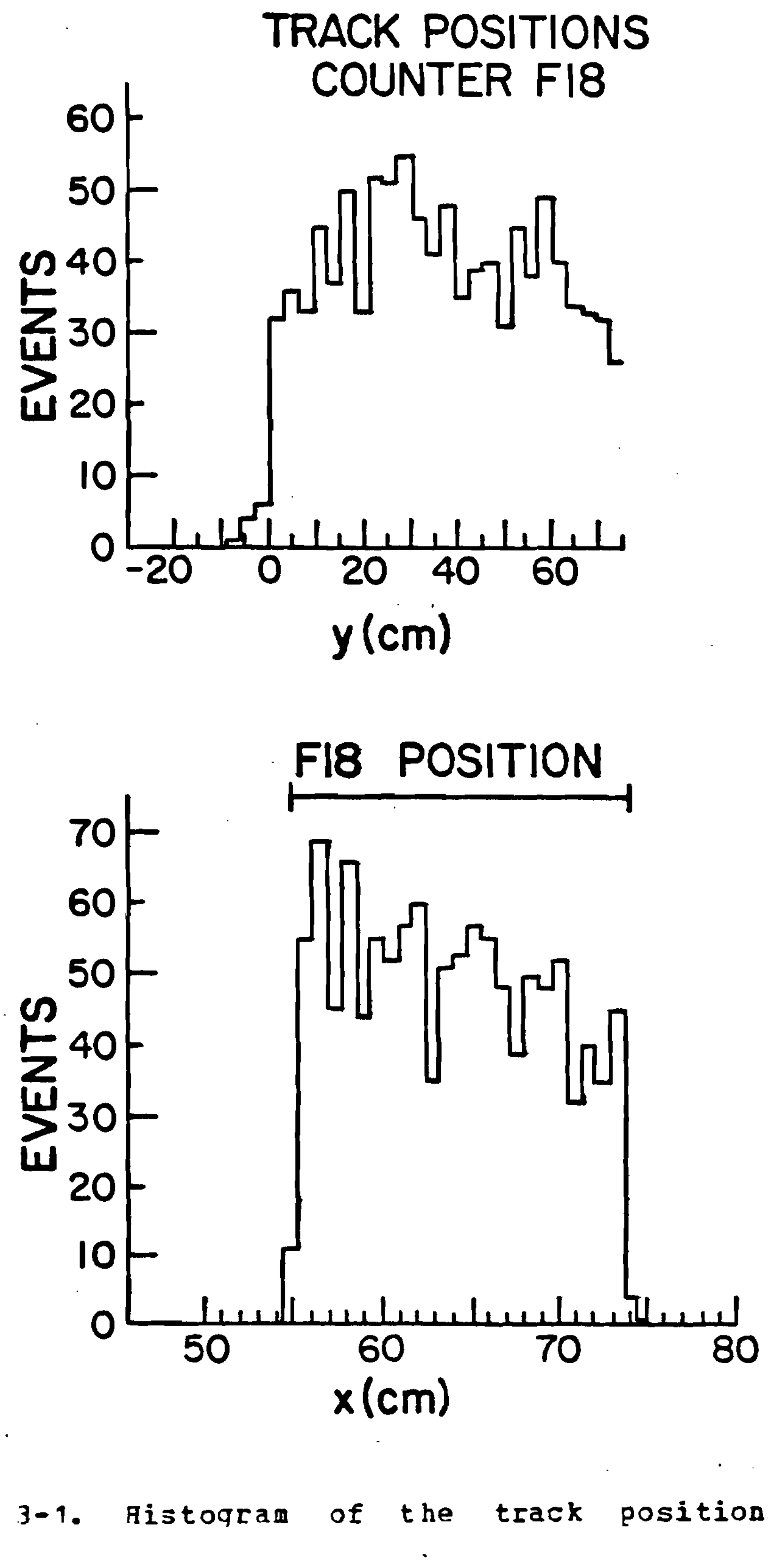

Figure 3-1. Histogram of the track positions at the F hodoscope when counter F18 is on.

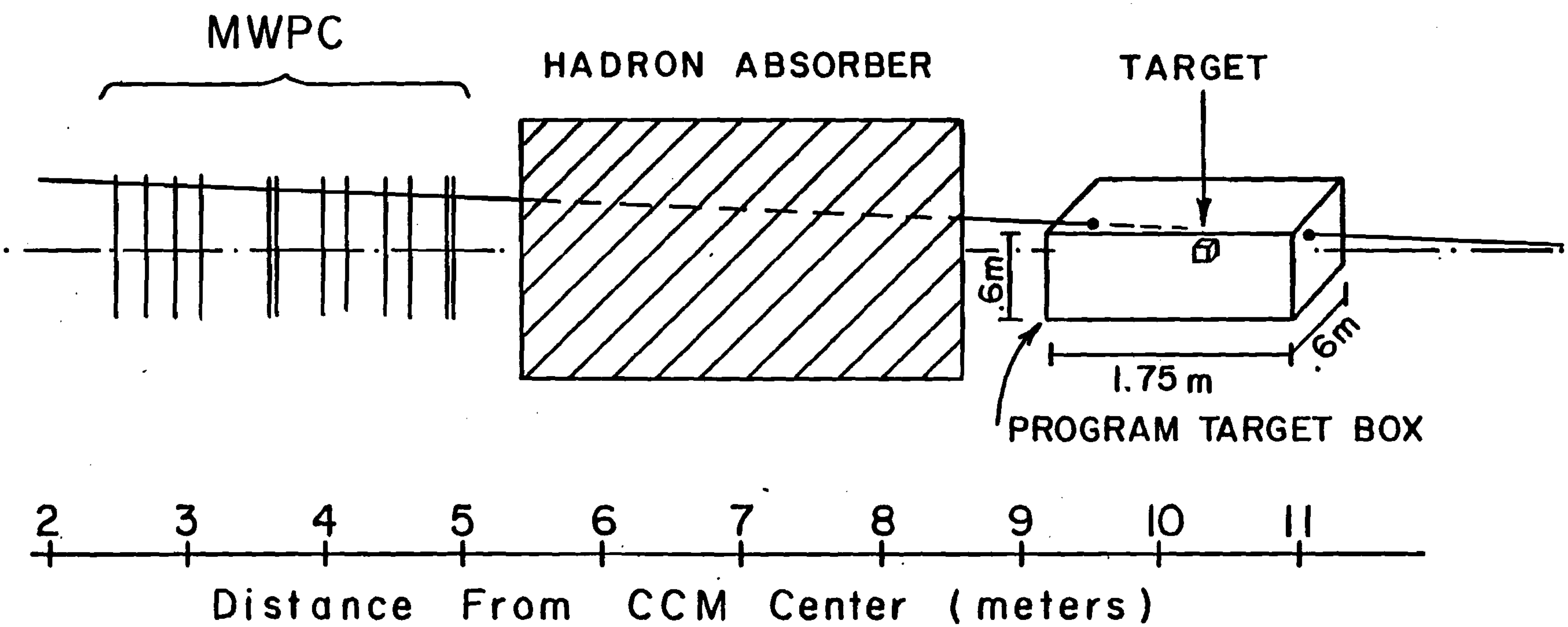

Figure 3-2. Diagram showing extrapolated track piercing the program's target box.

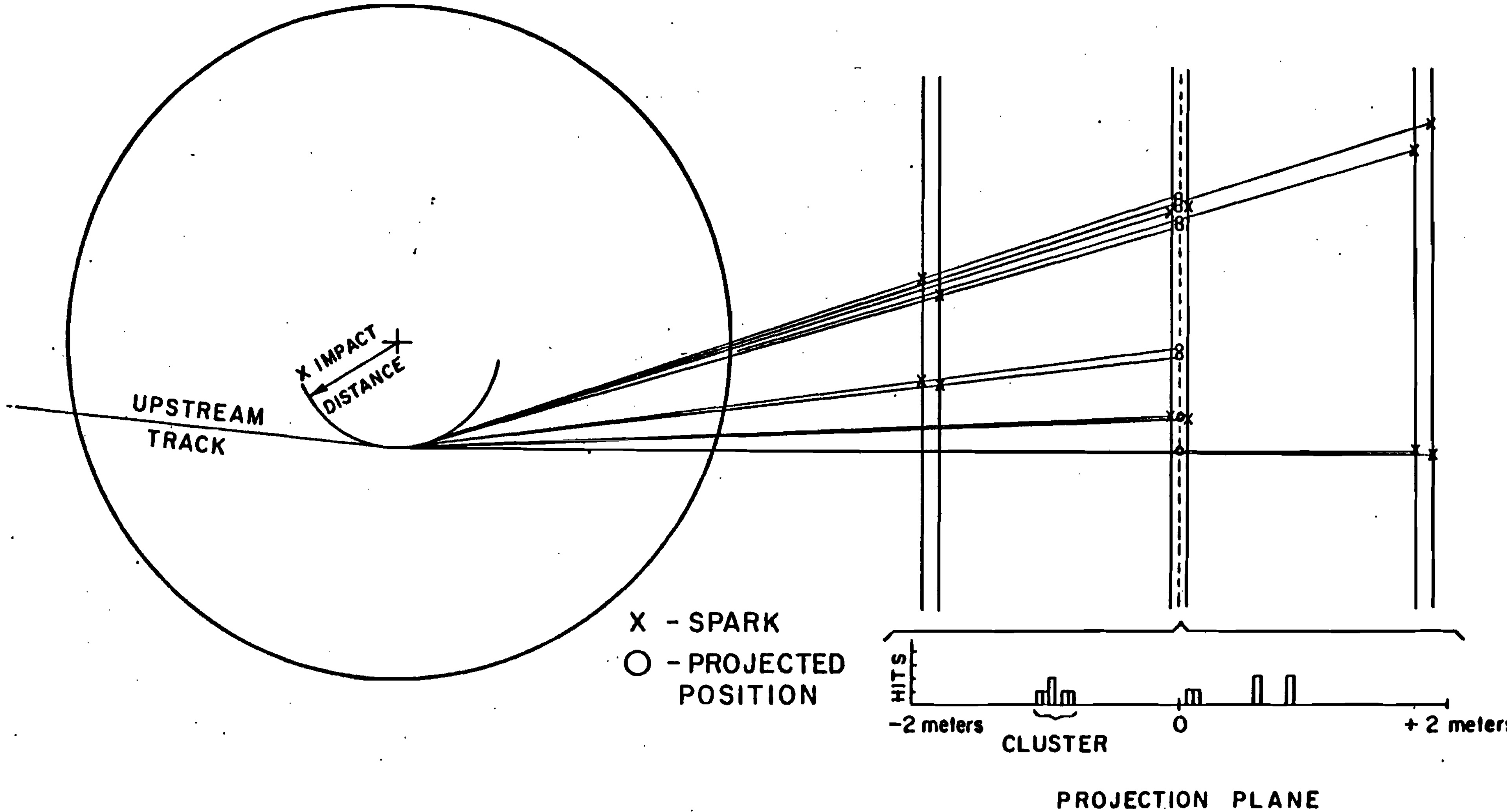

Figure 3-3. Diagram demonstrating the track finder.

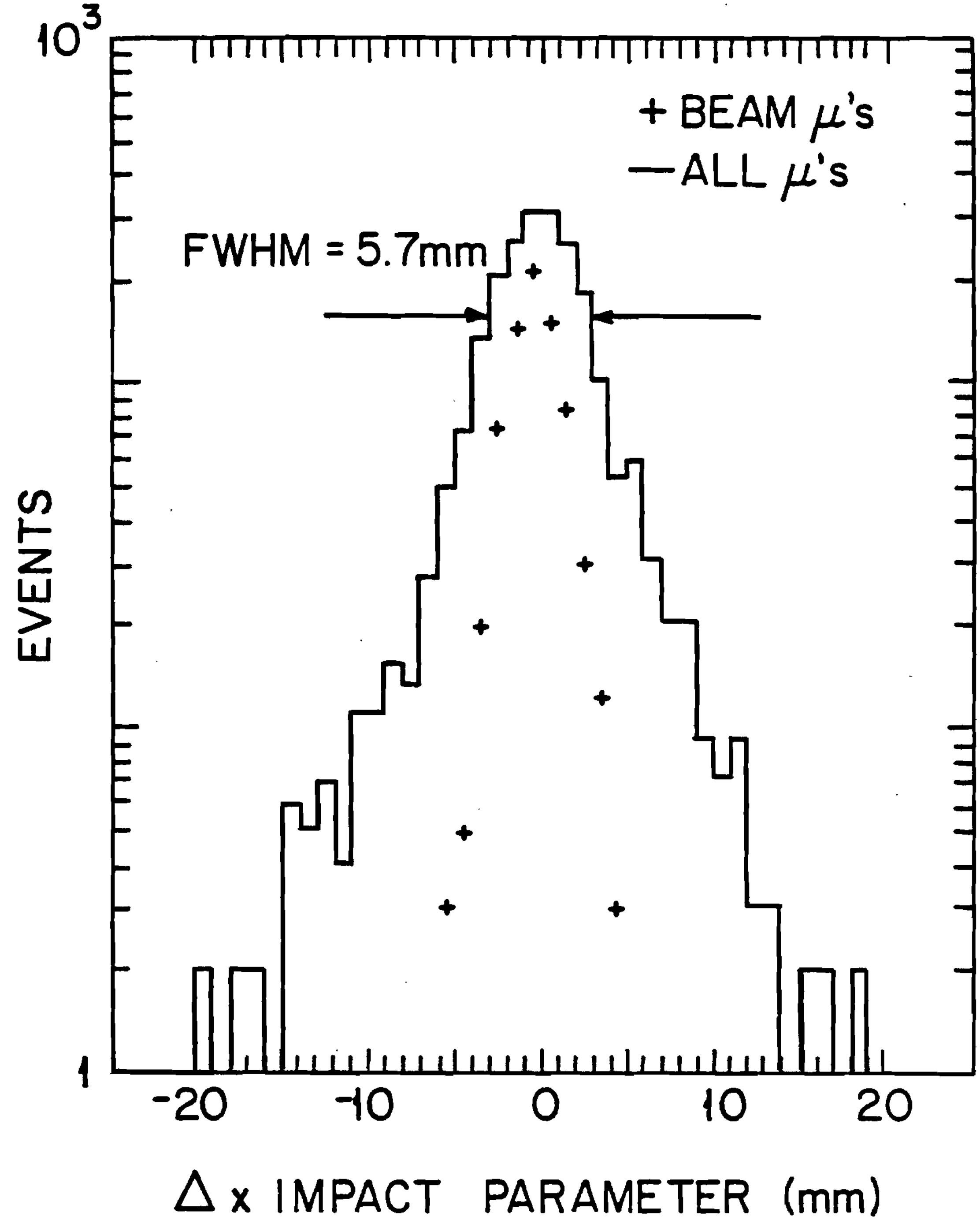

Figure 3-4. Difference of upstream and downstream track's impact parameters.

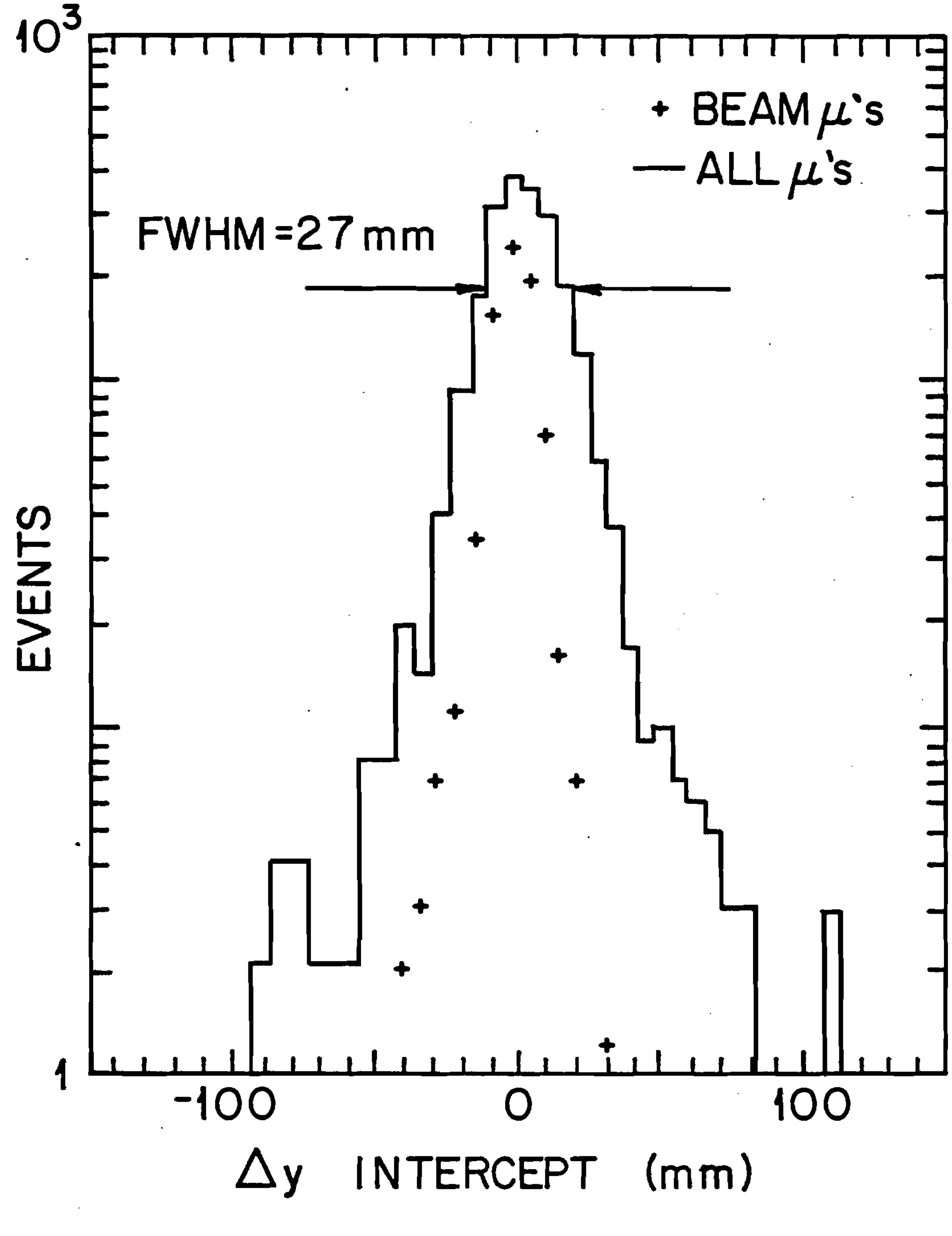

Figure 3-5. Difference of upstream and downstream track's y intercepts.

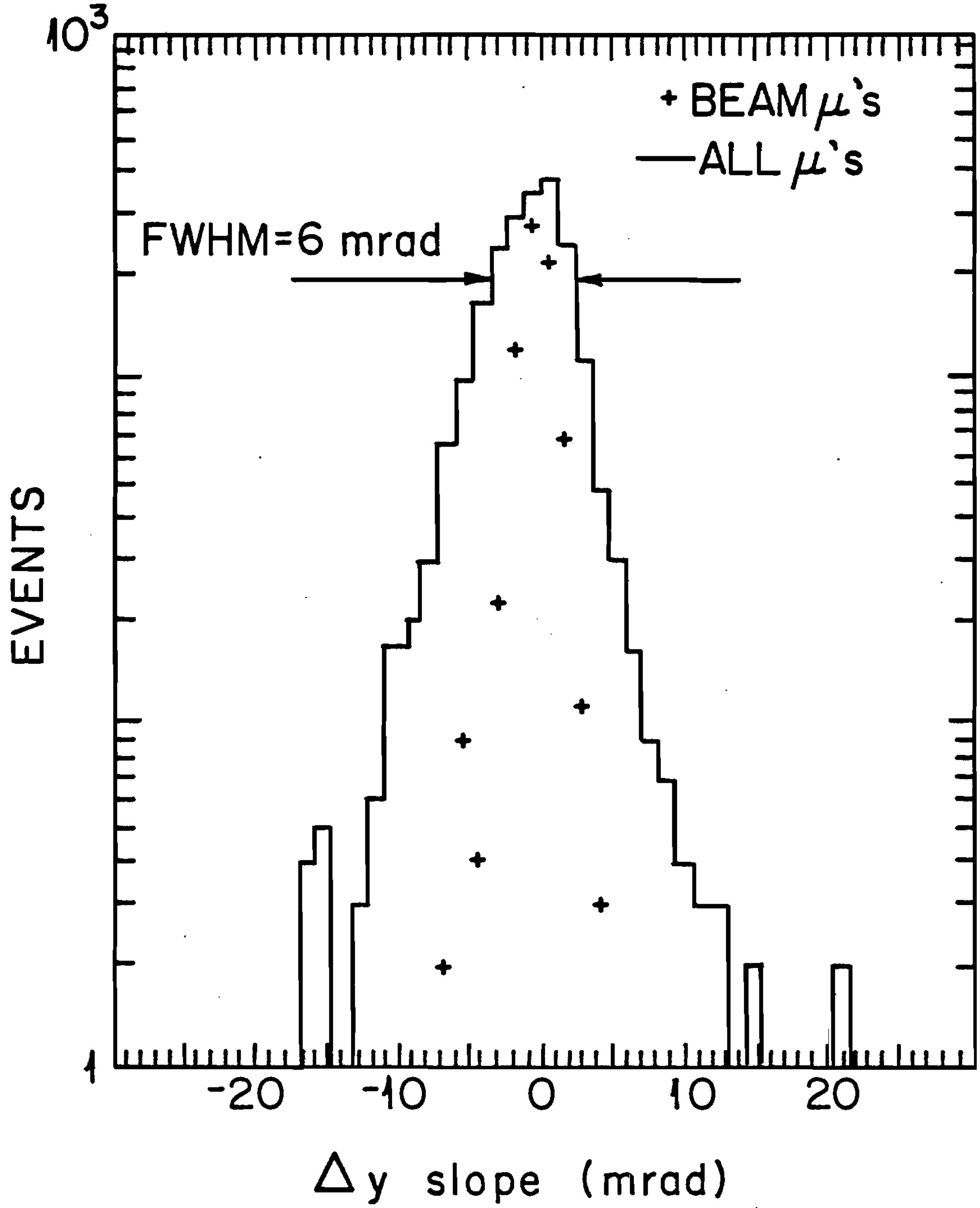

Figure 3-6. Difference of upstream and downstream track's y slope.

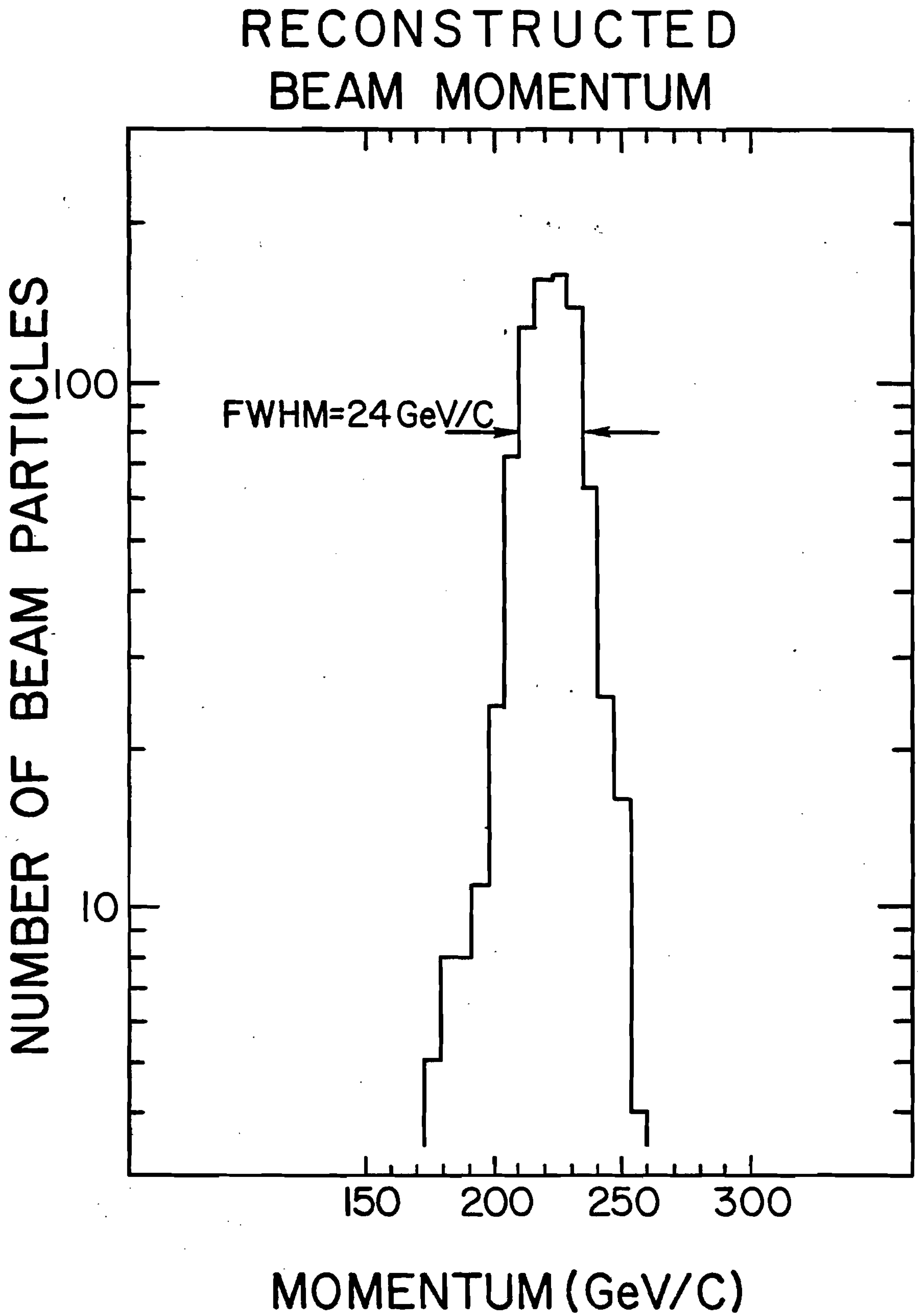

Figure 3-7. Reconstructed beam momentum.

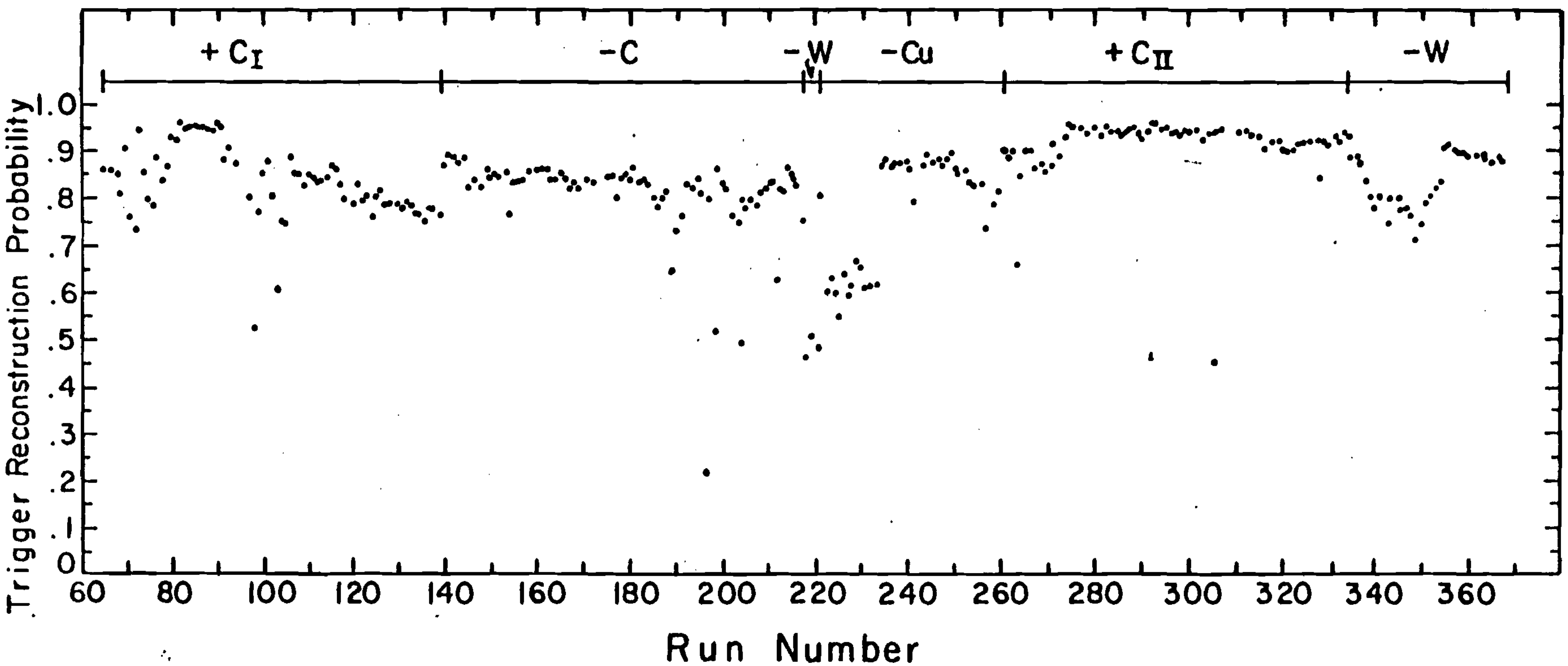

Figure 3-8. Percentage of triggers in which the reconstruction program found two or more muons.

Chapter IV Analysis

INTRODUCTION

This chapter describes the methods used to convert the data from events with given kinematics to normalized cross sections. The first section describes the conditions we required of events to keep them in the data sample. The second section describes our use of the beam tagging system to get normalizations. The Monte Carlo program is then described. Finally, the experiment's backgrounds are discussed.

CUTS

There were three classes of clearly bad triggers that were easily removed by simple cuts: (a) events that contained a beam or halo muon, (b) events that did not originate in the target, and (c) events that did not satisfy the trigger logic. Figures 4-1 and 4-2 show the mass and momentum spectra for part of the tungsten data before and after cuts were applied to remove the above backgrounds.

The first step was to get rid of muons that come into the lab either in the beam or in the halo around the beam. The momentum spectra shown in Figure 4-2 clearly show an excess of high momentum muons with the same sign as the beam (in this case, μ^-) over opposite sign muons. The beam/halo cuts were designed to eliminate the high-momentum like-sign muons without throwing away 'real' events, as indicated by the opposite sign (and presumably good) muons.

The halo muons were identified by their extrapolated position at the target. Muons that were too far from the target center (in the xy plane) were cut. Because of the multiple scattering in the hadron shield, the maximum allowed distance from the target center for a muon was momentum dependent. The final cut, as shown in Figure 4-3, was that the product of the momentum and the distance to the center of the target had to be less than 6 GeV/c-meters.

The beam muons were defined as high momentum muons which had only a small angle θ with respect to the beam direction. The cut used, as shown in Figure 4-4, was:

$$p_{\mu} - 6 \text{ GeV/mrad} * \theta < 100 \text{ GeV/c}. \quad (4\text{-}1)$$

The final momentum spectra (Figure 4-2), after all cuts, showed no charge asymmetry, indicating that beam and halo muons had been eliminated.

The events that did not come from the target were eliminated by cutting on the probability that a pair of tracks intersected (formed a vertex) in the target. The difficulty in determining if a pair of tracks pointed at the target was due to multiple scattering in the hadron shield.

The joint probability distribution[15] P for a multiple scattering of angle θ_x and displacement x is:

$$P(x,\theta_x) = \exp[4p^2 x_0(\theta_x^2/z - 3\theta_x x/z^2 + 3x^2/z^3)/.00441] \tag{4-2}$$

where:

z = The length of the scattering material (= 3m).

x_0 = The radiation length of the material (= 1.76cm).

p = Momentum of the particle.

Since the momentum loss in going through the shield was about 4.5 GeV/c for muons whose momenta ranged between 8 and 225 GeV/c, p was not always well defined. Instead of p^2, we used $p_i p_f$, where the subscripts mean before and after the shield. The scattering in y is independent of that in x and the same distribution applies. Since probability is proportional to $\exp(-\chi^2/2)$, the χ^2 (chi-square) for a set of displacements in x and y can easily be calculated. The total χ^2 is just the sum of the x and y χ^2.

If three or more muons were in one event, the χ^2 test assumed that the vertex was in the center of the target. If only two muons were in the event, the vertex (in x and y) was chosen to minimize the sum of the χ^2 for the two tracks. The requirements imposed (shown in Figure 4-5) were that no individual track have a χ^2 greater than 7.8 and that (in the case of a two muon event) that the total χ^2 be less than 7.8. The track pair χ^2 distribution shown in Figure 4-5 is for pairs that survived the single track cut (hence the knee at 7.8). The solution for the minimum χ^2 (assuming a z position at the target) also gave the best guess for the track parameters (slopes and intercepts) of the muons as they left the target. These new parameters were then used in calculating the event kinematics (mass, p_T, x_f, and $\cos\theta^*$).

The effectivness of the χ^2 method can be seen by examining in detail two mass regions in Figure 4-1. The region from 2.7 GeV/c^2 to 3.4 GeV/c^2 is mostly J/Ψ's produced in the target. The region 1.4 to 1.7 GeV/c^2 is mostly J/Ψ's produced in the shield. The factor of 2 shift in the mass comes from forcing the vertex to be at the target. If one allows the z position of the vertex in the vertex χ^2 minimization to shift also, Figure 4-6 shows the origin of these two classes of events clearly. Note that the low mass data set contains some real low mass events that came from the target. Figure 4-7 shows the χ^2 confidence level distribution for the two sets of events assuming they came from the target. Because the shield events had χ^2's about 10 times larger than the target events, the shield events were all at very low confidence levels and so were easily separated from the good events. The cut at $\chi^2 = 7.8$ corresponds to a confidence level cut of 2%. Also note that the flatness of the distribution for the target J/Ψ's indicates that our formula represents a legitimate χ^2. Thus the χ^2 test can tell if an event does not originate in the target.

Finally, a check was made that the scintillator counters actually pierced by the muon tracks satisfied the trigger requirements (the dimuon and mass logic). This cut was very effective in eliminating low mass events that triggered the experiment due to extra scintillator hits.

The last two, and most obvious, event requirements, that the muon pair originate in the target and satisfy the trigger logic, accounted for almost all of the trigger rejections. For the mass region of greatest interest in this report ($M > 4$ GeV/c^2), the target and logic requirements were responsible for 97% of the rejections. Of the remaining data above 4 GeV/c^2, only 15% was thrown out for containing a beam/halo muon.

We corrected for the rejection of good events by the above cuts by applying these same cuts in the Monte Carlo program that estimated the detection efficiency of the experiment.

Beam Particle Identification

The beam composition was tagged by the four beam Cerenkov counters C_2, C_3, C_4, and C_5 (see chapter II). Signals from these counters, when in coincidence with a beam timing signal from the beam defining scintillators, were counted with CAMAC scalers. Also scaled were various coincidences between the counters. The Cerenkov counter's thresholds were set just below proton threshold for all the negative beam runs and for the first positive beam runs. For the second set of positive runs, C_2 and C_4 were set just below kaon threshold. The resulting particle definitions were:

TABLE 4-I

Particle Definitions for the Carbon Runs

	C_2	C_3	C_4	C_5
First positive run				
Pi^+ and K^+	1	1	1	-
Proton	0	0	0	-
Second positive run				
Pi^+	1	1	1	1
K^+	0	1	0	1
Proton	0	0	0	0
Negative runs				
$\bar{p}$	Zero or one counters on			
Pi^-	$\equiv$ not $\bar{p}$			

For the metal target runs, the rates were too high for the counters to work effectively, so all particles were simply assumed to be negative pions.

The latched Cerenkov counter patterns from the carbon runs (both positive and negative beams) were used to calculate the efficiencies and accidental probabilities given below:

TABLE 4-II

Cerenkov Counter Performance

Counter	Eff	Acc
C_2	.987	.087
C_3	.986	.017
C_4	.977	.004
C_5	.952	.010

From this, plus the measured ratios of particle types in the beam (see Table 2-I, Chapter II), the contamination of any given particle tag from other types of particles can be calculated. The kaon sample contained about 1% of both pions and protons. The positive pion sample contained about a 1% kaon contamination because during the first positive run kaons were not separated out. The other possible contaminations for the positive beam were insignificant.

For the negative data, if an all counters off definition for $\overline{p}$ is used, the expected contamination from pions is .1%. If events with one and only one counter on are included in the sample the contamination increases to 2%. This second definition is the one we actually used.

All of these contamination levels are smaller than our error in the overall normalization and so will be ignored.

Normalization

The normalization factor (NF = picobarns/[event-nucleus]) is given by the formula:

$$NF = A/\{N_A * d * t * B_0 * [1 - e^{-t/L}] * (L/t)\} \qquad (4-3)$$

A = Target atomic mass number

N_A = Avogadro's number

d = Target density

t = Target length

L = Absorption length for given beam and target[33]

B_0 = Integrated beam flux

For the various targets:

TABLE 4-III

Target Properties

	t (cm)	d (gm/cm^3)	L (cm)				
			p	pi$^+$	K$^+$	$\bar{p}$	pi$^-$
C	31.16	2.20	36.6	50.1	58.1	34.2	48.5
Cu	15.24	8.96	14.8	18.2	21.2	13.7	18.4
W	10.60	17.08	10.1	12.8	15.4	10.9	12.2

Expressing NF as = D/B_o, then:

TABLE 4-IV

Target Normalization Factor D

(picobarns/(event-nucleus)) * 10^{11}

	p	pi^+	K^+	$\bar{p}$	pi^-
C	4.32	3.91	3.76	4.44	3.94
Cu	-	-	-	12.8	11.4
W	-	-	-	26.4	25.2

The integrated flux (B_o) used was the measured flux (B_m) times a correction factor k that took in to account various known problems with the apparatus. The problems included:

TABLE 4-V

Normalization Correction Factors

(A) The computer's occasional failure to reset the CAMAC scalers after each event,

(B) Failure to count correctly the number of particles in the beam when two or more particles were in one beam bucket (This applied to the metal targets only. The carbon runs vetoed such buckets.),

(C) Short term problem in the P hodoscope trigger logic which effectively turned off two of the 72 counters in the bank,

(D) Reconstruction efficiency.

The magnitude of the corrections used were:

ITEM	TARGET			
	C^+	C^-	Cu	W
(A)	.977	.996	.982	.955
(B)	1.00	1.00	1.20	1.23
(C)	.957	1.00	.920	1.00
(D)	.94	.94	.90	.92
k	.897	.936	.988	1.08

Note: Item (C), in parts of the analysis, was included in the Monte Carlo efficiencies instead of as a normalization correction. Then B_0 (in 10^{11} particles) and NF (in pb/(event-nucleus)) are given as:

TABLE 4-VI

Event Normalization Factors

	C					Cu	W
	p	pi^+	K^+	pi^-	$\bar{p}$	pi^-	pi^-
B_m	3.22	1.45	.0433	3.28	.016	3.07	4.17
B_0	2.89	1.30	.0388	3.07	.015	3.04	4.50
NF	1.50	3.01	96.8	1.28	290.	3.75	5.60
Error	.15	.30	11.0	.13	200.	.60	.90

Because of problems with the beam scalers on the negative runs, the measured B_m for $\bar{p}$ was unreliable. Instead, we used the results of Aubert *et al.*, and set

$B_m(\bar{p}) = .5 \pm .35\%$ of $B_m(\pi^-)$.

The errors in the normalization were set at one-half of the quadrature sum of the difference from one of the correction factors in Table 4-V plus a 10% error for the Monte Carlo and other effects.

<u>The Monte Carlo Program</u>

The acceptance of the experiment was investigated using a Monte Carlo program. The program functioned by generating a set of events with some kinematic parameters fixed (such as mass, x_f, p_T) and others randomly selected (such as the rotation of the plane of the event about the beam axis). The path of the muons in each generated event was traced through the program's model of the apparatus. The number of tries that successfully simulated a good event divided by the total number of tries was then taken as the probability that such an event would be detected by the apparatus. For each set of fixed parameters, 1000 tries were made or enough so that the proportional error on the final probability was less than 10%, which ever was larger.

The model of the apparatus used included the effects of multiple scattering and energy loss (with fluctuations) in the various materials in the experiment (iron, air, scintillators, <u>etc.</u>). Also included was a detailed description of the trigger logic. These two sets of effects, multiple scattering and the trigger logic, were very important in determining if an event would succeed. As a test of the importance of the multiple scattering, a set of events was generated with all of the same parameters as the actual events with masses > 4 GeV/c^2. These events had only a 75% average probabilitiy of success. (We ran one hundred tries for each event.) Since the acceptance for any event inside our kinematic range was generally between 10% to 40%, this test shows that the chance scattering of the muons in an event had comparable effects on the acceptance as did the actual kinematics of the event.

As a program check, two separate Monte Carlo programs were independently written and their results agreed.

A second check, for internal consistency, was made on the effect of the mass logic cut. The mass logic cut was set at one of two values for most of the experiment, either 13 (about .75 GeV/c^2) or 25 (about 2.8GeV/c^2). (See Appendix A.) The carbon target runs were done at 13, the metal targets runs at 25. The differences in the efficiency for the two cut values were well understood for masses above 3 GeV/c^2 and no problems were encountered. Figure 4-8 shows this by comparing the cross section at the J/Ψ as a function of x_f for the carbon data in which the same set of data was cut first with the logic set at 13 then at 25. The ratio of the cross sections as a function of x_f is clearly consistent with 1.0 and independent of x_f. The total cross sections agree to within 1%. (There is a 20% differnece in the actual number of events.)

In the mass range below the J/Ψ, the situation deteriorated badly. Figure 4-9 shows the cross section ratios as a function of mass and x_f in the region 2. < M < 2.7 GeV/c^2. In this region the proportional change in the efficiency (for a cut at 25) can be 15% to 20% or more in a mass interval of only 150 MeV/c^2. Modeling this change adequately with the Monte Carlo would have required breaking this interval into many small mass regions and calculating separate efficiencies for each. Rather than using this expensive and cumbersome solution, we empirically derived a correction formula that changed the Monte Carlo efficiency so that the cross section remained the same in going from a cut of 13 to 25. The correction factor was a function of both mass and x_f. The cross section ratios with the corrected efficiencies are shown in Figure 4-9. Below 2.0 GeV/c^2, no attempt was made to calculate cross sections for the metal targets. It should be repeated that these corrections were only used on the data below the J/Ψ. They were not needed above this mass.

Monte Carlo events were generated according to several different schemes. In the first case, events were generated at grid points in mass, x_f, and p_T space and in mass, x_f, and $\cos\theta^*$ space. The distributions used for the random variables were either obvious (such as a flat distribution for the azimuthal angle about the beam) or arrived at by a bootstrap method combined with intelligent first guesses. Figures 4-10 (mass vs x_f), 4-11 (x_f vs p_T), and 4-12 (x_f vs $\cos\theta^*$) show various slices through these grid spaces. As can be seen, except for $\cos\theta^*$, the dependence of the efficiency is slowly varying over the kinematic region of interest.

In the second scheme, the test events were generated at the same point in mass, x_f, p_T, and $\cos\theta^*$ as the 2000 actual high mass events. This second set of Monte Carlo points was used in the pion structure function analysis reported in Chapter VI.

Resolution

The measured mass resolution at the J/ψ is given below.

TABLE 4-VII, Mass Resolution

Beam/Target	FWHM (MeV/c^2)	Mass shift (MeV/c^2)
p/C	320	15
pion/C	330	12
pion/Cu	310	23
pion/W	350	27

The above numbers were found by fitting a Monte Carlo given shape to actual data. The Monte Carlo indicated that the mass resoution was proportional to the mass. The resolution measured in the carbon data was only slightly improved (about 6%) by the use of the target counter information (see Chapter II). Given the loose dependence that the χ^2 method had on the exact target position (on the scale of a 4" target block), as shown in Figure 4-6, only a small improvement was expected.

The Monte Carlo was also used to calculate the resolution in x_f and p_T. The resolution is only slightly mass dependent.

Table 4-VIII, x_f and p_T Resolution

	Sigma	Shift
x_f	.02	.002
p_T(>1GeV/c)	280 MeV/c	-30 MeV/c
p_T(≅0)	-	130 MeV/c

The shifts were large at small p_T because there was only one direction for shifts to occur.

Backgrounds

There were two main sources of background signal to be considered: (a) secondary production (ie, dimuons produced from the interaction of hadrons that were themselves produced in the target) and (b) muons from uncorrelated sources (such as pions decaying in the drift space between the target and hadron shield). The lack of an effect from secondary production can be seen in the production of J/Ψ's in the carbon target. Figure 4-13 shows the ratio of $d\sigma/dx_f$ for J/Ψ's from the first and third target segments. If there were secondary production, the extra events would show as an excess at low x_f in the third target segment. No such effect is seen, the χ^2 for a constant value being 9 for 9 degrees of freedom. The lack of an effect is not surprising because the J/Ψ production cross section rapidly decreases for secondary particles with momentum less than 100 GeV/c.

See Figure 4-14.

Sources of uncorrelated muons would be expected to produce like-sign muon pairs almost as easily as opposite-sign pairs.[17] As Figure 4-15 shows, the like-sign spectrum above 4 GeV/c^2 in mass is about 1% of the opposite-sign spectrum. In this region sources of uncorrelated muons can be ignored. Below the J/ψ mass, however, the like-sign background was important. We corrected the data for this by simply subtracting out of the data an amount equal to the like-sign component.

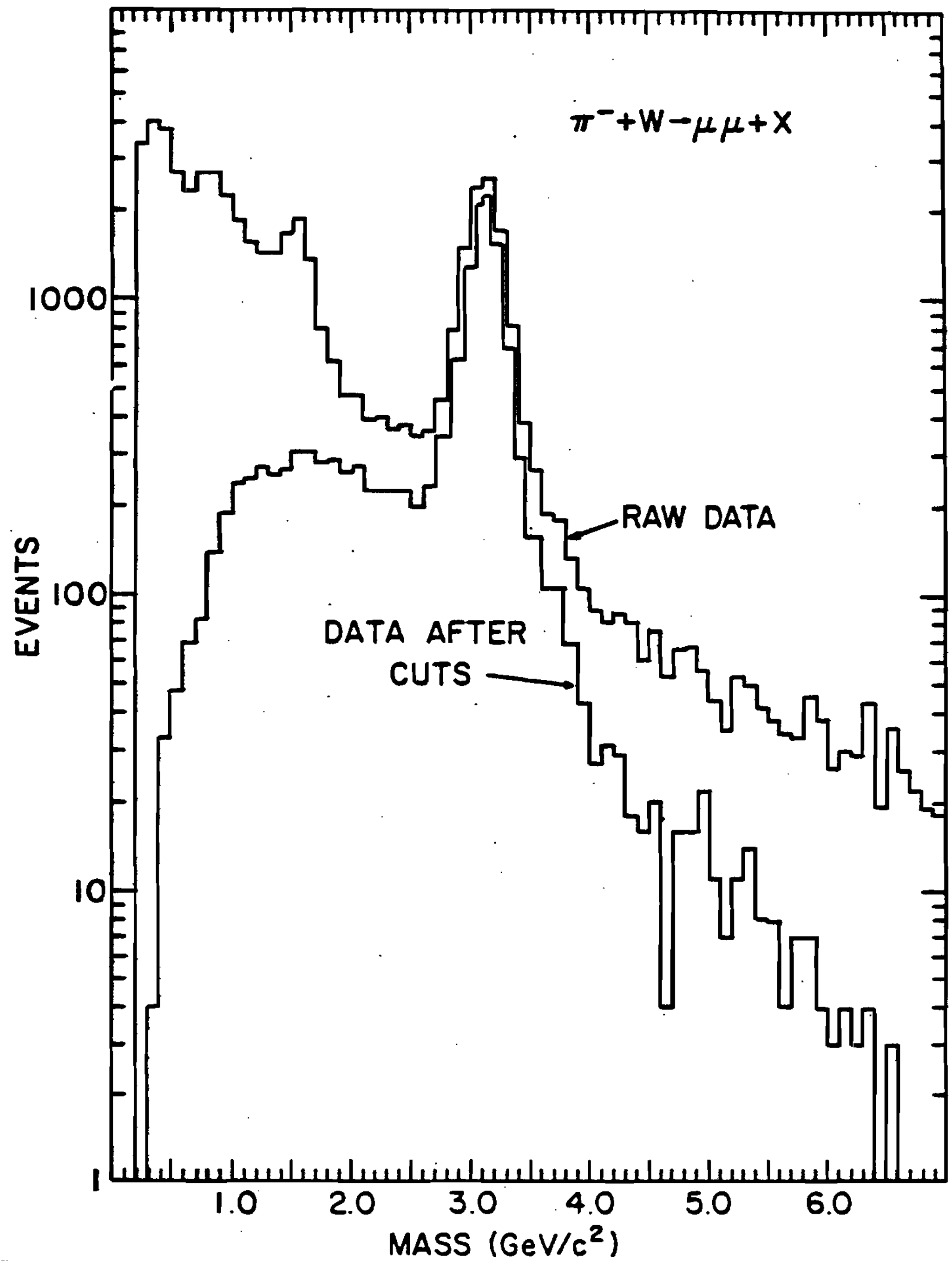

Figure 4-1. Event spectrum for the tungsten data before and after the bad triggers were removed.

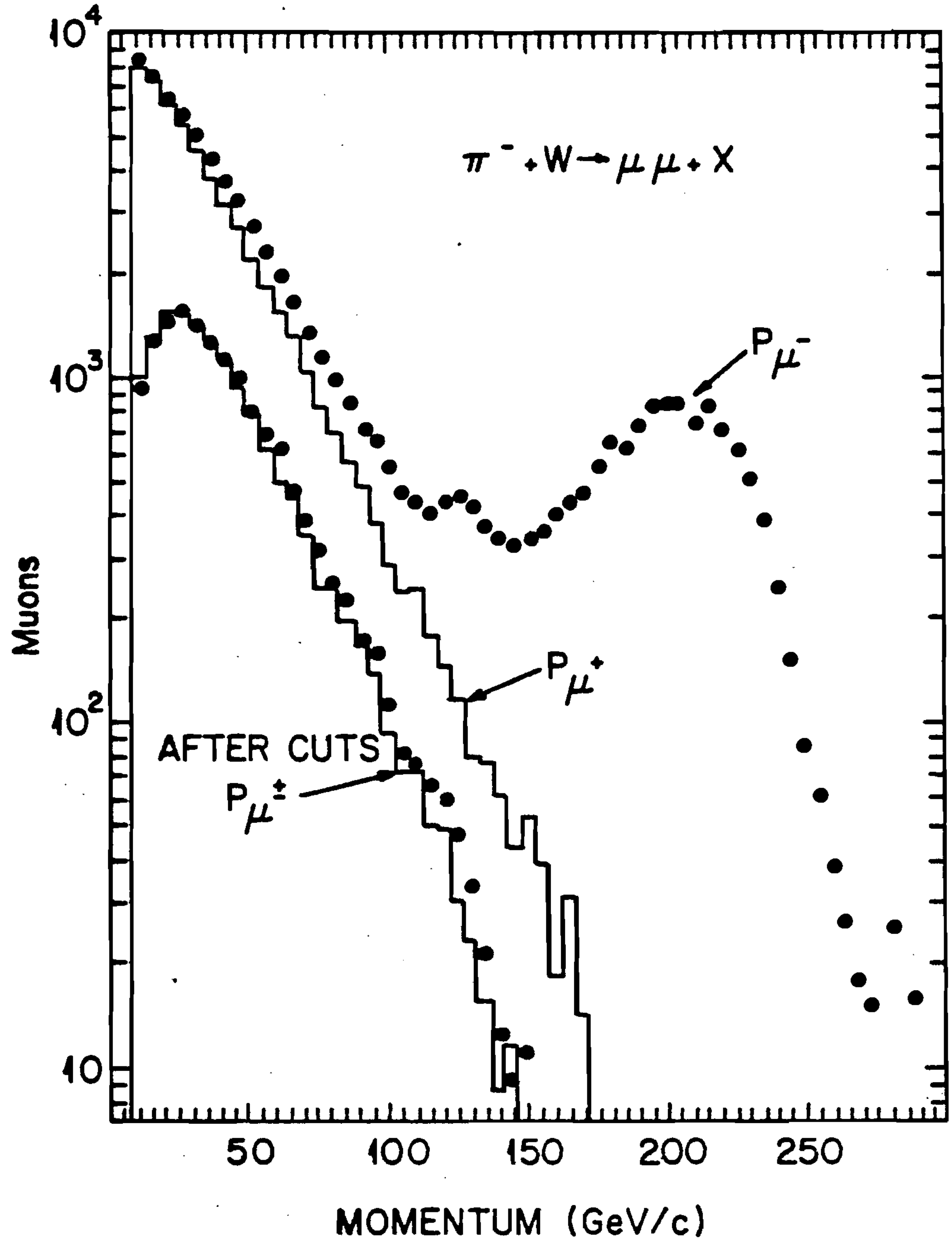

Figure 4-2. Momentum spectrum before and after bad triggers were removed. After the cuts, the two spectra (for ± muons) were essentially the same.

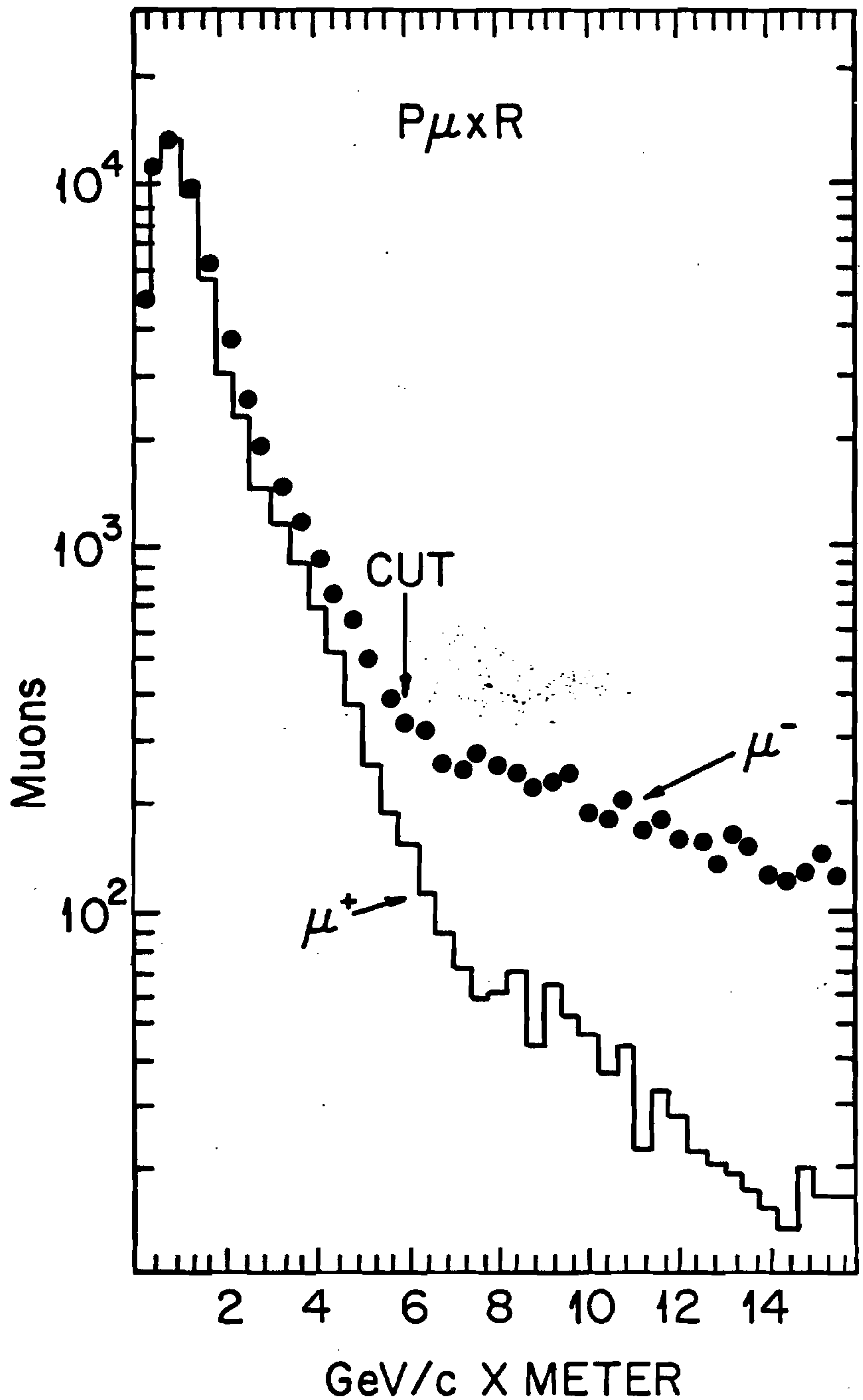

Figure 4-3. Halo muon cut.

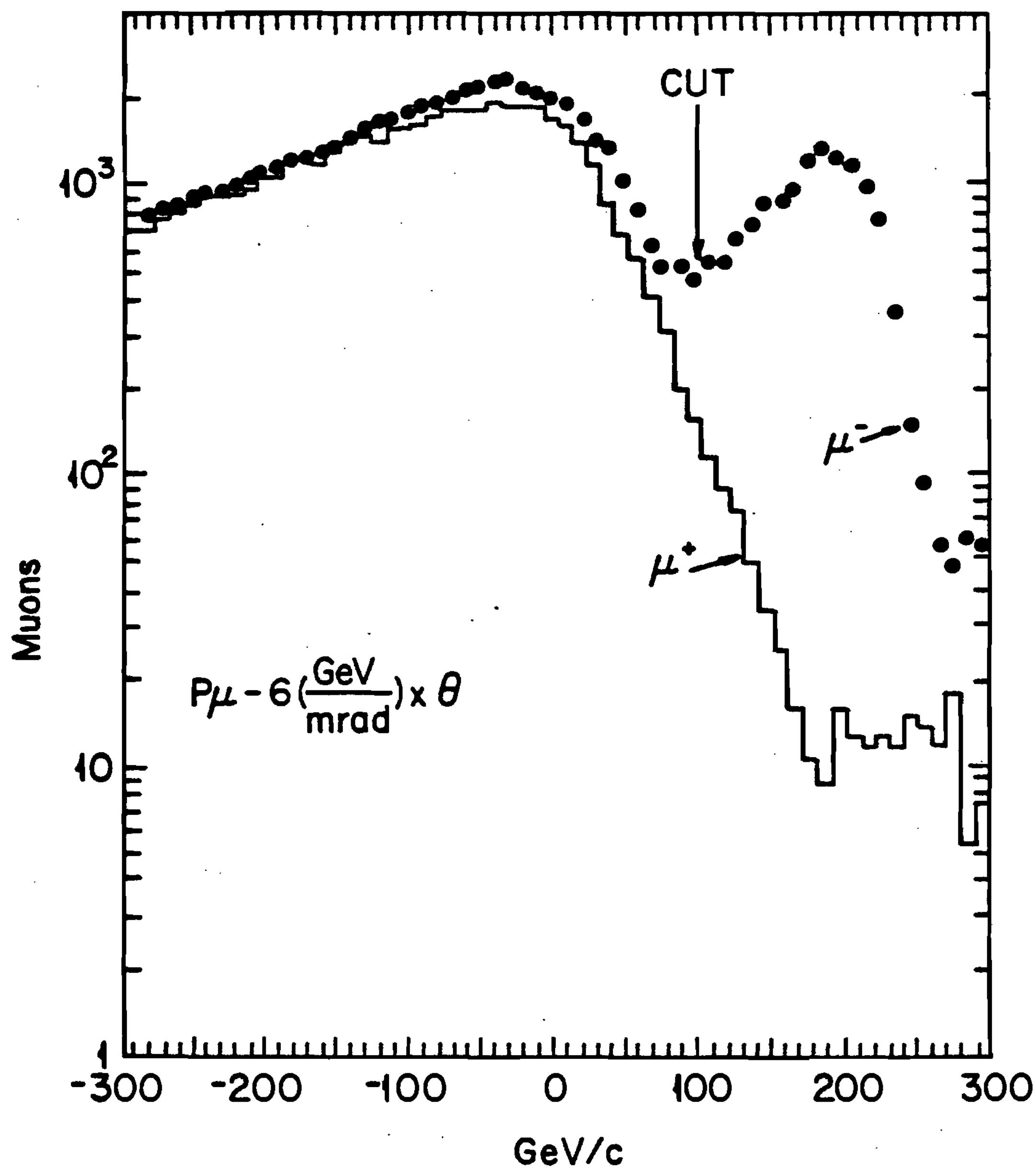

Figure 4-4. Beam muon cut.

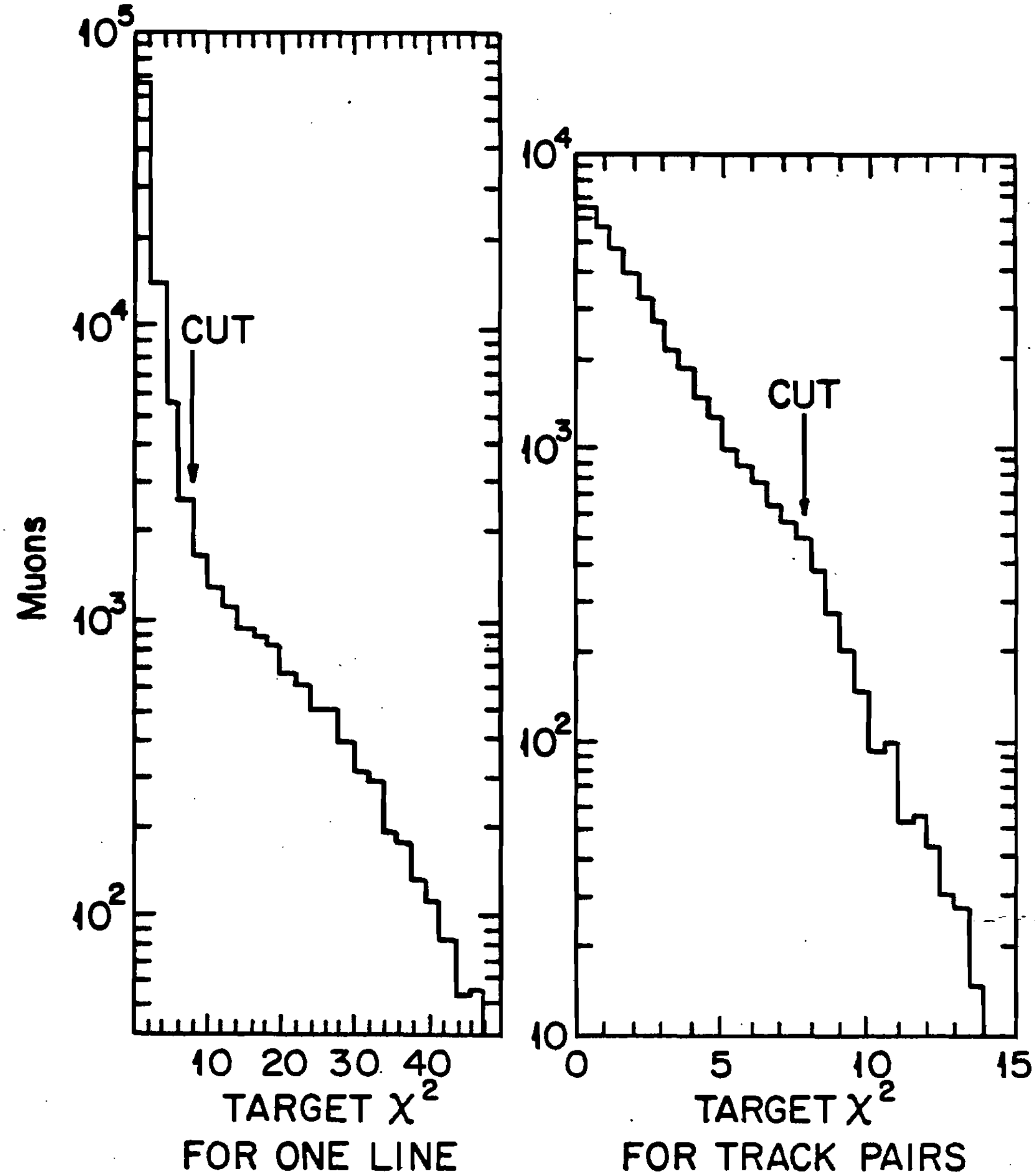

Figure 4-5. χ^2 that single tracks and track pairs came from the target.

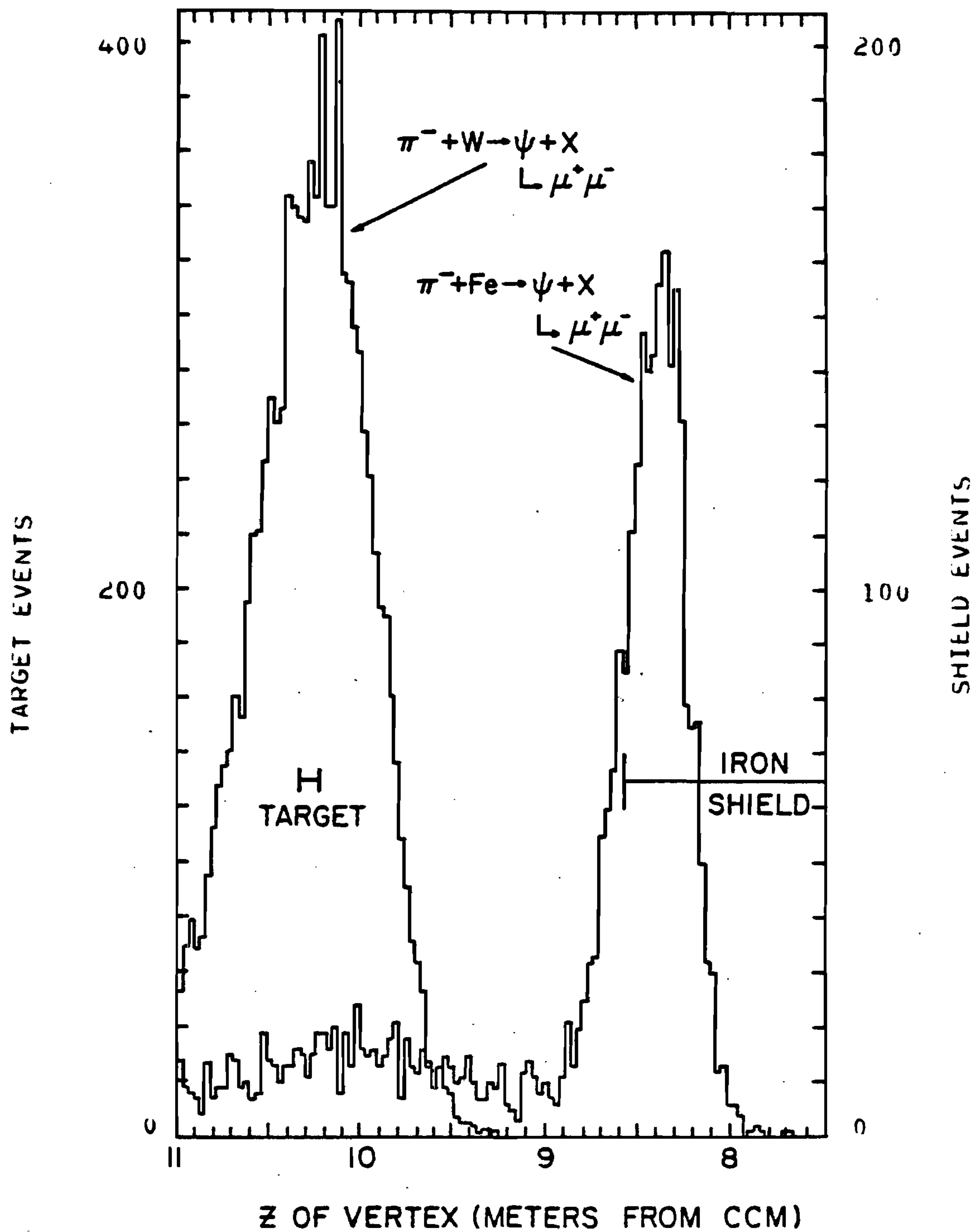

Figure 4-6. Fitted z position for J/Ψ's produced in the target and shield.

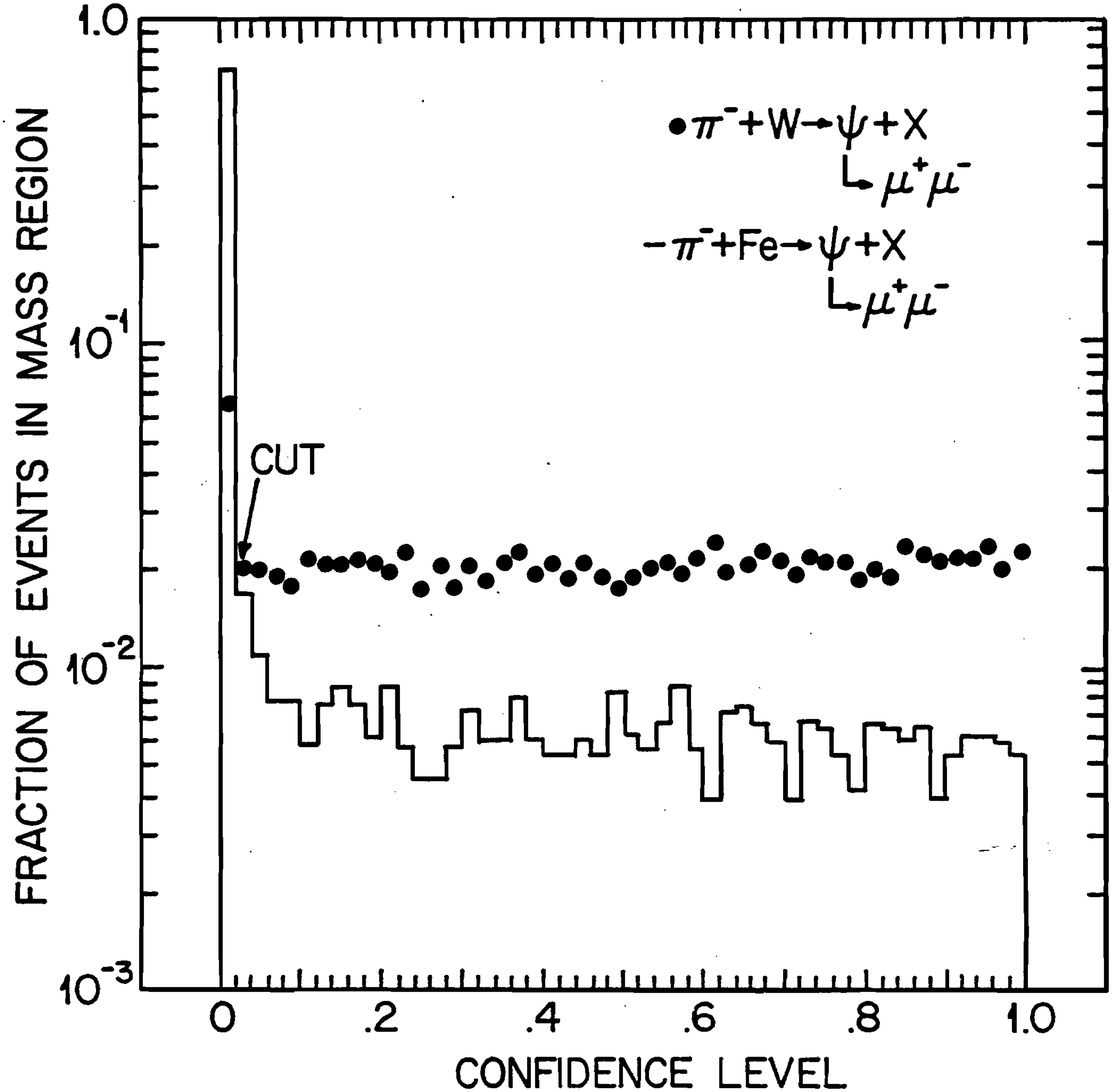

Figure 4-7. Histogram of the X^2 confidence level that events were generated in the target for events that came from the target and from the shield.

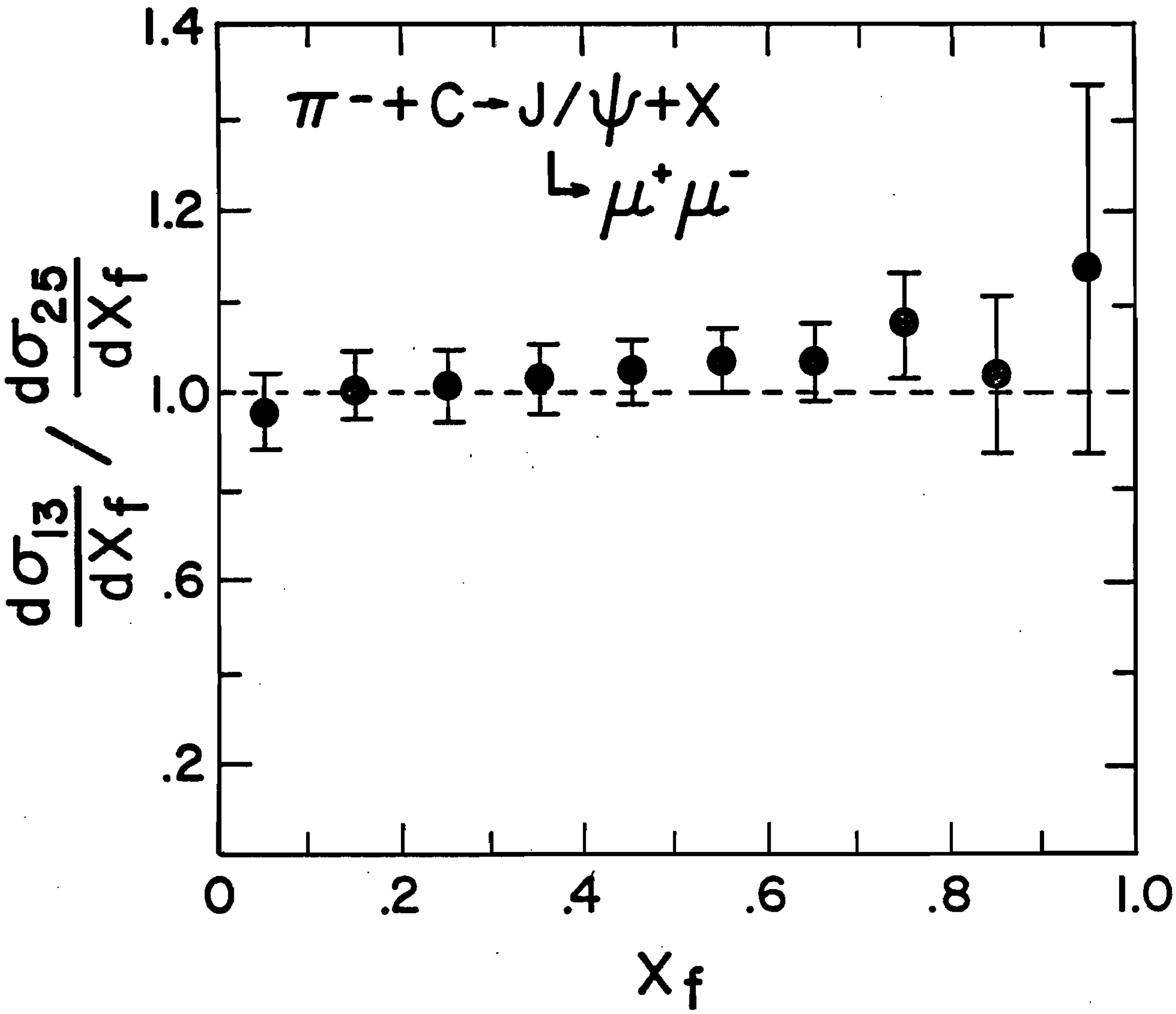

Figure 4-8. Ratio of the cross sections for J/Ψ events as a function of x_f for mass logic cuts of 13 and 25.

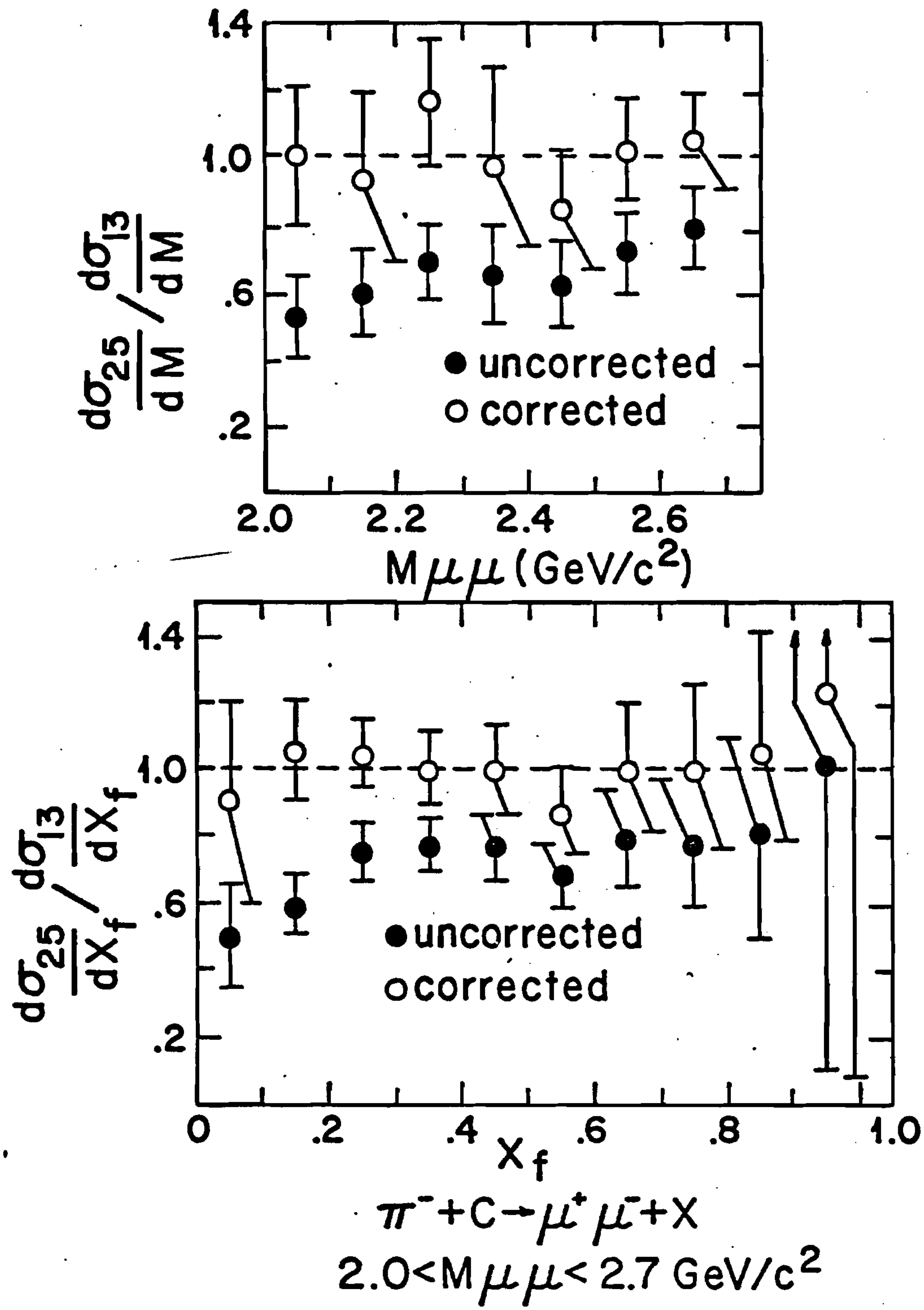

Figure 4-9. Ratio of the cross sections for events with 2 < M < 2.7 GeV/c^2 at cuts of 13 and 25 before and after the correction to the Monte Carlo is applied.

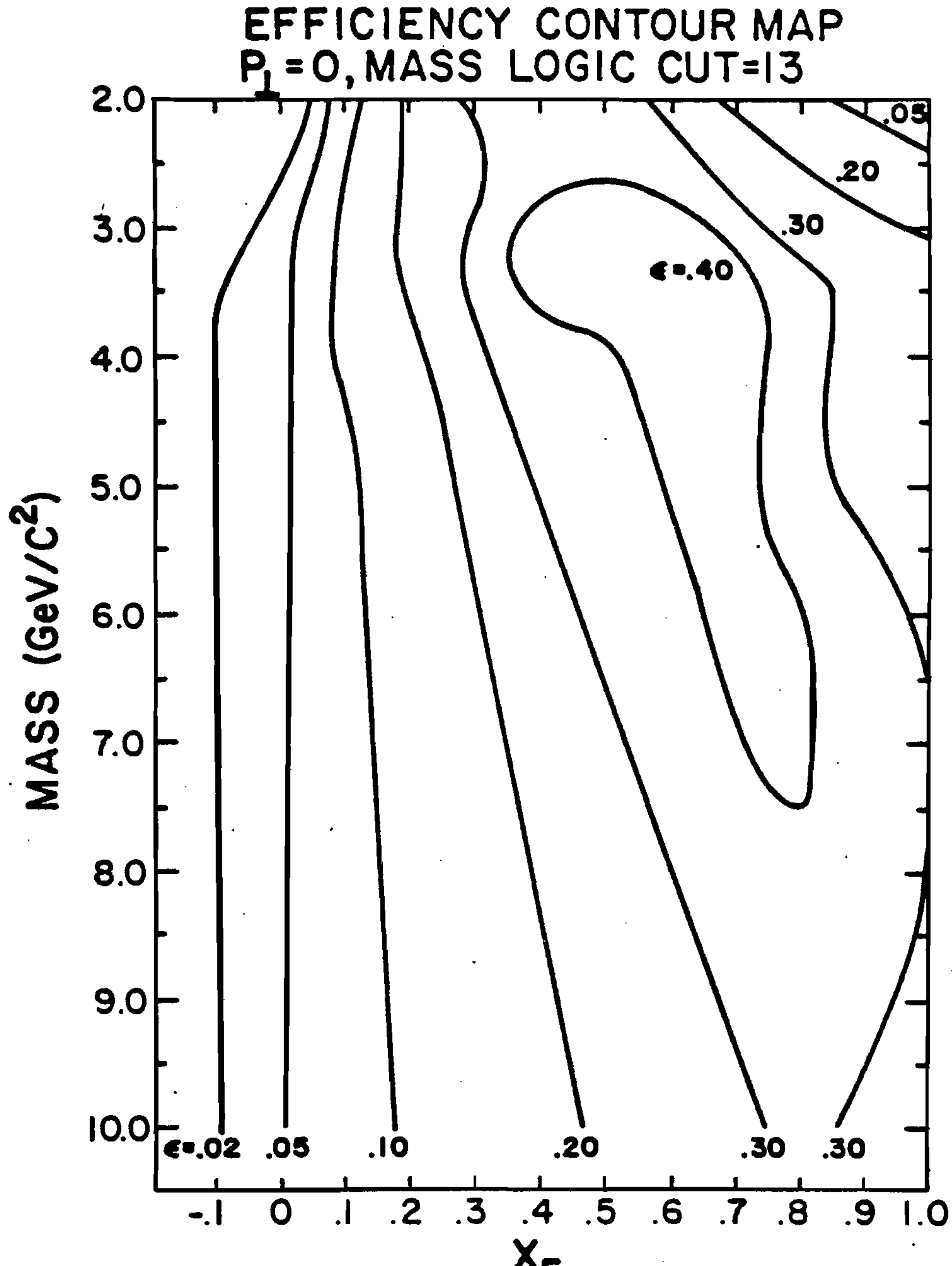

Figure 4-10. Contour plot of the acceptance as a function of mass and x_f.

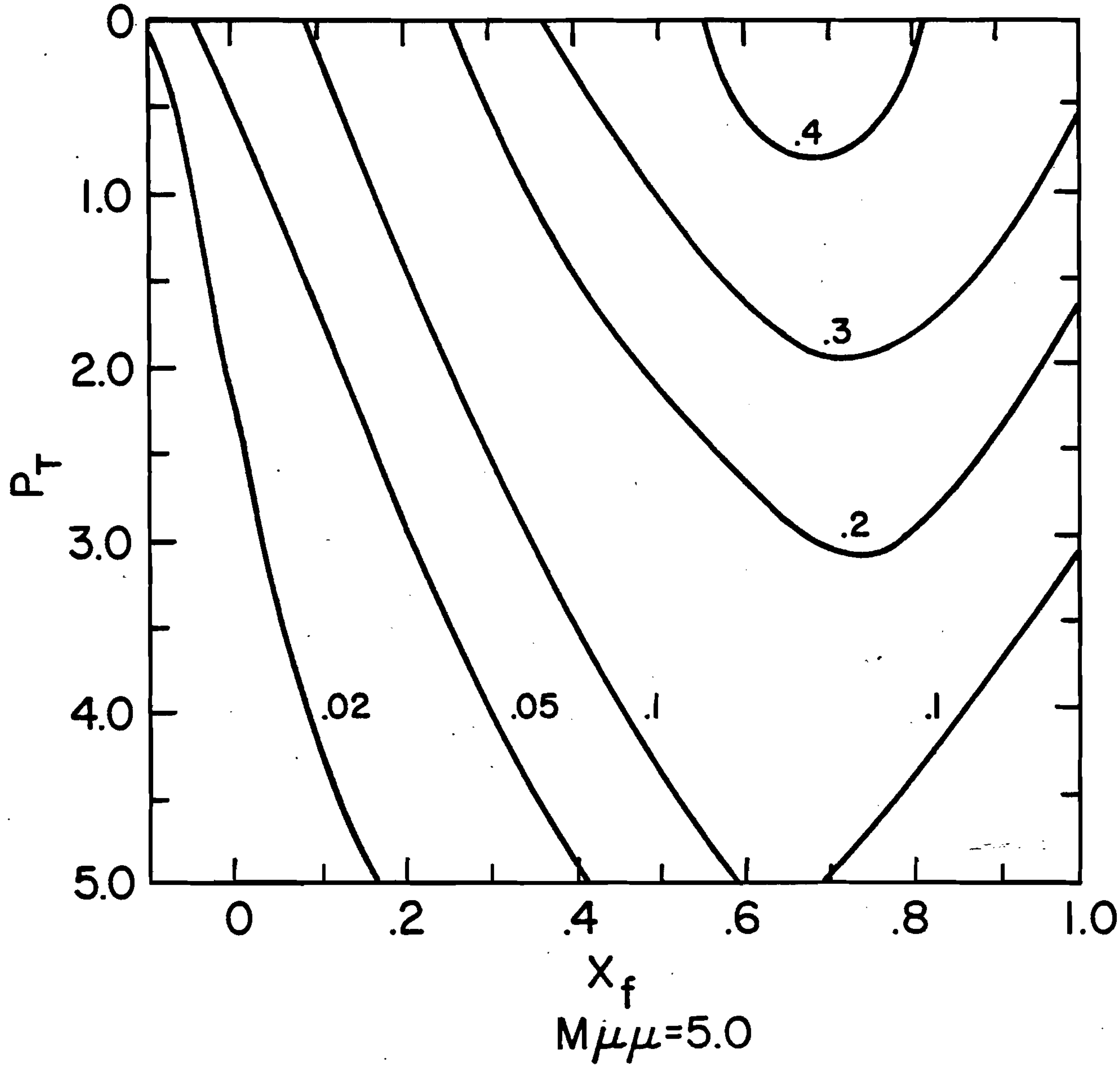

Figure 4-11. Contour plot of the acceptance as a function of x_f and p_T.

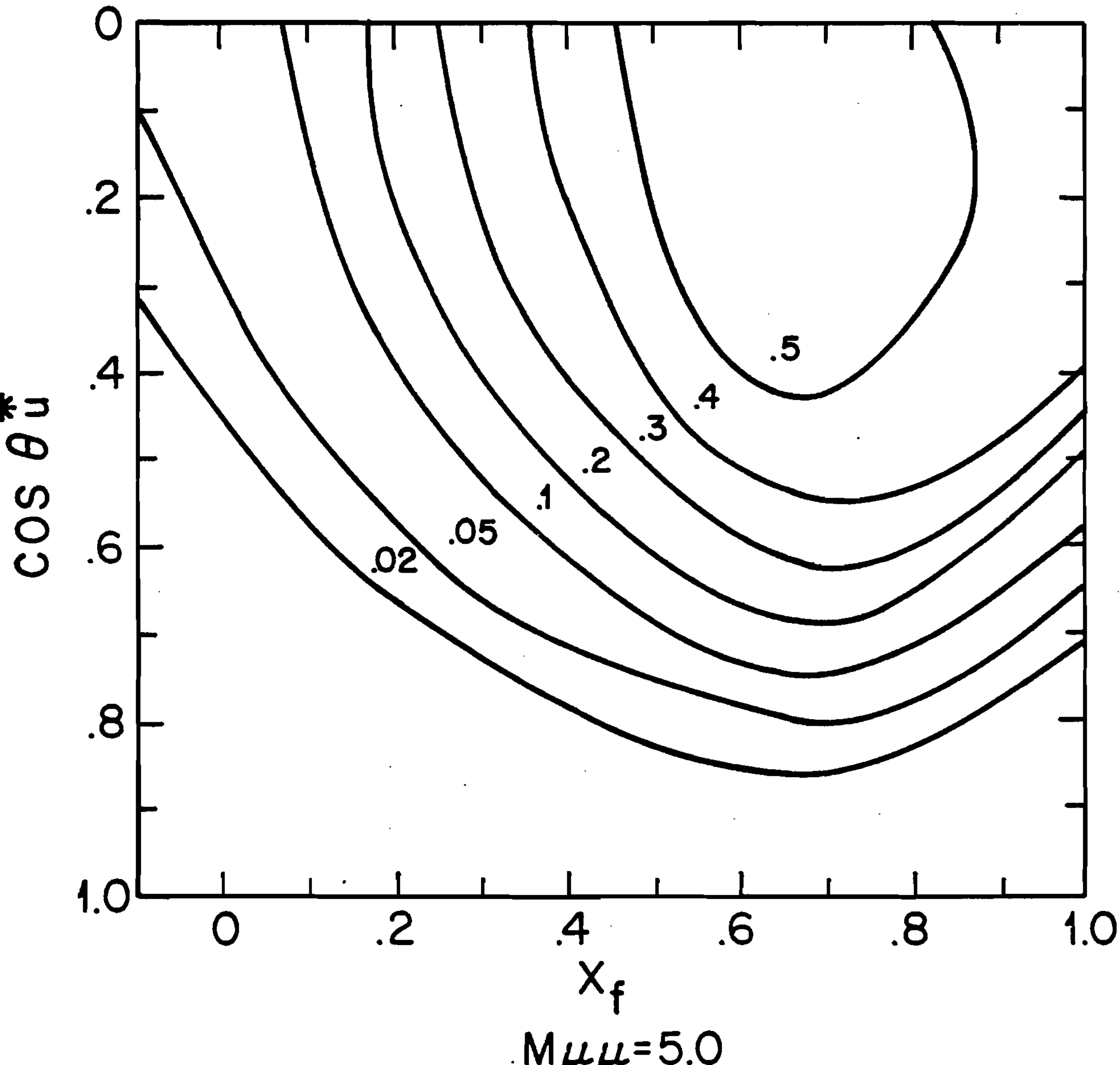

Figure 4-12. Contour plot of the acceptance as a function of x_f and $\cos\theta^*$.

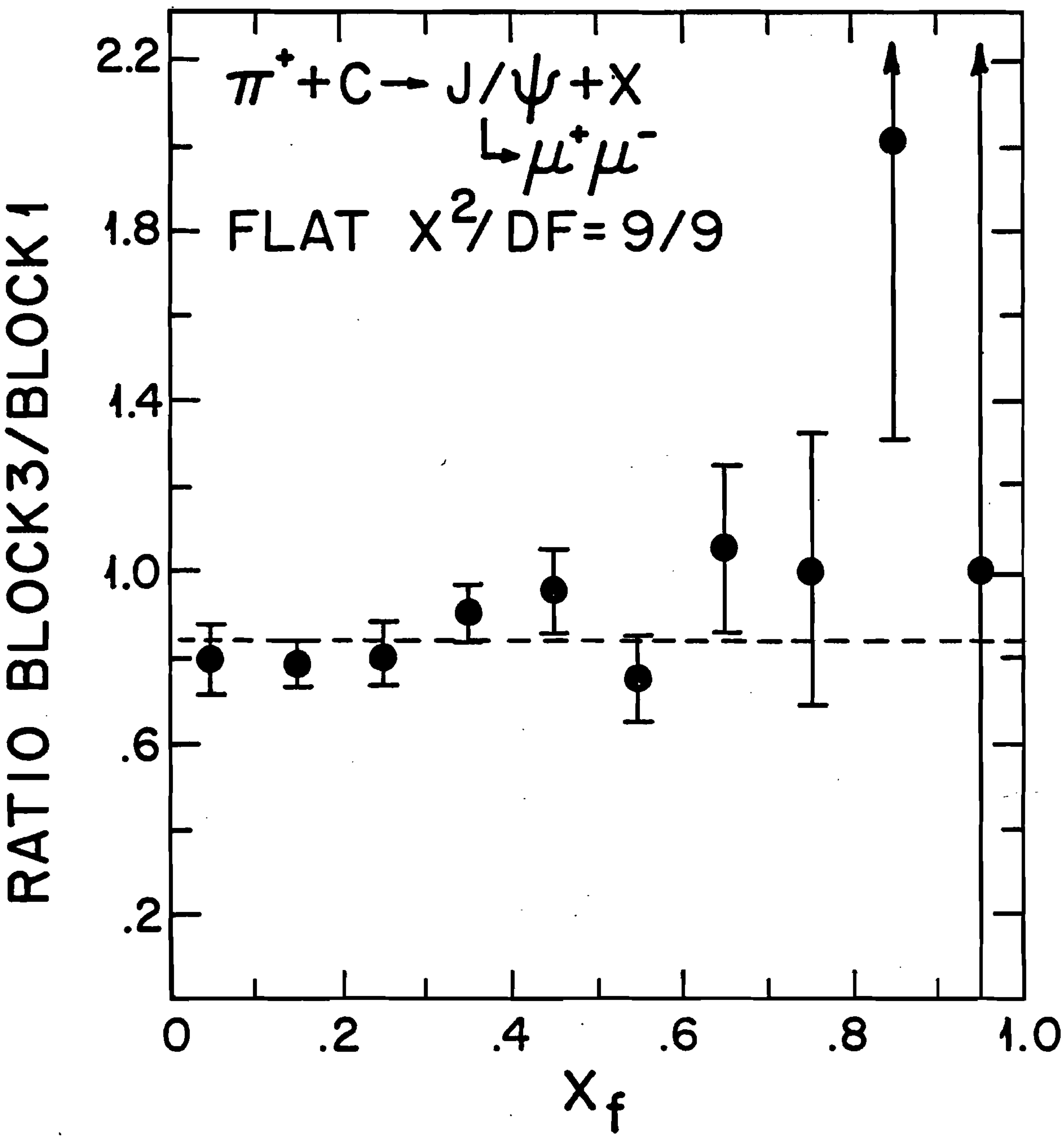

Figure 4-13. Ratio of the cross sections for J/Ψ events produced in carbon target blocks 1 and 3.

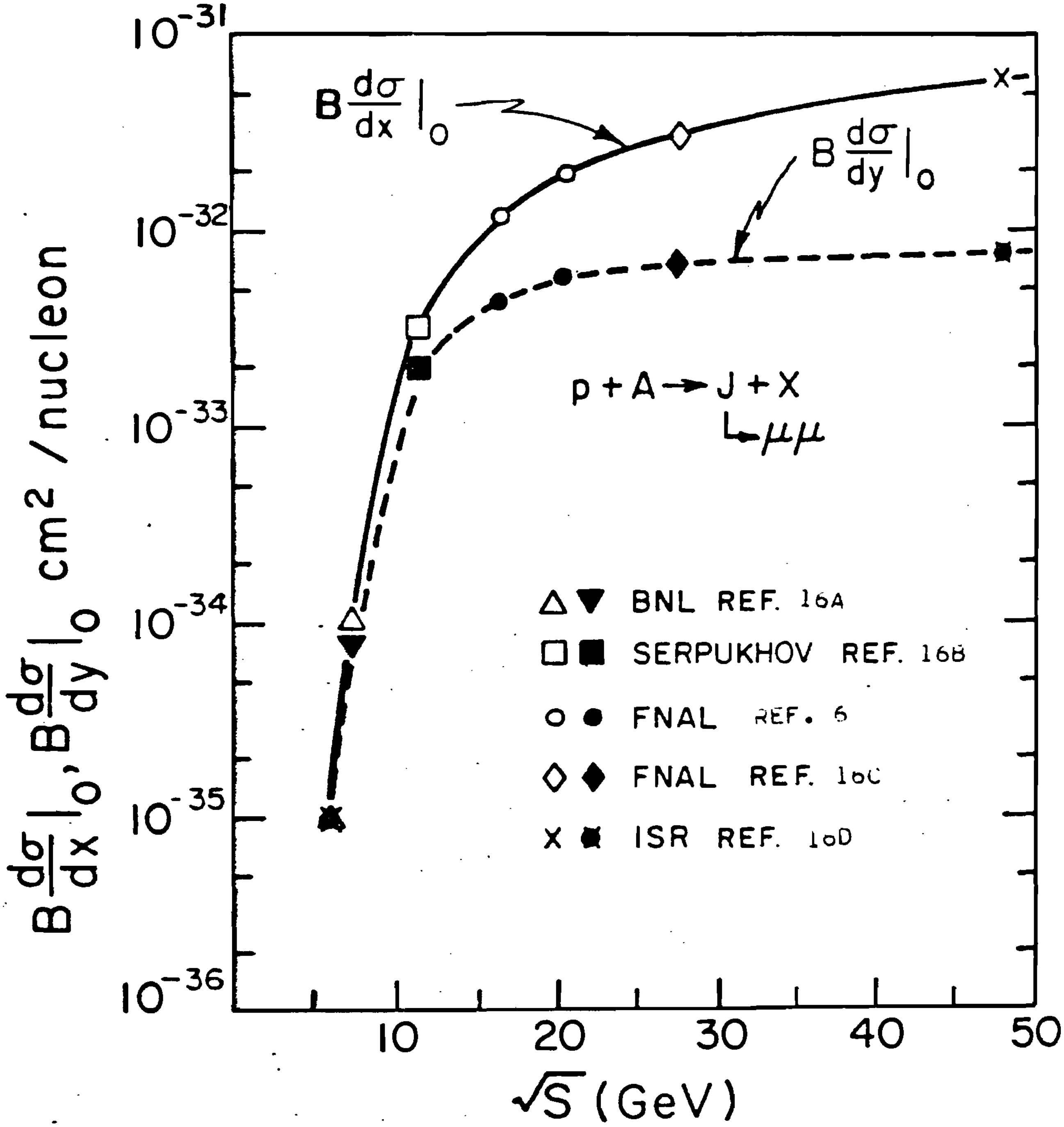

Figure 4-14. Dependence of J/Ψ production on center of mass energy.

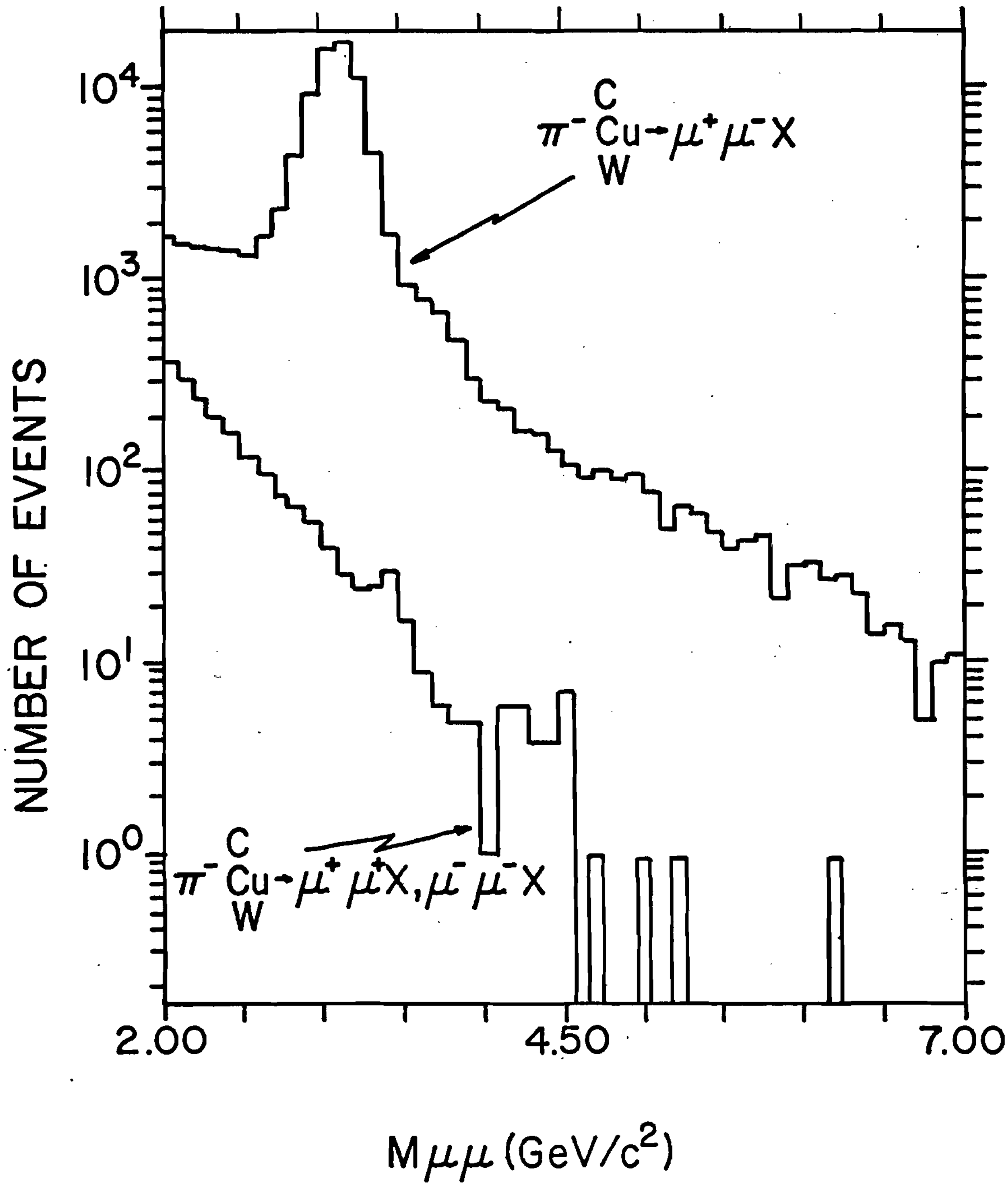

Figure 4-15. Like-sign background compared to opposite-sign production.

Chapter V Distributions

INTRODUCTION

This chapter presents the data in the form of differential cross sections and gives the results of selected fits to the data. In particular, fits are given to projections which involve only one kinematic parameter. The next chapter (VI) continues the discussion of the data in the framework of the Drell-Yan model.

For the x_f and p_T distributions, the data have been divided into several mass regions. The regions, and the symbols used for each in the graphs that follow, are:

Table 5-I, Mass Regions

1.5 To 2.0, open triangles
2.0 To 2.7, solid squares
2.7 To 3.5 (J/Ψ), open circles
3.5 To 4.0 (Ψ'), solid triangles
4.0 To 5.0, open squares
5.0 To 6.5, solid circles
6.5 To 8.0, open diamonds
8.0 To 11.0, solid diamonds

In the tables given in this chapter, the error on a number is given directly below that number in the table.

Distributions

Figures 5-1 through 5-7 show the mass spectra (in $cm^2/(GeV/c^2)$/nucleus) for the different targets and particle types and for $x_f > 0$. In the pion spectra displayed, the bin sizes change from 100 MeV/c^2 wide for $M < 5$ GeV/c^2 to 200 MeV/c^2 for $5 < M < 6.8$ GeV/c^2 to 300 MeV/c^2 for $M > 6.8$ GeV/c^2. Figures 5-8 through 5-13 give the p_T spectra for various masses, targets, and beams. The graphs show $d\sigma/(p_T dp_T)$. The actual p_T distributions (ie, without the $1/p_T$ weight) go to zero as p_T goes to zero as shown in Figure 5-14. Figures 5-15 through 5-26 show the x_f spectra.* Two sets of x_f graphs are shown, one for $d\sigma/dx_f$ and the other for $E^{cm} d\sigma/dx_f$. Though the fits to $E^{cm} d\sigma/dx_f$ generally have a lower X^2, the $d\sigma/dx_f$ cross sections are shown so that the x distributions can be used without having to unfold the p_T dependence (through the definition of E^{cm}).

The tables in Appendix B (page 224) give $[E^{cm}/(2\pi p^{cm}_{max})] d^2\sigma/(dx_f p_T dp_T)$ for the J/Ψ and Ψ' for p, pi^+, and pi^- beams. Also included is a list of high mass

---

* The x used here is defined as the momentum of the pair parallel to the beam in the beam-target center of mass divided by the maximum allowed momentum. The maximum momentum takes into account the need to divert some of the center of mass energy into a final state baryon and the rest mass of the pair. This definition allows x to reach 1 for any mass. The next chapter on the Drell-Yan model, however, uses the mass independent definition of x in which the maximum momentum is simply half of the center of mass energy. The center of mass definition assumed that the target was a single nucleon of mass .938 GeV/c^2.

events (> 4 GeV/c^2) by target, for the π^- beam, giving mass, x_f, p_T and weighted cross section (pb/nucleus) for each event.

Table 5-II gives the measured $<p_T>$ and Table 5-III gives $<p_T^2>$. The spectra were fit to two forms. First, for p_T > 1 GeV/c, the fit (Table 5-IV) was to $A*\exp(-B*p_T)$, and second, for all p_T, the fit (Table 5-V) was to $A*\exp[-B(p_T^2 + C^2)^{1/2}]$. The second form was used in order to model the flattening of the spectra at low p_T while retaining the exponential fall off at high p_T. The results of the second class of fits are shown on the graphs.

Tables 5-VI and 5-VII give the fits of the x_f distributions to the form $A(1-x_f)^B$. For all fits at low mass (< 2.7 GeV/c^2), the x_f fits were only done for x_f > .2 because the large subtraction of like-sign background that was needed to extract the yield below x_f = .2 made the data less statistically precise. The restriction of the fits to high x_f was also applied at all masses to the pion data because the actual cross sections seemed to be flatter at low x_f then the power law fit would imply, especially at the J/Ψ.

Table 5-VIII gives the total measured cross section for x_f > 0 for various masses. Separate cross sections are

reported for resonance and continuum production at the J/Ψ and Ψ'. As shown in Figure 5-27, the region around the resonances was fit with a power law background to represent the continuum and a Monte Carlo suggested line shape for the J/Ψ and Ψ'. The integrated results of the fits are given in the table. Because the fits were not exact and because the tails of the resonances extended beyond the mass limits, the sum of resonance and continuum did not always equal the total cross section for the mass region.

Table 5-II

$\langle p_T \rangle$

Beam/ Target	Mass Region 1.5 2.0	2.0 2.7	2.7 3.5	3.5 4.0	4.0 5.0	5.0 6.5	6.5 8.0	8.0 11.0
π^+/C	0.77	0.83	1.08	1.09	1.12	1.37	----	----
	.10	.10	.10	.11	.13	.16		
π^-/C	0.76	0.90	1.08	1.07	1.11	0.92	1.15	----
	.10	.10	.10	.10	.11	.12	.17	
π^-/Cu	----	0.90	1.12	1.15	1.12	1.18	1.13	1.29
		.10	.10	.10	.11	.11	.15	.19
π^+/W	----	0.92	1.15	1.21	1.17	1.24	1.13	1.18
		.10	.10	.10	.10	.11	.12	.12
Proton	0.71	0.83	1.05	1.05	0.84	----	----	----
	.10	.10	.10	.11	.12			
K^+/C	----	----	1.12	----	----	----	----	----
			.11					
$\bar{p}$/C	----	----	1.07	----	----	----	----	----
			.13					

Table 5-III

$\langle p_T^2 \rangle$

Beam/ Target	Mass Region 1.5–2.0	2.0–2.7	2.7–3.5	3.5–4.0	4.0–5.0	5.0–6.5	6.5–8.0	8.0–11.0
pi^+/C	0.87	0.95	1.54	1.67	1.59	2.07	----	----
	.10	.11	.10	.22	.25	.33		
pi^-/C	0.82	1.09	1.55	1.52	1.51	1.10	1.58	----
	.10	.10	.10	.12	.14	.13	.35	
pi^-/Cu	----	1.05	1.65	1.81	1.70	1.86	1.59	2.07
		.10	.10	.13	.15	.20	.31	.55
pi^-/W	----	1.11	1.75	1.98	1.88	2.06	1.71	1.61
		.10	.10	.12	.13	.16	.22	.19
Proton	0.71	0.88	1.43	1.53	0.88	----	----	----
	.10	.10	.10	.23	.30			
K^+/C	----	----	1.56	----	----	----	----	----
			.16					
$\bar{p}/C$	----	----	1.47	----	----	----	----	----
			.23					

Table 5-IV

Fits to $d\sigma/(p_T dp_T) = A\ \exp[-B*p_T]$

$A = nb\ GeV^{-2}\ c^{2}\ nucleus^{-1}$

$B = GeV^{-1}\ c$

Beam/ Target	Mass Region							
	1.5 2.0	2.0 2.7	2.7 3.5	3.5 4.0	4.0 5.0	5.0 6.5	6.5 8.0	8.0 11.0
Pi^{+}/C								
A	558.	256.	755.	4.40	3.12	----	----	----
	280.	128.	120.	.82	2.81			
B	2.99	3.19	2.44	1.70	1.79	----	----	----
	.33	.31	.07	.09	.62			
X^{2}/DF	9/16	13/9	27/22	9.5/6	1.1/4			
Pi^{-}/C								
A	414.	316.	711.	26.4	12.2	2.68	----	----
	126.	106.	85.	8.2	5.6	4.48		
B	2.67	2.95	2.34	2.46	2.54	2.25		
	.19	.22	.04	.19	.30	1.11		
X^{2}/DF	20/19	12/8	65/22	8/8	5.1/6	9/3		
Pi^{-}/Cu								
A	----	1390	2600	122.	36.6	59.5	----	----
		511	419	40.	12.9	40.6		
B		2.75	2.18	2.48	2.13	2.96		
		.22	.01	.19	.19	.42		
X^{2}/DF		14/16	71/25	25/24	6/10	7.4/8		

Table 5-IV, cont.

pi$^-$/W								
A	----	5870	9320	294.	139.	82.	2.25	11.4
		1560	1540	64.	24.	28.	1.65	9.8
B		2.93	2.19	2.05	2.16	2.24	0.94	2.00
		.14	.02	.10	.04	.19	.44	.56
χ^2/DF		13/18	146/27	20/22	22/22	11/12	3.3/6	0.7/4
Proton								
A	587.	267.	599.	6.75	0.55	----	----	----
	278.	173.	91.	8.20	0.88			
B	3.16	3.22	2.59	2.12	1.35			
	.32	.48	.07	.83	1.27			
χ^2/DF	8/13	4/6	42/20	5/6	1.4/2			
K^+								
A	----	----	267.	----	----	----	----	----
			229.					
B			1.64					
			.59					
χ^2/DF			1.6/3					

Table 5-V

Fits to $d\sigma/(p_T dp_T) = A \exp(-B[p_T^2 + C^2]^{1/2})$

A = microbarns GeV^{-2} c^2 $nucleus^{-1}$

B = GeV^{-1} c

C = GeV/c

Beam/ Target	Mass Region							
	1.5 2.0	2.0 2.7	2.7 3.5	3.5 4.0	4.0 5.0	5.0 6.5	6.5 8.0	8.0 11.0
pi^+/C								
A	1.00	13.4	23.2	98.5	.0036	----	----	----
	.71	9.6	2.9	114.	.0031			
B	3.19	4.24	3.18	1.23	1.72			
	.35	.26	.02	.30	.30			
C	0.42	1.35	1.63	1.23	0.86			
	.20	.14	.04	.30	.52			
χ^2/DF	16/25	18/13	35/31	18/10	4/8			
pi^-/C								
A	0.85	32.2	99.4	0.54	.011	.0023	----	----
	.30	40.1	37.9	.38	.013	.0051		
B	3.00	4.15	3.42	3.10	3.89	1.87		
	.18	.34	.08	.21	.29	.83		
C	0.40	1.55	1.92	1.58	2.26	0.90		
	.11	.22	.07	.17	.23	.82		
χ^2/DF	27/28	13/12	33/35	20/12	6/10	13/12		

Table 5-V, cont.

pi^-/Cu								
A	----	6.76	56.6	11.0	.302	.890	----	----
		4.37	9.1	5.5	.403	.951		
B		3.14	2.85	3.49	2.66	3.28		
		.18	.02	.14	.38	.31		
C		1.02	1.60	1.80	1.27	1.65		
		.18	.02	.11	.39	.25		
X^2/DF		20/25	38/34	44/33	9/14	12/12		
pi^-/W								
A	----	1220	421.	27.4	278.	.710	.0072	.061
		199	68.	20.5	251.	.610	.0044	.111
B		4.16	2.96	3.05	3.72	2.65	1.63	3.58
		.08	.02	.18	.16	.24	.38	.45
C		1.77	1.84	1.96	2.46	1.47	0.21	2.33
		.04	.01	.16	.16	.25	.50	.49
X^2/DF		25/27	60/36	20/31	38/31	18/16	10/10	2.4/6

Table 5-V, cont.

Proton								
A	.647	5.33	1190	97.5	.005	----	----	----
	.375	3.42	434	139.	.001			
B	3.13	3.82	4.12	2.80	2.65			
	.30	.25	.07	.48	.30			
C	0.37	1.35	2.32	1.43	0.73			
	.19	.14	.06	.35	.21			
X^2/DF	14/22	8/10	39/29	10/10	2.7/6			
K^+								
A	----	----	23.4	----	----	----	----	----
			4.6					
B			2.64					
			.05					
C			2.14					
			.05					
X^2/DF			2.8/7					

Table 5-VI

Fits to $d\sigma/dx_f = A(1-x)^B$

$A = \text{nb } (x_f \text{ unit})^{-1} \text{ nucleus}^{-1}$

Beam/ Target	Mass Region							
	1.5 2.0	2.0 2.7	2.7 3.5	3.5 4.0	4.0 5.0	5.0 6.5	6.5 8.0	8.0 11.0
π^+/C								
A	272.	78.8	304.	6.33	2.09	----	----	----
	50.	13.5	36.	1.38	.40			
B	3.95	2.90	2.34	1.61	1.80			
	.33	.24	.07	.23	.20			
χ^2/DF	10/10	18/13	8/14	2.3/6	4.4/3			
π^-/C								
A	258.	69.2	302.	7.44	2.84	1.05	----	----
	36.	9.8	35.	1.14	.63	.26		
B	3.30	2.30	2.22	1.57	1.31	1.39		
	.17	.14	.05	.14	.23	.27		
χ^2/DF	14/12	28/13	17/14	15/13	7/6	11/6		
π^-/Cu								
A	----	418.	1520	52.4	15.3	6.14	----	----
		78.	250	9.6	3.1	1.39		
B		2.63	2.38	1.95	1.20	0.88		
		.15	.05	.12	.14	.15		
χ^2/DF		19/13	31/14	19/13	4.5/6	3.3/6		

Table 5-VI, cont.

π^-/W								
A	----	1010	4600	129.	57.	25.9	6.20	3.01
		174	750	22.	10.	5.1	1.75	.90
B		2.00	2.25	1.41	1.18	1.06	0.97	0.60
		.10	.04	.07	.08	.12	.22	.18
χ^2/DF		46/14	39/14	20/14	13/14	7.2/6	4.7/6	6.9/6
Proton								
A	236.	90.	300.	5.52	0.76	----	----	----
	38.	14.	32.	1.05	.21			
B	4.75	4.67	4.32	3.27	1.42			
	.27	.23	.07	.34	.36			
χ^2/DF	5.4/9	14/9	45/16	3.8/7	5.2/6			
K^+								
A	----	----	290.	----	----	----	----	----
			56.					
B			2.97					
			.32					
χ^2/DF			2.5/6					
$\bar{p}$								
A	----	----	502.	----	----	----	----	----
			374.					
B			4.30					
			.58					
χ^2/DF			5.7/5					

Table 5-VII

Fits to $E^{cm} d\sigma/dx_f = A(1-x)^B$

A = nb GeV $(x_f \text{ unit})^{-1}$ nucleus^{-1}

Beam/ Target	Mass Region 1.5 – 2.0	2.0 – 2.7	2.7 – 3.5	3.5 – 4.0	4.0 – 5.0	5.0 – 6.5	6.5 – 8.0	8.0 – 11.0
π^+/C								
A	602.	218.	1140	28.0	8.65	----	----	----
	103.	36.	124	5.7	3.65			
B	2.63	1.95	1.75	1.17	1.10			
	.30	.22	.06	.21	.55			
χ^2/DF	8/10	18/13	14/14	2.5/6	3.5/3			
π^-/C								
A	624.	208.	1150	31.4	13.2	6.26	----	----
	80.	26.	121	4.5	2.7	1.65		
B	2.18	1.46	1.65	1.08	0.83	1.10		
	.15	.12	.04	.13	.20	.26		
χ^2/DF	7/12	15/13	14/14	16/13	5.3/6	12/6		
π^-/Cu								
A	----	1220	5660	220.	75.8	37.9	----	----
		221	923	40.	14.9	8.3		
B		1.75	1.77	1.43	0.83	0.65		
		.13	.04	.11	.12	.13		
χ^2/DF		10/13	20/14	21/13	4.9/6	3.8/6		

Table 5-VII, cont.

π^-/W								
A	----	3100	17800	566.	292.	163.	45.4	29.2
		524	2890	96.	51.	31.	12.4	8.3
B		1.21	1.70	0.96	0.86	0.83	0.77	0.53
		.08	.03	.06	.07	.10	.21	.18
χ^2/DF		24/14	10/14	17/14	18/14	5.7/6	4.6/6	7.1/6
Proton								
A	538.	250.	982.	21.1	3.43	----	----	----
	82.	36.	99.	4.0	.92			
B	3.51	3.70	3.50	2.64	0.96			
	.25	.22	.04	.33	.34			
χ^2/DF	3.4/9	19/9	53/16	4.1/7	5.5/6			
K^+								
A	----	----	997.	----	----	----	----	----
			187.					
B			2.28					
			.30					
χ^2/DF			3.1/6					
$\bar{p}$								
A	----	----	1640	----	----	----	----	----
			1200					
B			3.55					
			.58					
χ^2/DF			6.4/5					

Table 5-VIII

Total Cross Sections

(nb/nucleus, $x_f > 0$)

Mass	pi^+ C	pi^- C	pi^- Cu	pi^- W	P C	K^+ C	$\bar{p}$ C
1.5>2.0	55.4	63.3	----	----	45.1	----	----
	6.8	6.7			5.5		
2.0>2.7	17.8	22.5	122.	375.	12.5	----	----
	2.4	2.5	20.	60.	1.7		
2.7>3.5	82.5	90.2	403.	1350	54.5	72.0	92.0
	9.2	9.1	64.	216	6.1	12.0	64.0
J/Ψ	80.2	86.4	385.	1300	52.7	----	----
	10.4	10.2	61.	200	6.8		
J/Ψ cnt	2.8	4.5	21.1	72.7	1.80	----	----
	.7	.7	3.4	13.1	.58		
3.5>4.0	2.04	2.88	15.1	54.3	1.29	----	----
	.23	.35	2.5	8.7	.21		
Ψ'	0.96	1.54	8.85	30.5	0.61	----	----
	.23	.25	1.63	4.9	.14		
Ψ' cnt	0.53	0.92	5.55	19.9	0.32	----	----
	.12	.14	.97	3.6	.10		

Table 5-VIII, cont.

4.0>5.0	0.73	1.29	6.81	24.7	0.33	----	----
	.23	.21	1.19	4.2	.07		
5.0>6.5	0.14	0.40	3.06	11.7	.047	----	----
	.04	.09	.59	2.0	.029		
6.5>8.0	.041	.091	0.48	2.96	----	----	---
	.021	.028	.14	.71			
8.0>11.	.020	.064	0.28	1.84	----	----	----
	.020	.033	.10	.48			

cnt ≡ continuum in mass region

A_Dependence

The dependence of the π^- cross section on the atomic number of the target, paramaterized in the form $\sigma_0 A^{\alpha}$, is shown in Figures 5-28 through 5-30 as a function of different kinematic parameters (mass, p_T, and x_f). The errors include the systematic errors listed in Chapter IV for the normalization. The cross section in the various kinematic intervals was well represented by the power law dependence as shown in Figure 5-31.

Figure 5-29 shows the dependence of α on p_T at various masses. A systematic rise of α with p_T is seen in the J/ψ interval but not for the regions above or below the J/ψ. Similar results have been reported in other inclusive hadron production experiments,[19] particularly for π^- induced J/ψ's.[18] Figure 5-30 shows no significant variation in α with x_f. The mass dependence (with $x_f > 0$) of α shown in Figure 5-28 includes previous measurements at lower mass.[6] The main feature is a rise in α with mass, reaching a plateau of $\alpha = 1.12 \pm .05$ at masses above the J/ψ. A similar plateau in α has been observed in the proton data,[6,20] shown for comparison in Figure 5-32, although there the plateau value is 1.02.

The Upsilon

Using the measured atomic mass number dependence for the π^- data, the different targets were combined to give per nucleon cross sections. The combined mass spectrum is shown in Figure 5-33. The continuum above 4 GeV/c^2 was fit to the form $d\sigma/dM = aM^b$. The upsilon region was fit as a gaussian of σ_m = 380 MeV/c^2 (the width calculated by the Monte Carlo program). The result was b = 5.6 ± .05 and $B\sigma_{upsilon}$ = .4 ± .35 pb/nucleon. This gives a 95% confidence limit of $B\sigma_{\Upsilon}$ < 1.4pb/nucleon for incident π^- at 225 GeV/c. The sensitivity of this result can be compared to the reported limit on proton induced upsilons at 200 GeV/c. In a 1.0 GeV/c^2 wide mass region, we find $B\sigma_{\Upsilon}$/continuum = .4 ± .4 while Yoh *et al.*,[4] report .1 ± .1.

p_T Dependence

In Figure 5-34, the mean transverse momenta for π^- induced events with x_f > 0 are ploted versus pair mass. Data from other measurements are shown for comparison. The mean p_T increases with mass up to M ≅ 4 GeV/c^2, where it reaches a plateau value of approximately 1.2 GeV/c. A similar plateau was seen for the proton induced data of Yoh *et al.*, but at a value 200 MeV/c lower. Proton induced data from our experiment also exhibits a lower $\langle p_T \rangle$ at M = 4

GeV/c^2. The dependence of $\langle p_T \rangle$ on x_f is displayed in Figure 5-35 for several intervals of pair mass. Within uncertainties of ∓ 100 MeV/c, no variation of $\langle p_T \rangle$ with x_f is observed.

x_f Dependence

The x_f spectra for both pions and protons (again see Figures 5-15 through 5-25) show a steady flattening in x_f as the mass increases. The change in the fitted power with mass is fairly monotonic, except for some of the fits in which the J/Ψ x_f dependence is somewhat steeper than the mass regions below it.

At the J/Ψ, we also have x_f distributions for $\bar{p}$ and K^+ beams. The $\bar{p}$ distribution resembles the proton distribution whereas the K^+ looks somewhat like the pion data.

A detailed treatment of J/Ψ production will be discussed in the thesis of Kari Karhi of The University of Chicago. The high mass data is best discussed in the framework of the Drell-Yan model, the subject of the next chapter.

Polar (Helicity) Angle Distribution

The final kinematic parameter of interest is the polar angle. This is defined as the angle between the positively charged muon and some vector $\vec{p}$ measured in the rest frame of the muon pair. In the annihilation reaction shown in Figure 1-2, one should use the $q\bar{q}$ collision axis as $\hat{p}$. The $q\bar{q}$ collision axis is just the hadron collision axis in the 'naive' Drell-Yan model in which $p_{T,quark} = 0$. However, experiments have shown that muon pairs, and hence the the colliding quarks, have large p_T. Moreover, because the reaction progresses through an intermediate one-particle state, information is lost concerning the momenta of the quarks. In particular, the p_T of the individual quarks (and thus direction of the $q\bar{q}$ axis) cannot be deduced from the kinematics of the final state muons. Generally, one tries to get around this problem by defining $\hat{p}$ in terms of the direction of the hadrons that contain the quarks.

There are several different ways to define $\hat{p}$ in terms of the beam ($\hat{p}_{beam}$) and target ($\hat{p}_{target}$) trajectories in the pair rest frame. Some commonly used directions for $\hat{p}$ are shown in Figure 5-36 and are defined (in terms of unit direction vectors) as:

$$\hat{p} = \hat{p}_{beam} \quad \text{(t-channel)} \qquad (5-1)$$

$$= \hat{p}_{target} \quad \text{(u-channel)}$$

$$= \hat{p}_{beam} + \hat{p}_{target} \quad \text{(s-channel or recoil channel)}$$

$$= \hat{p}_{beam} - \hat{p}_{target} \quad \text{(Collins-Soper)}.$$

These various directions are all the same when the p_T's of the quarks (and thus of the muons) are zero. The Collins-Soper angle[21] was proposed to give the a best guess of θ for $p_T \neq 0$ by assuming the p_T comes from the two quarks in equal amounts.

The distribution of the polar angle has been examined for the mass regions $2.0 < M < 2.7$ GeV/c^2, $2.7 < M < 3.5$ GeV/c^2 (the J/ψ), and $M > 3.5$ GeV/c^2. The distributions are shown in Figures 5-37 through 5-40 (reproduced from the thesis of Cathy Newman) with their best fits to $1 + \lambda \cos^2\theta^*$. Results of the fits are given in Table 5-IX. The continuum regions above and below the J/ψ show strong dependence on θ^* regardless of the definition of θ^* used, whereas the J/ψ data is consistent with a flat angular distribution.

Because of the indeterminate source of the pair's p_T and the possible dependence of the production mechanism on p_T, it should be noted that we see no significant differences in the polar angle distributions for samples with $p_T < 1.0$ GeV/c versus $p_T > 1.0$ GeV/c. See Figures 5-41 and 5-42.

The mass dependence of these distributions reflects a clear change in the underlying production mechanisms for the

J/ψ compared with the continuum. Indeed, the continuum results are consistent with the prediction of $\lambda = 1$ in the Drell-Yan model where two spin 1/2 fermions annihilate into a 1^- intermediate state.

Table 5-IX

HELICITY ANGULAR DISTRIBUTION FITS

Angle	Flat χ^2/DOF	$1+\cos^2\theta^*$ χ^2/DOF	$1+\lambda\cos^2\theta^*$ λ	χ^2/DOF
		$2.0 < M_{\mu\mu} < 2.7$ GeV/c^2		
s channel	77.5/9	15.7/9	1.10±.16	15.3/8
t channel	67.4/9	15.7/9	.71±.11	8.8/8
u channel	102.5/9	34.2/9	1.72±.22	22.4/8
Collins-Soper	79.7/9	25.6/9	1.14±.17	25.0/8
		J/ψ		
s channel	19.0/9	240.0/9	.03±.06	18.7/8
t channel	36.7/9	101.0/9	.33±.06	2.2/8
u channel	12.3/9	131.0/9	.09±.07	10.7/8
Collins-Soper	7.0/9	212.0/9	-.10±.07	4.7/8
		$M_{\mu\mu} > 3.5$ GeV/c^2, all p_T		
s channel	32.3/9	104.0/9	.05±.10	32.0/8
t channel	49.7/9	11.1/9	.82±.15	9.8/8
u channel	47.8/9	17.7/9	1.31±.26	16.2/8
Collins-Soper	44.6/9	6.6/9	1.30±.23	4.9/8
		$M_{\mu\mu} > 3.5$ GeV/c^2, $p_T > 1$ GeV/c		
s channel	11.7/7	25.4/7	.16±.19	11.0/6
t channel	30.4/9	15.8/9	.65±.17	12.4/8
u channel	29.4/7	13.7/7	1.42±.39	12.5/6
Collins-Soper	36.4/9	11.2/9	1.47±.32	8.8/8
		$M_{\mu\mu} > 3.5$ GeV/c^2, $p_T < 1$ GeV/c		
s channel	13.1/7	11.9/7	.50±.22	7.4/6
t channel	26.0/9	3.3/9	1.05±.24	3.3/8
u channel	28.2/9	12.6/9	1.11±.31	12.5/8
Collins-Soper	31.6/9	12.6/9	1.17±.29	12.2/8

Production Ratios

The other clear prediction of the Drell-Yan model, as mentioned in Chapter I, is that the cross section ratio of pi^+ to pi^- incident on an isoscalar target (such as carbon) should go to 1/4 at high mass. Figure 5-43 shows the measured ratio as a function of pair mass for $x_f > 0$. The ratio is consistent with unity at the J/Ψ, as expected for a strong production mechanism. Above 3.1 GeV/c^2 the ratio falls toward 1/4 as predicted.

Because the data indicate that the Ψ' is not produced with the same cross section for pi^+ and pi^-, a small (3%) correction was calculated and applied to the J/Ψ ratio to take into account the unequal contributions from the reactions $pi^{\pm}$ C > Ψ' > J/Ψ + anything. This correction was based on our measurement of total Ψ' production and the measured branching ratios.[22]

The solid curve on the graph is the prediction of the Drell-Yan model using the pion structure function derived in the next chapter. The shape of the curve, however, is more sensitive to the assumed shape of the nucleon sea. Here we have used the sea given by the Columbia-Fermilab-Stony Brook collaboration[4] because it is measured in a q^2 region closer to our own than are the fits based on the deep inelastic scattering experiments. (The curve shows a clear dependence on which sea is assumed and the CFSB sea fits our data best.)

The ratio of π^- to proton cross section, with its rise to over 100 at a mass of 10 GeV/c^2 (see Figure 5-44), is also in dramatic agreement with expectations. (The proton results are from Yoh, *et al.*)

Conclusion

The last two sections on the production ratios and polar angle clearly indicate that the data are in good agreement with the Drell-Yan model. The implication then is that the model can be applied to the data to deduce the pion structure function. This is discussed in the next chapter.

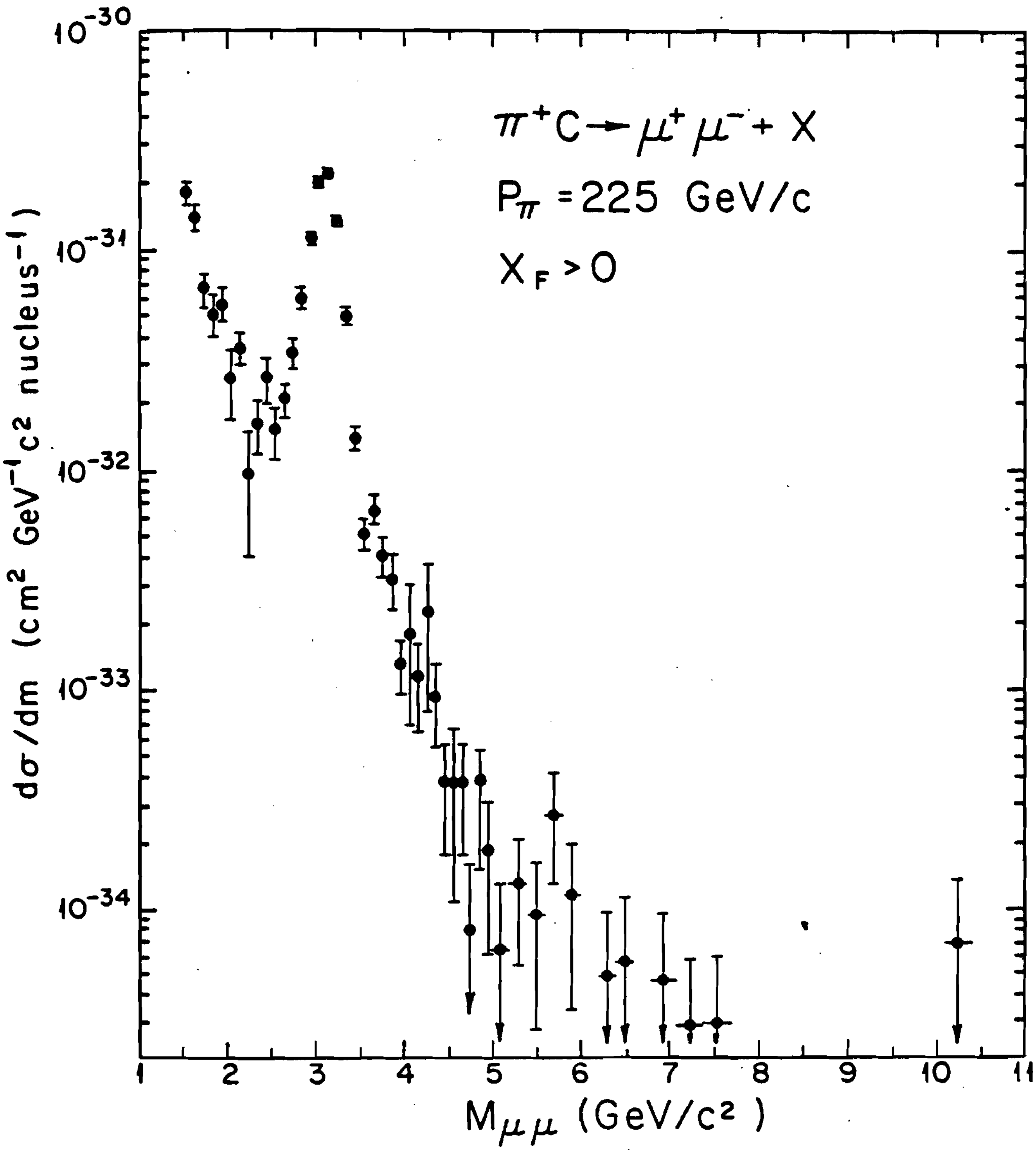

10^{-30}
10^{-31}
10^{-32}
10^{-33}
10^{-34}
$d\sigma/dm$ (cm^2 GeV^{-1}c^2 nucleus^{-1})
$\pi^+C \rightarrow \mu^+\mu^- + X$
$P_\pi = 225$ GeV/c
$X_F > 0$
1 2 3 4 5 6 7 8 9 10 11
$M_{\mu\mu}$ (GeV/c²)

Figure 5-1.

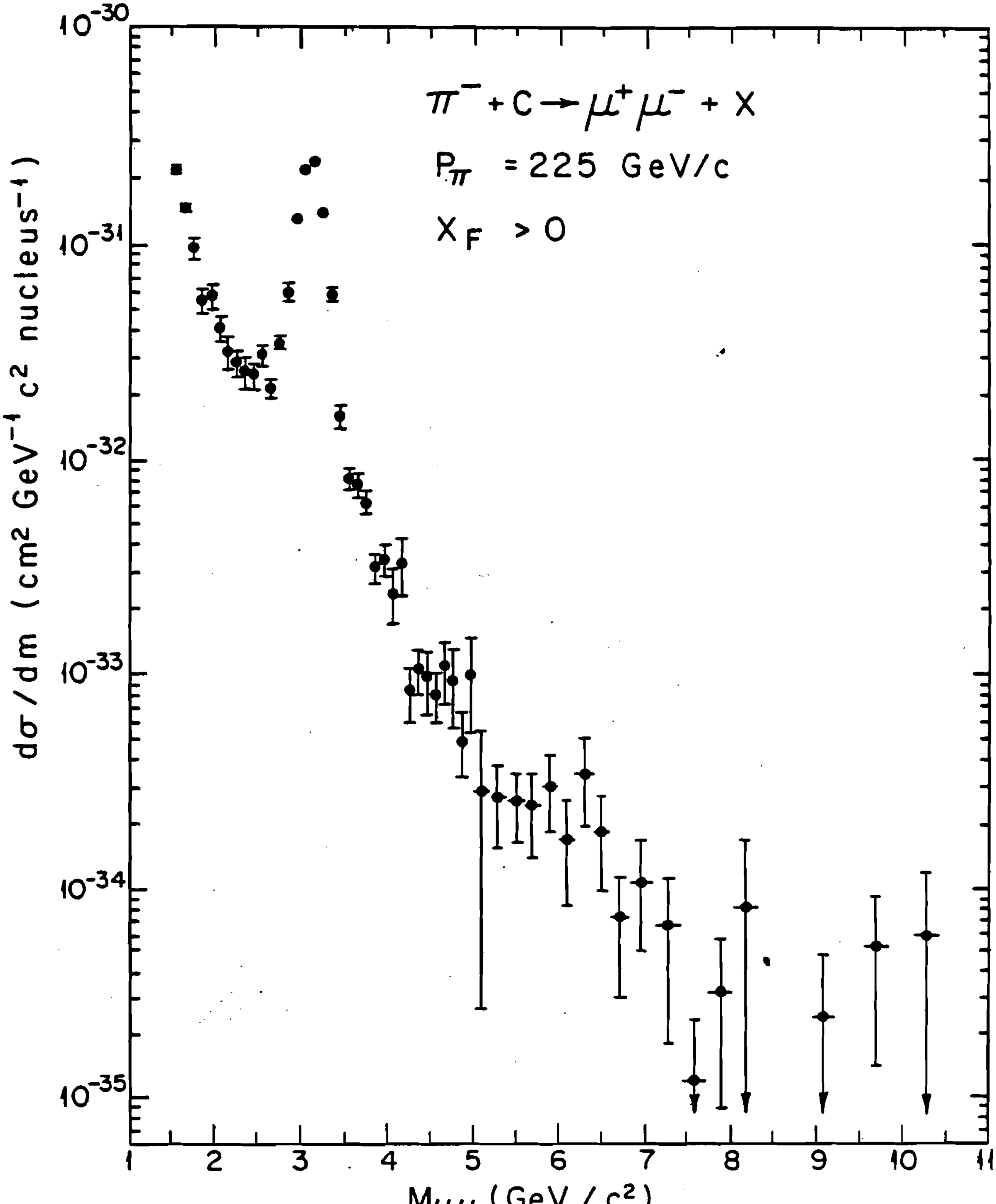

$\pi^- + C \rightarrow \mu^+\mu^- + X$
$P_\pi = 225$ GeV/c
$X_F > 0$
$d\sigma/dm$ (cm² GeV⁻¹ c² nucleus⁻¹)
$M_{\mu\mu}$ (GeV / c²)

Figure 5-2.

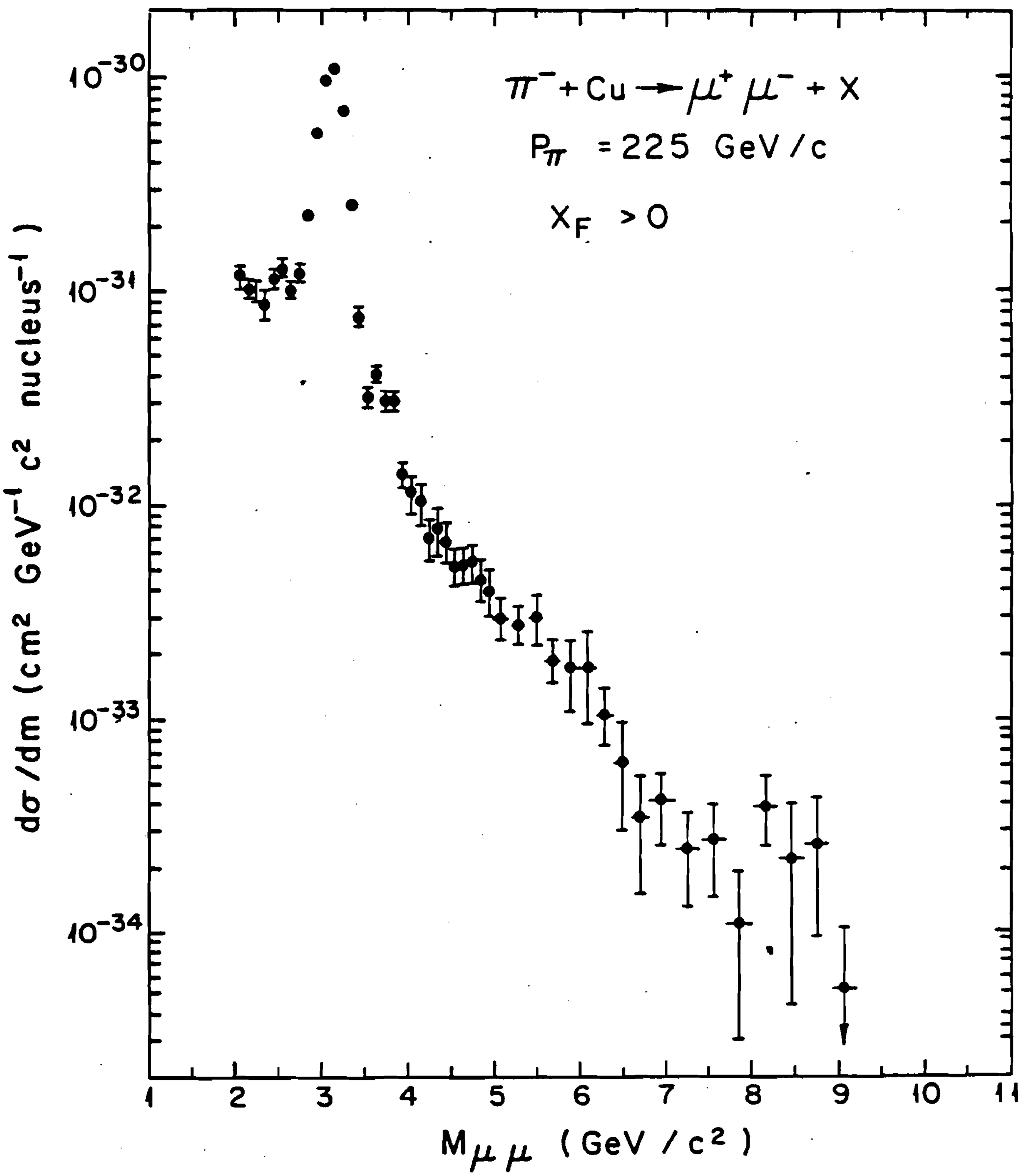
$\pi^- + Cu \rightarrow \mu^+ \mu^- + X$
P_π = 225 GeV/c
X_F > 0
dσ/dm (cm² GeV⁻¹ c² nucleus⁻¹)
M μμ (GeV / c²)
10⁻³⁰
10⁻³¹
10⁻³²
10⁻³³
10⁻³⁴
1
2
3
4
5
6
7
8
9
10
11

Figure 5-3.

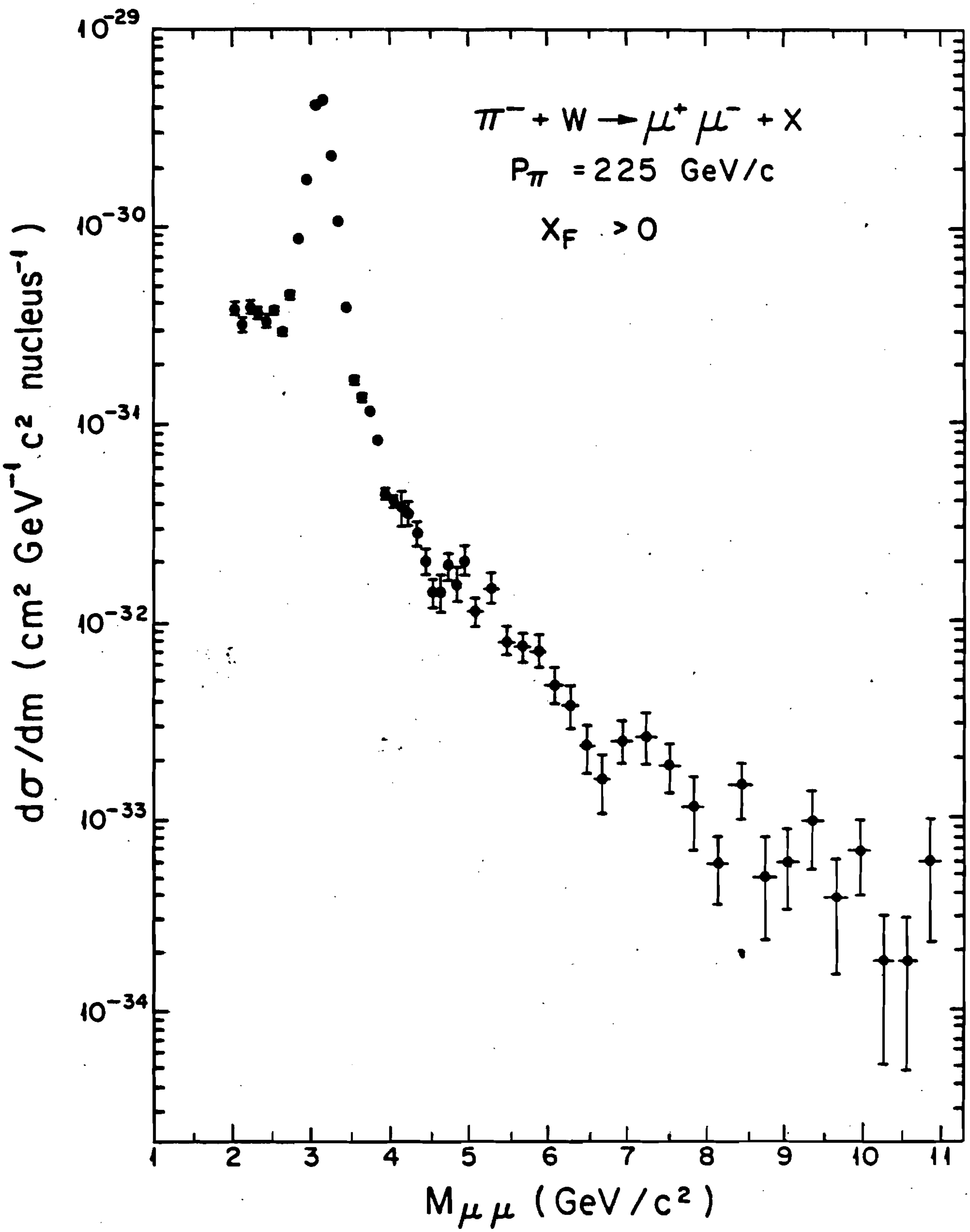

$\pi^- + W \rightarrow \mu^+ \mu^- + X$
$P_\pi = 225$ GeV/c
$X_F > 0$
$d\sigma/dm$ (cm² GeV⁻¹ c² nucleus⁻¹)
$M_{\mu\mu}$ (GeV/c²)
10^{-29}
10^{-30}
10^{-31}
10^{-32}
10^{-33}
10^{-34}
1
2
3
4
5
6
7
8
9
10
11

Figure 5-4.

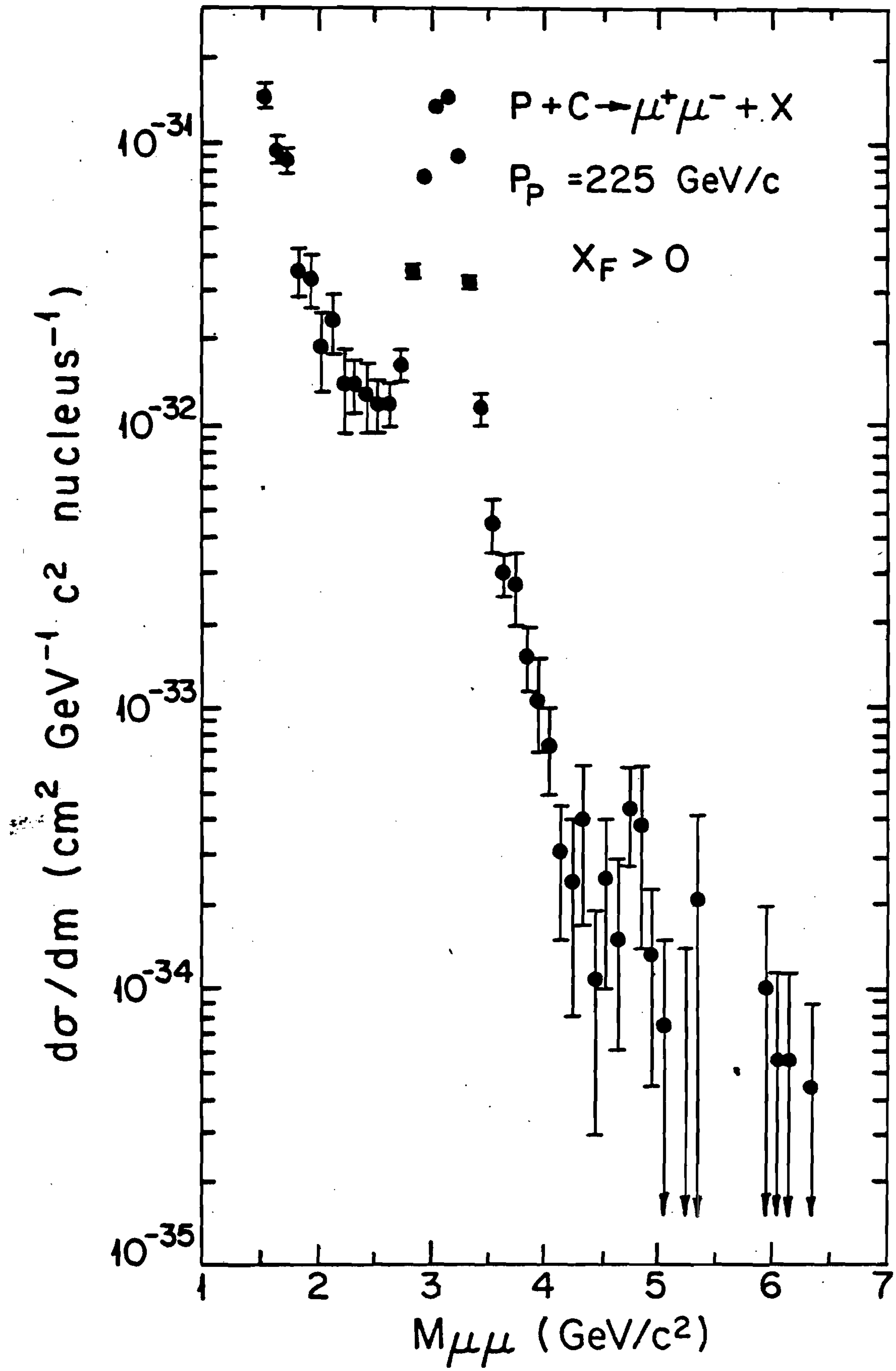
P + C → μ⁺μ⁻ + X
P_P =225 GeV/c
$X_F > 0$
dσ/dm (cm² GeV⁻¹ c² nucleus⁻¹)
10⁻³¹
10⁻³²
10⁻³³
10⁻³⁴
10⁻³⁵
1
2
3
4
5
6
7
Mμμ (GeV/c²)

Figure 5-5.

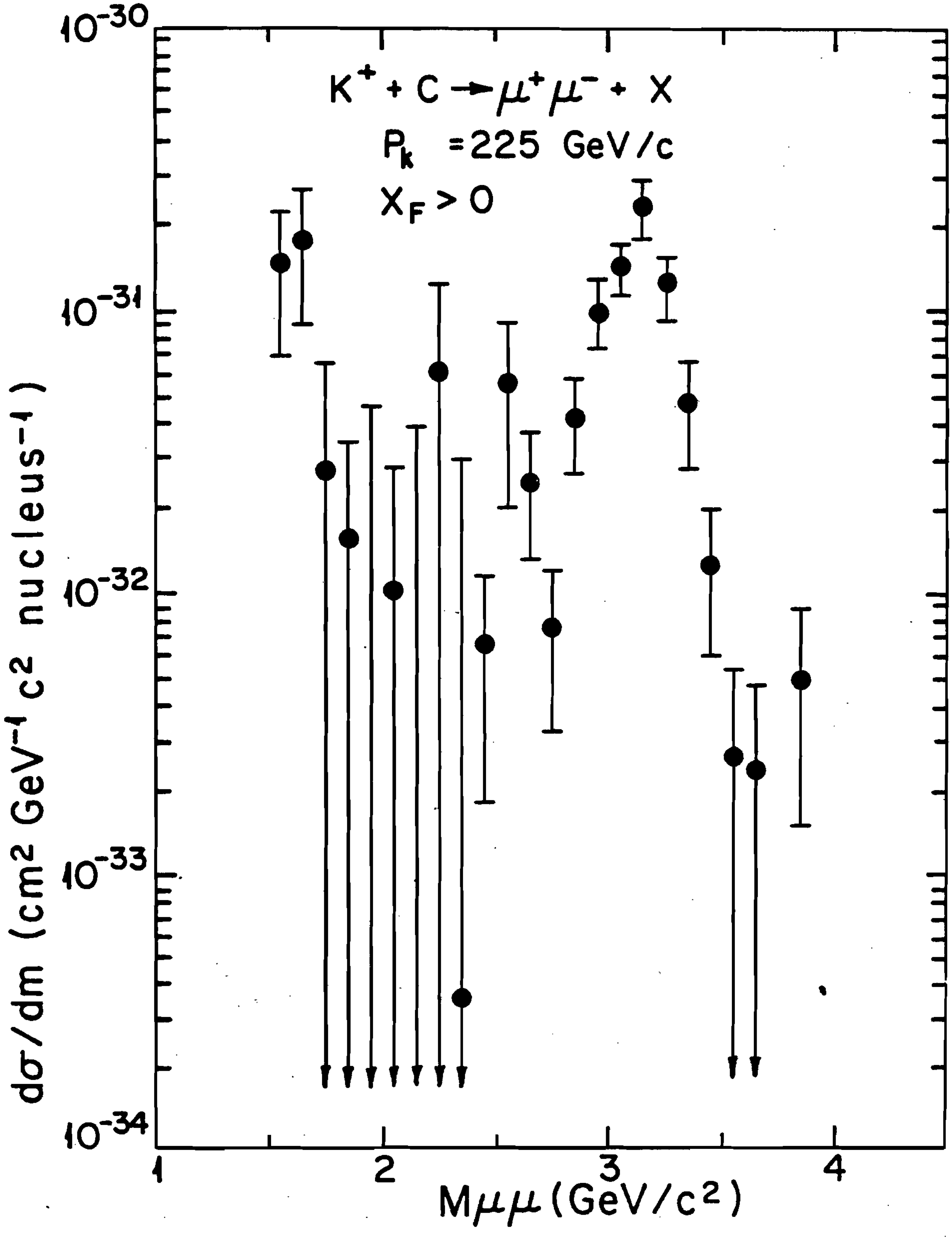

K⁺ + C → μ⁺μ⁻ + X
Pk =225 GeV/c
XF > 0
10-30
10-31
10-32
10-33
10-34
dσ/dm (cm² GeV⁻¹ c² nucleus⁻¹)
1
2
3
4
Mμμ (GeV/c²)

Figure 5-6.

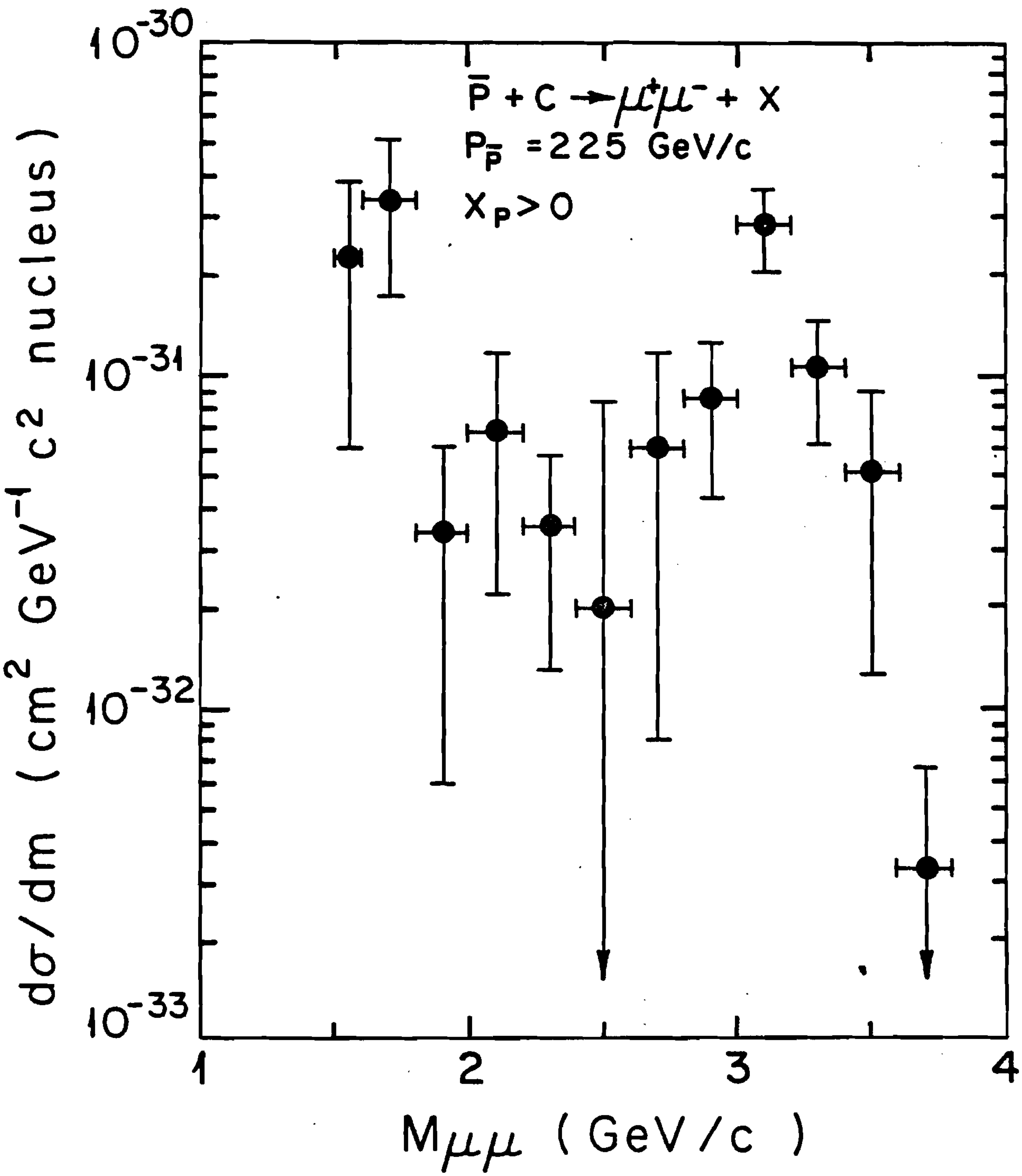
$\bar{P} + C \rightarrow \mu^+\mu^- + X$
$P_{\bar{P}}$ = 225 GeV/c
$X_P > 0$
10^{-30}
10^{-31}
10^{-32}
10^{-33}
1
2
3
4
dσ/dm (cm² GeV⁻¹ c² nucleus)
Mμμ (GeV/c)

Figure 5-7.

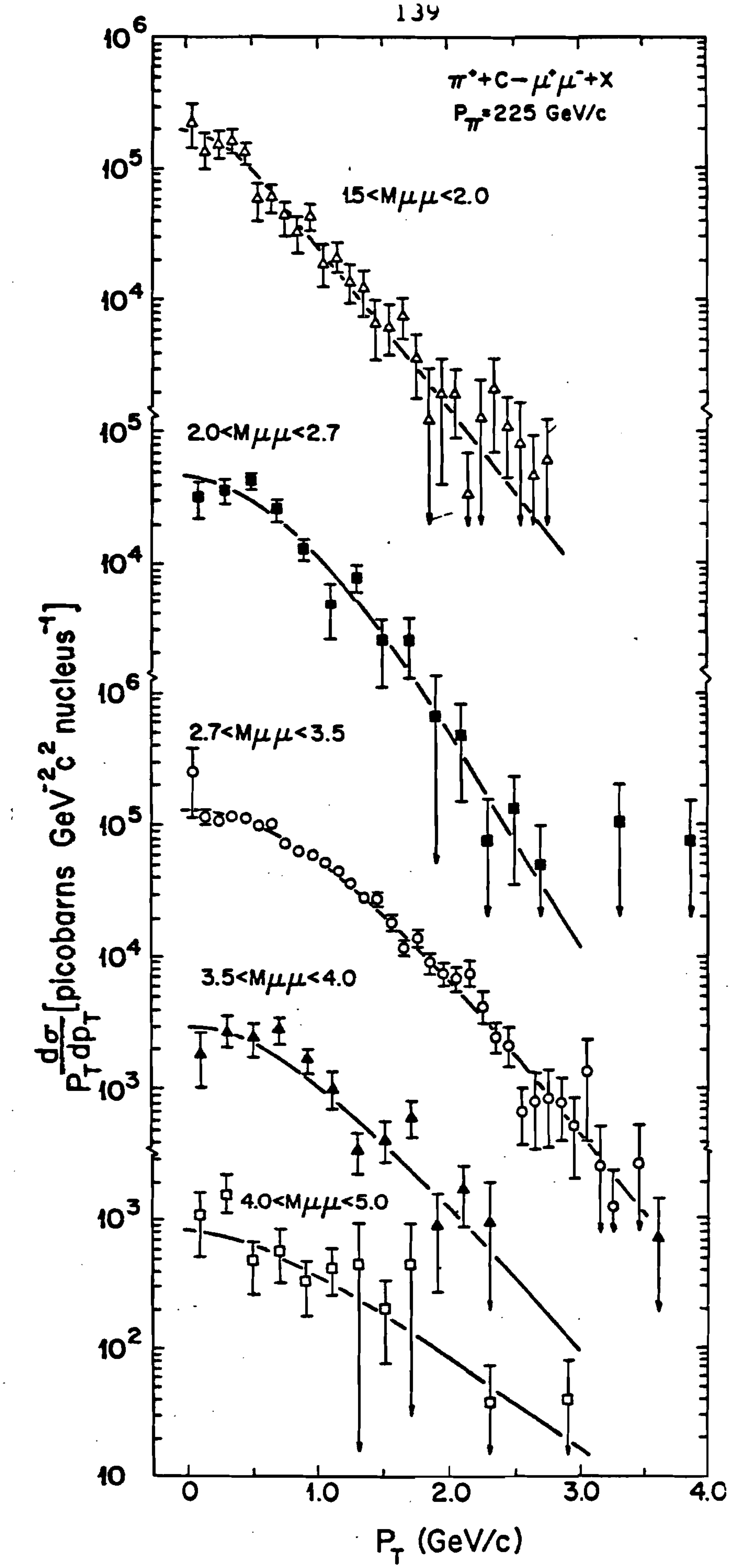

π⁺+C→μ⁺μ⁻+X
Pπ=225 GeV/c
1.5<Mμμ<2.0
2.0<Mμμ<2.7
2.7<Mμμ<3.5
3.5<Mμμ<4.0
4.0<Mμμ<5.0
dσ/(PT dPT) [picobarns GeV⁻² c² nucleus⁻¹]
PT (GeV/c)

Figure 5-8.

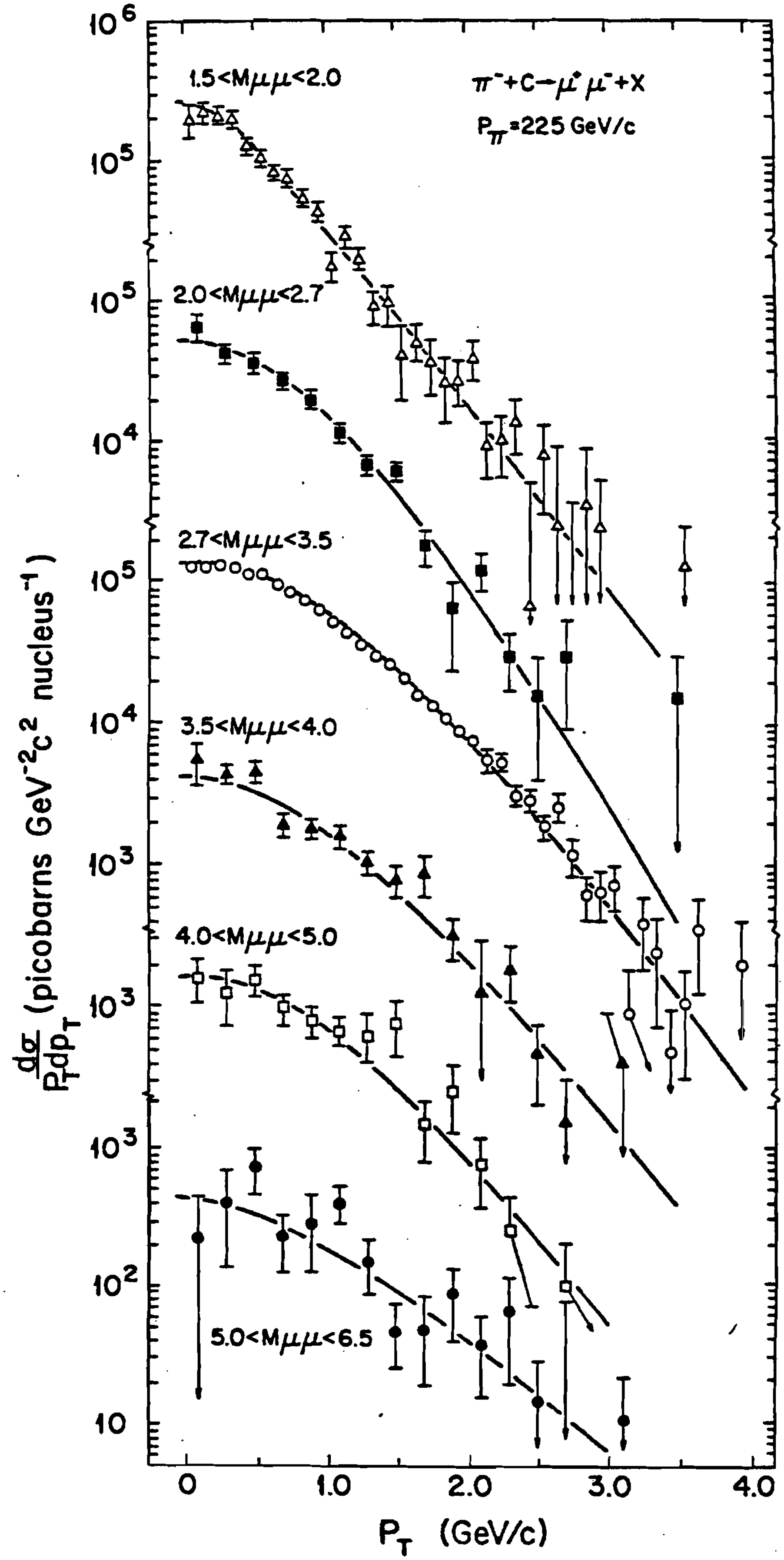
1.5<Mμμ<2.0
π⁻+C→μ⁺μ⁻+X
P_π=225 GeV/c
2.0<Mμμ<2.7
2.7<Mμμ<3.5
3.5<Mμμ<4.0
4.0<Mμμ<5.0
5.0<Mμμ<6.5
dσ/P_T dp_T (picobarns GeV⁻²c² nucleus⁻¹)
P_T (GeV/c)
0
1.0
2.0
3.0
4.0
10⁶
10⁵
10⁴
10³
10²
10

Figure 5-9.

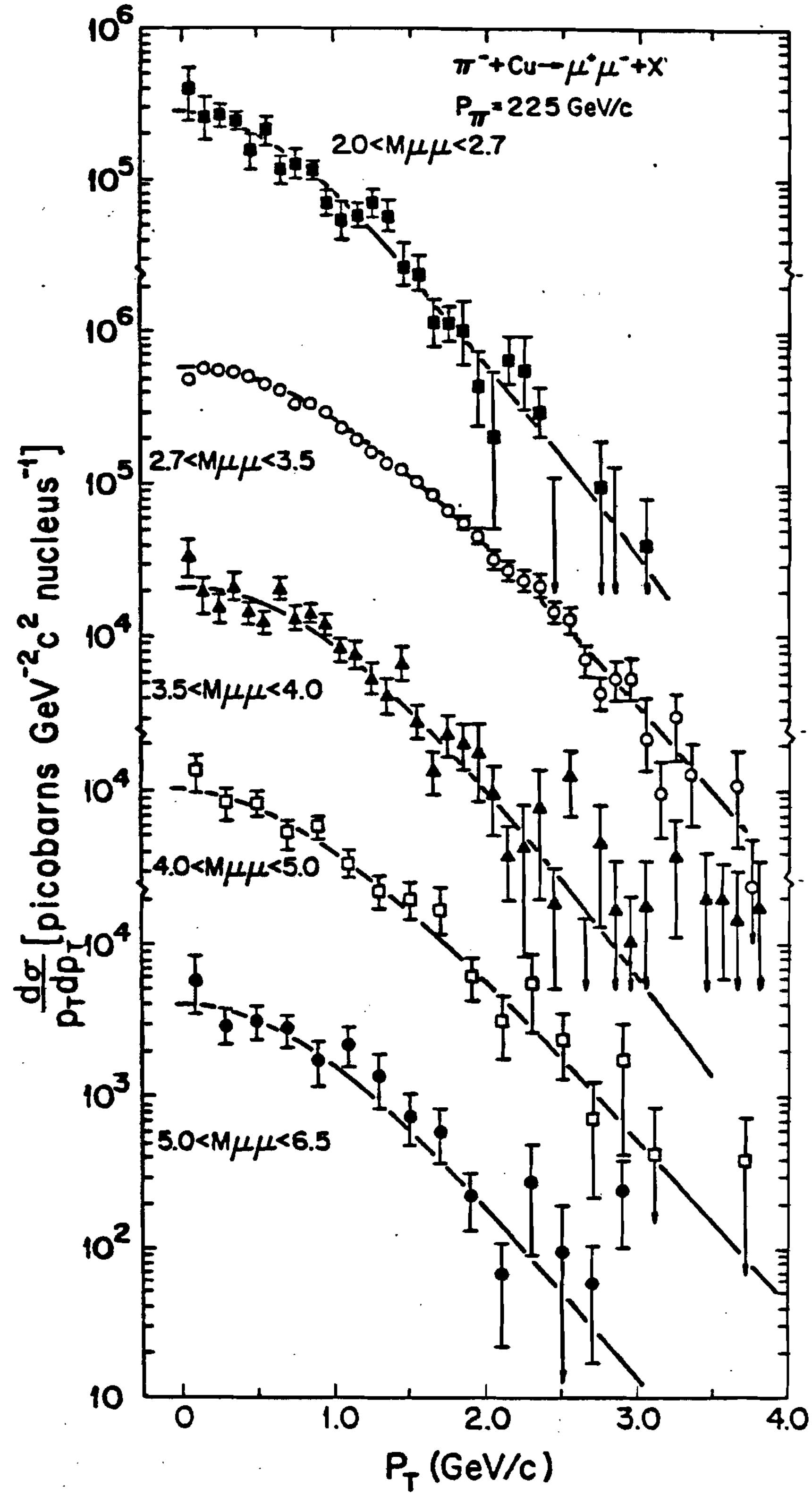
$\pi^- + Cu \rightarrow \mu^+\mu^- + X$
$P_\pi = 225$ GeV/c
2.0<Mμμ<2.7
2.7<Mμμ<3.5
3.5<Mμμ<4.0
4.0<Mμμ<5.0
5.0<Mμμ<6.5
$\frac{d\sigma}{p_T dp_T}$ [picobarns GeV^{-2}c^2 nucleus^{-1}]
P_T (GeV/c)
10
10^2
10^3
10^4
10^5
10^6
0
1.0
2.0
3.0
4.0

Figure 5-10.

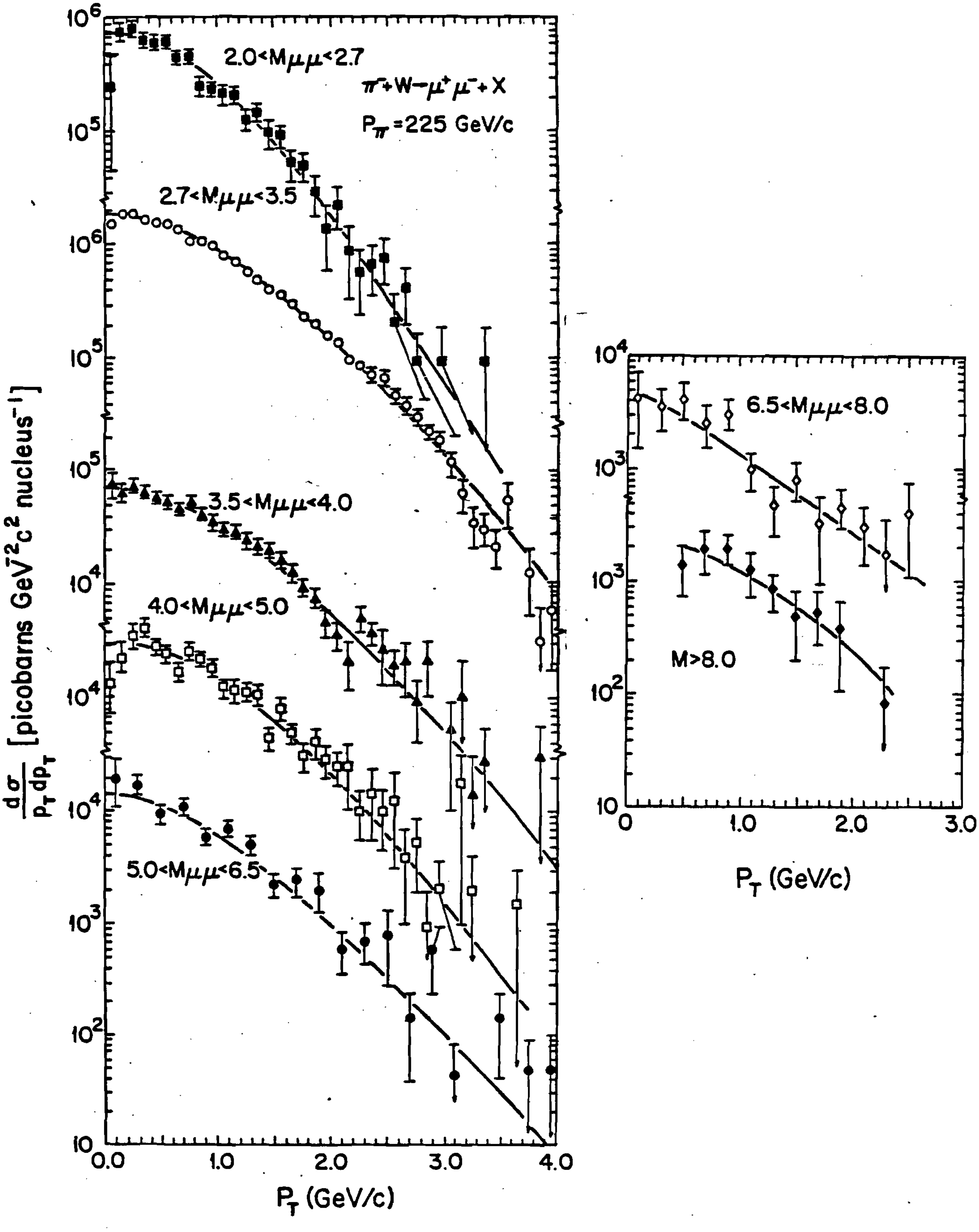
2.0<Mμμ<2.7
π⁻+W→μ⁺μ⁻+X
Pπ=225 GeV/c
2.7<Mμμ<3.5
3.5<Mμμ<4.0
4.0<Mμμ<5.0
5.0<Mμμ<6.5
6.5<Mμμ<8.0
M>8.0
dσ/pTdpT [picobarns GeV⁻²c² nucleus⁻¹]
PT (GeV/c)
PT (GeV/c)

Figure 5-11.

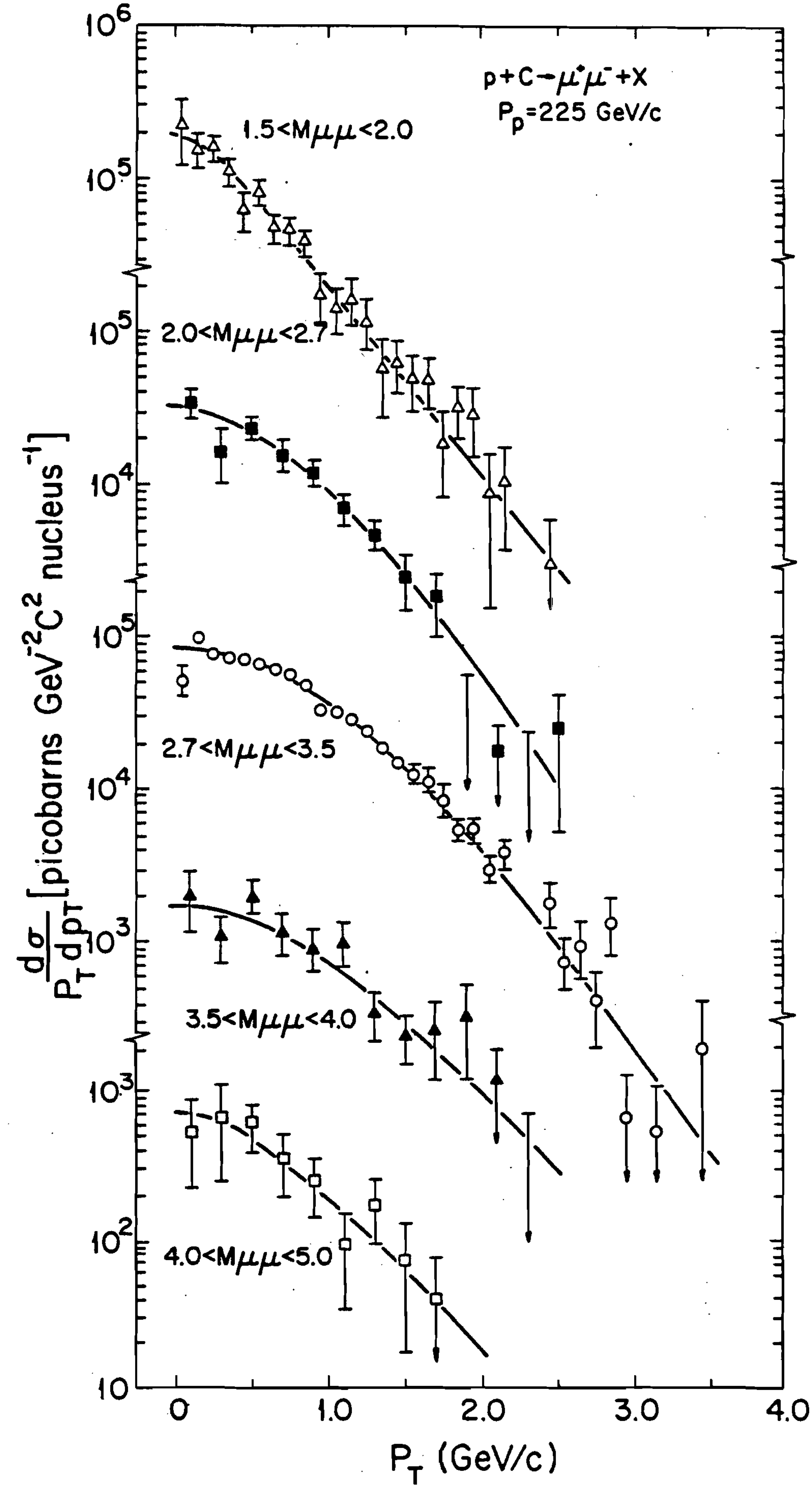
p+C→μ⁺μ⁻+X
P_p=225 GeV/c
1.5<Mμμ<2.0
2.0<Mμμ<2.7
2.7<Mμμ<3.5
3.5<Mμμ<4.0
4.0<Mμμ<5.0
$\frac{d\sigma}{P_T dp_T}$ [picobarns GeV^{-2}C^2 nucleus^{-1}]
P_T (GeV/c)
0
1.0
2.0
3.0
4.0
10
10^2
10^3
10^4
10^5
10^6

Figure 5-12.

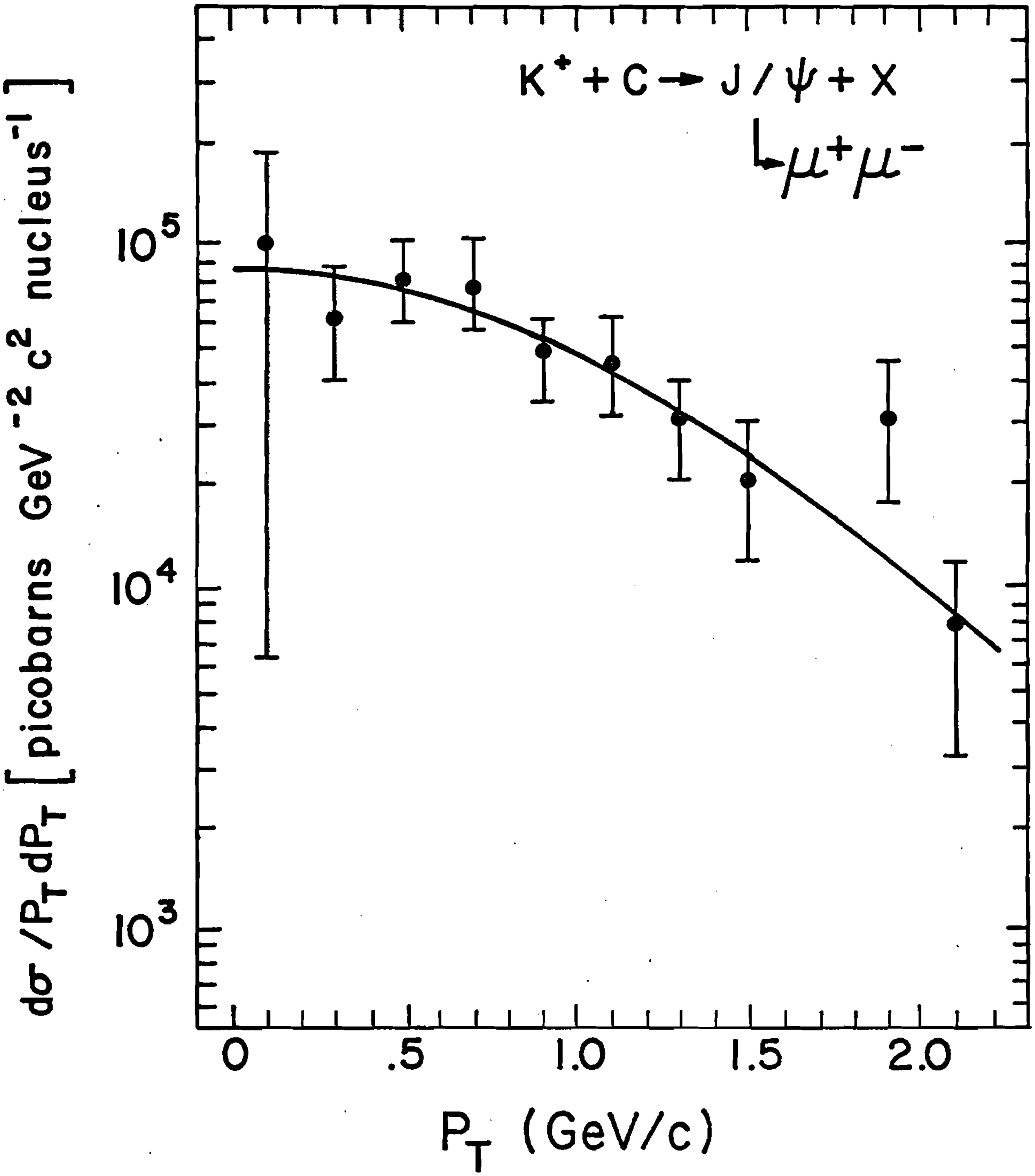
K⁺ + C → J/ψ + X
↳ μ⁺μ⁻
dσ/P_T dP_T [picobarns GeV⁻² c² nucleus⁻¹]
10⁵
10⁴
10³
0
.5
1.0
1.5
2.0
P_T (GeV/c)

Figure 5-13.

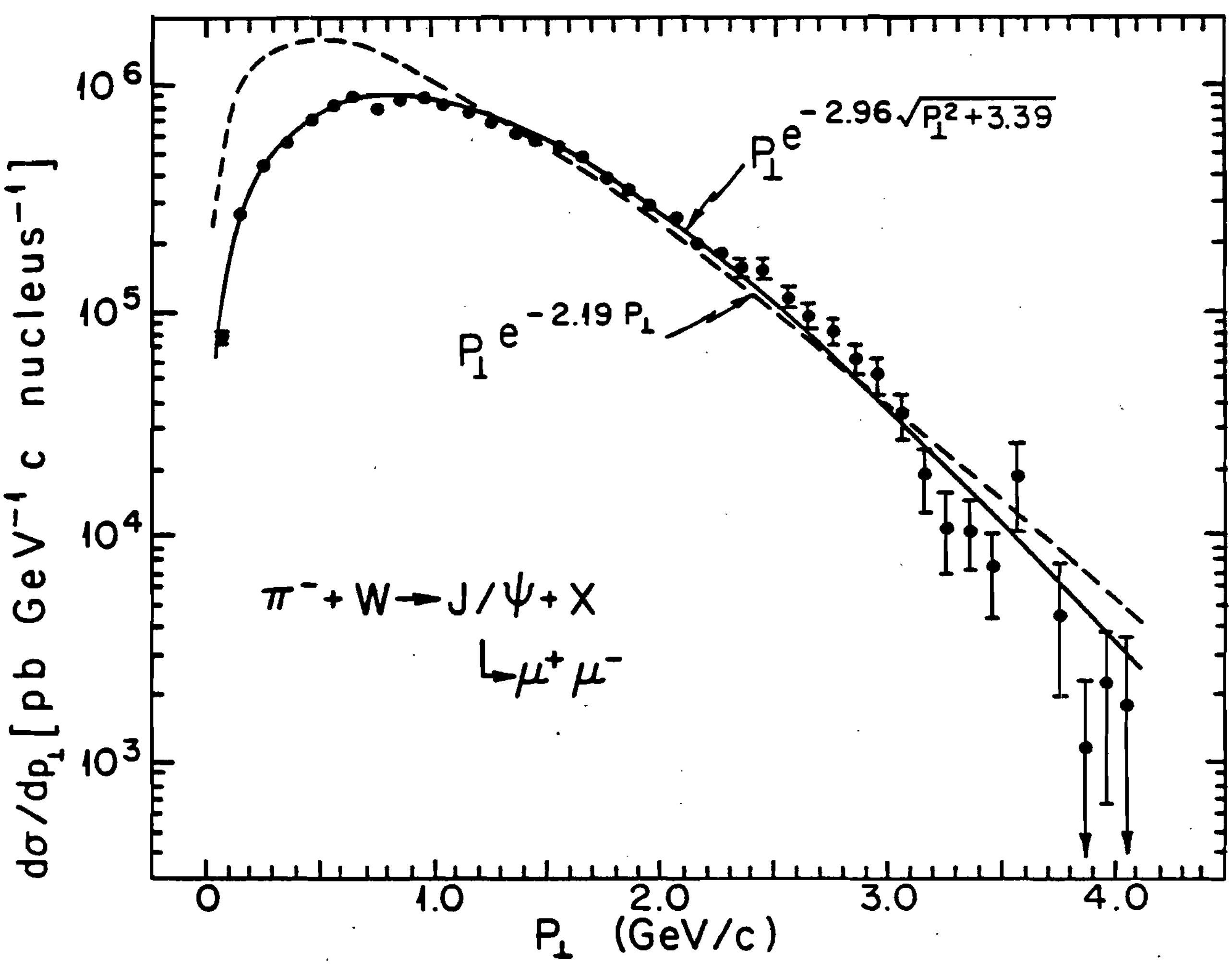

10^6
10^5
10^4
10^3
$d\sigma/dp_\perp$ [pb GeV^{-1} c nucleus^{-1}]
0
1.0
2.0
3.0
4.0
$P_\perp$ (GeV/c)
$P_\perp e^{-2.96\sqrt{P_\perp^2+3.39}}$
$P_\perp e^{-2.19 P_\perp}$
$\pi^- + W \rightarrow J/\psi + X$
$\rightarrow \mu^+ \mu^-$

Figure 5-14.

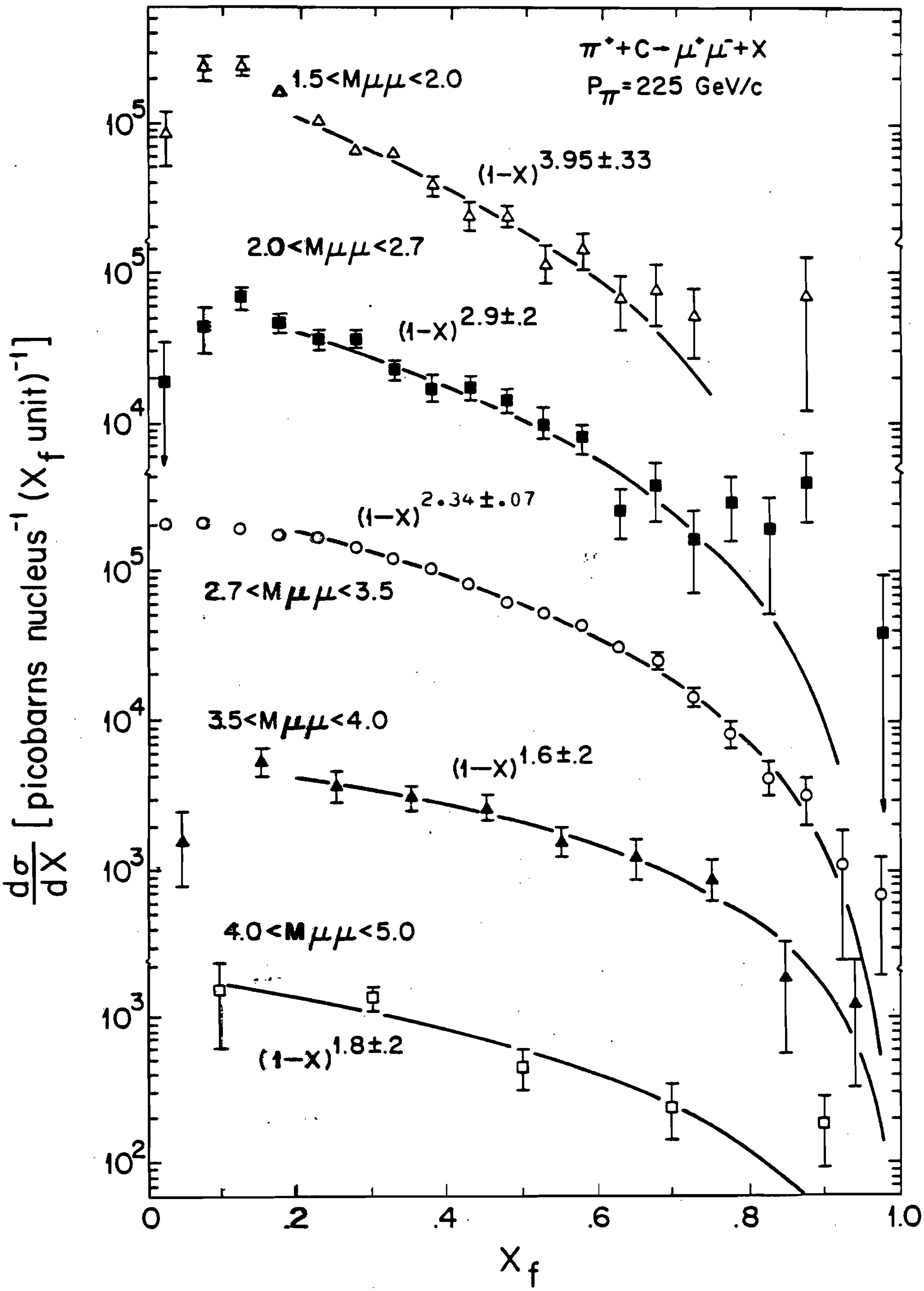

$\pi^{+}+C\rightarrow\mu^{+}\mu^{-}+X$
$P_{\pi}=225$ GeV/c
$1.5<M\mu\mu<2.0$
$(1-X)^{3.95\pm.33}$
$2.0<M\mu\mu<2.7$
$(1-X)^{2.9\pm.2}$
$(1-X)^{2.34\pm.07}$
$2.7<M\mu\mu<3.5$
$3.5<M\mu\mu<4.0$
$(1-X)^{1.6\pm.2}$
$4.0<M\mu\mu<5.0$
$(1-X)^{1.8\pm.2}$
$\frac{d\sigma}{dX}$ [picobarns nucleus^{-1} (X_f unit)$^{-1}$]
X_f

Figure 5-15.

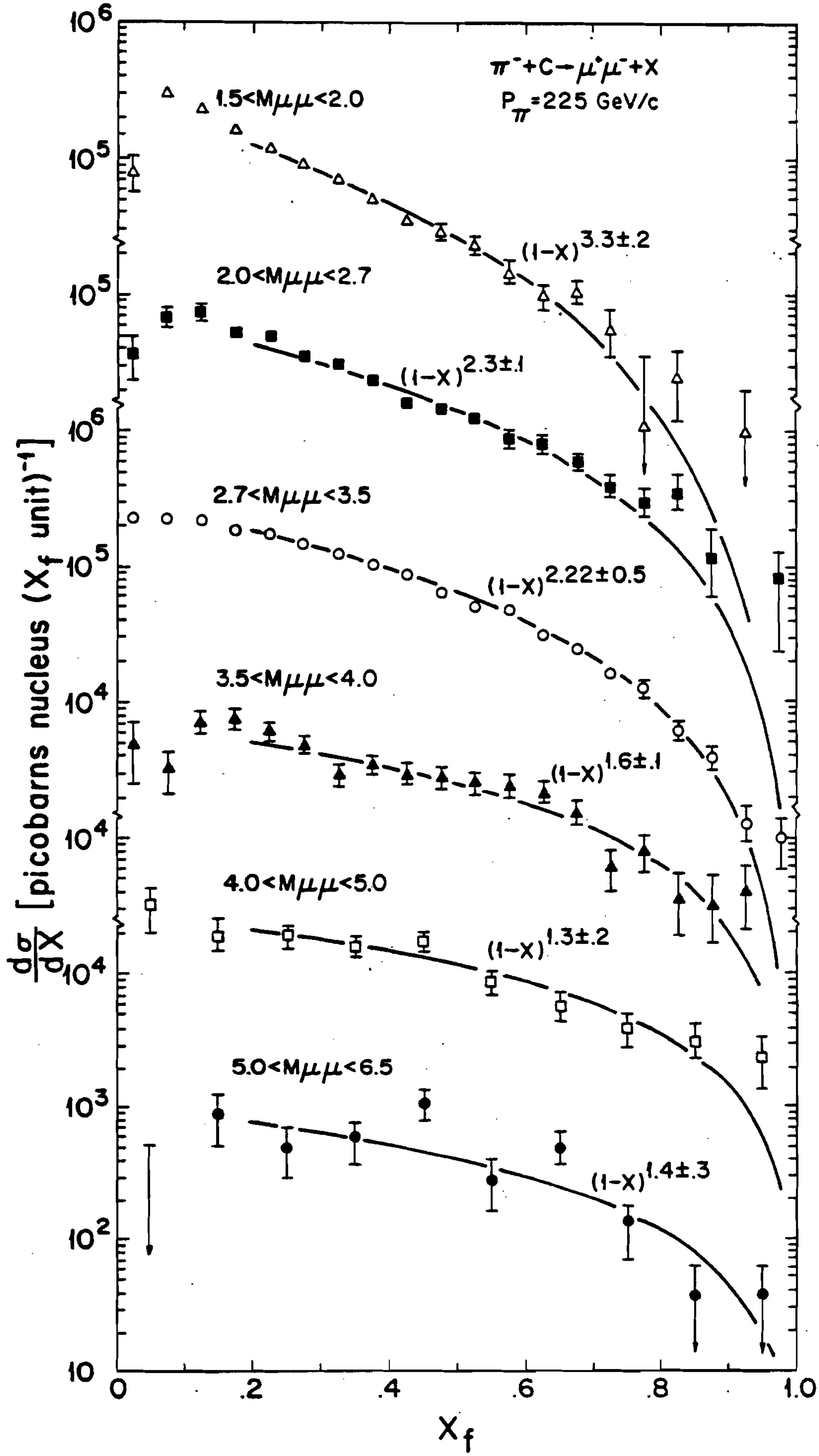

π⁻+C→μ⁺μ⁻+X
Pπ=225 GeV/c
1.5<Mμμ<2.0
(1-X)^3.3±.2
2.0<Mμμ<2.7
(1-X)^2.3±.1
2.7<Mμμ<3.5
(1-X)^2.22±0.5
3.5<Mμμ<4.0
(1-X)^1.6±.1
4.0<Mμμ<5.0
(1-X)^1.3±.2
5.0<Mμμ<6.5
(1-X)^1.4±.3
dσ/dX [picobarns nucleus (Xf unit)^-1]
Xf

Figure 5-16.

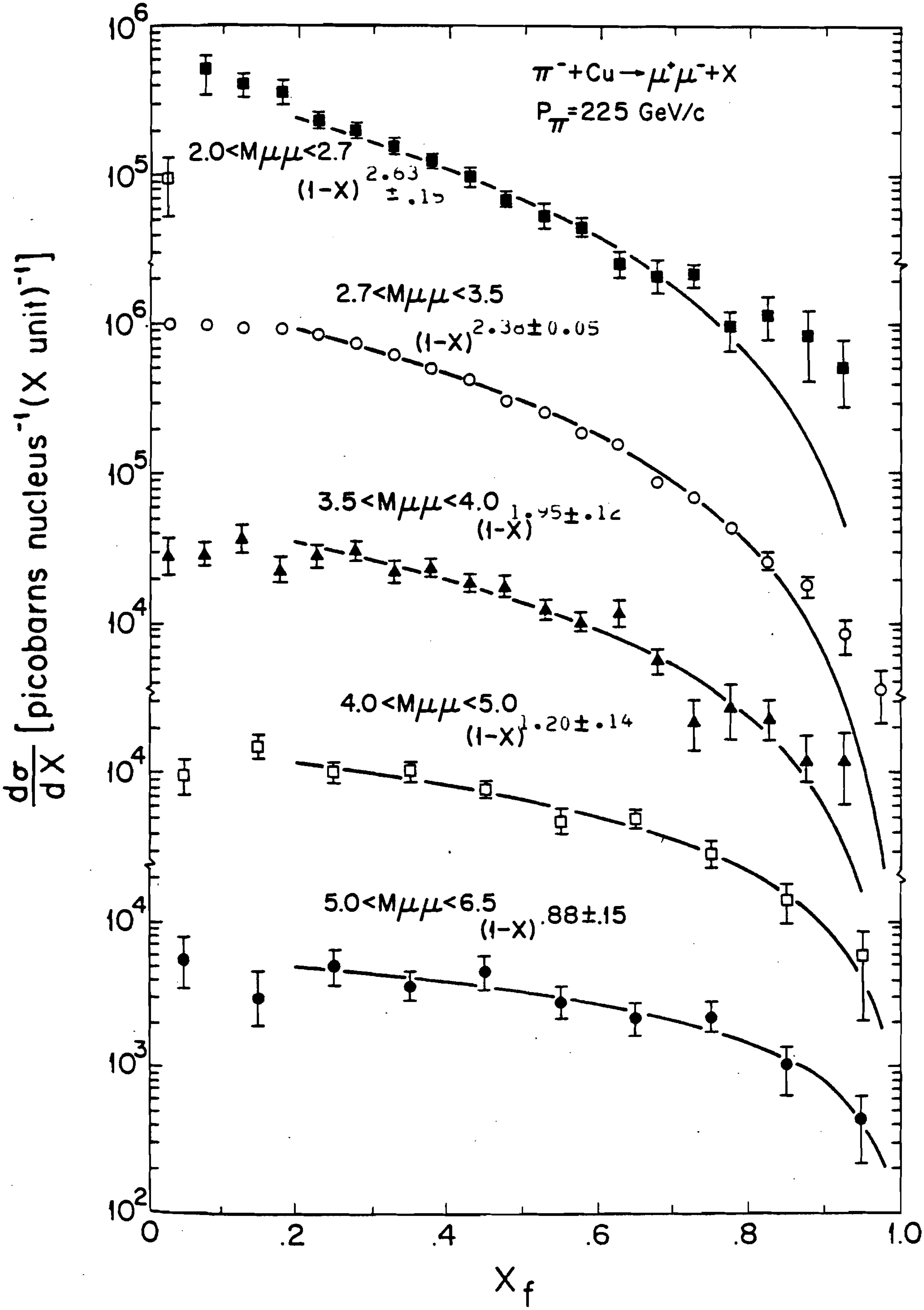
π⁻+Cu→μ⁺μ⁻+X
Pπ=225 GeV/c
2.0<Mμμ<2.7
(1-X) 2.63 ±.15
2.7<Mμμ<3.5
(1-X)2.38±0.05
3.5<Mμμ<4.0
(1-X)1.95±.12
4.0<Mμμ<5.0
(1-X)1.20±.14
5.0<Mμμ<6.5
(1-X).88±.15
dσ/dX [picobarns nucleus⁻¹(X unit)⁻¹]
Xf
0
.2
.4
.6
.8
1.0
10⁶
10⁵
10⁴
10³
10²

Figure 5-17.

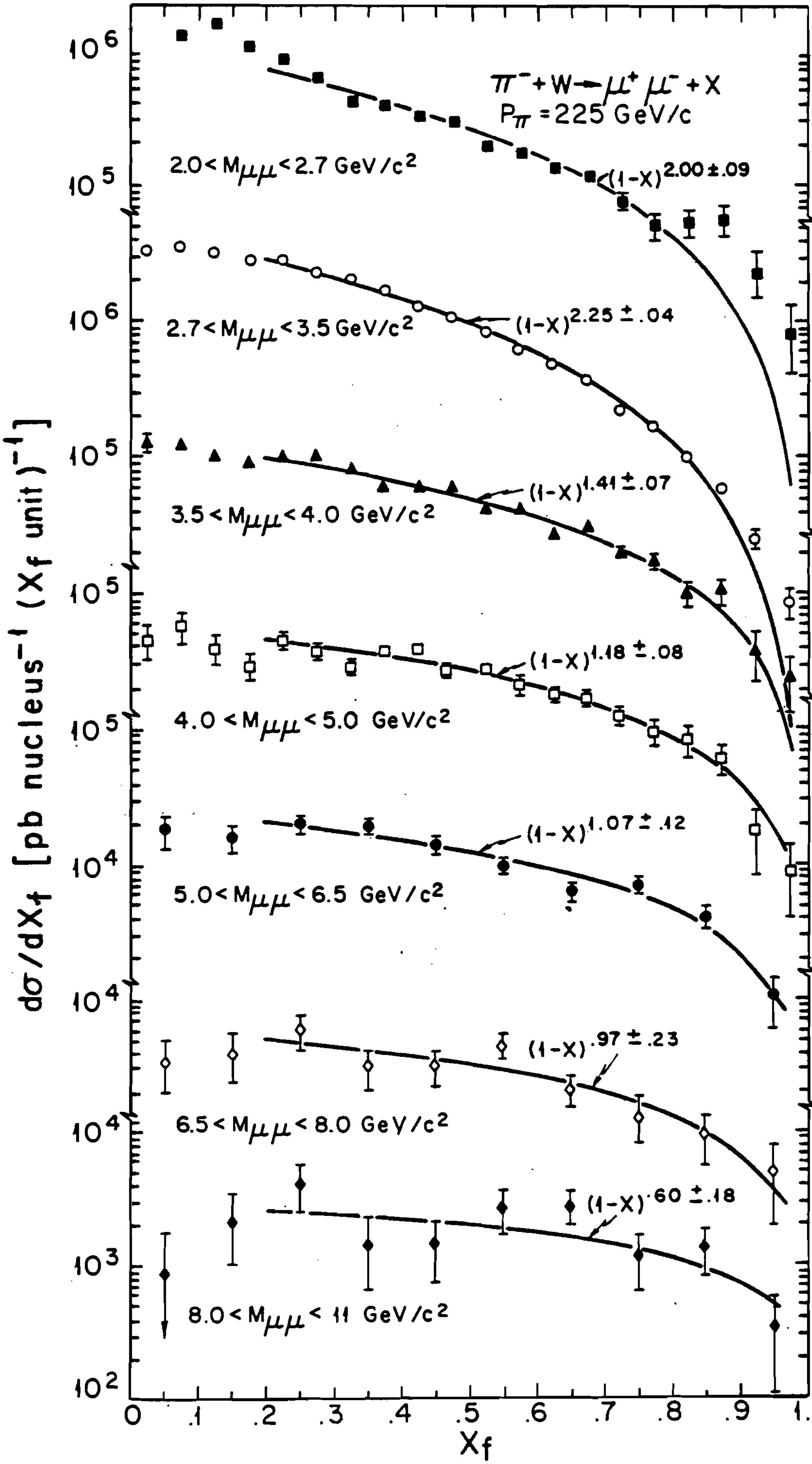

$\pi^- + W \to \mu^+ \mu^- + X$
$P_\pi = 225$ GeV/c
$2.0 < M_{\mu\mu} < 2.7$ GeV/c^2
$(1-X)^{2.00 \pm .09}$
$2.7 < M_{\mu\mu} < 3.5$ GeV/c^2
$(1-X)^{2.25 \pm .04}$
$3.5 < M_{\mu\mu} < 4.0$ GeV/c^2
$(1-X)^{1.41 \pm .07}$
$4.0 < M_{\mu\mu} < 5.0$ GeV/c^2
$(1-X)^{1.18 \pm .08}$
$5.0 < M_{\mu\mu} < 6.5$ GeV/c^2
$(1-X)^{1.07 \pm .12}$
$6.5 < M_{\mu\mu} < 8.0$ GeV/c^2
$(1-X)^{.97 \pm .23}$
$8.0 < M_{\mu\mu} < 11$ GeV/c^2
$(1-X)^{.60 \pm .18}$
$d\sigma/dX_f$ [pb nucleus^{-1} (X_f unit)$^{-1}$]
X_f

Figure 5-18.

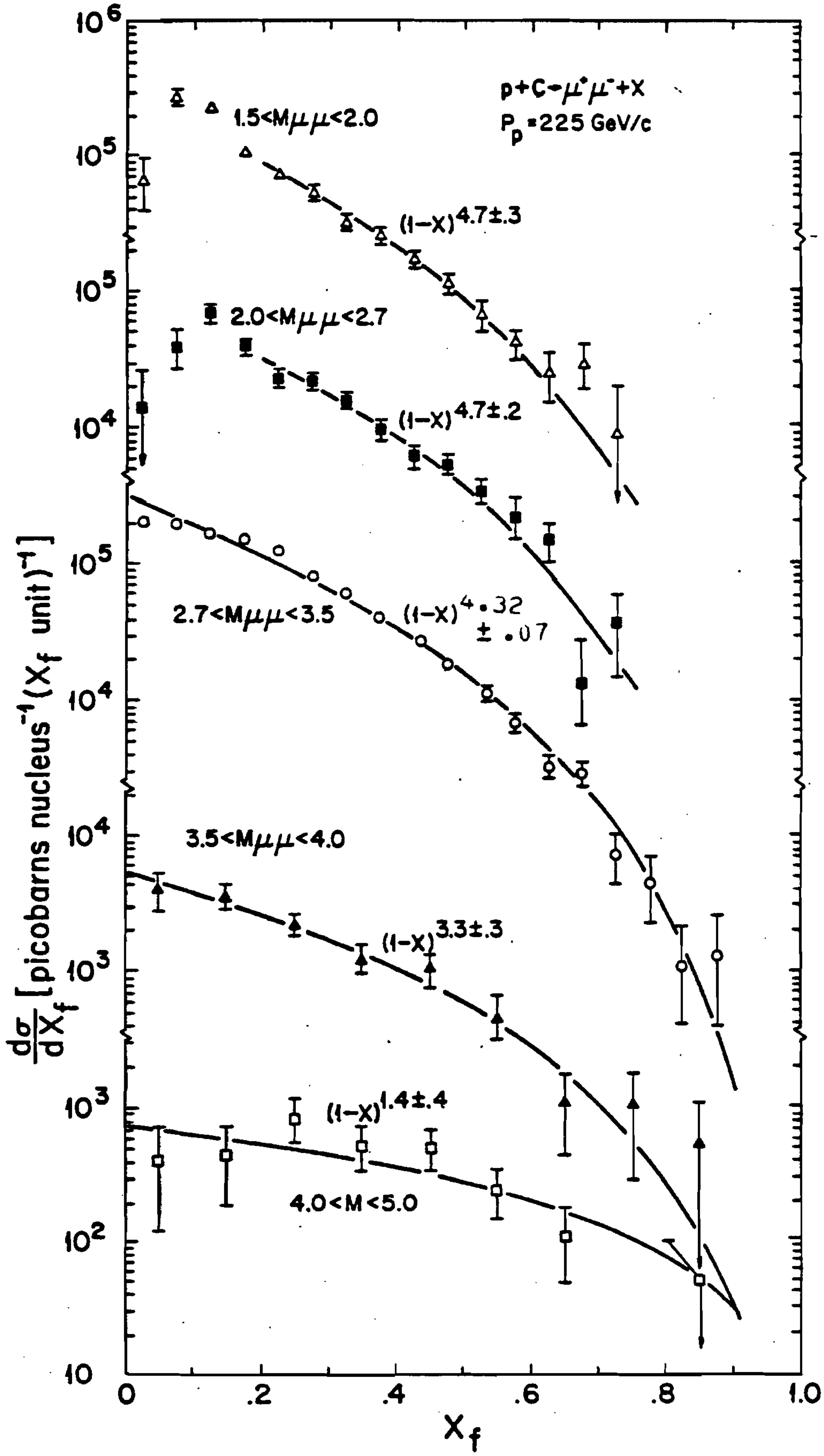
p+C→μ⁺μ⁻+X
Pp=225 GeV/c
1.5<Mμμ<2.0
(1-X)^4.7±.3
2.0<Mμμ<2.7
(1-X)^4.7±.2
2.7<Mμμ<3.5
(1-X)^4.32 ±.07
3.5<Mμμ<4.0
(1-X)^3.3±.3
(1-X)^1.4±.4
4.0<M<5.0
dσ/dXf [picobarns nucleus⁻¹ (Xf unit)⁻¹]
Xf

Figure 5-19.

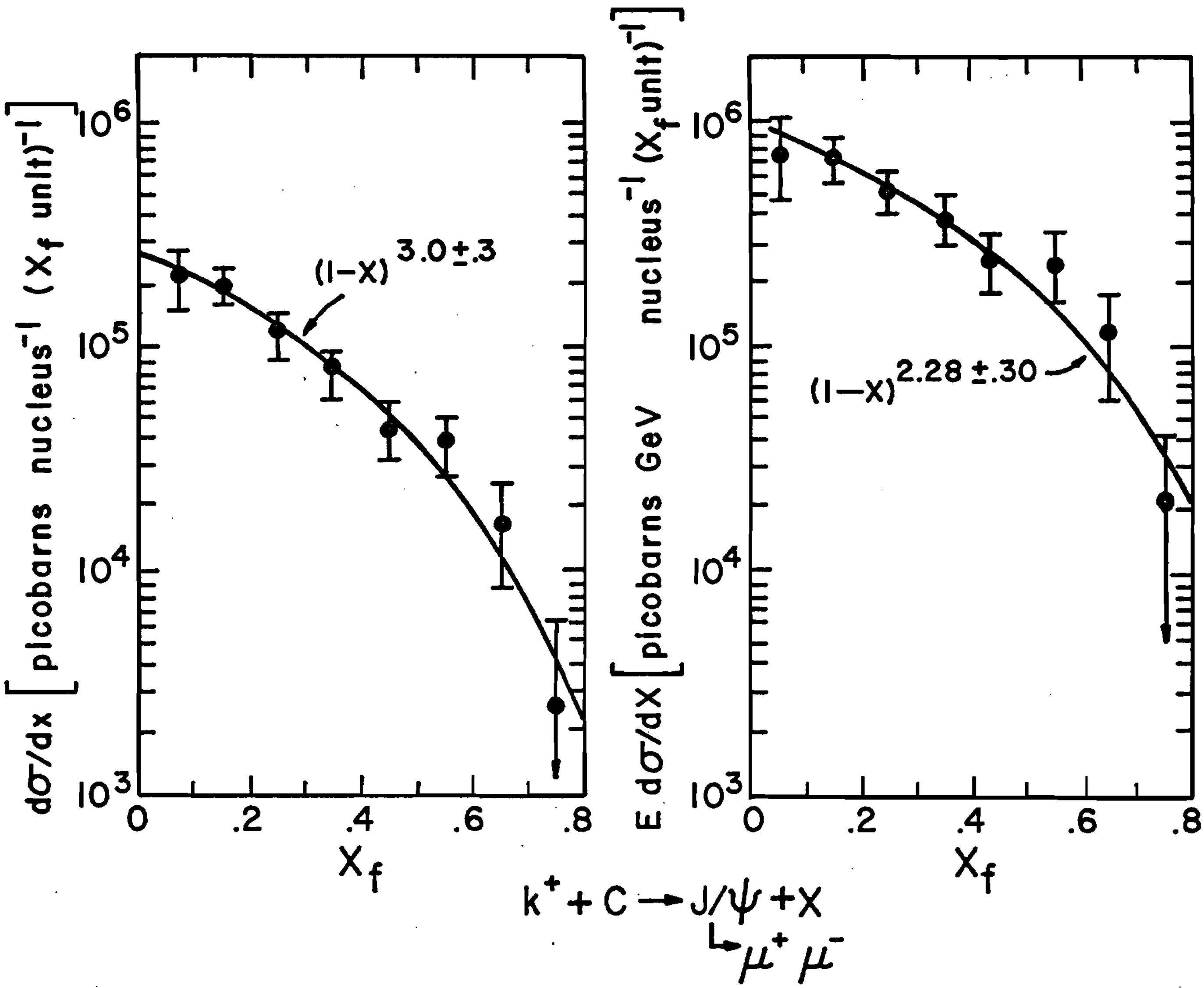

dσ/dx [picobarns nucleus⁻¹ (Xf unit)⁻¹]
(1−X)^3.0±.3
E dσ/dX [picobarns GeV nucleus⁻¹ (Xf unit)⁻¹]
(1−X)^2.28±.30
Xf
k⁺ + C → J/ψ + X
→ μ⁺ μ⁻

Figure 5-20.

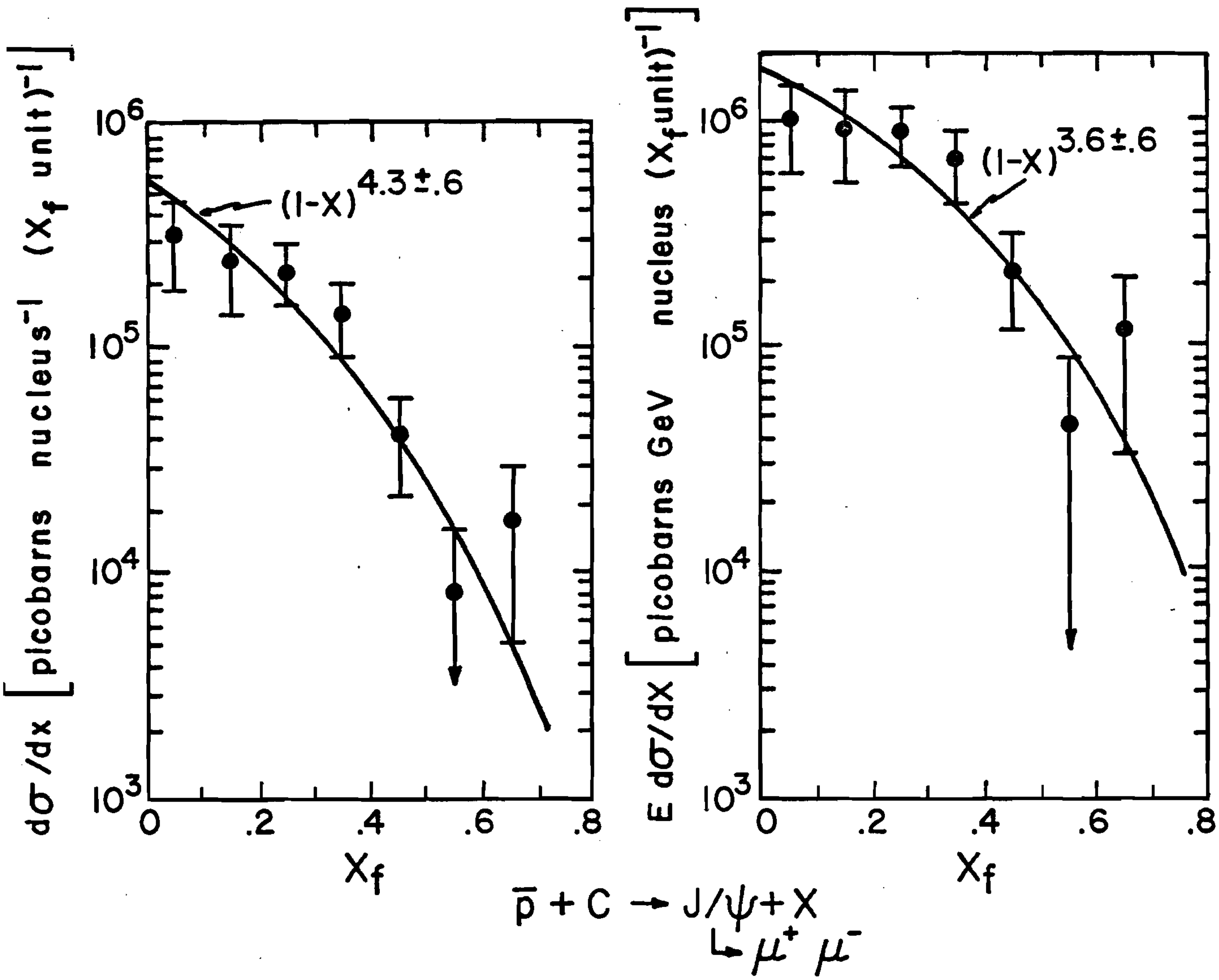

$d\sigma/dx$ [picobarns nucleus^{-1} (X_f unit)$^{-1}$]
$(1-X)^{4.3\pm.6}$
$E\, d\sigma/dX$ [picobarns GeV nucleus (X_f unit)$^{-1}$]
$(1-X)^{3.6\pm.6}$
10^6
10^5
10^4
10^3
0 .2 .4 .6 .8
X_f
$\bar{p} + C \rightarrow J/\psi + X$
$\mu^+ \mu^-$

Figure 5-21.

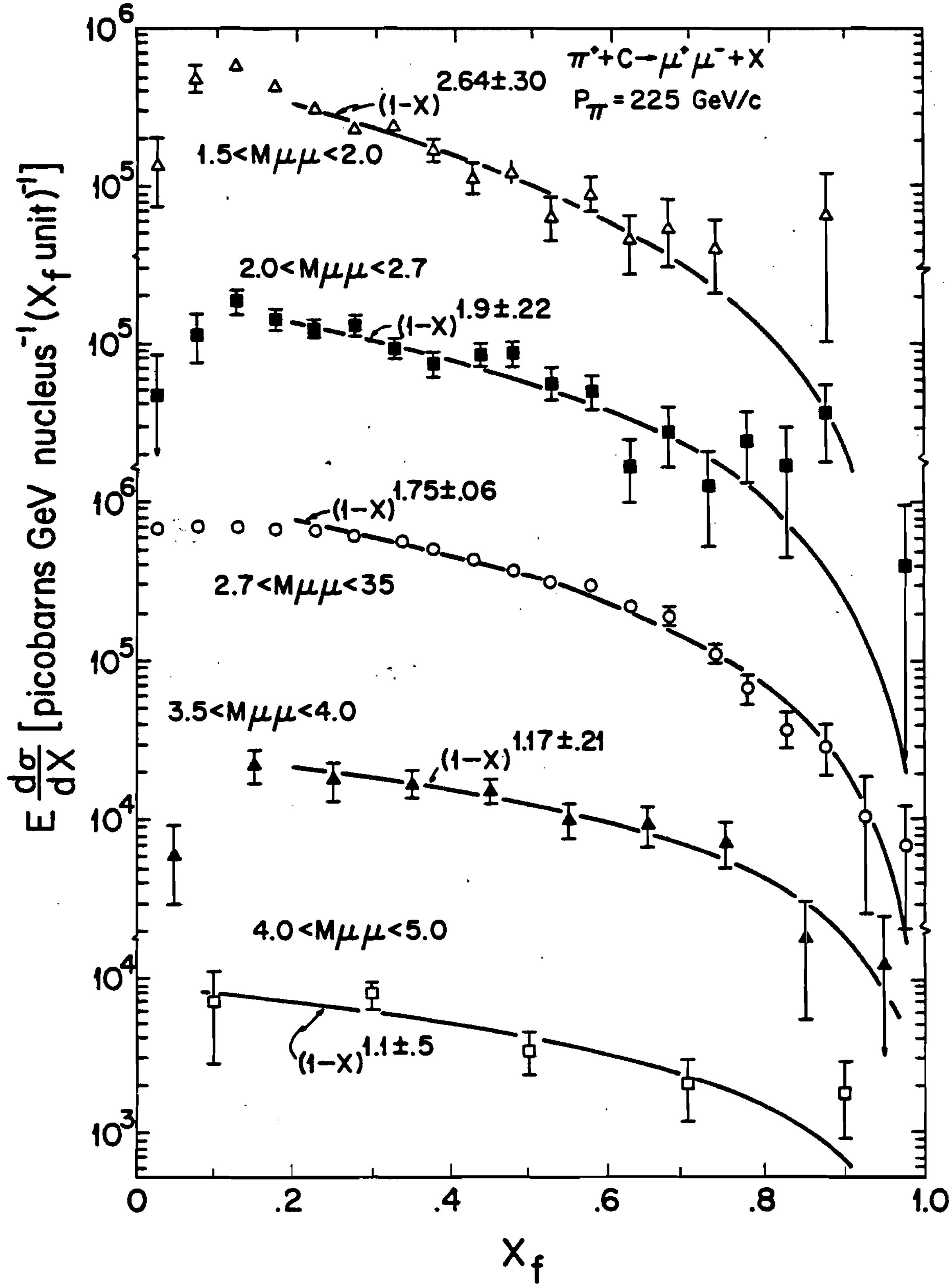
$\pi^+ + C \rightarrow \mu^+\mu^- + X$
$P_\pi = 225$ GeV/c
$(1-X)^{2.64\pm.30}$
$1.5<M\mu\mu<2.0$
$2.0<M\mu\mu<2.7$
$(1-X)^{1.9\pm.22}$
$(1-X)^{1.75\pm.06}$
$2.7<M\mu\mu<35$
$3.5<M\mu\mu<4.0$
$(1-X)^{1.17\pm.21}$
$4.0<M\mu\mu<5.0$
$(1-X)^{1.1\pm.5}$
$E\frac{d\sigma}{dX}$ [picobarns GeV nucleus^{-1}(X_f unit)$^{-1}$]
X_f
0
.2
.4
.6
.8
1.0
10^6
10^5
10^4
10^3

Figure 5-22.

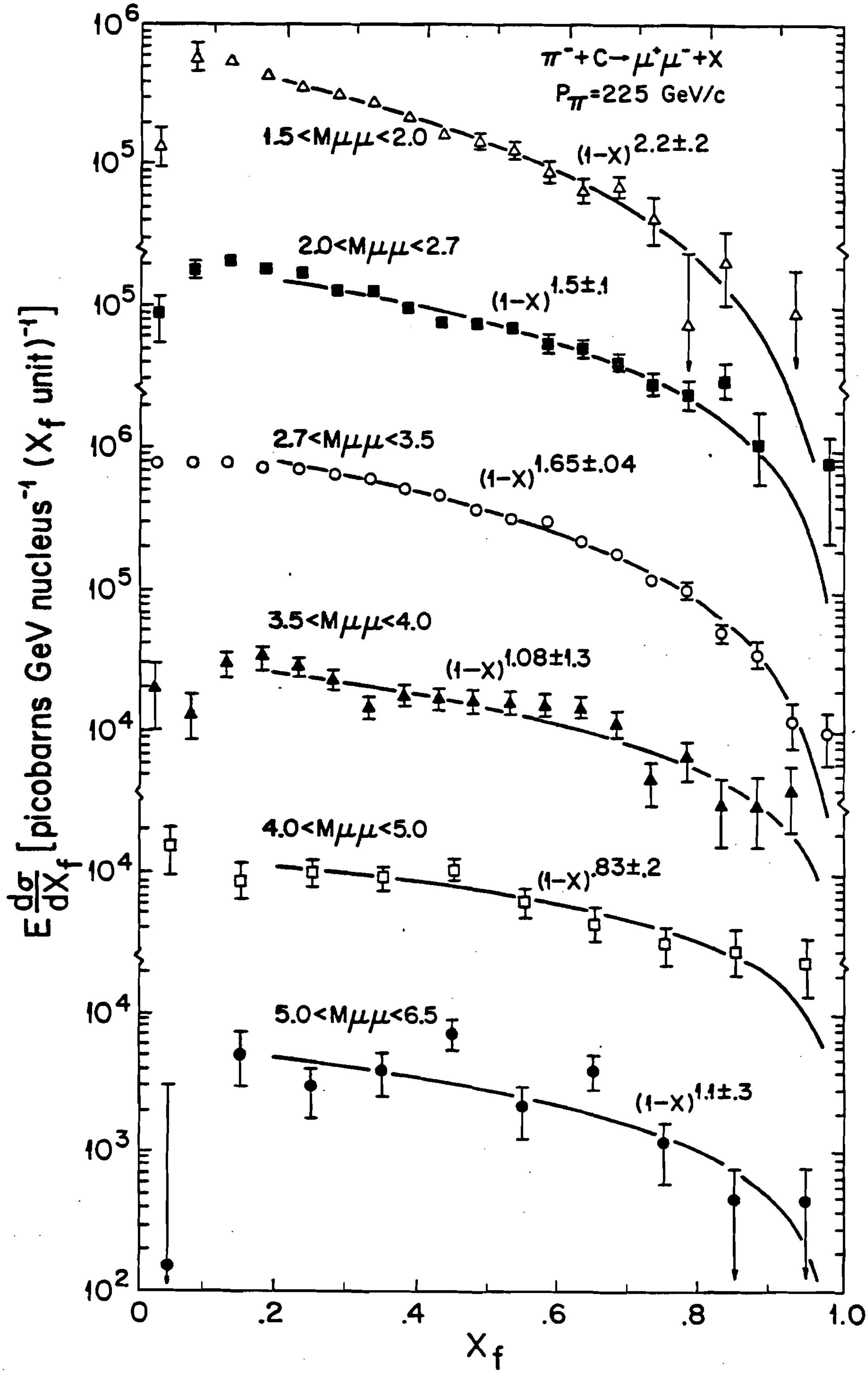

$\pi^- + C \to \mu^+\mu^- + X$
$P_\pi = 225$ GeV/c
$1.5 < M\mu\mu < 2.0$
$(1-X)^{2.2\pm.2}$
$2.0 < M\mu\mu < 2.7$
$(1-X)^{1.5\pm.1}$
$2.7 < M\mu\mu < 3.5$
$(1-X)^{1.65\pm.04}$
$3.5 < M\mu\mu < 4.0$
$(1-X)^{1.08\pm1.3}$
$4.0 < M\mu\mu < 5.0$
$(1-X)^{.83\pm.2}$
$5.0 < M\mu\mu < 6.5$
$(1-X)^{1.1\pm.3}$
$E\frac{d\sigma}{dX_f}$ [picobarns GeV nucleus^{-1} (X_f unit)$^{-1}$]
X_f

Figure 5-23.

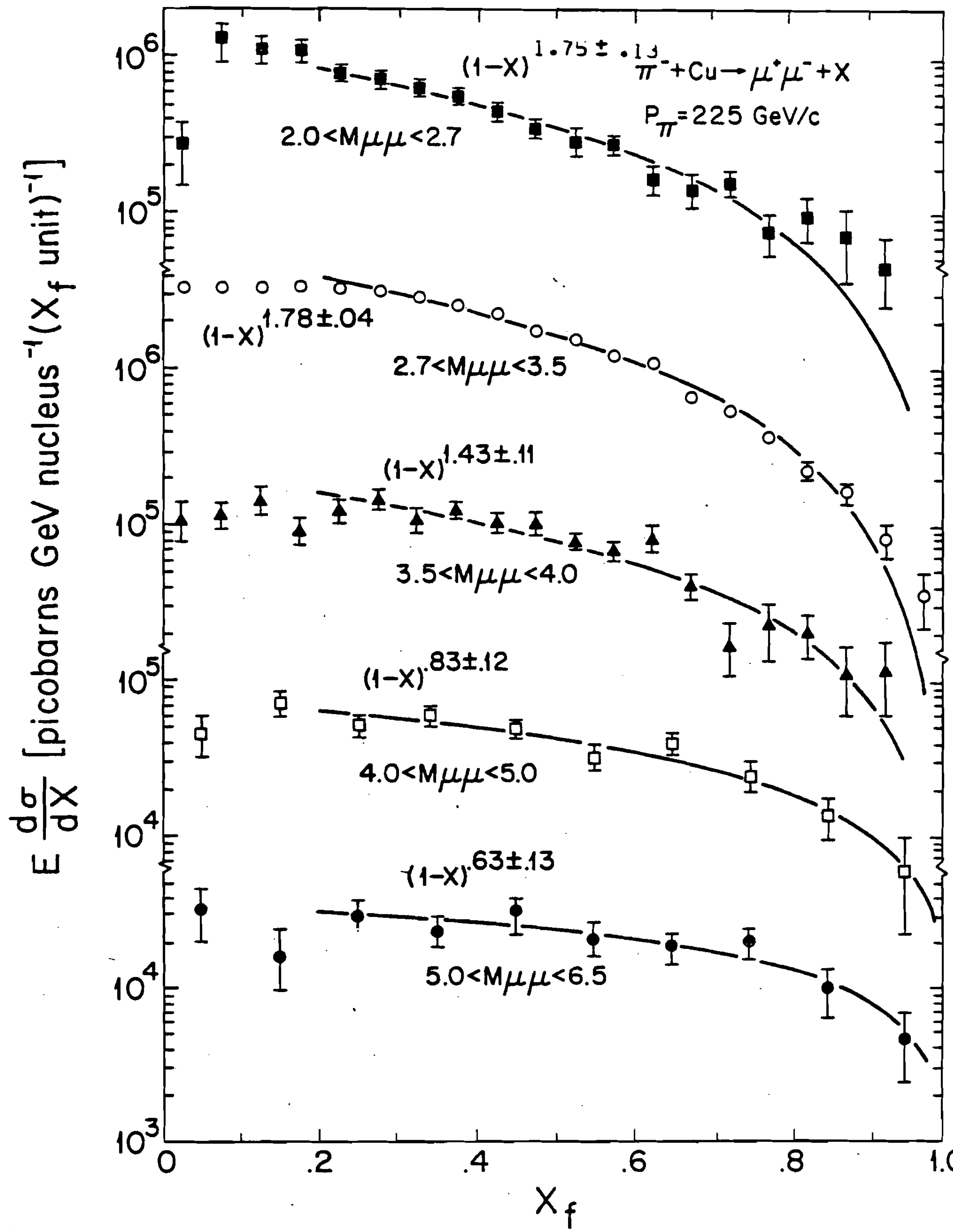

$(1-X)^{1.75\pm.13}$
$\pi^- + Cu \rightarrow \mu^+\mu^- + X$
$P_\pi = 225$ GeV/c
$2.0 < M\mu\mu < 2.7$
$(1-X)^{1.78\pm.04}$
$2.7 < M\mu\mu < 3.5$
$(1-X)^{1.43\pm.11}$
$3.5 < M\mu\mu < 4.0$
$(1-X)^{.83\pm.12}$
$4.0 < M\mu\mu < 5.0$
$(1-X)^{.63\pm.13}$
$5.0 < M\mu\mu < 6.5$
$E\frac{d\sigma}{dX}$ [picobarns GeV nucleus^{-1}(X_f unit)$^{-1}$]
X_f

Figure 5-24.

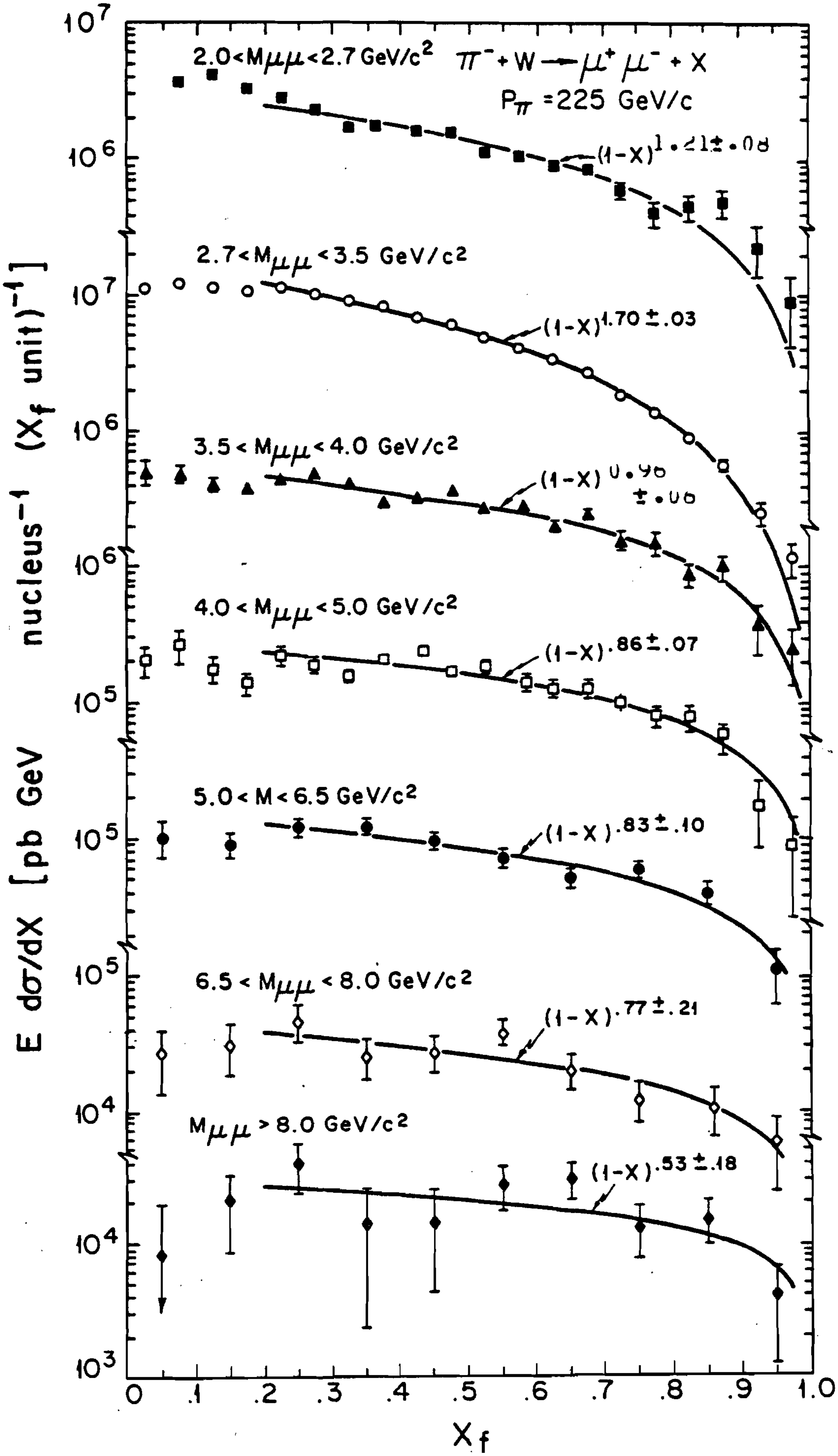

2.0<Mμμ<2.7 GeV/c²
π⁻ + W → μ⁺ μ⁻ + X
Pπ =225 GeV/c
(1-X)^1.21±.08
2.7<Mμμ<3.5 GeV/c²
(1-X)^1.70±.03
3.5<Mμμ<4.0 GeV/c²
(1-X)^0.96 ±.06
4.0<Mμμ<5.0 GeV/c²
(1-X)^.86±.07
5.0<M<6.5 GeV/c²
(1-X)^.83±.10
6.5<Mμμ<8.0 GeV/c²
(1-X)^.77±.21
Mμμ>8.0 GeV/c²
(1-X)^.53±.18
E dσ/dX [pb GeV nucleus⁻¹ (X_f unit)⁻¹]
X_f

Figure 5-25.

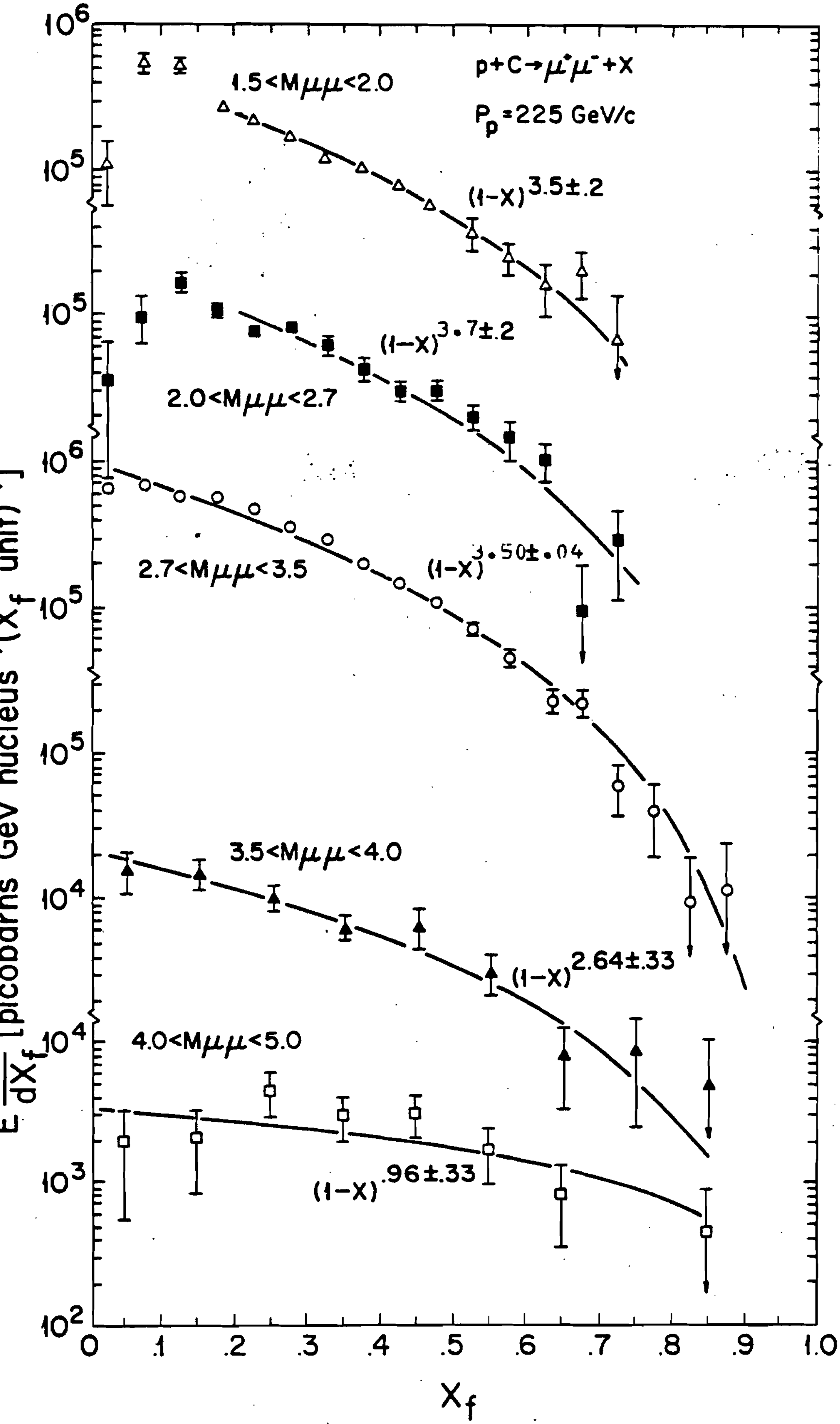
p+C→μ⁺μ⁻+X
P_p=225 GeV/c
1.5<Mμμ<2.0
(1-X)^3.5±.2
2.0<Mμμ<2.7
(1-X)^3.7±.2
2.7<Mμμ<3.5
(1-X)^3.50±.04
3.5<Mμμ<4.0
(1-X)^2.64±.33
4.0<Mμμ<5.0
(1-X)^.96±.33
E dσ/dX_f [picobarns GeV nucleus^-1 (X_f unit)^-1]
X_f

Figure 5-26.

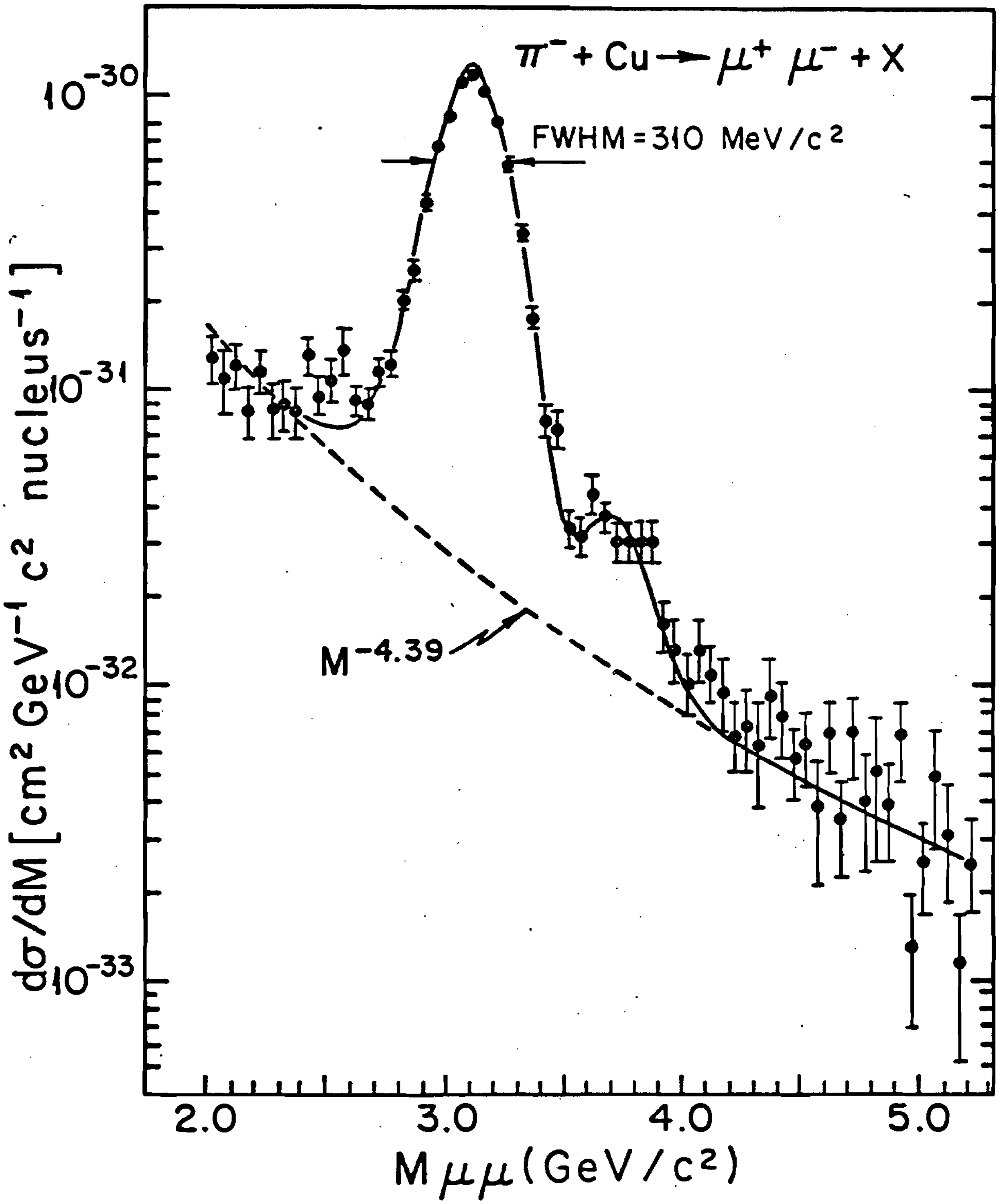

Figure 5-27. Separation of the resonances from the continuum.

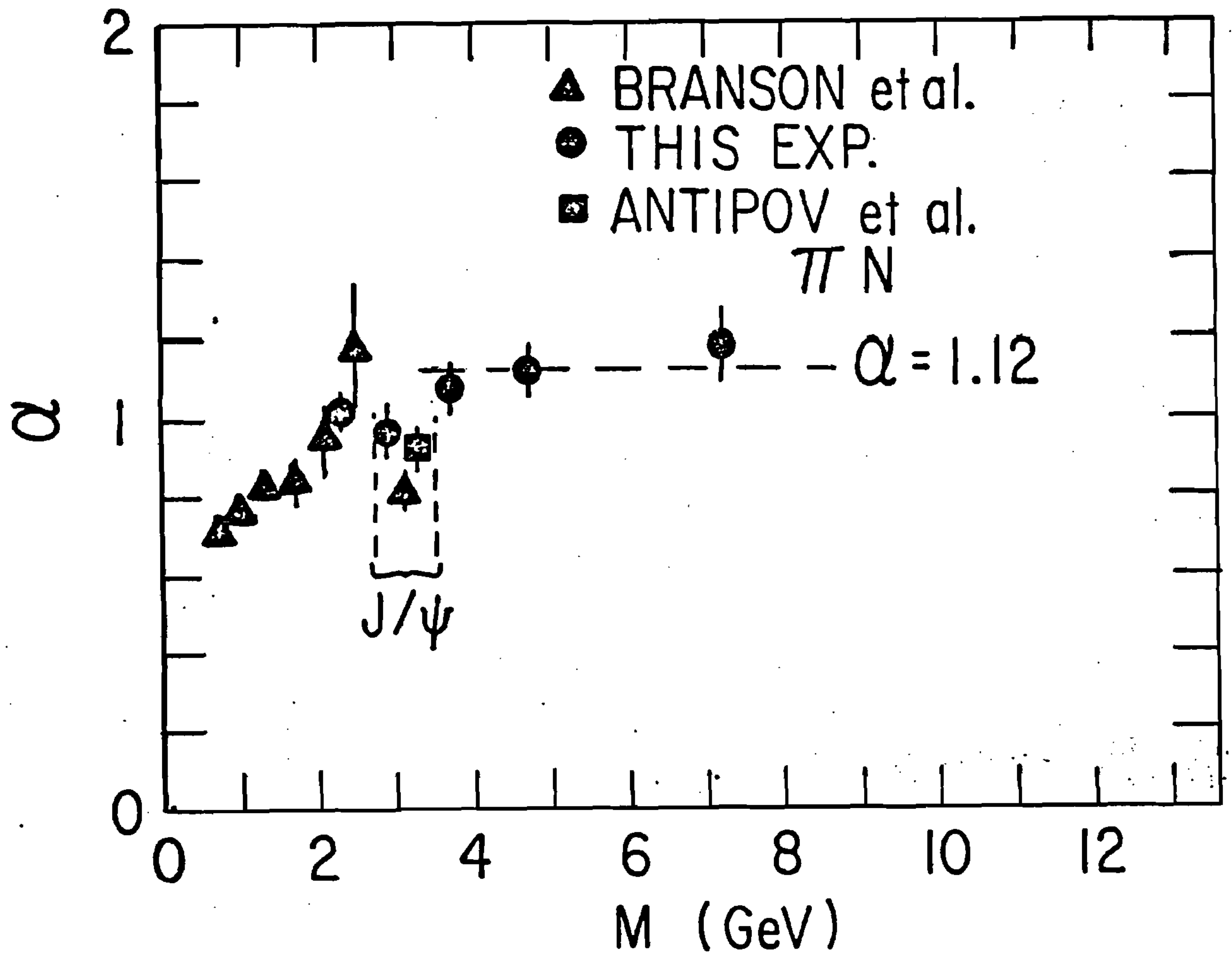

Figure 5-28. Atomic mass number dependence versus mass for pion induced events.

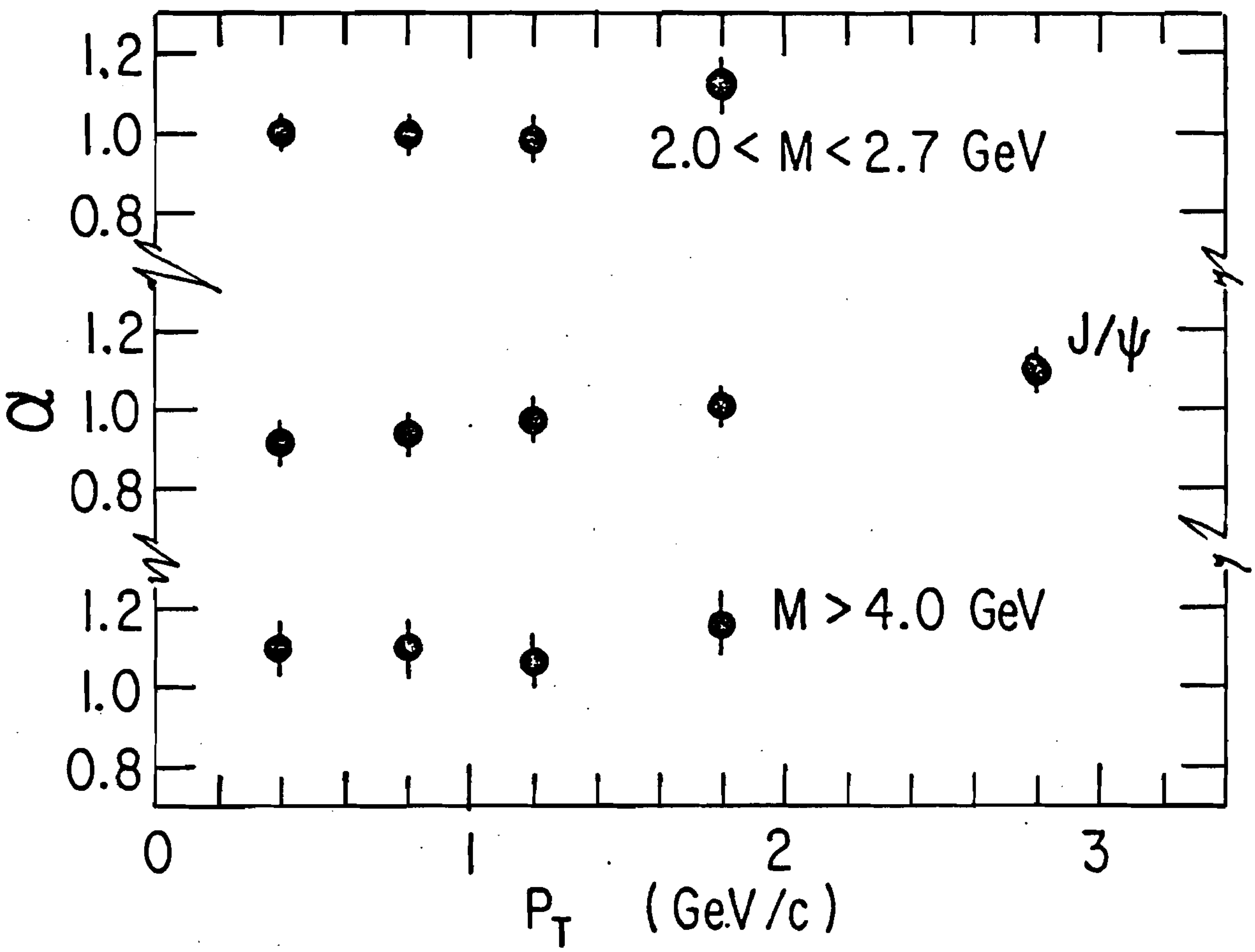

Figure 5-29. Atomic mass number dependence versus p_T.

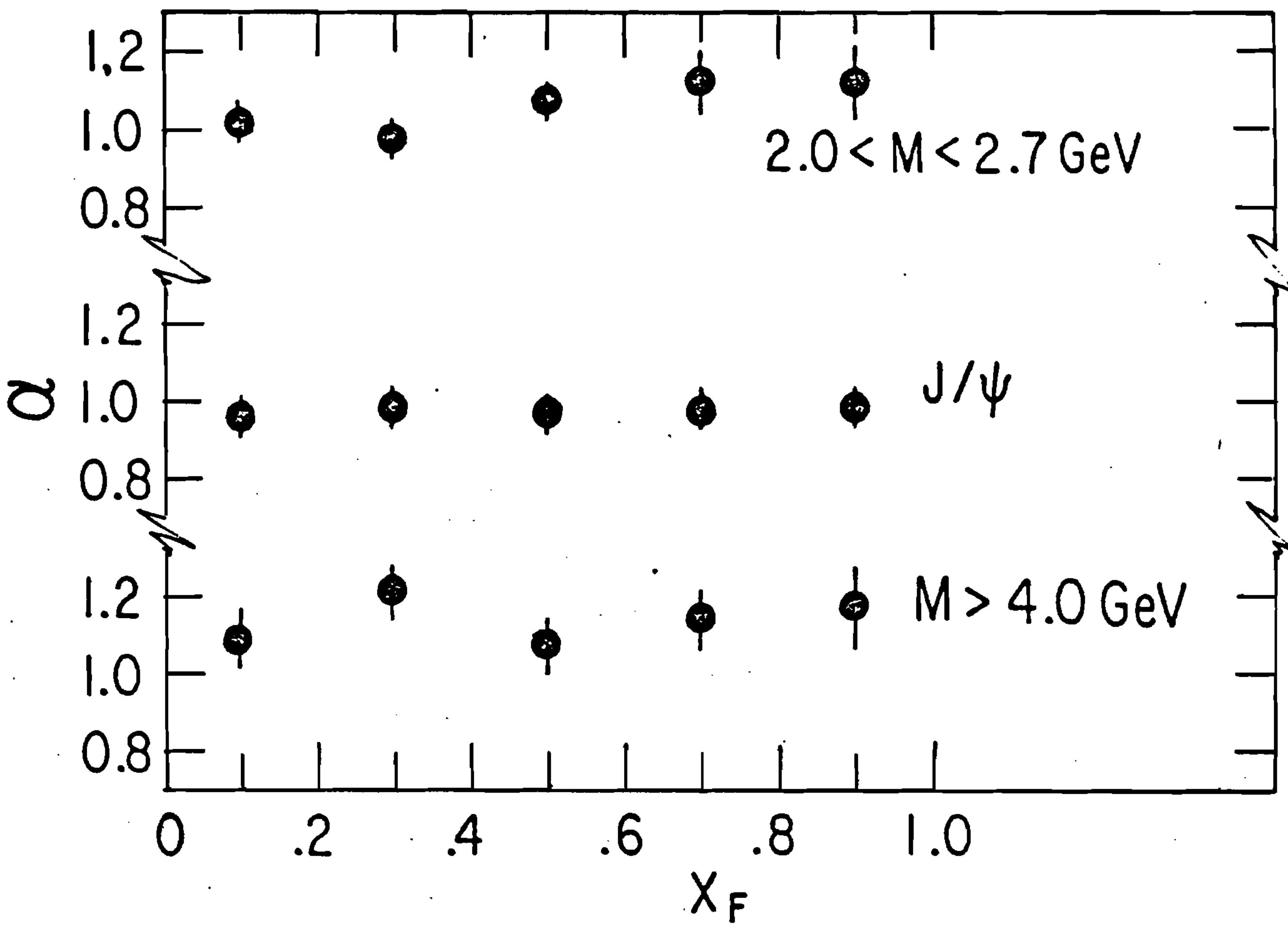

Figure 5-30. Atomic mass number dependence versus x_f.

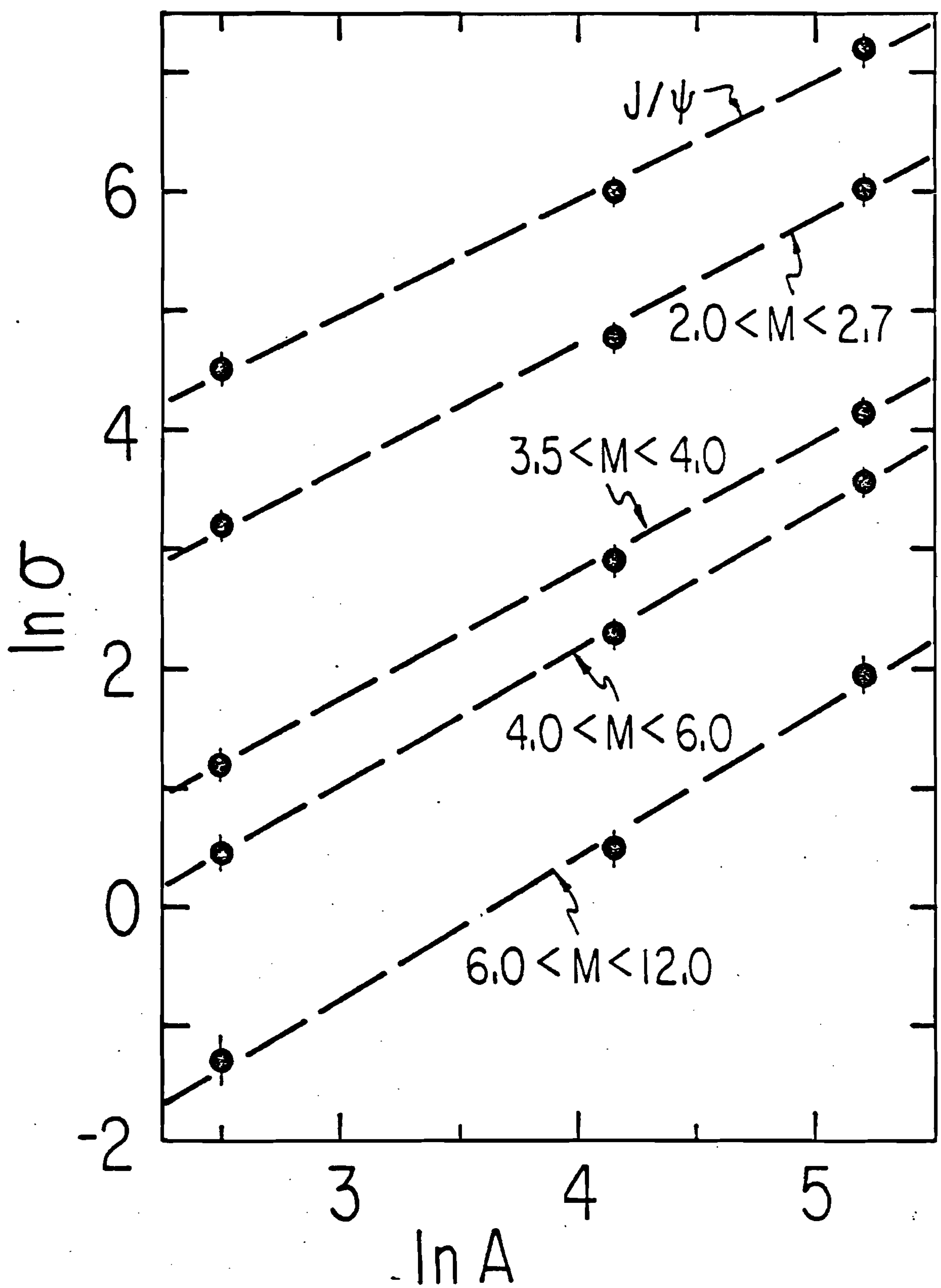

Figure 5-31. Atomic mass number power law fits.

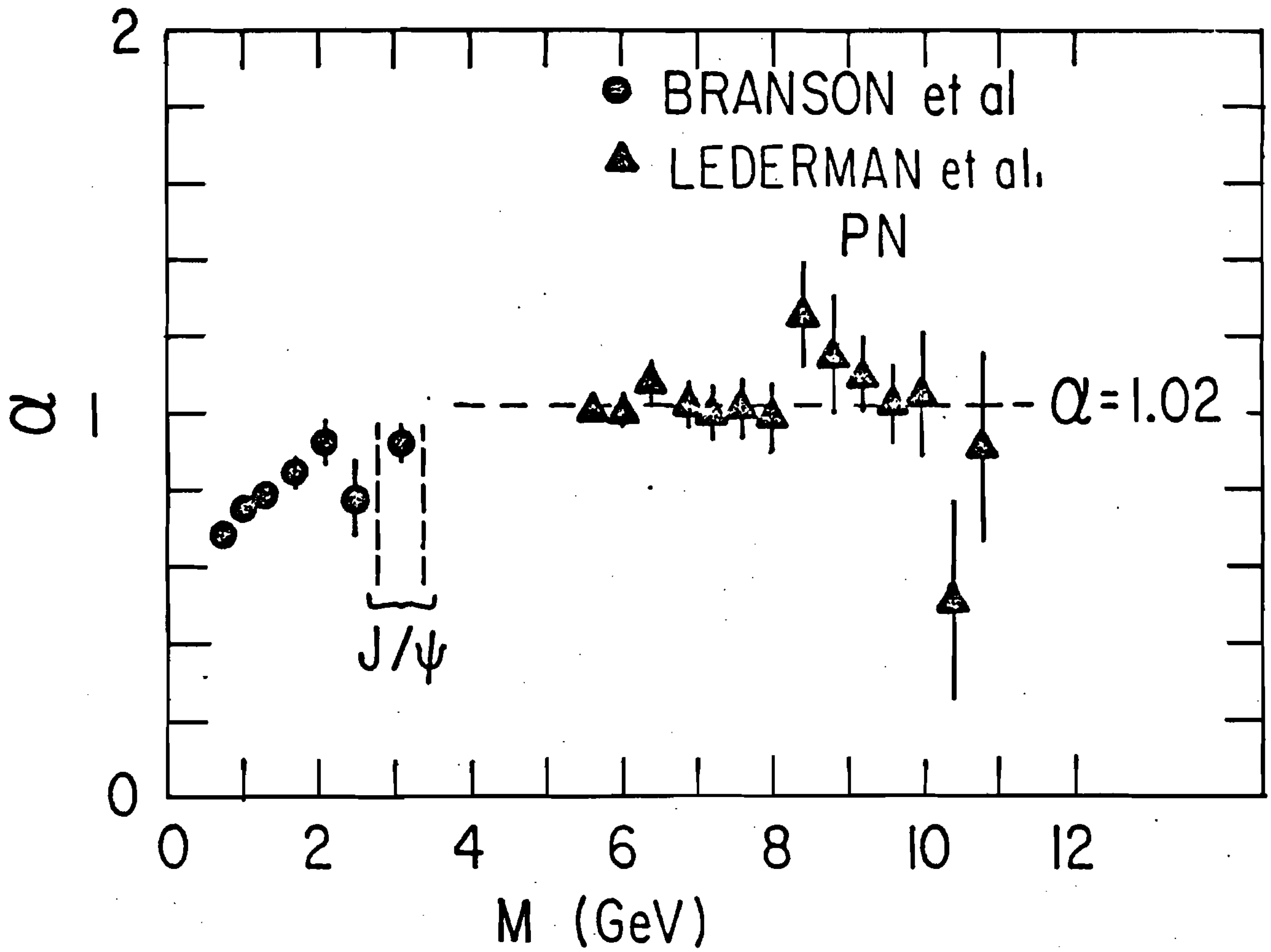

Figure 5-32. Atomic mass number dependence versus mass for proton induced events.

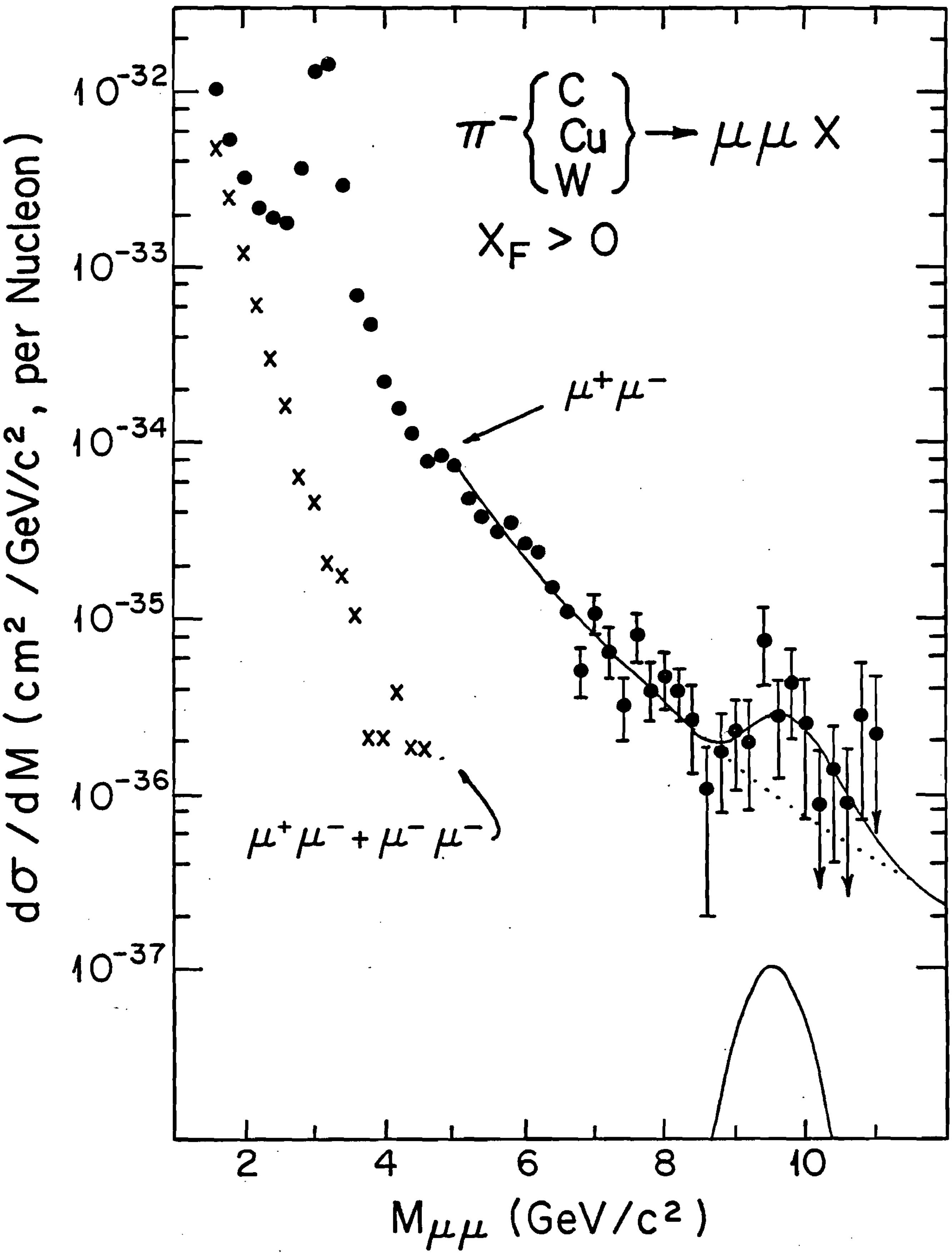

Figure 5-33. Cross section fit for the upsilon.

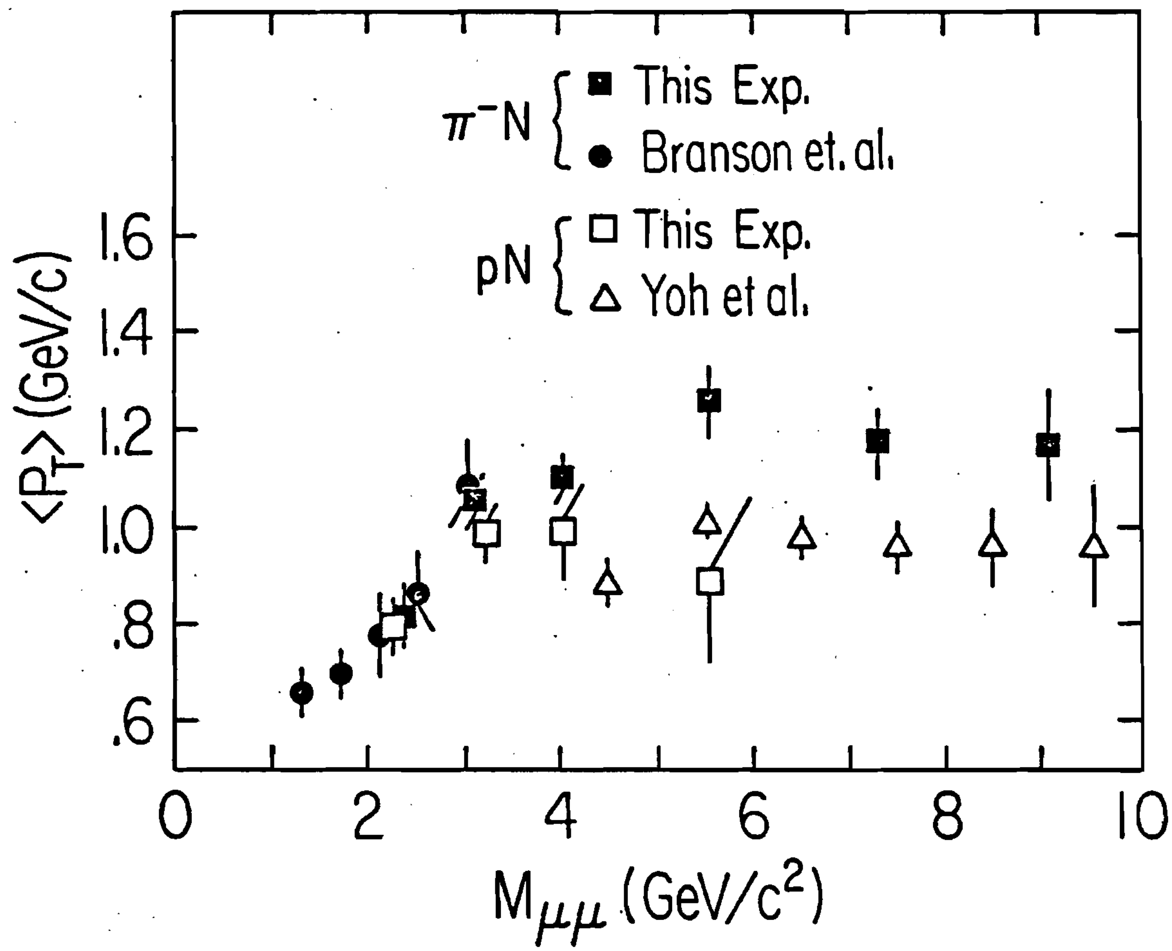

Figure 5-34. Average p_T versus mass.

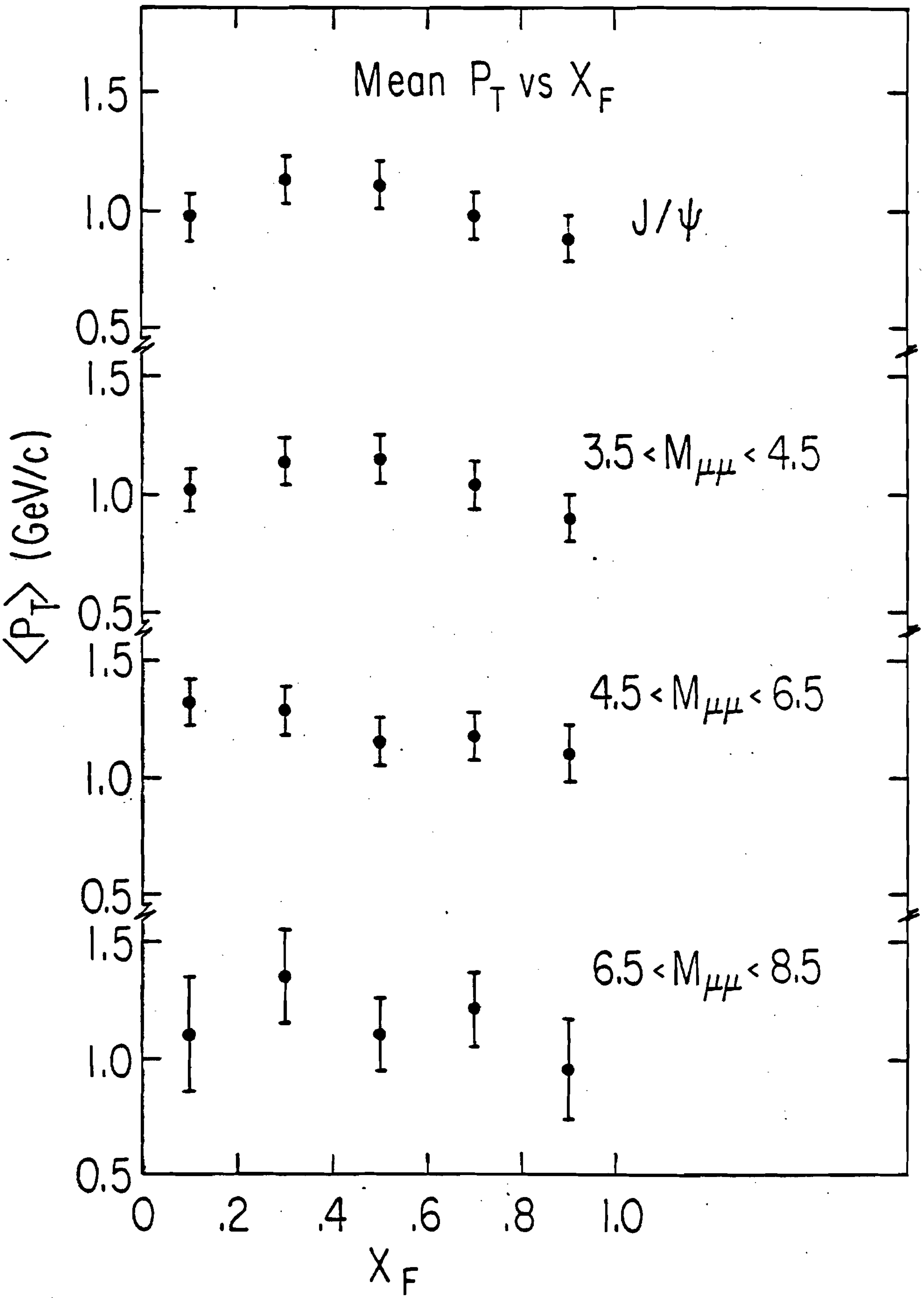

Figure 5-35. Average p_t versus x_f.

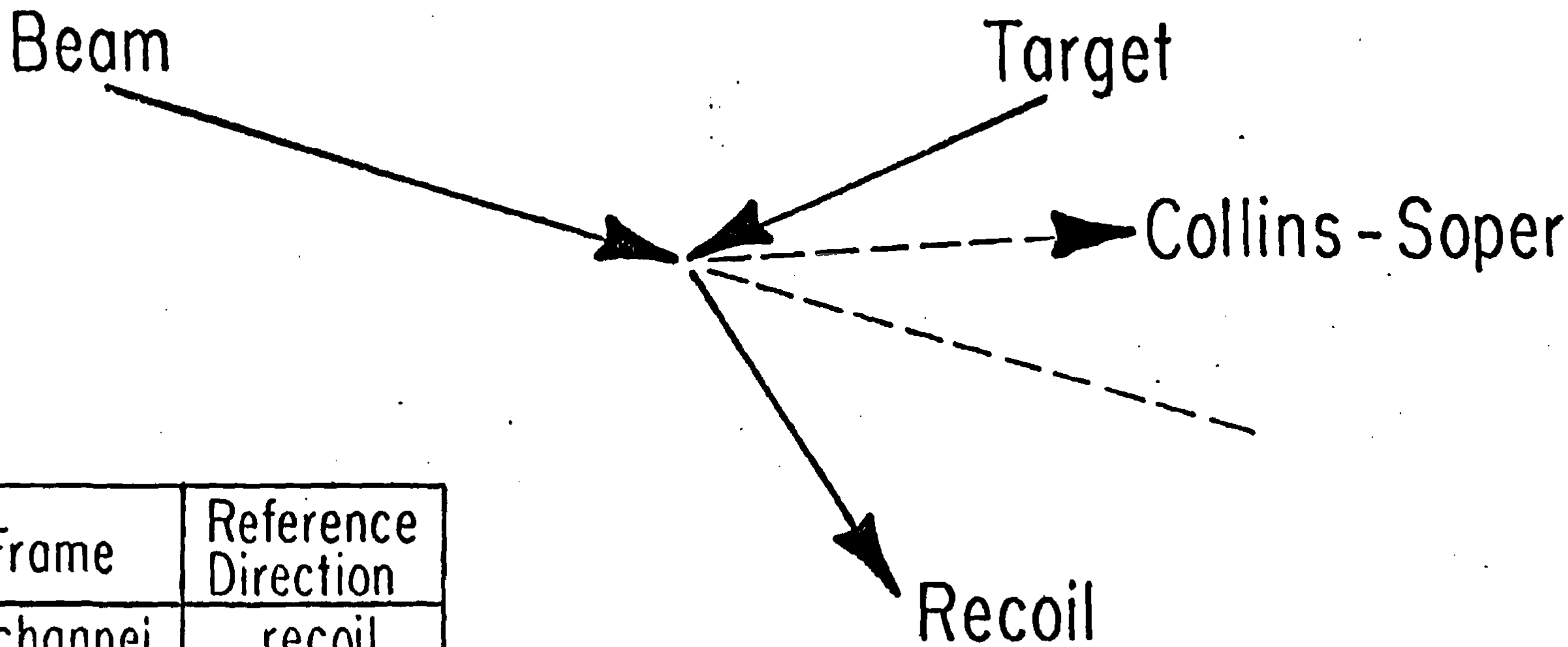

Frame	Reference Direction
s-channel	recoil
t-channel	beam
u-channel	target
Collins-Soper	$\hat{P}_B - \hat{P}_T$

Mu-Pair C.M. System

Figure 5-36. Polar angle definitions.

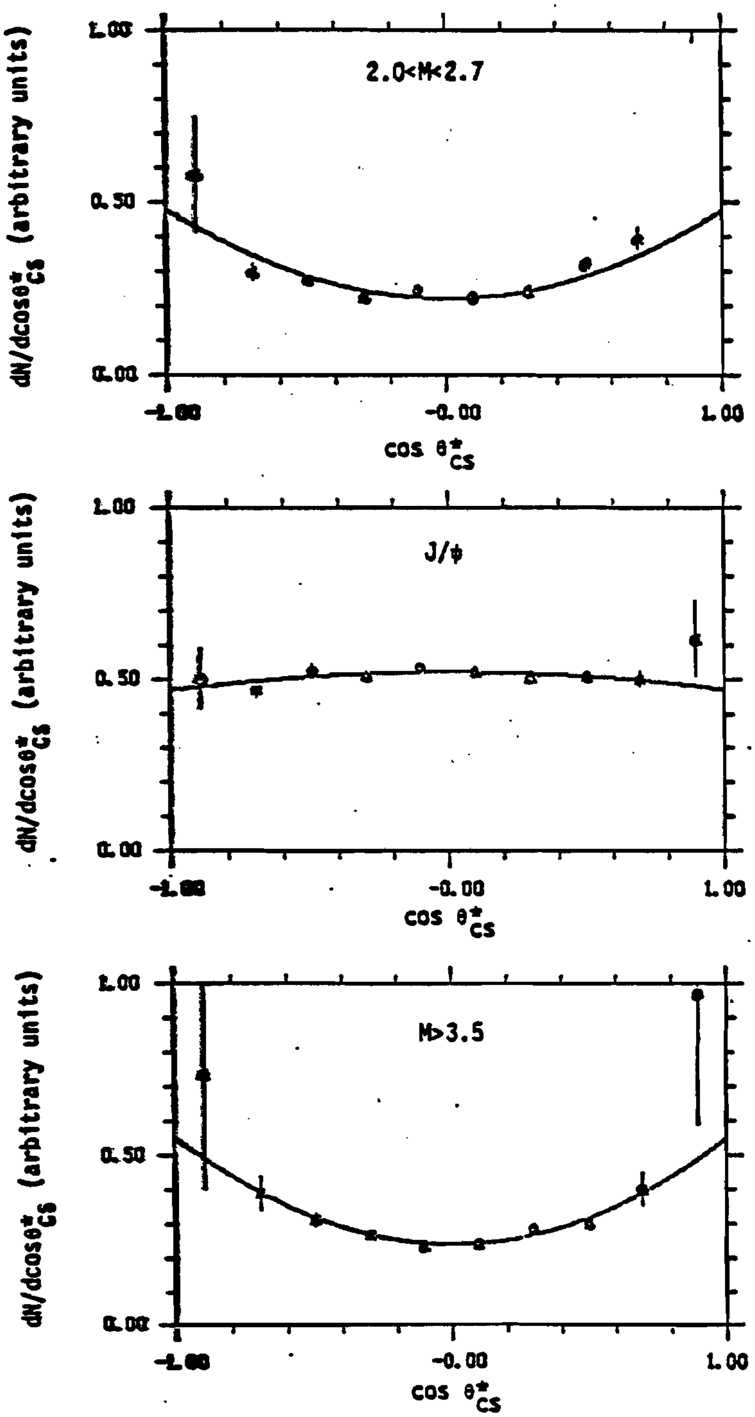

Figure 5-37. Polar angle distributions for the Collins-Soper angle at various masses.

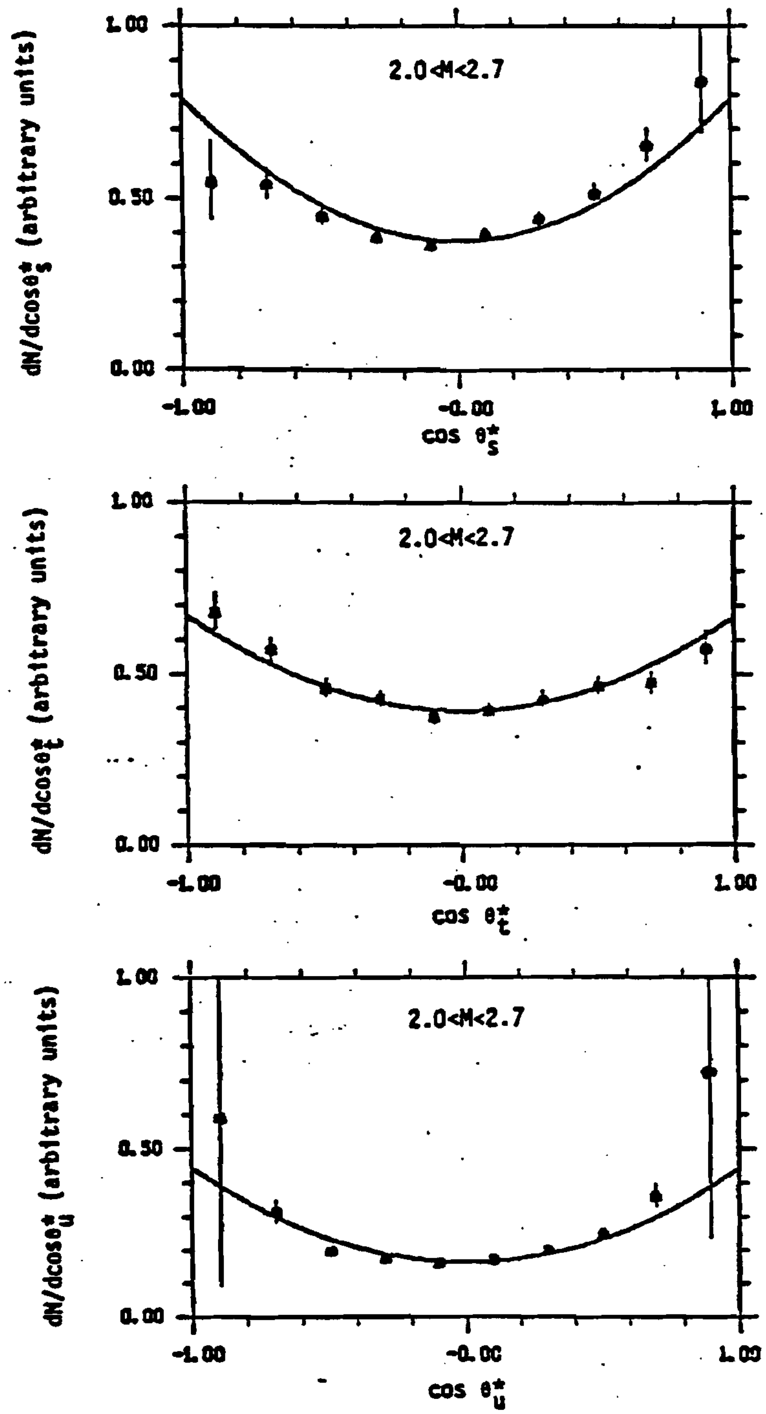

Figure 5-38. Polar angle distributions in s, t, and u channels for $2 < M < 2.7$ GeV/c^2.

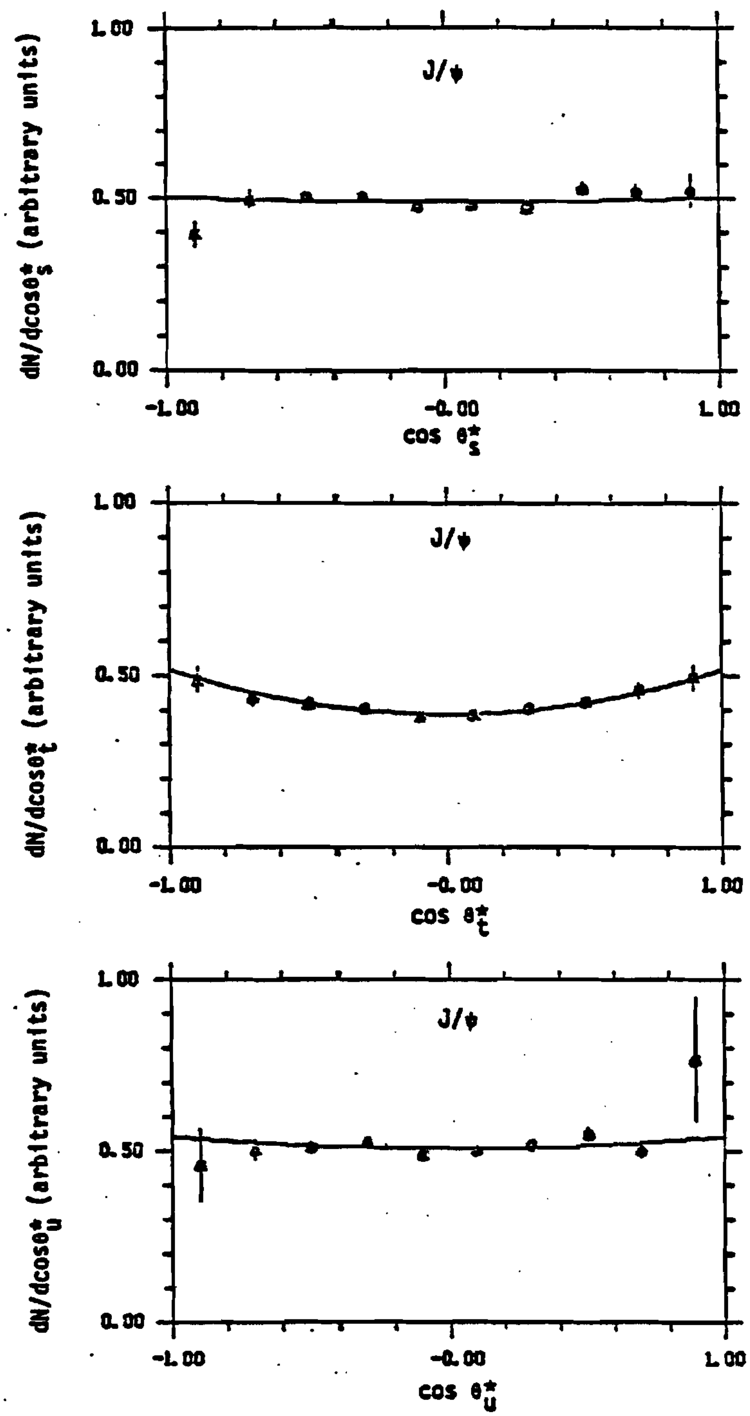

Figure 5-39. Polar angle distributions in s, t, and u channels for the J/Ψ.

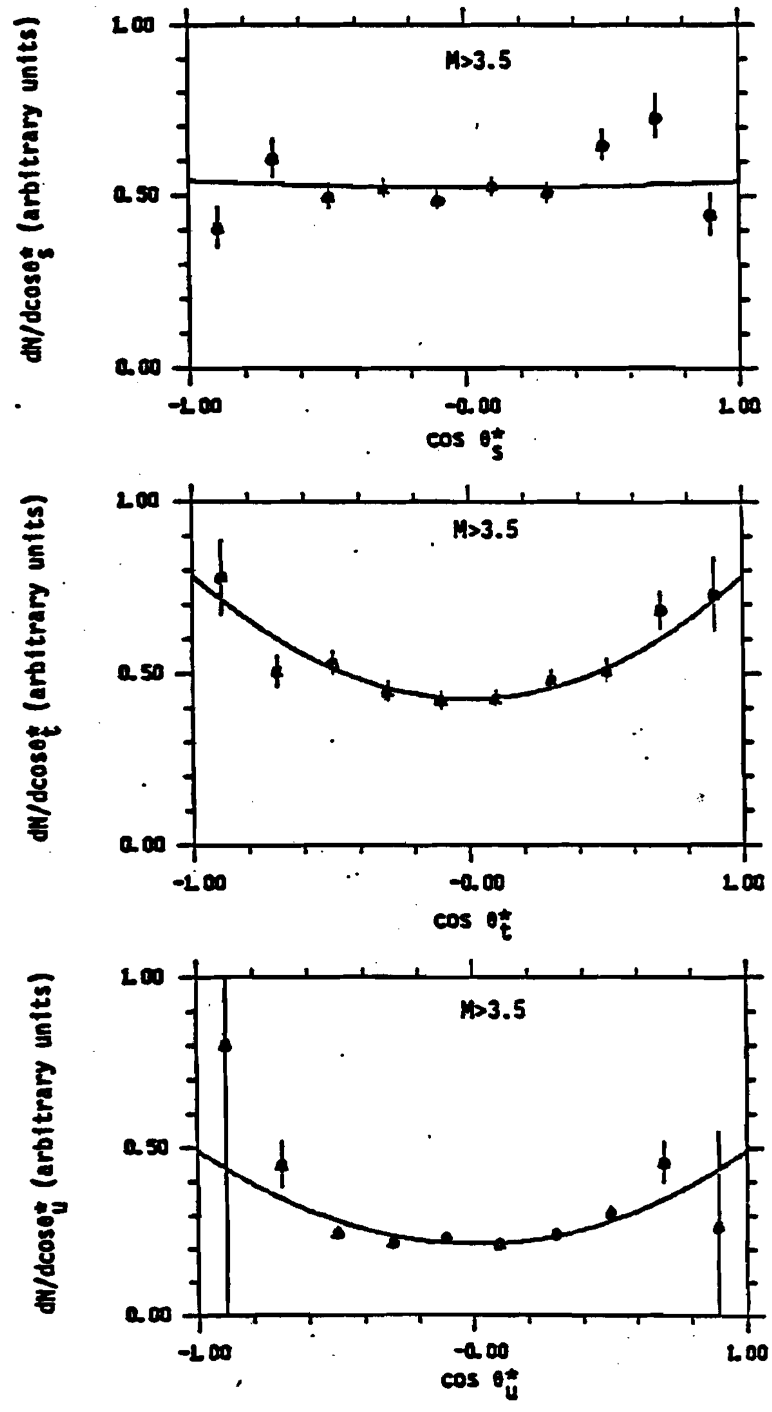

Figure 5-40. Polar angle distributions in s, t, and u channels for M > 3.5 GeV/c^2.

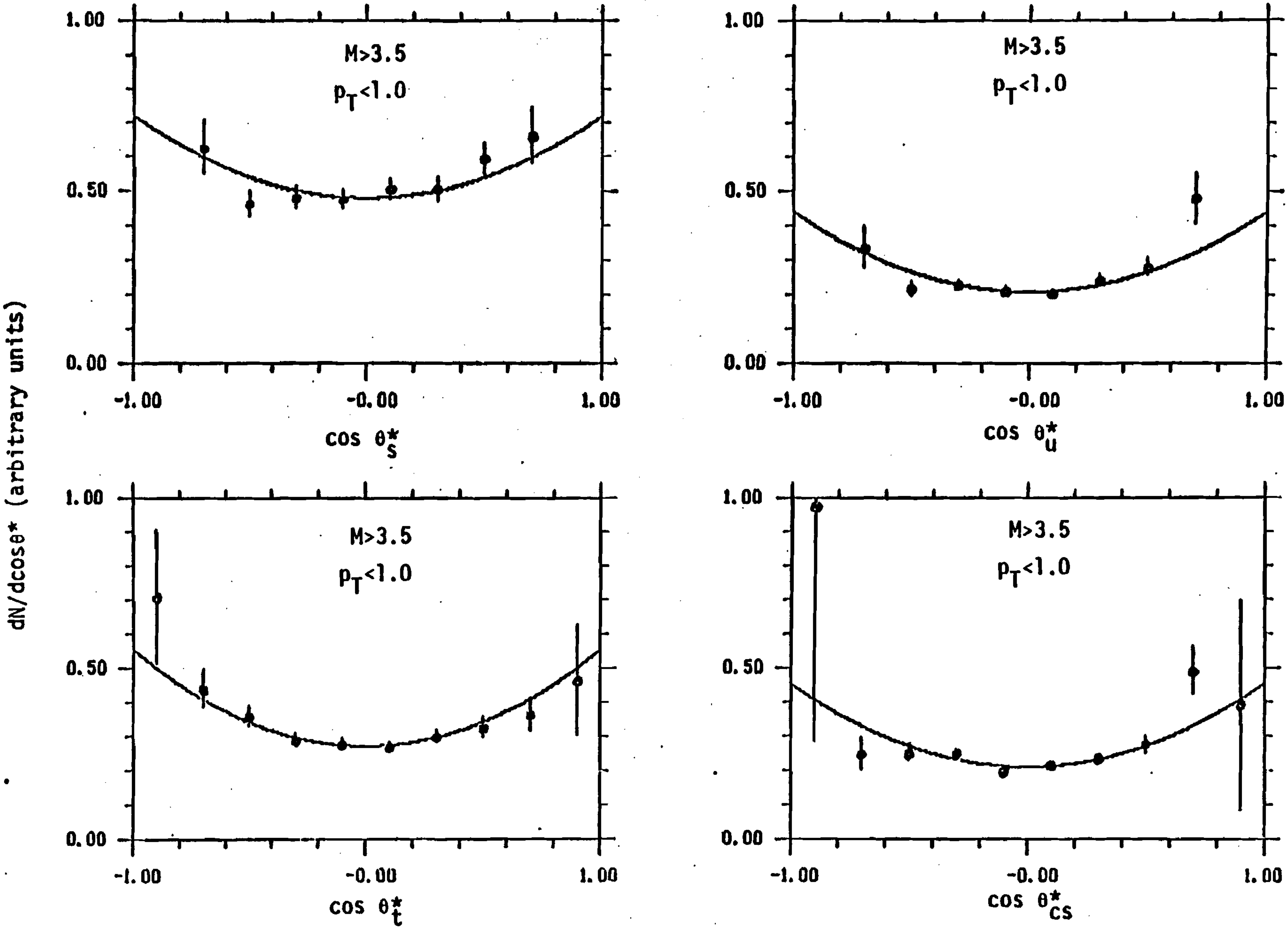

Figure 5-41. Polar angle distributions for p_T < 1.0.

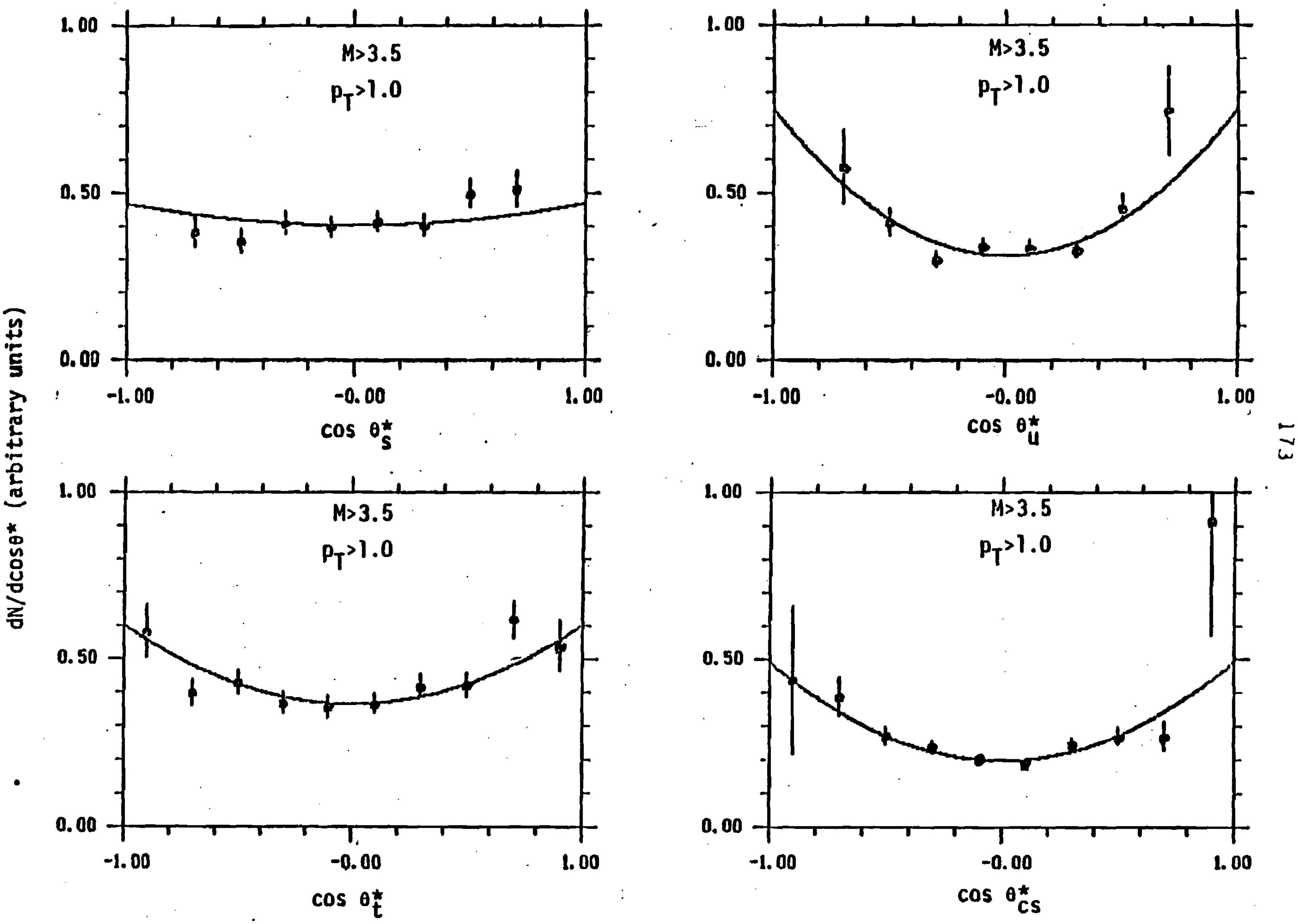

Figure 5-42. Polar angle distributions for $p_T > 1.0$.

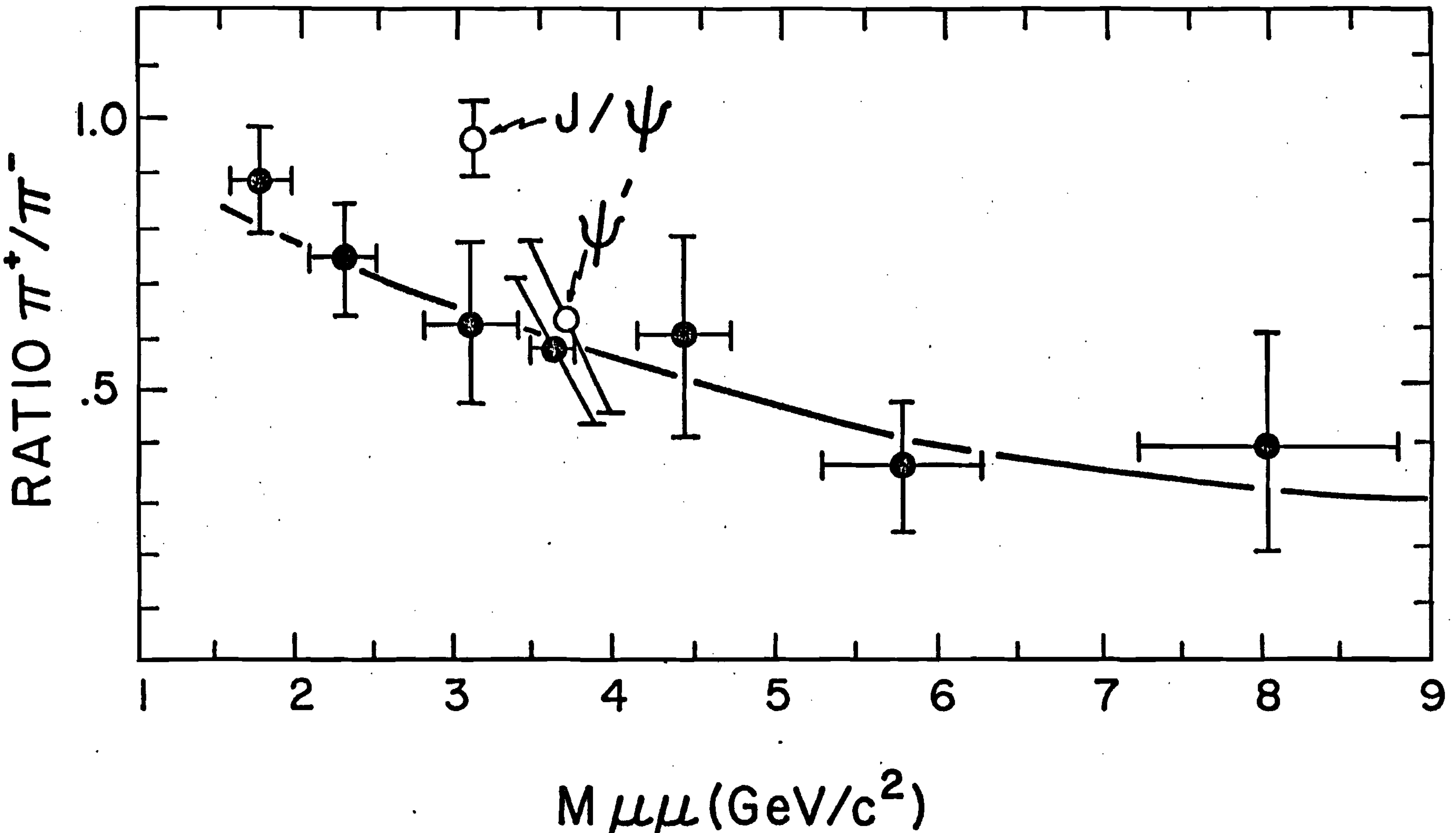

Figure 5-43. Production ratio of π^+ induced dimuons to π^- induced dimuons on carbon as a function of mass. Curve is calculated using our pion structure function, the nucleon valence quark distribution of Buras and Gaemers, and the nucleon sea quark distribution of CFSB.

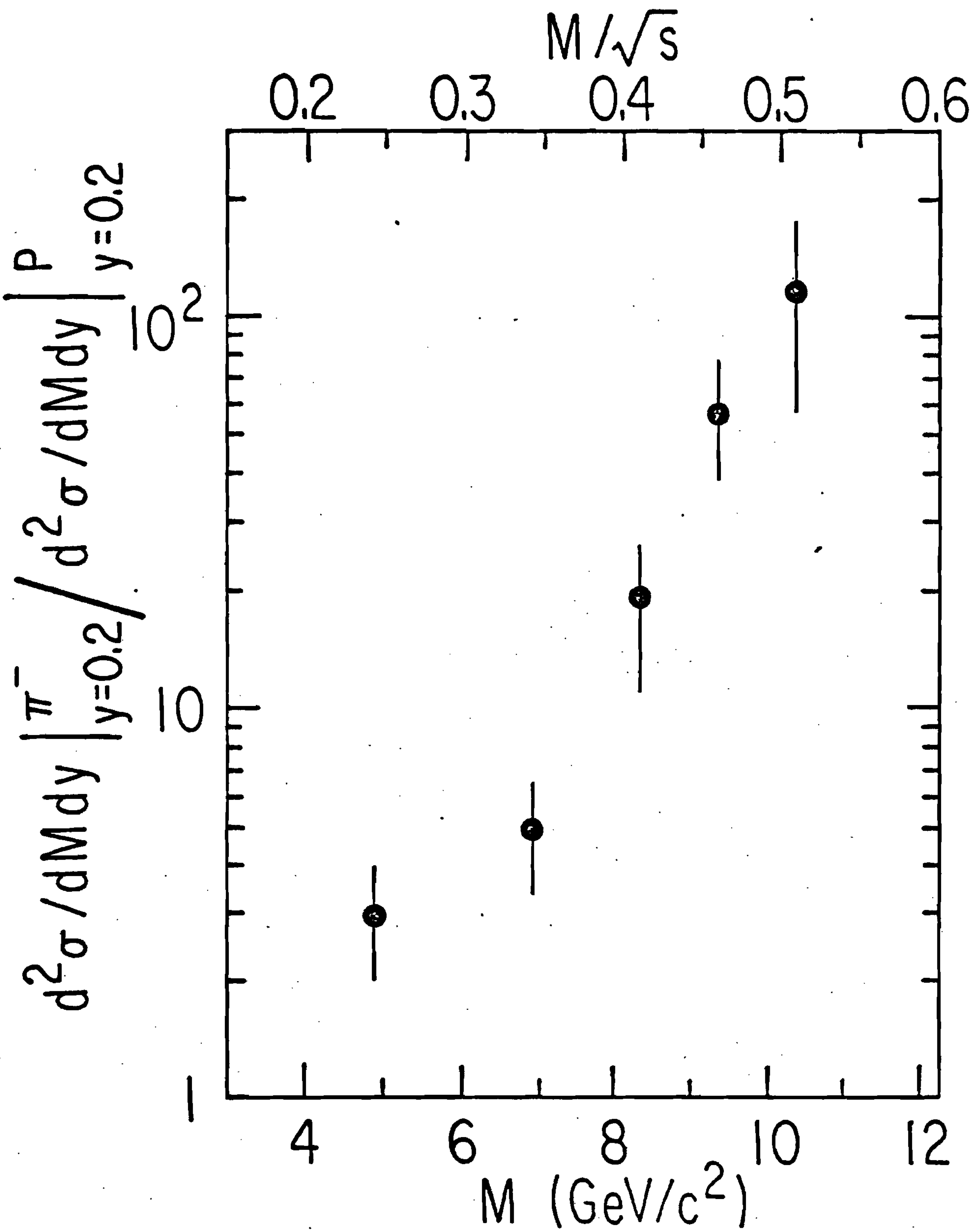

Figure 5-44. Production ratio of pi^{-} induced dimuons to proton induced dimuons as a function of mass.

Chapter VI Pion Structure Function

INTRODUCTION

As seen in Chapter V, the pion data are consistent with the Drell-Yan model. This chapter describes how the model was applied to deduce the pion structure function. A detailed description of how the data were processed is given and then the results are presented.

The Data Set

In order to get the most statistical power from our experiment, the π^- induced cross sections from all three targets were combined into one data set. Our measured atomic mass number dependence of $A^{1.12}$ was used to express the data in picobarns/nucleon. The data points are shown in Figure 6-1 where the variables are defined as:

$$M = \text{Invariant pair mass } (\text{GeV}/c^2) = [x_1 x_2 s]^{1/2} \quad (6-1)$$

$$x_f = 2p_{||} s^{-1/2} = x_1 - x_2 ; \; p_{||} \text{ in center of mass}$$

$$x_1 = [x_f + (x_f^2 + 4M^2/s)^{1/2}]/2 = x_{pion}$$

$$x_2 = [-x_f + (x_f^2 + 4M^2/s)^{1/2}]/2 = x_{nucleon}$$

Two methods were used to fit the data. In the first method, the data were binned and fit to a functional form by a least squares method. The second method used the data as a set of points and found the functional form that gave the maximum likelihood for that data set.

Bin Method

In the bin method, the data were first binned separately by target type. Each event was assigned a weight:

$$w_i = (NF / eff) * x_1^2 x_2^2 s^2 \qquad (6\text{-}2)$$

where:

NF = cross section / nucleon / event for a given target

eff = acceptance efficiency

$x_1^2 x_2^2 s^2 = M^4$ when p_T effects are ignored.

For a bin B and target j with N events, the bin value and error was:

$$\text{Bin value} = A_{B,j} = \sum_{i=1}^{N} w_i \,/\, \text{Area}_B \qquad (6\text{-}3)$$

$$\text{Bin Error} = E_{B,j}^2 = \sum_{i=1}^{N} w_i^2 \,/\, \text{Area}_B^2 + (A_{B,j} * EA * \ln(AN_j))^2$$

Area_B = Area of bin B (in x_1, x_2 units)

AN_j = Atomic mass number of target j

EA = Error on atomic mass number dependence.

The targets were then combined according to:

$$D_B = \sum_{j=1}^{3} 1 \,/\, E_{B,j}^2 \qquad (6\text{-}4)$$

$$A_B = \left(\sum_{j=1}^{3} A_{B,j} / E_{B,j}^2\right) / D_B$$

$$E_B^2 = 1 / D_B$$

Bin centers were the weighted averages of the events in the bins.

For a given value of the function, F_B, at bin B, the χ^2 was formed and then minimized.

$$\chi_0^2 = \sum_{Bins} (F_B - A_B)^2 / E_B^2 \qquad (6\text{-}5)$$

Many of the bins had very few events in them (ie, 1 to 3) and we felt that the error assigned to the bins should be more carefully defined. In Poisson statistics, the error is proportional to the square root of the expected number of events N_B^*. The definition for E_B assumes $N_B^* = N_B$, the actual number of events. We defined two conversion factors, W_B and W'_B, that relate N_B to E_B and A_B:

$$A_B = W_B * N_B \qquad (6\text{-}6)$$

$$E_B^2 = W'_B * N_B$$

So W_B was an average weight for the events in that bin. Then we defined a new 'expected number of events' using this average weight:

$$N_B^* = F_B / W_B \qquad (6\text{-}7)$$

and a new estimate for the expected error:

$$E_B^{*2} = W'_B * N_B^* \qquad (6\text{-}8)$$

These errors were used in the minimization. Note that W_B and W'_B stayed the same. We found that some type of error redefinition method was necessary to insure that the minimization routine came up with the correct answer when a known distribution was put in as a test sample. The above method accomplished this.

<u>Maximum Likelihood</u>

The likelihood of a set of uncorrelated events happening is just the product of the probability of occurence for each event. In the maximum likelihood method we tried to find an event probability distribution (which is proportional to the cross section times the probability that an event will be seen) that matched the actual distribution of data points. The probability that an event would be seen at some x_1,x_2 is:

$$P(x_1,x_2) = F(x_1,x_2) * eff(x_1,x_2) \; / \; Norm \qquad (6\text{-}9)$$

where:

$F(x_1,x_2)$ = Functional form being fit (differential cross section)

$eff(x_1,x_2)$ = Acceptance efficiency (probability that event will be seen)

Norm = The normalization constant for the given form of $F(x_1,x_2)$

The normalization is calculated by summing up $F(x_1,x_2)$ * $eff(x_1,x_2)$ for a set of M points uniformly scattered over the region being fit:

$$\text{Norm} = \sum^{M} (F(x_1, x_2) * \text{eff}(x_1, x_2)) \;/\; M \qquad (6-10)$$

The likelihood L of a given set of N points actually occurring was then:

$$L = \prod_{i=1}^{N} P(x_1, x_2), \text{ or} \qquad (6-11)$$

$$\ln[L] = \sum_{i=1}^{N} \ln[P(x_1, x_2)]$$

$$= \sum_{i=1}^{N} \ln[F(x_1, x_2)] + \sum_{i=1}^{N} \ln[\text{eff}(x_1, x_2)] - \sum_{i=1}^{N} \ln[\text{Norm}]$$

$$= \sum_{i=1}^{N} \ln[F(x_1, x_2)] - N * \ln(\text{Norm}) + \text{constant}$$

where the constant is independent of the functional form of F. The likelihood was then maximized by minimizing -ln(L). Minimization in both the bin and likelihood methods was done using the MINUIT minimization program.

Drell-Yan Model

As stated in chapter I, the Drell-Yan cross section formula is:

$$d^2\sigma/(dx_A dx_B) = (4\pi\alpha^2 s/(9M^4)) \sum_i \{e_i^2 \qquad (6-12)$$

$$[x_A f_i^A(x_A) x_B f_{\bar{i}}^B(x_B) + x_A f_{\bar{i}}^A(x_A) x_B f_i^B(x_B)]\}$$

There are a number of simplifications in its application to this experiment. For a pion, charge conjugation and isospin invariance imply that the quark distribution function is the same for both of the valence quarks (d and $\bar{u}$ for a π^-). Further, if the kinematic region is restricted to $x_1 > 0.25$, the contribution of sea quarks in the pion is expected to be negligible (we estimate less than 4%) in this region. Then for pion-nucleon collisions the sum over quark flavors reduces to two terms corresponding to the two valence quarks in the pion. The cross section becomes:

$$M^4 d^2\sigma/(dx_1 dx_2) = 4\pi\alpha^2 s/9 * \tag{6-13}$$

$$[4/9\ x_1\bar{u}^{pi}(x_1)x_2 u^N(x_2) + 1/9\ x_1 d^{pi}(x_1)x_2\bar{d}^N(x_2)]$$

or since $\bar{u}^{pi}(x_1) = d^{pi}(x_1)$:

$$M^4 d^2\sigma/(dx_1 dx_2) = (4\pi\alpha^2 s/9)\ F^{pi}(x_1)\ G^N(x_2) \tag{6-14}$$

$$F^{pi}(x_1) = x_1\bar{u}^{pi}(x_1)$$

$$G^N(x_2) = 4/9\ x_2 u^N(x_2) + 1/9\ x_2\bar{d}^N(x_2)$$

There are two useful sum rules that apply to the valence quark distribution of the pion.

A) $\int_0^1 \bar{u}^{pi}(x)\ dx$ = Number of $\bar{u}$ valence quarks in the pion. (Should equal 1 if the color assumption is correct.) (6-15)

B) $\int_0^1 x\bar{u}^{pi}(x)\ dx$ = Fraction of pion momentum carried by the $\bar{u}$ valence quark.

C) $\int_0^1 x\bar{u}(x)dx / \int_0^1 \bar{u}(x)dx = \langle x\rangle$, average x of the $\bar{u}$ valence quark.

Structure Function Fits

In extracting the structure function by the bin method, two different ways of defining the bin edges were used. The first used bin edges of constant x_1 and x_2 (rectangular bins). The second definition used bins of constant $x_1 * x_2$ and $x_1 - x_2$ (constant mass and x_f when p_T is ignored) giving curved bin edges. See Figure 6-2. In both cases the fits were done in the x_1, x_2 plane. For both the bin and maximum likelihood methods, the mass region was cut at $4.0 < M < 8.75$ GeV/c^2. The limits were set to avoid contributions from the resonances (the J/Ψ, Ψ' and upsilon).

As a first test, the rectangular bin method was used to test the hypothesis that the cross section could be factorized as in equation 6-14. The range of x_1 ($0.25 < x_1 < 1.0$) was divided into 14 bins and the range of x_2 ($.05 < x_2 < .28$) was divided into 9 bins. The 85 populated bins were fit to 23 variables, 14 of which represented values of $F^{pi}(x_1)$ and 9 of which represented $G^N(x_2)$. Each bin was a product of two of the variables, one from each subset. This represented a test of the factorization hypothesis free of any assumed functional form for the structure functions. We found a χ^2 of 65 for 61 degrees of freedom for this fit, indicating good agreement with the factorization hypothesis.

We still needed additional information to fix the separate normalizations of the pion and nucleon structure functions. To do this, we forced the nucleon structure function, as given above, to have the same normalization as the nucleon structure function derived by others from deep inelastic lepton scattering experiments[23,24] and proton induced lepton pair experiments[4]. In particular, we used the valence quark distributions of Buras and Gaemers (with $Q^2 = -M^2$) and the sea distribution of the Columbia-Fermilab-Stony Brook collaboration. As stated in the previous chapter, we prefer the CFSB sea over the sea given by Buras and Gaemers because it more accurately reproduces our measurement of the pi^+/pi^- production ratio. Figure 6-3 shows the data points given by the factorization test for the nucleon function normalized to the same area as the theoretical curve. The agreement is excellent (a χ^2 of 5.1 for 8 degrees of freedom). Also shown are various curves of the form $(1-x_2)^n$, also normalized to the same area over the region $.05 < x_2 < .28$. They demonstrate the fact that we had very little lever arm in x_2 and so we could not distinguish between different forms of $G^N(x_2)$. Indeed, the theoretical curve using the sea of Buras and Gamers matched the data points almost as well as the hybrid form we used, the only difference being a 20% change in the normalization. Because of the insensitivity of the data to the exact form of $G^N(x_2)$, we have sometimes simply parameterized the nucleon function in the form $(1-x_2)^n$, letting the minimizing routine find the best value for n. The pion normalization was then fixed by forcing the nucleon fit to have the same normalization as the theoretical curve.

The data were first fit to the following parameterizations:

$$F^{pi}(x_1) = a\ x_1^{1/2}(1-x_1)^b \qquad (6\text{-}16)$$

$$G^N(x_2) = d\ (1-x_2)^c,\ d = \text{forced normalization} \qquad (6\text{-}17)$$

The theoretical predictions[25,26] for b range from 0 to 2. The leading square root term in F^{pi} follows the suggestion of several authors[27] that $\lim_{x\to 0} F^{pi}(x) = x^{1/2}$. The $x^{1/2}$ term also allows the sum rule (6-15A) to have a finite value. The results of the fits are given in Table 6-I, and are in fair agreement for all three methods.

Table 6-I, Comparision of Methods

	a	b	c	X^2/DF	#pt	$<M^2>$
Curved edge	0.73	1.28	3.30	69/75	1970	25.7
	.05	.08	.50			
Square edge	0.58	1.10	3.00	64/81	1372	28.3
	.05	.08	.70			
Max L. H.		1.37	4.05		2057	
		.05	.40			

The differences in the parameter values between methods give a better representation of the systematic errors in our methods than do the statistical errors quoted. On the basis on this comparison of different methods, we have increased the error bars on the pion fits by a factor of two in the work that follows. Figure 6-4 shows the results of the bin method with the points from the factorization test for the pion.

As a check on the sensitivity of the pion fit to the assumed shape of $G^N(x)$, we fixed the parameterization of $G^N(x)$ at specific values and then did the minimization. The results were:

Table 6-II, Pion Dependence on $G^{N}(x) = (1-x)^{n}$

n	a	b	χ^2/DF	Con. Level
2	0.71	1.20	75/76	0.50
	.10	.14		
3	0.73	1.26	69/76	0.69
	.11	.14		
4	0.75	1.33	71/76	0.63
	.11	.14		
5	0.79	1.40	81/76	0.36
	.12	.14		
Theory	0.71	1.21	72/76	0.58
	.10	.14		

Con. level = confidence level

No strong dependence was seen.

As a consistency check, the pion and nucleon structure functions obtained above were used to calculate the muon pair cross section as a function of x_f for various mass regions. Figure 6-5 shows that the calculation is in good agreement with the data.

Figure 6-6 shows the structure function applied to the whole mass range $M < 11$ GeV/c^2 and $x_f > .1$. The x_f limit was chosen so that data from earlier experiments[6] could be included. The calculation falls below the data by a factor of 2 at 2 GeV/c^2 and a factor of 15 at 0.6 GeV/c^2.

p_T Effects

We have investigated the sensitivity of our results to transverse momentum.[28] We were prevented from doing elaborate checks due to a lack of statistics, and so investigated the p_T effects in only two simple ways. First, we divided the data into two samples of $p_T < 1$ GeV/c and $p_T > 1$ GeV/c. We also forced the parameterization of $G^N \sim (1-x)^3$ because there was not enough data in these smaller samples to fit both F^{pi} and G^N. As Table 6-III shows, the pion function was the same within statistics.

Table 6-III, Pion Fits verses p_T

	a	b	c	χ^2/DF	#pt	$\langle M^2 \rangle$
$p_T<1.0$	0.32	1.18	$\equiv 3$	87/75	1069	25.4
	.06	.16				
$p_T>1.0$	0.37	1.24	$\equiv 3$	62/69	901	26.1
	.06	.14				

In the second method, we tried to include p_T effects in the model (though in a very naive way). In our model, the p_T is assumed to come from the p_T of the quarks. Each quark is assumed to have an intrinsic $p_T = 1$ GeV/c, so that the total p_T goes from 0 to 2 GeV/c. Events with higher p_T are dropped from the sample. We assumed that the cross section stays exactly the same as 6-14 except that now the distribution functions also contain a delta function for the quark p_T, ie, the cross section was then:

$$d^6\sigma/(dx_1 d\theta_1 dp^2_{T,1} dx_2 d\theta_2 dp^2_{T,2}) = 4\pi\alpha^2/(9M^2)\ h_1(\vec{p}_1)\ h_2(\vec{p}_2) \tag{6-18}$$

$$x_1 h_1(\vec{p}_1) = F^{pi}(x_1)\ \delta(p_{T,1} - 1)/(4\pi)$$

$$x_2 h_2(\vec{p}_2) = G^N(x_2)\ \delta(p_{T,2} - 1)/(4\pi)$$

After integrating over $p_{T1,2}$, one gets:

$$d^2\sigma/(dx_1 dx_2) = 4\pi\alpha^2/(9x_1x_2)\ F^{pi}(x_1)\ G^N(x_2)\ \langle 1/M^2\rangle_{PT} \tag{6-19}$$

or, setting $H(x_1,x_2) = x_1x_2s\ \langle 1/M^2\rangle_{PT}$:

$$x_1^2 x_2^2 s^2 d^2\sigma/(dx_1 dx_2) = 4\pi\alpha^2 s/9\ F^{pi}(x_1)\ G^N(x_2)\ H(x_1,x_2)$$

Note that in the case that p_T is ignored, the above equations reduce to what we had before (ie, $H(x_1,x_2) = 1$). For the p_T model we used, H reduced to:

$$H(x_1,x_2) = x_1x_2\ (A^2 - 4)^{-1/2} \tag{6-20}$$

$$A = [(p^2_{L1}+1)^{1/2} + (p^2_{L2}+1)^{1/2}]^2 - p_{T,total} - 2$$

$$p_{L1,2} = x_{1,2}s^{1/2}/2$$

The values of $x_{1,2}$ were found using Newton's method to solve:

$$M^2 = (p_1 + p_2)^2 \text{ (4 vectors)} \tag{6-21}$$

$$x_f = x_1 - x_2$$

The fit was done in the region $4 < (x_1 x_2 s)^{1/2} < 8.75$ GeV. The inclusion of p_T caused x_1 and x_2 to assume lower values than when p_T was ignored. Because $x_1 x_2 s$ was generally less then M^2 and because the bin edges were defined in terms of x_1 and x_2, about half of the events with $M > 4$ GeV/c^2 failed to make the data sample. F^{pi} was again fit to the form in equation 6-16. The results were:

Table 6-IV, p_T Model Fits

	a	b	c	χ^2/DF	#pt	$<M^2>$
$p_{T,quark}=0$	0.73	1.26	≡ 3	69/76	1970	25.7
	.11	.14				
$p_{T,quark}=1$	0.45	1.44	≡ 3	115/73	876	33.5
	.08	.20				

The pion fits do not change significantly.

Neither method of including p_T appears to affect the pion structure function significantly. More sophisicated treatments of the effects of p_T are probably not justified given this insensitivity and the limited amount of data we have.

Mass Dependence

The mass dependence was investigated in a manner similar to the first method described in the previous section. The sample was divided into two sets $4 < M < 5.3$

GeV/c^2 and $5.3 < M < 8.75$ GeV/c^2 and F^{pi} fitted to the form of 6-16. The results were:

Table 6-V, Mass Dependence Fits

	a	b	c	χ^2/DF	#pt	$\langle M^2 \rangle$
$M < 5.3$	0.73	1.22	≡ 3	26/33	1418	20.3
	.12	.18				
$M > 5.3$	0.69	1.29	≡ 3	40/39	552	39.6
	.18	.22				

The results show no significant mass dependence for the pion structure function.

Fermi Motion

The effect of Fermi motion was investigated with a Monte Carlo that generated two sets of data with the distribution $M^4 d^2\sigma/(dx_1 dx_2) \sim (1-x_1)^1 (1-x_2)^5$. One set included the effects of Fermi motion in generating the kinematics of an event (basically by smearing the value of s), the other did not. The two sets were then put through the fitting procedure. The results were:

Table 6-VI, Fermi Motion Effects

	Pion	Nucleon
No Fermi motion	1.03 ± .06	4.9 ± .4
With Fermi motion	.98 ± .06	4.7 ± .4

No significant effect was seen.

Sum Rules

Finally, the sum rules given earlier in the chapter were integrated using the fit $\bar{u}^{pi}(x) = .73x^{-1/2}(1-x)^{1.28}$.

$$\text{Sum A)} \quad \int_{.25}^{1} \bar{u}^{pi}(x)\,dx = .25 \pm .07 \qquad (6\text{-}21)$$

$$\text{Sum B)} \quad \int_{.25}^{1} x\bar{u}^{pi}(x)\,dx = .11 \pm .03$$

Note that a 20% normalization error has been folded in to reflect both the uncertainty in the nucleon normalization and in the atomic mass number dependence.

One would like to continue the integration of 6-21A to x = 0 to see if the integral was consistent with color (see equation 6-15). The integral, however, depends heavily on the low x behaviour of $\bar{u}(x)$. To study this, we fit $F^{pi} = a\,x^{e}\,(1-x)^{b}$ for several values of e. The results of the fits and the value of the sum rules for x =0 → 1 were:

Table 6-VII, Sum Rule Results

e	a	b	c	X^2/DF	Con. Level	Sum A	Sum B	<x>
0.00	0.40	0.97	3.5	74/75	0.51	∞	0.20	0.00
	.06	.14	1.0				.04	
0.25	0.54	1.13	3.4	71/75	0.62	1.70	0.18	0.11
	.08	.14	1.0			.34	.04	.02
0.50	0.73	1.28	3.3	69/75	0.66	0.91	0.16	0.18
	.11	.15	1.0			.18	.03	.04
0.75	0.99	1.43	3.1	70/75	0.64	0.65	0.15	0.23
	.14	.15	1.0			.13	.03	.04
1.00	1.35	1.59	3.0	72/75	0.55	0.52	0.15	0.29
	.20	.16	1.0			.10	.03	.06

All of the fits given are fairly good. The wide range in the value of sum rule A (.5 to infinity) means that we cannot make any firm statement about color without first assuming a specific low x dependence. Conversely, if one believes in color, so that sum A ≡ 1, then we can make a statement about the probable low x dependence of the structure function.

We can also make a fairly confident statement about the percentage of a pion's momentum carried by the two valence quarks. This percentage (= 2* Sum B = .3 to .4) is not strongly dependent on the low x behaviour of $\bar{u}(x)$. The other 60 to 70% of the momentum is presumably carried by the sea quarks and gluons.

Conclusion

This experiment has made significant advances in both experimental technique and in the understanding of hadron physics. On the experimental side, our use of a very fast and complex trigger logic has demonstrated the feasibility of the use of intricate, real-time, logic to select for rare events.

In the realm of hadron physics, our measurements have presented evidence for many interesting effects.

(1) We find that the atomic mass number dependence of pion induced dimuons increases with mass up to masses of about 4 GeV/c^2, where it reaches a plateau of $A^{1.12}$. This power law dependence seems definitely to be greater than 1, as opposed to the proton dependence which appears to plateau at a value of 1.

(2) We have set the first limits for the production cross section of pion induced upsilons: $B\sigma_T < 1.4$ pb/nucleon, 95% confidence limit at $s^{1/2} = 20$ Gev.

(3) We have shown that the p_T of pion induced dimuons reaches a plateau of about 1.2 GeV/c at high masses, a value 200 MeV/c higher than the proton induced dimuon p_T plateau at similar energies.

(4) We have presented data on the production of J/Ψ particles with various beams, including $\bar{p}$ and K^{+} beams.

(5) We have found dramatic agreement between the predictions of the Drell-Yan model and experiment. The important features of the data and some of their implications are:

(a) A $1 + \cos^2\theta^*$ dependence of the cross section at high masses. This indicates the existence of spin 1/2 particles inside of the hadrons that can interact together through a 1^- intermediate state.

(b) The π^+/π^- ratio. The value of this ratio at high masses and the manner of approach to this value has several implications:

i) The agreement with a high mass limit of 1/4 indicates that the charges on the d and u quarks are of the ratio 1:2.

ii) The manner of approach to the ratio indicates that the nucleon sea quark distribution goes as $(1-x)^{10}$ for $|Q^2| > 4\ GeV^2/c^4$ and $x_N < .3$.

iii) The fact that the ratio is not 1 indicates that the reaction is basically electromagnetic and that the 1^- intermediate state is probably a virtual photon.

(c) The π^-/proton ratio is one of the first clear indications that one of the valence quarks in the pion is in fact an antiquark.

(6) We have used the framework of the Drell-Yan model to make the first clear derivation of the pion structure function.

(a) We have shown that for $x_{pi} > .25$, $x\bar{u}(x)$ agrees well with the functional form $x^{1/2}(1-x)^b$, with $1.2 < b < 1.4$.

(b) We have shown that the normalization of the structure function indicates that 30 to 40% of the pion's momentum is carried by the valence quarks.

(c) And we have shown that if one assumes that $\lim_{x \to 0} \bar{u}(x) = x^{-1/2}$, then the data are in excellent agreement with the color hypothesis and that color is important for more then just bookkeeping.

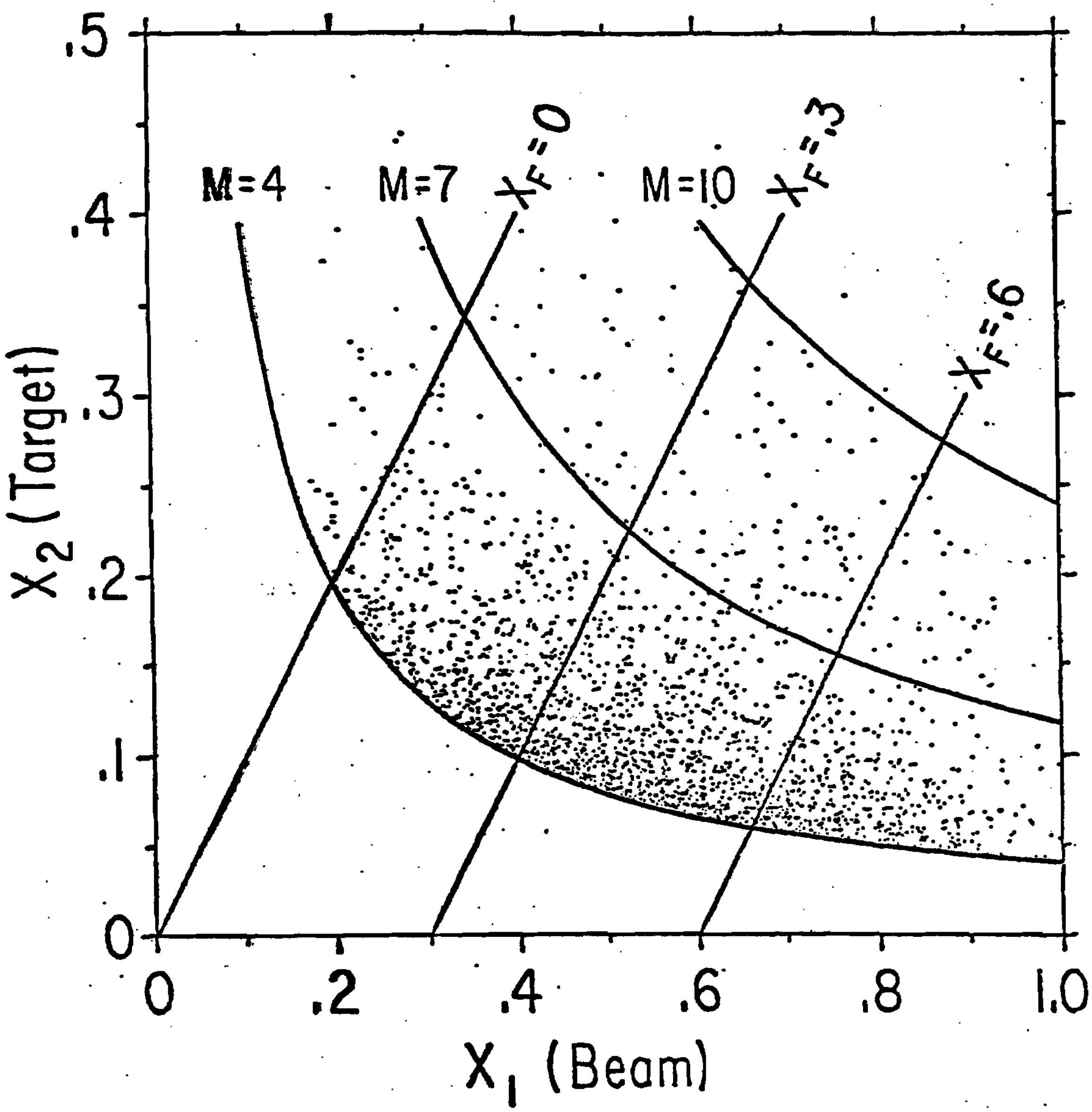

Figure 6-1. Scatter plot showing location of events in the data set.

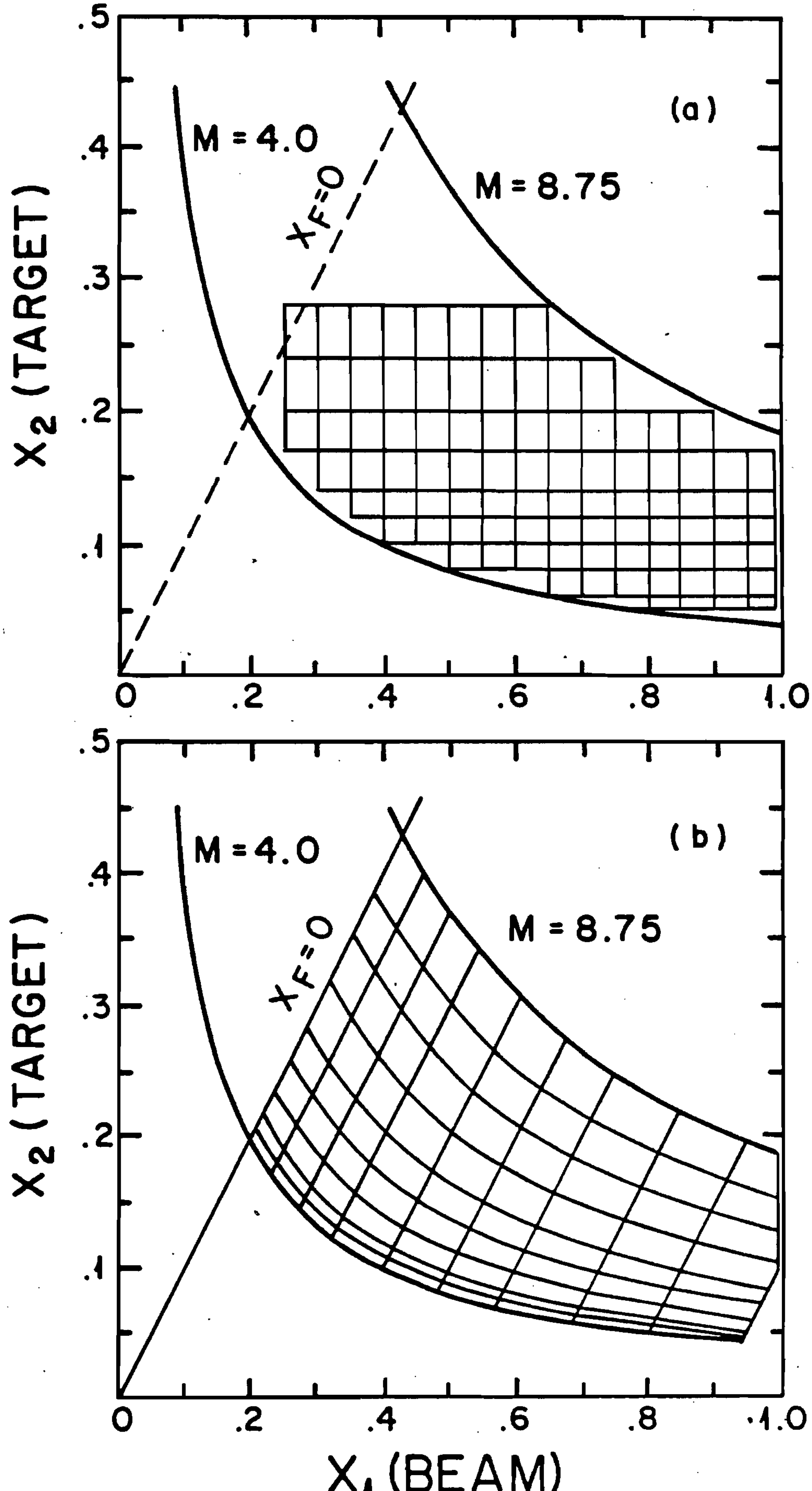

Figure 6-2. Definition of bin edges used in fits.

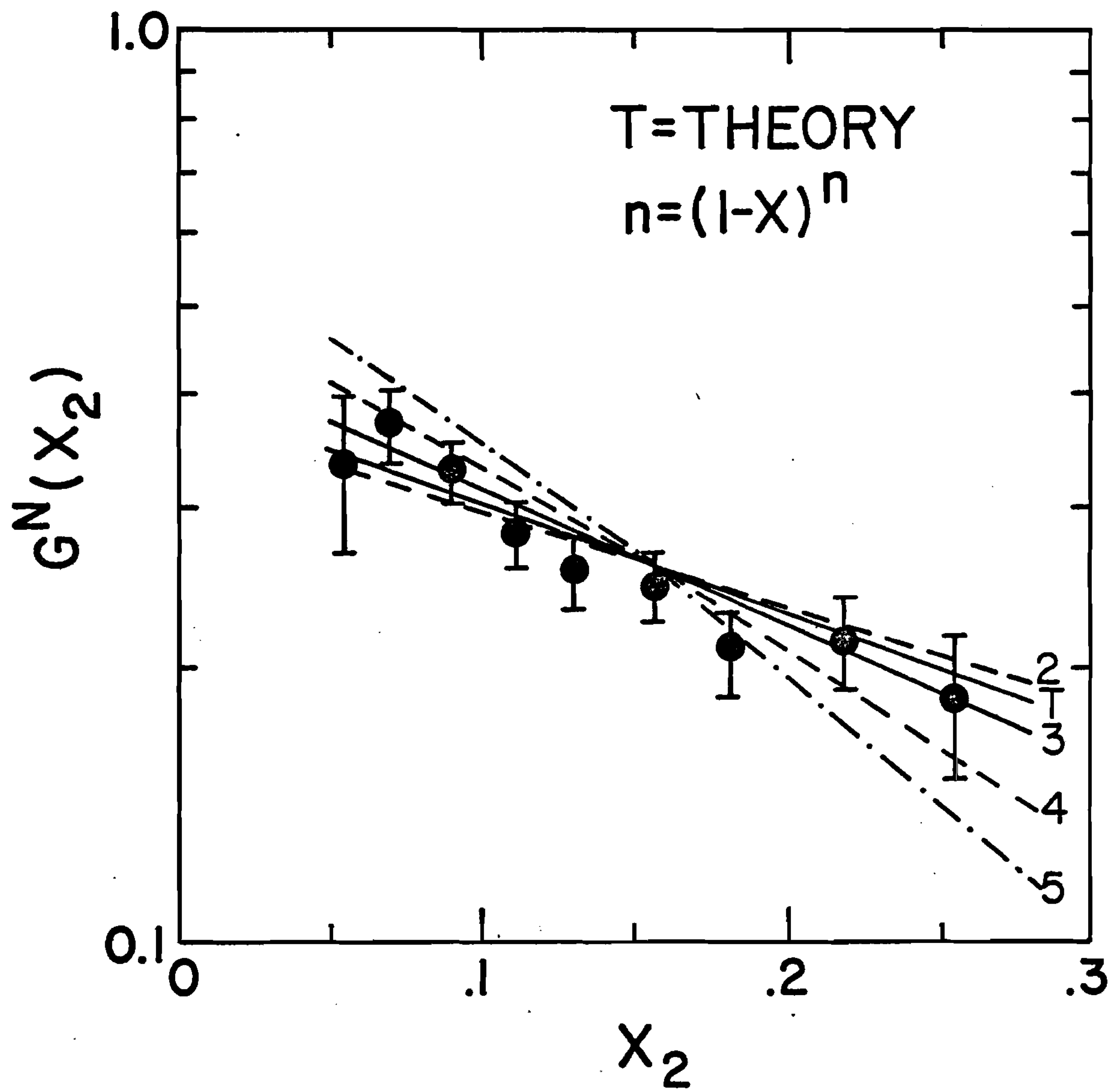

Figure 6-3. Comparison of parameterizations for the nucleon structure function. Data points are from the factorization test fit.

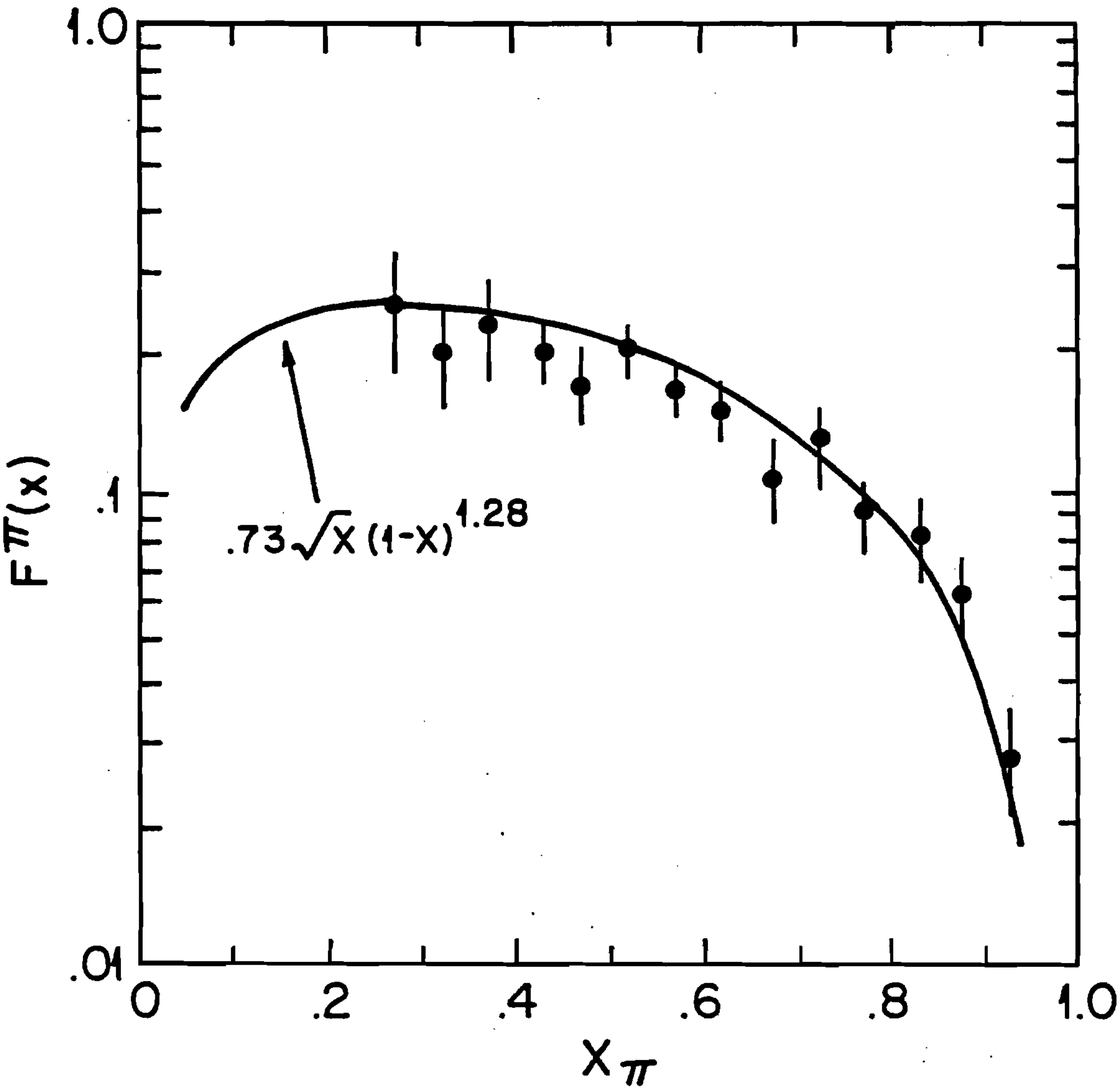

Figure 6-4. The pion structure function.

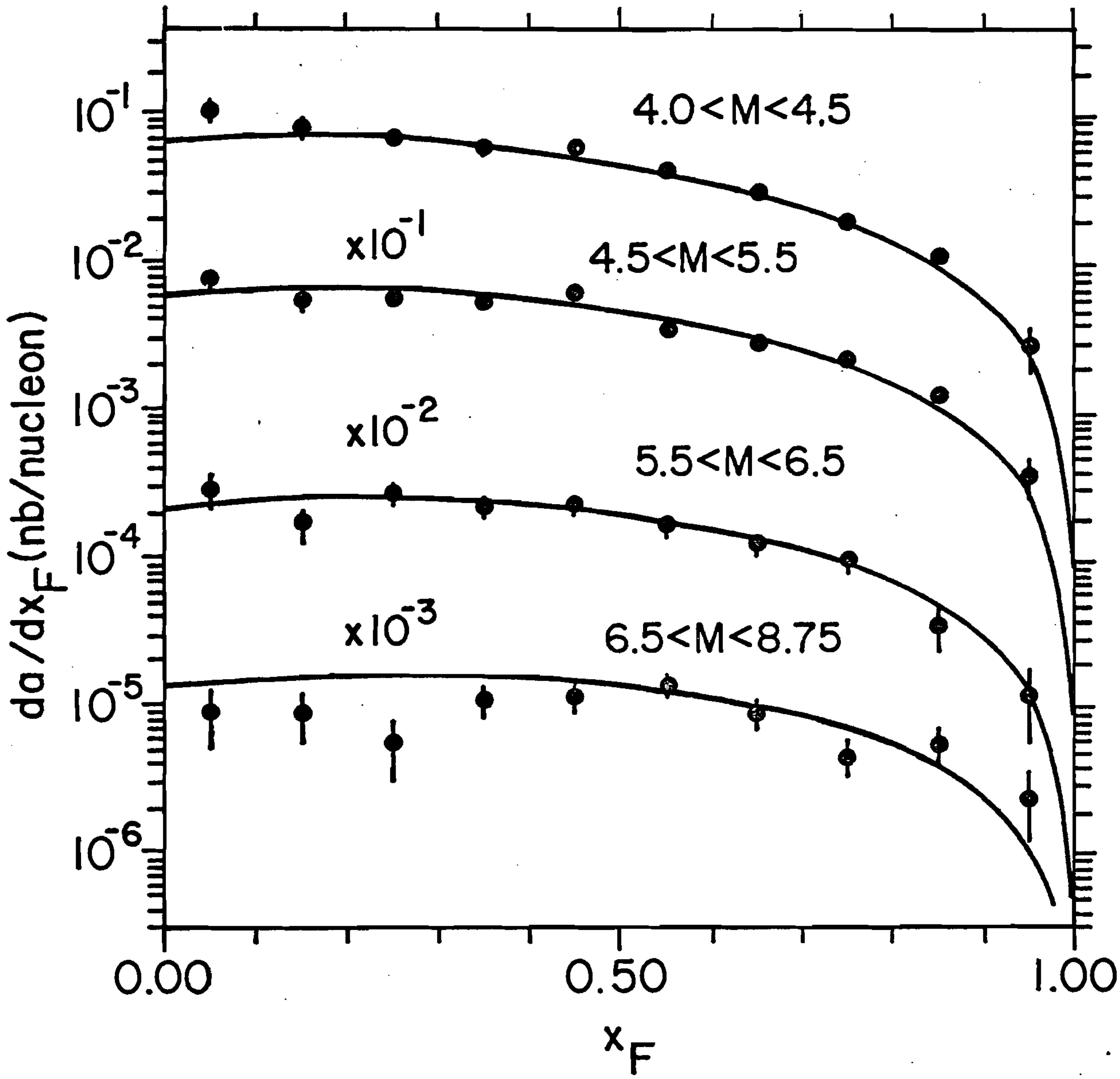

Figure 6-5. Feynman-x distribution of pi$^-$ induced muon pairs with masses beteen 4.0 and 8.75 GeV/c^2. The curves are based on our fits for the structure functions.

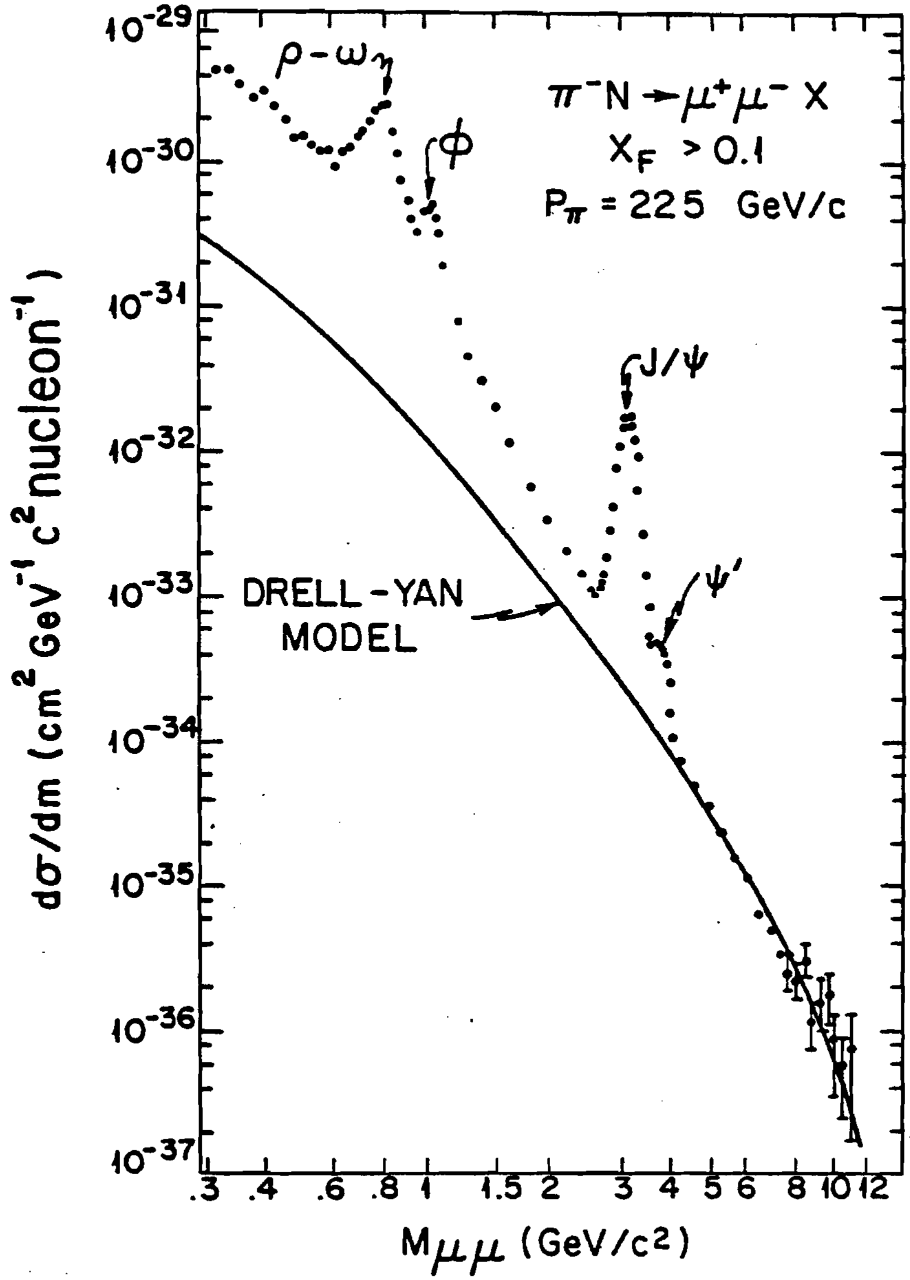

Figure 6-6. Comparison of Drell-Yan model to the measured cross section. The low mass points are from reference 6. The pion sea[29] was assumed to be $0.1(1-x)^5$.

Appendix A

Design Of A Fast Mass Dependent Trigger*

I. Introduction

The new physics accessible to experiments that produce lepton pairs has encouraged a number of groups to search for events of higher and higher lepton pair mass and hence lower cross sections.[4,6,30] These groups seek answers to several intriguing questions such as the role of the Drell-Yan mechanism in the production of muon pairs and the existence of resonances with masses greater than the J/Ψ. Our group investigated these and other questions in a recent experiment at Fermilab that used a 225 GeV/c hadron beam to study the reaction:

$$\text{hadron} + \text{nucleus} \rightarrow \mu^{+}\mu^{-} + \text{anything}. \qquad (A-1)$$

The spectrometer, shown in Figure A-1, consisted of a very large dipole analyzing magnet (formerly the Chicago Cyclotron Magnet) with multi-wire proportional chambers forward of the magnet and spark chambers after the magnet to measure tracks. Large iron absorbers protected the spectrometer from the flood of hadrons, and identified the muons by a range requirement. The information for the trigger came from three large scintillator hodoscope banks

---

* This Appendix has been submitted as a separate paper to Nuclear Instruments and Methods.

labelled J, F, and P in Figure A-1. The resulting apparatus accepted about a quarter of all muon pairs (a "dimuon" event), independent of mass. The apparatus accepted muons from the decay of the ρ (750 MeV/c^2) $\rightarrow \mu^+\mu^-$ equally well as those from the decay of the Υ (9.5 GeV/c^2). With low mass dimuon production about a million times more common than the events of interest, recording every dimuon event would have required unacceptable amounts of time for data taking and analysis.

We clearly needed a mass dependent trigger. The desired trigger determined the dimuon mass by combining three different quantities, the momenta of the two muons, p_1 and p_2, and their relative opening angle, θ, according to

$$M^2_{\mu\mu} = 2p_1p_2(1-\cos\theta). \quad \text{(A-2)}$$

These quantities, which depend on the observed muon tracks, are usually calculated "off-line" with the aid of a large computer. Additionally, the trigger incorporated the following features:

(1) Short decision time: under 500 ns after an event, including signal transit time as well as time for the mass calculation.

(2) No loss of acceptance or lengthening of the decision time due to additional particles in the

spectrometer.

(3) Immunity to rf noise from large spark chambers only one meter away.

(4) Short design and construction time (under 9 months).

Our solution was to use gate matrix techniques to generate the three kinematic quantities, p_1, p_2, and θ, from the pattern of the muon trajectories observed in the scintillator counter banks. A simple hardwired digital processor then calculated the mass. Section II of this report describes the trigger concept in detail, section III describes the circuit design, and section IV dicusses the performance of the trigger.

II. The Trigger

The trigger can be divided into two parts: the dimuon logic, which required that two or more muons be produced in an event, and the mass logic, the main subject of this report, which actually estimated the invariant mass of the pair. The entire trigger logic had to be completed in under 300ns, a time constraint imposed on the trigger by the memory time of the tracking chambers and the propagation time delay of signals going from one end of the apparatus to the other.

The dimuon trigger had two stages. Stage 1, called the pretrigger, started the mass calculation. It required that the J scintillator bank (see Figure A-2a), which was divided into four sectors, have hits in diagonally opposite quadrants and that the F bank (see Figure A-2b) have hits in both its top and bottom halves, these conditions being necessary to do the mass calculation as will be explained below. Stage 2 of the dimuon logic ran in parallel to the mass logic and further checked for the presence of two muons by requiring horizontally separated hits in the F and P banks. This parallel logic also imposed a minimum opening angle requirement at the J bank. The mass logic later required a larger opening angle. The dimuon logic was built almost entirely with standard NIM logic modules. Each stage lasted 150 ns.

The object of the mass logic was to obtain a coarse estimate of the logarithm of the mass of the muon pair from the formula:

$$\log(M_{\mu\mu}^{2}/2) = \log(p_{1}) + \log(p_{2}) + \log(1-\cos\theta). \qquad \text{(A-3)}$$

We chose to trigger on the logarithm of the mass as then only additions rather than multiplications need be performed. The mass logic calculated the logarithms of the quantities p_1, p_2, and $(1-\cos\theta)$ as well as the mass itself in less than 120 ns. The remainder of this section discusses the calculation of these quantities from the hits observed in the J and F hodoscope banks.

The first of the hodoscope banks used in the mass logic, the J, was placed in front of the magnet. It consisted of two parts, (1) 24 horizontal position measuring counters called the J_x counters, and (2) 16 vertical position measuring counters called the J_y counters. See Figure A-2a. Note that each counter only extended half way across the acceptance of the spectrometer. By considering only events that have muons going through different quadrants of the J hodoscope we avoided ambiguous solutions for the location of the two muons. As a further check that the hits came from two or more muons, we required that the hit quadrants be diagonally opposite each other.

The second counter bank, called the F bank and shown in Figure A-2b, had 56 horizontal position measuring counters, divided into 28 top and 28 bottom counters.

Assuming both muons orginated in the target, the separations of their hits in the J_x and J_y banks determined their opening angle. The relative displacement of the muon hits in the J_x and F banks, which lie on either side of the magnet, determined the muon momenta. To make the linking between hits in the J_x and F banks unambiguous, we required that one muon go through the top half of the counter arrays, the other through the bottom half. Figure A-3 shows a typical event that satisfies these requirements.

The essence of our method was the way in which a coincidence between a pair of counters that measured a quantity of interest (momentum or opening angle) was converted into a digital measure of that quantity. The logic formed all possible two-fold coincidences between the elements of two counter banks using a large matrix of AND gates. Each gate in the matrix represented a value of the quantity computed, either a momentum or an angle. The range of possible values was quantized into a small number of bins, and the outputs of all gates associated with the same bin value were ORed together. Figure A-4 shows a simplified diagram of a circuit that does this. The ORed outputs formed a set of lines labelled in ascending order of value. An event that satisfied the pretrigger requirements would have one or more of these lines true. (Multiple hits in a counter bank can turn on more than one line.)

We then fed the output lines into the input channels of a priority encoder circuit in their labelled order, ie, line one went into input channel one, and so on. The encoder circuit put out as a digital number the channel number of the highest true input. The grouping of the matrix bins and the selection of the scale of the quantities computed were carefully chosen so that the channel number was the value of the quantity wanted. The number of channels used was chosen to match the resolution of the measurement. To take a specific case, every combination of an upper J_x counter with an upper F counter corresponded to some value of $\log(p_{up})$. Each combination was assigned to an encoder channel according to

$$\text{Channel number} = 10\log_{10}(p_{up}) - 7, \qquad \text{(A-4)}$$

which gave fifteen channels for 7 GeV/c < p_{up} < 160 GeV/c.

Two steps were required to measure the opening angle. First, coincidence matrices found the horizontal and vertical separations. All possible two-fold combinations of the output of these matrices formed a second matrix which grouped the output lines by the value of $10\log_{10}(1-\cos\theta) + 33$. We imposed a minimum opening angle cut at this point by not connecting up the line for the smallest opening angle. The resulting twenty output lines for 35 mrad < θ < 320 mrad were fed into an encoder.

Taking the three digital numbers that corresponded to

$\log(p_{up})$, $\log(p_{down})$, and $\log(1-\cos\theta)$, a simple digital adder described below then produced a number which increased monotonically with the dimuon mass. The mass logic then accepted or cut an event based of this mass number.

III. The Circuit Design

The mass logic, built at Princeton University, used MECL 10K integrated circuits.[31] We mounted the integrated circuits in Augut ECL wire-wrap boards.[32] These boards, which have built-in sockets already connected to ground and voltage planes (both -5.2V and -2V), simplified the construction and debugging of the circuit. Signal lines were wire-over-ground transmission lines terminated through 100 ohms to -2V. The circuit divided into four sections, (1) the input latches, (2) the matrix-encoders, (3) the adder-comparator, and (4) the testing circuit. Figure A-5 shows a flow diagram of the circuit.

The basic input latch circuit, shown in Figure A-6, had a NIM-to-MECL translator built from a differential amplifier with the threshold set at -.2 Volts and a type D master-slave flip-flop. This circuit required a data signal at least 8ns long. The -.2V came from a two resistor voltage divider between ground and -2V with a .01uF bypass capacitor to ground. Each four channel amplifier chip had its own volatge divider network. The pretrigger provided separate J and F latch signals.

The latch output then fed the matrix-encoder boards. The basic matrix board, as shown in Figure A-4, had four parts: fanout gates, the AND matrix, fanin gates, and an encoder circuit. We based the encoder circuit on the MC10165 priority encoder chip. When data was present, the encoder chip put out as a digital number the logical complement of the highest priority channel number. When there was no input, the output was the same as the output for the highest priority channel. Because of this strange behaviour, we followed this chip with a circuit that inverted the output, but only when there was data present and no data into higher order encoder chips. Such higher order chips, not shown in the figure, were used when more then 8 channels were needed. The encoder circuit formed the low order three bits of the final digital output by OR'ing the output of the individual inverter circuits (as only one circuit would be non-zero). The high order bits were determined by which inverter circuit was non-zero. We used a four bit number for the momentum and a five bit number for the opening angle.

The adder used two Arithmetic Logic Units (MC10181) to form the four low order bits of the double sum. The carry bits from each adder chip along with the high order fifth bit of the opening angle number formed a 3 bit address used to look up the two high order bits of the sum in a 8x2 bit memory made from two 8 channel multiplexer chips (MC10164). A six bit comparator, made from two MC10166 comparator chips, tested the final sum against a number set by front panel switches (the "cut value"). See Figure A-7. If the sum (called the mass number) was greater than the cut value, a true signal, translated to NIM levels, was sent to the master trigger.

Because of the large scale of the circuit (about five hundred chips), we also built into the mass logic a computer controlled on-line testing circuit. This circuit used a series of digital counters and decoders that cycled through a set of input combinations that tested every gate and wire in the system at least once, but not all combinations of inputs as that would have taken too much time. The order of the combinations tried was hardwired into the tester, the computer providing only an intializing signal and a step clock. For each combination, the computer read back through a simple CAMAC interface module the output of each matrix-encoder board, the final sum, the cut value, and the comparison result. The computer compared these numbers with the expected results. Two test cycles were used, one to test the opening angle board, the other to test the momentum boards. The entire test took about three seconds and was run approximately every four hours.

As a further check, we compared the mass logic results while taking actual data with that of an off-line computer program that simulated the same logic. This comparison was done with the mass logic both in and out of the master trigger. Between these two systems of checks, we can confidently say that the mass logic nevered failed during the four months that our experiment ran.

IV. Performance

This logic worked quite well. The redundancy in the trigger to insure the existence of two separated muons kept the trigger very clean. Indeed, in some runs, the final off-line analysis reconstructed two or more muons in up to 95% of the triggers. A reconstructed muon was defined as a track (ie, a set of hits in the chambers both before and after the magnet) that pointed at struck scintillator counters in all three hodoscope banks. Furthermore, the acceptance efficiency, shown in Figure A-8, was large and only slowly changing in the region of interest. The entire trigger logic took about 300ns, the mass logic taking about half of this.

With only six bits to cover the mass range of zero to twenty GeV/c^2, we did not expect great mass resolution from the logic. Figure A-9 shows the line shape of the ρ and J/Ψ as calculated by the logic. The nominal mass scale in GeV/c^2 is also shown. This figure shows that rejecting events with a mass number of 25 or less will cut about 96% of the ρ's and leave 88% of the J/Ψ's. The mass resolution includes the effect of extra hits in the counter banks (from delta rays, third muons, overlapping counters, etc). Because the logic would use the combination of hits that gave the highest mass, the extra hits caused high mass tails which were the main source of ineffectiveness in the trigger.

To quantify the effectiveness of the trigger, we used a figure of merit defined as the number of events the trigger accepted for each good J/Ψ recorded. Table A-I presents this number for various trigger cuts. The first entry in the table is from a previous experiment of ours[6] using basically the same set up, but which did not try to suppress low mass events. The second entry is from our present experiment with just the dimuon trigger requirements. The other entries came from runs that rejected events with a mass number less than or equal to the indicated number. The wide range (7 to 200) in the figure of merit for the present experiment demonstrates the flexibility of the trigger.

Table A-I

Trigger Figure Of Merit

Trigger Discription	Triggers Per J/Ψ
Previous Experiment	1000
This Ex. No Mass Logic	200
Mass Cut = 13	100
Mass Cut = 20	20
Mass Cut = 25	7

V. Conclusion

This mass dependent trigger logic provided a rejection factor of up to 150 against low mass events. This permitted the collection of a managable amount of data (about three million events on tape) with no significant loss of efficiency at high mass. It seems clear that as physicists try to study rarer events, complicated triggers such as described here will become more and more necessary. The success of this particular example points the way to the use of such systems in future experiments.

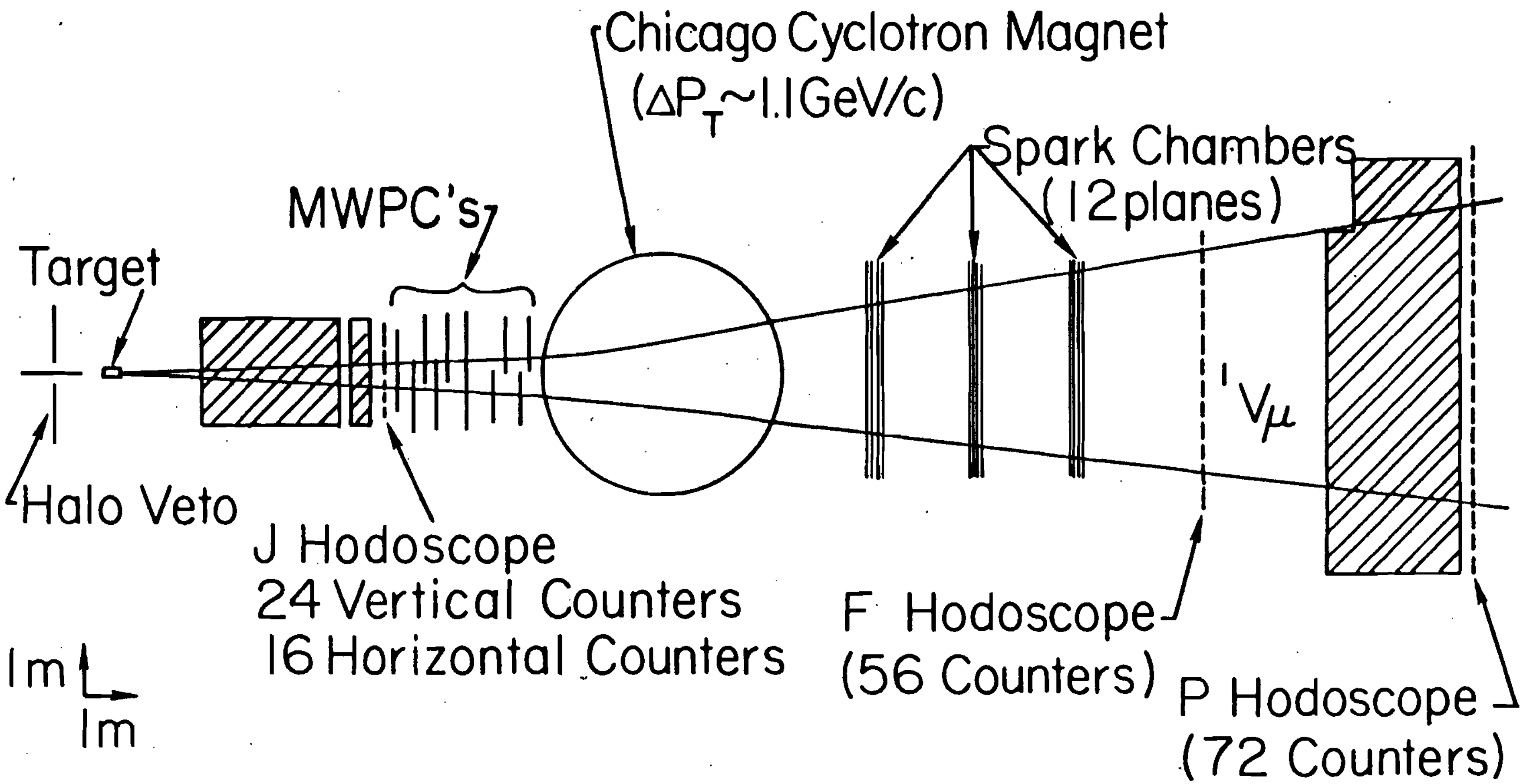

Figure A-1. Plan view of the spectrometer.

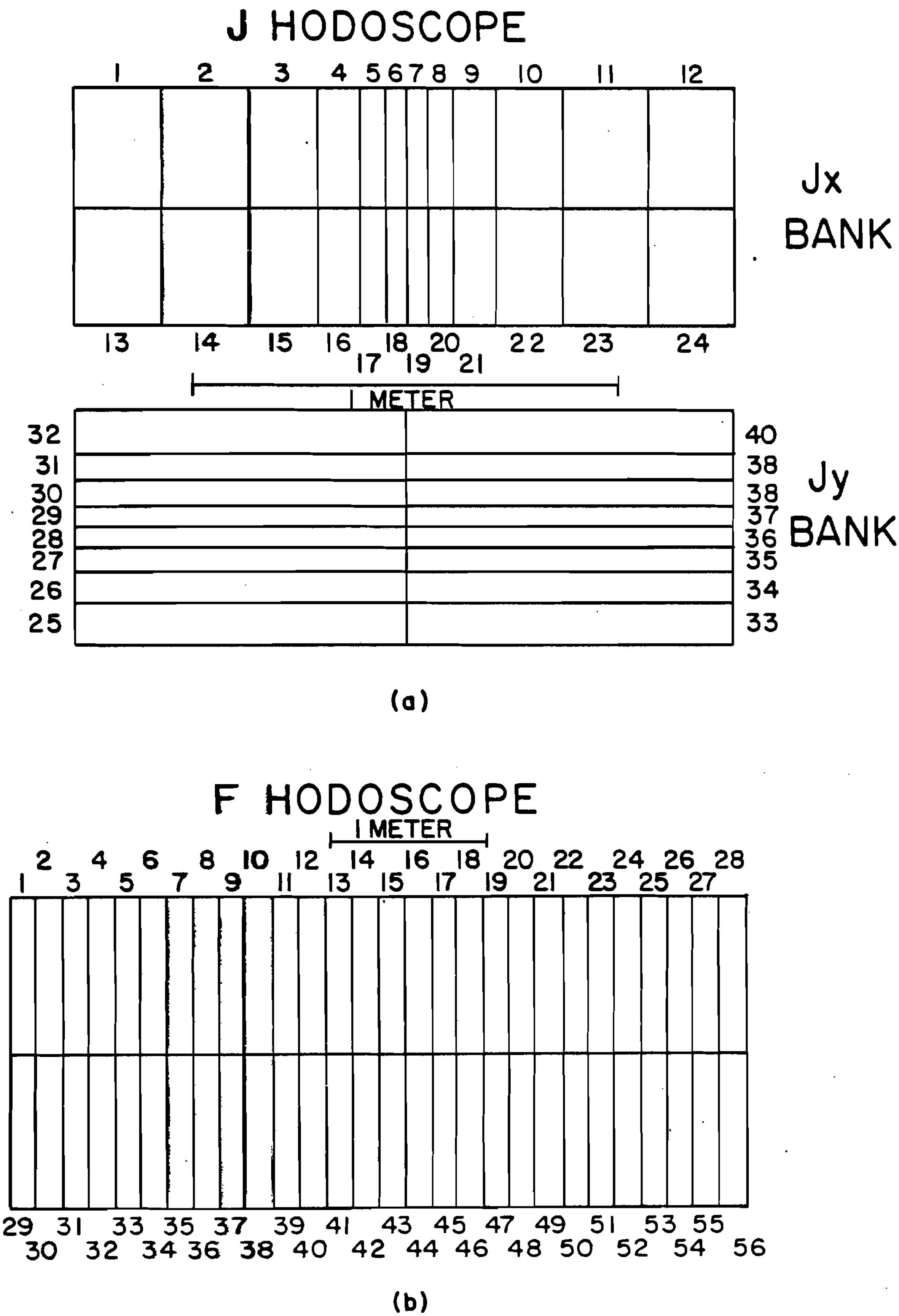

Figure A-2. Segmentation of the J and F hodoscopes. The J counters varied in width from 1.75 inches to 8 inches. The F counters were 7.25 inches wide.

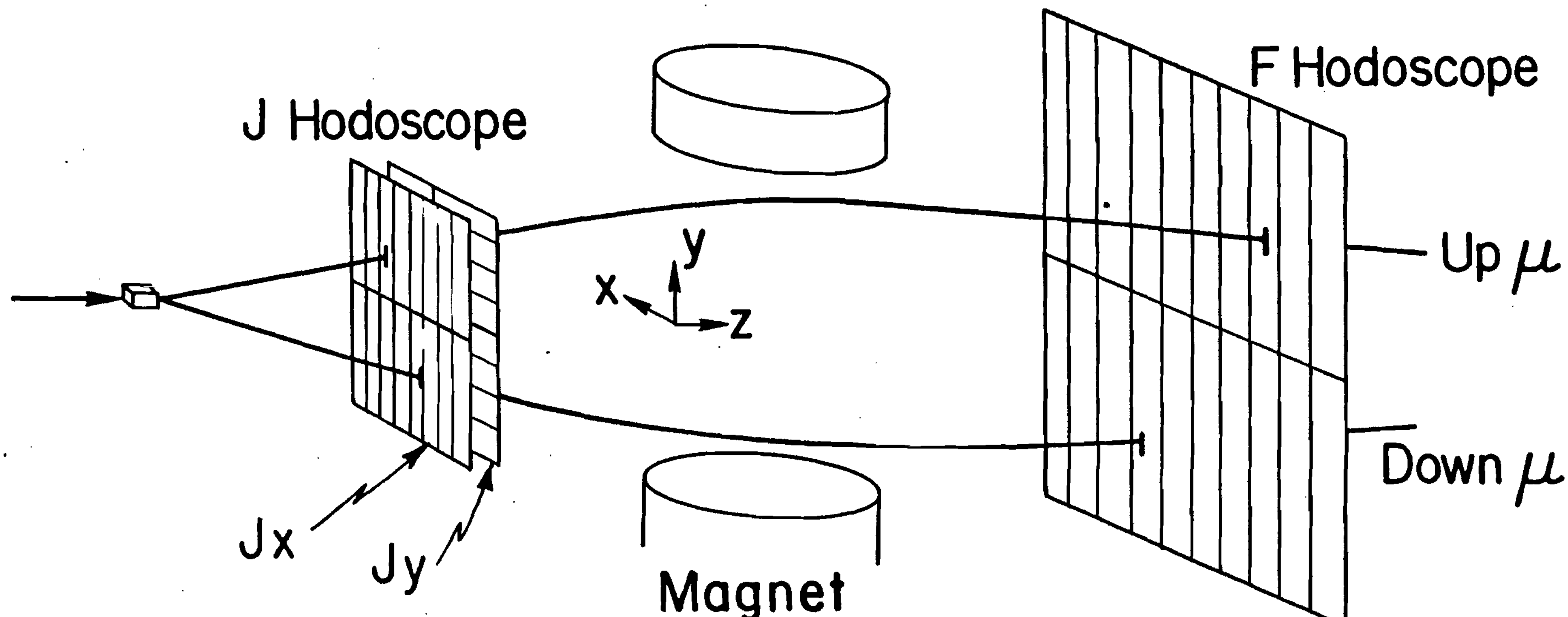

Figure A-3. A typical event showing the up-down and right-left requirements of the trigger logic that provided unambigous location and linking information.

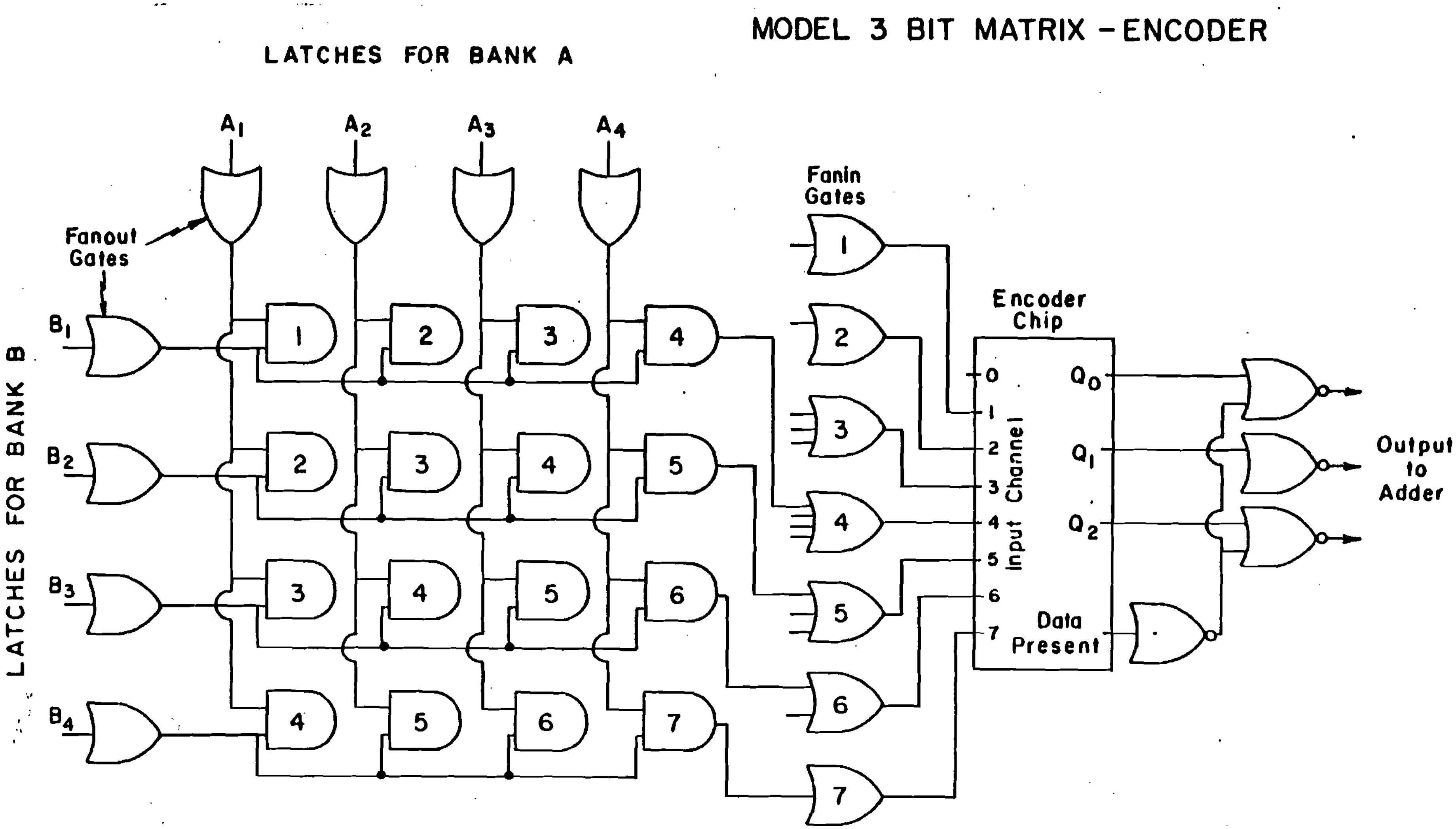

Figure A-4. A simple matrix-encoder board. The value associated with a coincidence node is the number inside the AND symbol. In practice, the momentum boards had 168 nodes each. The opening angle board had 5 separate matrices, with 16 to 96 nodes each.

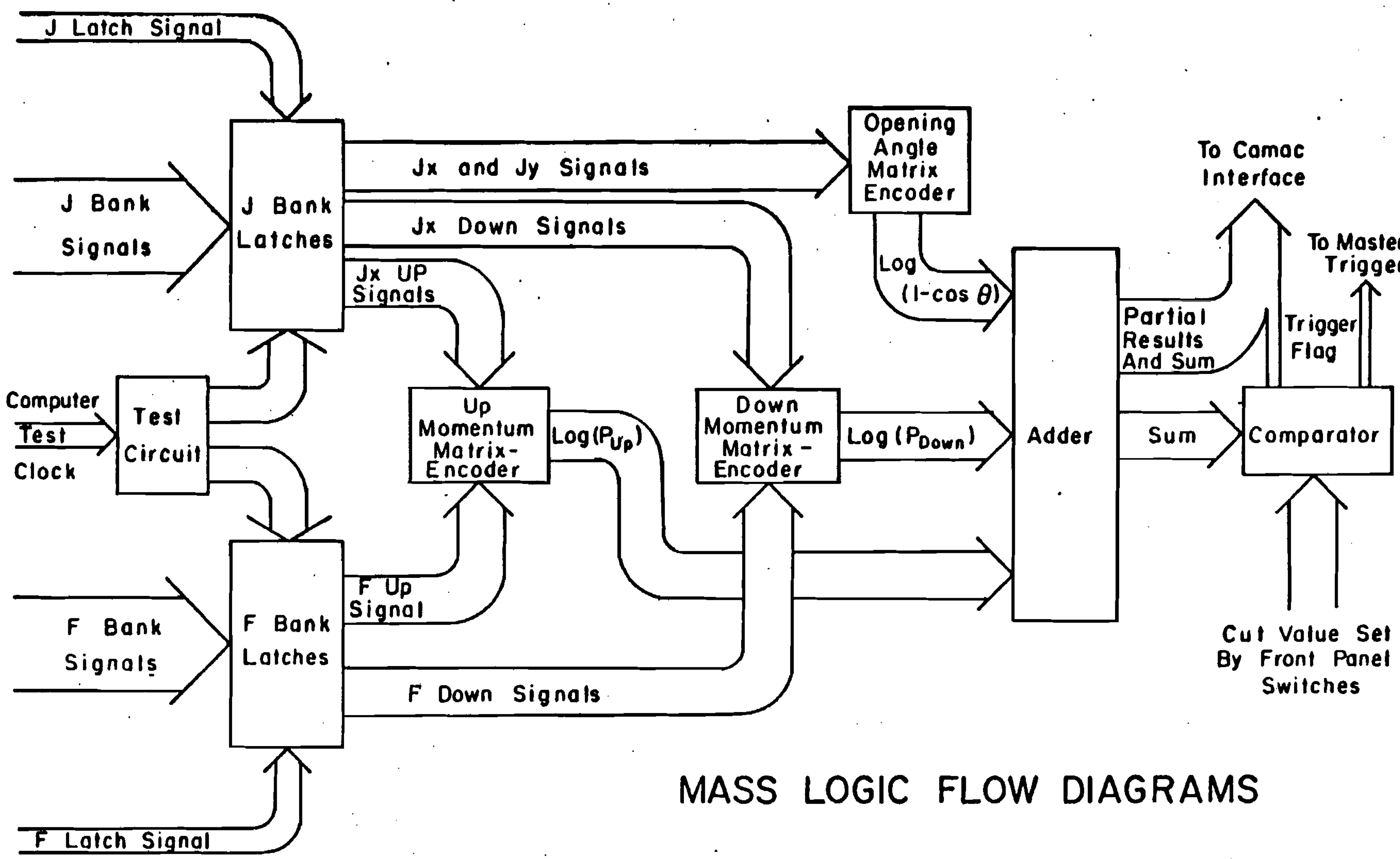

Figure A-5. Flow diagram of the mass calculator showing the general organization.

INPUT LATCH

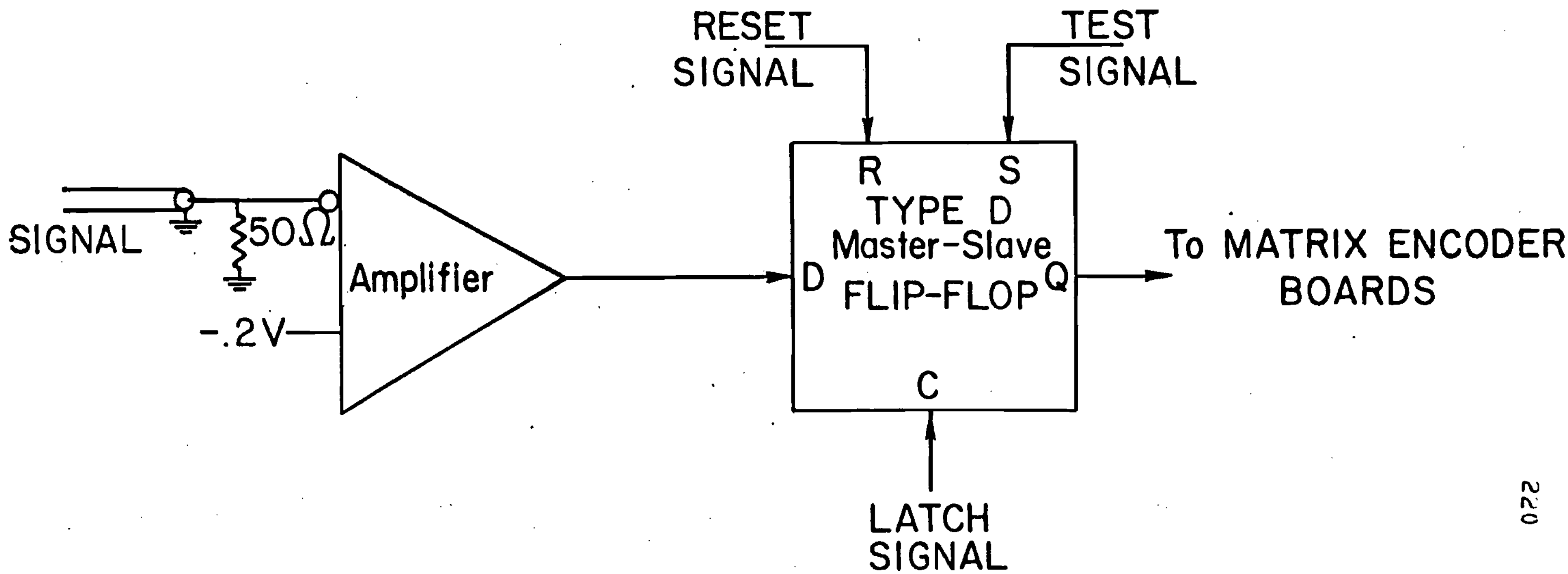

Figure A-6. Typical input latch. The amplifier was a MC10116 chip. The latch was a MC10131. The F bank signals were wired-ored in pairs at the amplifier output to reduce the number of combinations to managable levels.

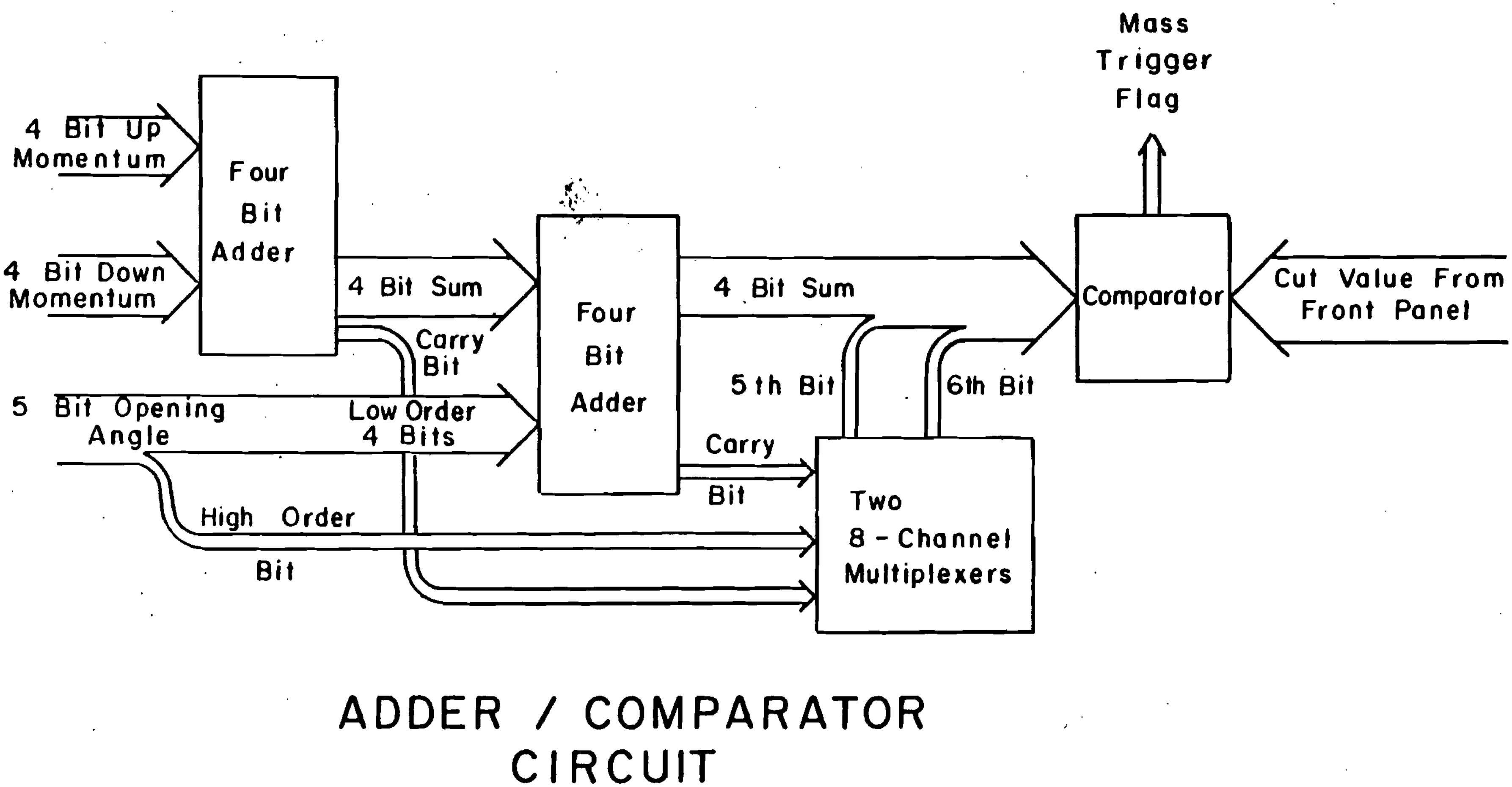

Figure A-7. Flow diagram of the adder/comparator circuit.

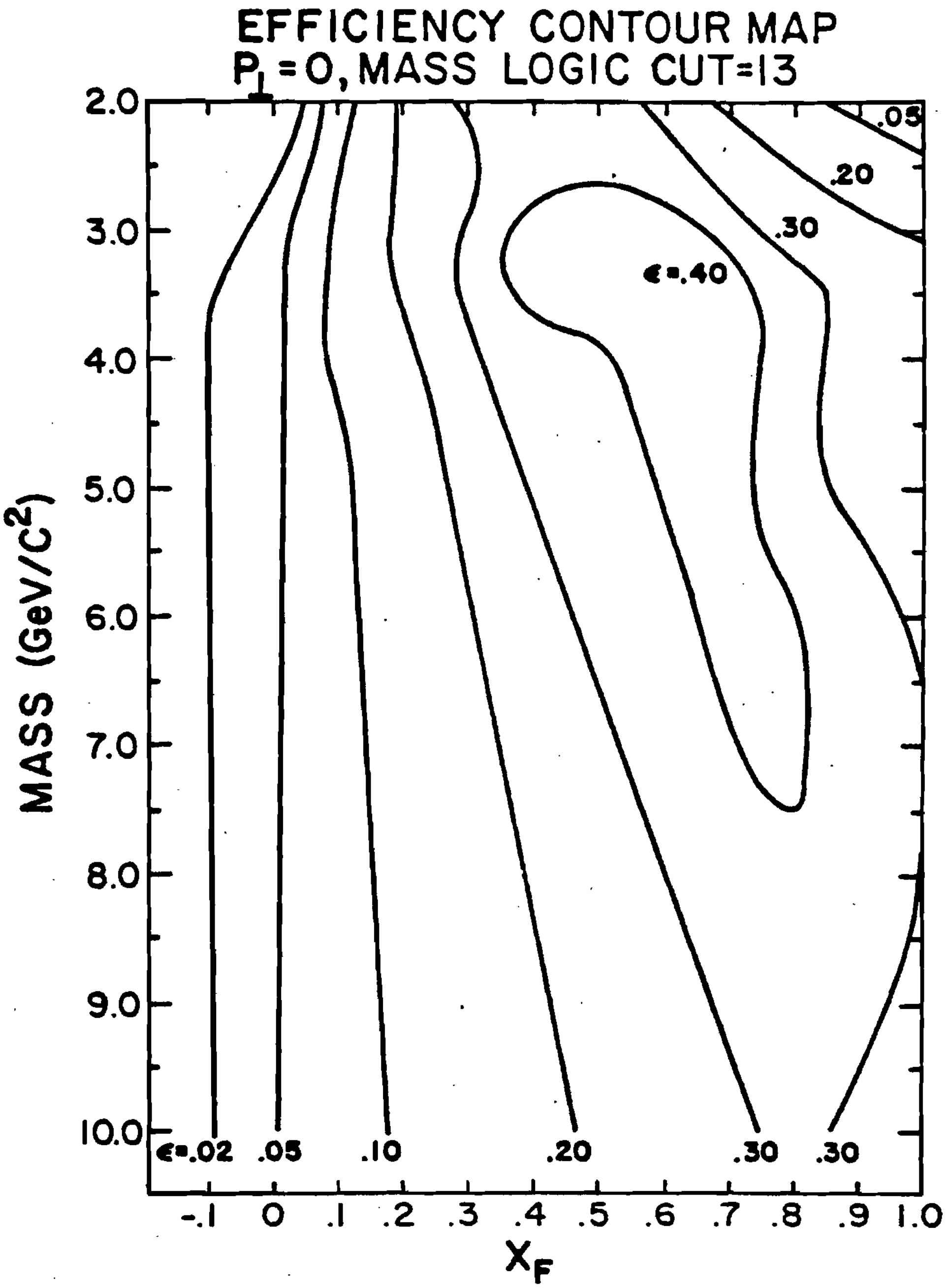

Figure A-8. Acceptance efficiency of the spectrometer for various masses and values of Feynman-x. The efficiency depends only weakly of p_T.

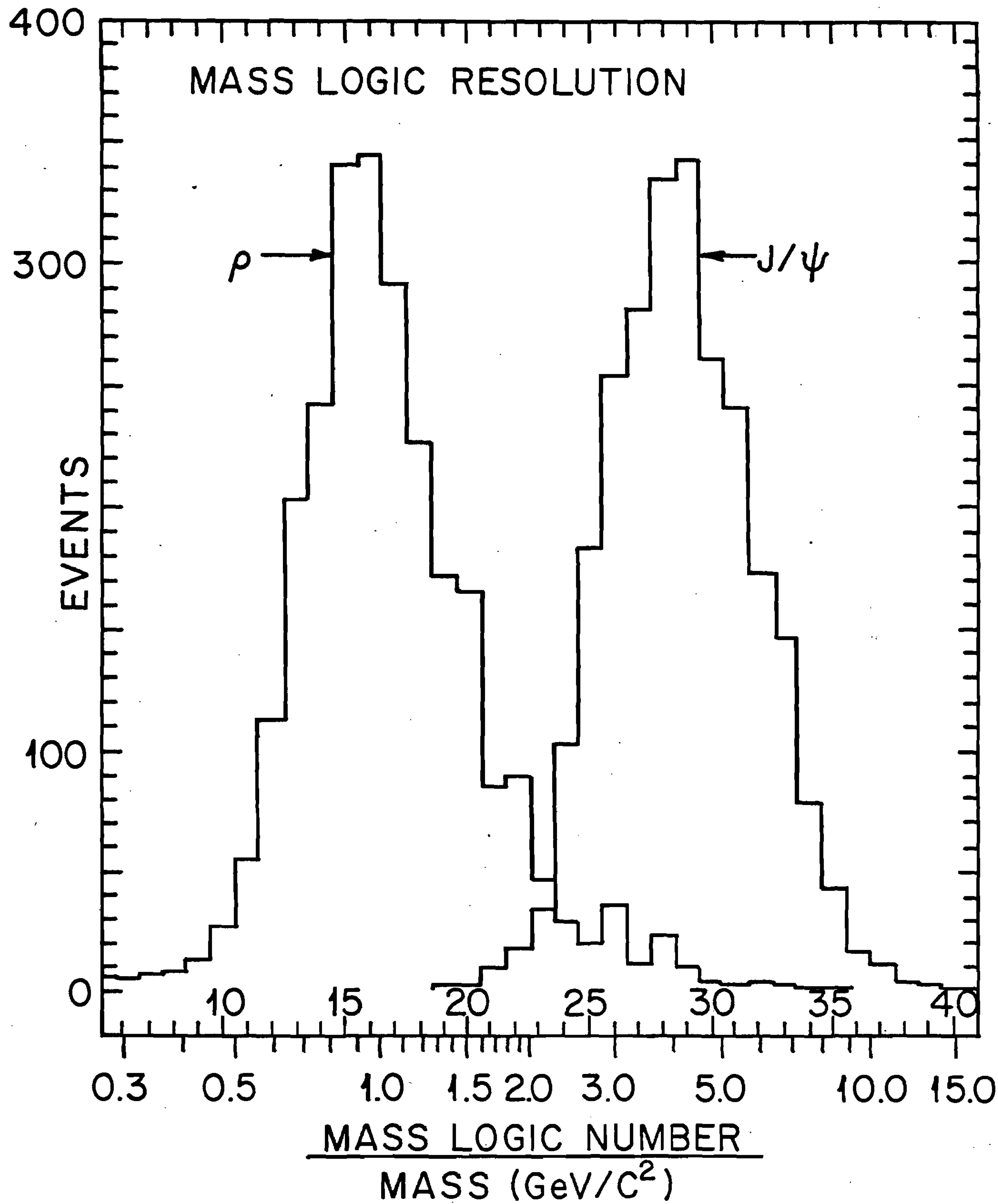

Figure A-9. The resolution of the mass logic for the producton of ρ's and J/Ψ's.

APPENDIX B

POS PION ON CARBON

2.7 < M < 3.5

XF

PT	.025	.075	.125	.175	.225	.275	.325	.375	.425	.475	.525	.575	.625	.675	.725	.775	.825	.875	.925	.975
.1	5.089	15.91	85.31	12.25	16.85	15.03	10.44	11.31	12.32	7.927	6.284	15.12	12.71	4.206	2.576	.6943	1.625	.9046	0.00	1.546
.3	10.59	15.62	16.10	9.566	16.53	10.39	12.08	10.46	9.866	8.683	8.767	5.812	6.932	4.313	1.974	.7843	.5428	.6722	0.00	0.00
.5	12.45	10.32	13.46	13.34	15.71	13.21	9.340	11.19	10.37	6.021	8.500	6.114	5.060	4.669	3.082	1.281	2.286	.9364	.4708	0.00
.7	13.67	11.32	9.919	11.24	8.253	9.255	8.729	6.300	7.495	8.071	4.985	4.841	3.488	2.461	2.768	1.650	.5431	0.00	0.00	0.00
.9	8.838	8.823	7.220	9.627	5.609	7.906	6.126	6.954	4.674	4.281	1.721	3.857	2.326	2.152	1.205	.6045	.1894	.2485	.6771	.3564
1.1	10.56	5.527	6.371	5.947	5.392	4.260	5.197	5.100	3.784	2.861	2.573	2.867	1.797	1.536	1.369	.5485	.1830	.3939	0.00	0.00
1.3	4.952	5.754	4.489	3.671	4.012	3.885	4.034	2.580	3.120	1.220	1.923	2.052	1.215	1.471	.3449	.5453	0.00	.4031	.2439	0.00
1.5	3.695	1.919	3.559	2.325	3.268	3.220	2.826	2.183	1.362	2.140	1.606	1.266	1.070	1.291	.4888	.4233	.1549	0.00	0.00	0.00
1.7	.5786	1.914	1.352	2.541	1.534	2.034	1.703	1.389	.9527	1.799	.9171	.8943	.3952	.3385	.3718	0.00	.1567	.2032	0.00	0.00
1.9	0.00	2.467	1.139	.9113	1.159	1.119	1.194	.5544	.6333	.6437	1.074	.5447	.5296	.2249	.1223	.1373	.1619	0.00	0.00	0.00
2.1	1.536	1.602	1.025	.7586	1.219	.6649	.6897	.7885	.9295	.3283	.4179	.0988	.2058	.2332	0.00	0.00	0.00	0.00	0.00	0.00
2.3	0.00	.6669	.7777	.4146	.4539	.8199	.2838	.3813	.2790	.2713	.3594	.2037	0.00	.1193	0.00	.1377	0.00	0.00	0.00	0.00
2.5	0.00	.2796	.2194	0.00	.2571	.2079	.3268	.5621	.1077	.0941	.0945	.1091	.1159	.1263	0.00	0.00	0.00	0.00	0.00	0.00
2.7	0.00	0.00	.2765	.2776	0.00	.3859	.1245	.1233	0.00	0.00	0.00	.1205	0.00	0.00	0.00	0.00	0.00	0.00	0.00	0.00
2.9	0.00	0.00	0.00	0.00	.3738	0.00	.3950	.2567	0.00	0.00	.1032	0.00	0.00	0.00	0.00	0.00	0.00	0.00	0.00	0.00
3.1	0.00	0.00	.1849	.6715	.1710	.2180	0.00	0.00	0.00	0.00	0.00	0.00	0.00	0.00	0.00	0.00	0.00	0.00	0.00	0.00
3.3	0.00	0.00	0.00	0.00	0.00	0.00	0.00	0.00	.1255	0.00	0.00	0.00	0.00	0.00	0.00	0.00	0.00	0.00	0.00	0.00
3.5	0.00	.2001	0.00	0.00	0.00	0.00	0.00	0.00	0.00	0.00	0.00	0.00	0.00	0.00	0.00	0.00	0.00	0.00	0.00	0.00
3.7	0.00	0.00	0.00	0.00	0.00	0.00	0.00	0.00	0.00	0.00	0.00	0.00	0.00	0.00	0.00	0.00	0.00	0.00	0.00	0.00
3.9	0.00	0.00	0.00	0.00	0.00	0.00	0.00	0.00	0.00	0.00	0.00	0.00	0.00	0.00	0.00	0.00	0.00	0.00	0.00	0.00

ERROR

PT	.025	.075	.125	.175	.225	.275	.325	.375	.425	.475	.525	.575	.625	.675	.725	.775	.825	.875	.925	.975
.1	2.998	4.802	70.41	3.409	3.789	5.376	3.036	3.103	2.784	1.983	2.341	9.417	4.131	2.331	2.141	.6943	1.625	.9046	0.00	1.546
.3	3.126	3.008	2.505	1.618	2.070	1.465	1.619	1.488	1.447	1.386	1.520	1.179	1.408	1.171	.8178	.5615	.5428	.6722	0.00	0.00
.5	2.820	2.037	1.828	1.590	1.597	1.354	1.114	1.227	1.198	.9342	1.143	.9964	.9296	.9588	.8594	.5744	.8655	.6690	.4708	0.00
.7	2.674	1.837	1.397	1.313	1.011	1.007	.9433	.8017	.8729	.9282	.7536	.7675	.6737	.6164	.6938	.5843	.3840	0.00	0.00	0.00
.9	2.121	1.550	1.140	1.102	.7588	.8446	.7226	.7686	.6366	.6249	.4059	.6261	.5082	.5231	.4028	.3027	.1894	.2485	.4810	.3564
1.1	2.242	1.219	1.019	.8275	.7099	.5858	.6261	.6235	.5465	.4908	.4778	.5151	.4238	.4109	.4130	.2744	.1830	.2785	0.00	0.00
1.3	1.576	1.190	.8108	.6237	.5862	.5392	.5345	.4300	.4817	.3151	.4101	.4280	.3371	.3934	.1992	.2727	0.00	.2851	.2439	0.00
1.5	1.324	.6857	.7310	.4985	.5171	.4912	.4469	.3921	.3127	.4121	.3684	.3383	.3229	.3729	.2446	.2445	.1549	0.00	0.00	0.00
1.7	.5786	.7381	.4529	.5213	.3619	.3992	.3554	.3188	.2643	.3752	.2767	.2829	.1976	.1955	.2147	0.00	.1567	.2032	0.00	0.00
1.9	0.00	.8972	.4326	.3244	.3348	.3105	.3083	.2097	.2240	.2276	.2979	.2226	.2369	.1591	.1223	.1373	.1619	0.00	0.00	0.00
2.1	.8931	.6667	.4219	.3108	.3523	.2515	.2440	.2630	.2805	.1642	.1869	.0988	.1455	.1649	0.00	0.00	0.00	0.00	0.00	0.00
2.3	0.00	.4716	.3900	.2419	.2274	.2903	.1639	.1907	.1613	.1568	.1798	.1441	0.00	.1193	0.00	.1377	0.00	0.00	0.00	0.00
2.5	0.00	.2796	.2194	0.00	.1819	.1471	.1887	.2520	.1077	.0941	.0945	.1091	.1159	.1263	0.00	0.00	0.00	0.00	0.00	0.00
2.7	0.00	0.00	.2765	.2776	0.00	.2230	.1245	.1233	0.00	0.00	0.00	.1205	0.00	0.00	0.00	0.00	0.00	0.00	0.00	0.00
2.9	0.00	0.00	0.00	0.00	.2647	0.00	.2283	.1816	0.00	0.00	.1032	0.00	0.00	0.00	0.00	0.00	0.00	0.00	0.00	0.00
3.1	0.00	0.00	.1849	.6715	.1710	.2180	0.00	0.00	0.00	0.00	0.00	0.00	0.00	0.00	0.00	0.00	0.00	0.00	0.00	0.00
3.3	0.00	0.00	0.00	0.00	0.00	0.00	0.00	0.00	.1255	0.00	0.00	0.00	0.00	0.00	0.00	0.00	0.00	0.00	0.00	0.00
3.5	0.00	.2001	0.00	0.00	0.00	0.00	0.00	0.00	0.00	0.00	0.00	0.00	0.00	0.00	0.00	0.00	0.00	0.00	0.00	0.00
3.7	0.00	0.00	0.00	0.00	0.00	0.00	0.00	0.00	0.00	0.00	0.00	0.00	0.00	0.00	0.00	0.00	0.00	0.00	0.00	0.00
3.9	0.00	0.00	0.00	0.00	0.00	0.00	0.00	0.00	0.00	0.00	0.00	0.00	0.00	0.00	0.00	0.00	0.00	0.00	0.00	0.00

DIFFERENTIAL CROSS SECTION
NB C**3 / GEV**2 / XF UNIT / NUCLEUS
NEG PION ON CARBON

2.7 < M < 3.5

XF

PT	.025	.075	.125	.175	.225	.275	.325	.375	.425	.475	.525	.575	.625	.675	.725	.775	.825	.875	.925	.975
.1	19.55	12.24	13.88	15.84	13.15	13.97	15.00	13.99	10.64	7.662	7.701	5.776	6.434	3.862	2.921	3.106	3.028	1.072	1.084	0.00
.3	23.57	16.81	12.27	13.61	16.80	12.36	12.48	13.10	11.27	7.965	6.669	6.702	7.276	5.949	3.883	2.460	1.185	1.713	0.00	.6088
.5	18.56	16.40	14.00	14.26	13.79	11.78	10.81	8.678	8.910	7.778	8.272	5.222	5.286	4.473	3.556	2.394	1.404	.4464	.2283	0.00
.7	11.49	13.91	12.20	11.25	9.754	9.402	9.398	8.914	6.758	5.976	5.088	5.235	4.294	2.408	1.865	1.893	1.185	.5478	0.00	.1728
.9	10.99	9.823	10.53	9.633	7.437	7.316	6.102	5.615	5.857	4.982	3.385	3.540	3.211	2.334	1.528	1.055	.8626	.7458	.1348	.1474
1.1	6.294	7.900	7.386	6.160	5.160	5.308	5.346	4.622	4.252	3.432	2.409	2.779	1.308	1.822	.7309	.8282	.2725	.1789	.1217	0.00
1.3	4.522	4.208	4.331	5.211	4.900	4.072	3.433	2.891	2.613	2.323	2.193	2.044	1.354	.7545	.9126	.5162	.4558	.2495	.2956	0.00
1.5	3.182	3.508	3.402	2.820	3.884	2.917	2.855	2.180	1.773	1.999	1.747	1.419	.6093	.8417	.6817	.5455	.1395	.0886	.0984	.1054
1.7	2.141	2.110	2.152	1.572	1.921	1.994	1.795	2.064	1.299	1.063	.4234	.9716	.5660	.3786	.2066	.4043	.1299	.0820	0.00	.0996
1.9	.6912	1.603	1.882	1.601	1.291	1.348	1.404	1.118	1.003	.5132	.4982	.5519	.4888	.3822	.0511	.1712	0.00	0.00	0.00	0.00
2.1	.5898	1.013	1.462	.6746	1.019	1.014	.9895	.4698	.6114	.5606	.6188	.5415	.2220	.1490	.1064	.1683	0.00	0.00	0.00	0.00
2.3	1.052	.3774	.7094	.5083	.7267	.5633	.5616	.3899	.4339	.2274	.1141	.2523	.1424	.1037	.1066	0.00	0.00	0.00	0.00	0.00
2.5	0.00	.3996	.3024	.3751	.3971	.5592	.0945	.3809	.2723	.0814	.3337	.3221	.0549	.1119	.0581	.0602	.0606	0.00	0.00	0.00
2.7	0.00	.2799	.4325	.2781	.3842	.3310	.5217	.3642	.0985	.0904	.1313	.0505	.0551	0.00	0.00	.0621	0.00	0.00	0.00	0.00
2.9	0.00	0.00	.2908	0.00	.0680	.1841	.0532	.1071	.1622	.0915	0.00	.0512	0.00	0.00	.0630	0.00	0.00	0.00	0.00	0.00
3.1	0.00	0.00	.1194	0.00	.1610	0.00	.1790	.0603	.1064	0.00	0.00	.0532	0.00	.0560	0.00	0.00	0.00	0.00	0.00	0.00
3.3	0.00	.1099	0.00	0.00	.1185	.2376	0.00	0.00	.0511	0.00	0.00	0.00	0.00	0.00	0.00	0.00	0.00	0.00	0.00	0.00
3.5	0.00	0.00	0.00	0.00	0.00	0.00	0.00	0.00	.0569	0.00	0.00	.0569	0.00	.0673	0.00	0.00	0.00	0.00	0.00	0.00
3.7	0.00	0.00	.1733	0.00	0.00	0.00	0.00	0.00	.0988	.0541	0.00	0.00	0.00	0.00	0.00	0.00	0.00	0.00	0.00	0.00
3.9	0.00	0.00	0.00	0.00	.1761	0.00	0.00	0.00	0.00	0.00	0.00	0.00	0.00	0.00	0.00	0.00	0.00	0.00	0.00	0.00

ERROR

PT	.025	.075	.125	.175	.225	.275	.325	.375	.425	.475	.525	.575	.625	.675	.725	.775	.825	.875	.925	.975
.1	4.996	3.515	3.232	2.555	2.196	2.336	2.383	3.124	1.716	1.486	1.522	1.244	1.508	1.038	.9372	1.387	2.039	.7567	1.084	0.00
.3	3.210	2.017	1.344	1.295	1.358	1.083	1.051	1.099	1.041	.8684	.8472	.8623	.9719	.9345	.7730	.7066	.4938	.7461	0.00	.5754
.5	2.310	1.621	1.208	1.068	.9687	.8419	.7832	.6983	.7243	.6861	.7325	.6067	.6267	.6178	.5870	.5265	.4472	.4024	.2283	0.00
.7	1.587	1.339	1.017	.8545	.7213	.6567	.6352	.6194	.5441	.5233	.4931	.5146	.4876	.3916	.3740	.4147	.3592	.2743	0.00	.1728
.9	1.543	1.077	.8982	.7190	.5703	.5302	.4699	.4514	.4648	.4390	.3697	.3913	.3898	.3523	.3063	.2732	.2734	.2830	.1348	.1474
1.1	1.150	.9508	.7187	.5443	.4484	.4257	.4152	.3881	.3775	.3504	.3316	.3324	.2351	.2420	.1955	.2215	.1364	.1256	.1217	0.00
1.3	.9196	.6629	.5246	.4879	.4209	.3617	.3216	.2967	.2870	.2839	.2856	.2782	.2323	.1832	.2152	.1722	.1725	.1441	.1707	0.00
1.5	.8176	.6263	.4535	.3516	.3691	.3043	.2930	.2553	.2328	.2582	.2523	.2334	.1574	.1965	.1692	.1820	.0988	.0886	.0984	.1054
1.7	.7963	.4828	.3706	.2711	.2669	.2576	.2379	.2541	.2029	.1881	.1223	.1944	.1665	.1339	.1033	.1529	.0919	.0820	0.00	.0996
1.9	.4024	.4349	.3640	.2844	.2284	.2218	.2194	.1948	.1832	.1325	.1332	.1476	.1474	.1351	.0511	.0989	0.00	0.00	0.00	0.00
2.1	.3410	.3644	.3289	.1953	.2130	.1991	.1905	.1304	.1483	.1401	.1502	.1503	.0993	.0950	.0752	.0972	0.00	0.00	0.00	0.00
2.3	.5374	.2197	.2372	.1811	.1879	.1565	.1502	.1233	.1369	.0929	.0659	.1030	.0823	.0733	.0754	0.00	0.00	0.00	0.00	0.00
2.5	0.00	.2309	.1749	.1699	.1503	.1688	.0669	.1348	.1114	.0575	.1181	.1219	.0549	.0791	.0581	.0602	.0606	0.00	0.00	0.00
2.7	0.00	.1979	.2175	.1608	.1579	.1353	.1651	.1377	.0697	.0639	.0758	.0505	.0551	0.00	0.00	.0621	0.00	0.00	0.00	0.00
2.9	0.00	0.00	.1686	0.00	.0680	.1064	.0532	.0757	.0939	.0647	0.00	.0512	0.00	0.00	.0630	0.00	0.00	0.00	0.00	0.00
3.1	0.00	0.00	.1194	0.00	.1139	0.00	.1036	.0603	.0753	0.00	0.00	.0532	0.00	.0560	0.00	0.00	0.00	0.00	0.00	0.00
3.3	0.00	.1099	0.00	0.00	.1185	.1375	0.00	0.00	.0511	0.00	0.00	0.00	0.00	0.00	0.00	0.00	0.00	0.00	0.00	0.00
3.5	0.00	0.00	0.00	0.00	0.00	0.00	0.00	0.00	.0569	0.00	0.00	.0569	0.00	.0673	0.00	0.00	0.00	0.00	0.00	0.00
3.7	0.00	0.00	.1733	0.00	0.00	0.00	0.00	0.00	.0988	.0541	0.00	0.00	0.00	0.00	0.00	0.00	0.00	0.00	0.00	0.00
3.9	0.00	0.00	0.00	0.00	.1761	0.00	0.00	0.00	0.00	0.00	0.00	0.00	0.00	0.00	0.00	0.00	0.00	0.00	0.00	0.00

NEG PION ON COPPER

2.7 < M < 3.5

XF

PT	.025	.075	.125	.175	.225	.275	.325	.375	.425	.475	.525	.575	.625	.675	.725	.775	.825	.875	.925	.975
.1	69.43	58.61	56.13	51.51	66.76	65.82	78.53	41.38	44.40	45.57	40.72	22.24	35.12	26.22	14.26	12.00	2.410	7.650	6.096	0.00
.3	92.97	81.63	48.63	58.13	66.10	56.34	50.80	51.71	46.04	38.95	45.50	25.63	26.06	18.50	15.81	8.836	5.852	4.432	6.462	2.135
.5	59.46	66.70	57.93	55.79	56.22	57.26	45.60	44.22	39.50	32.78	31.09	24.53	24.98	15.56	13.18	7.957	7.696	8.816	3.267	2.090
.7	40.93	47.08	53.54	47.26	44.33	46.13	41.92	36.77	37.24	27.38	20.89	18.91	18.11	8.410	9.500	5.369	5.113	1.623	.4875	1.070
.9	33.69	44.80	41.54	40.43	43.58	37.72	35.72	32.56	26.79	22.26	17.65	15.52	11.70	9.230	7.857	6.917	3.135	1.946	.9297	.8932
1.1	31.98	22.36	29.77	32.84	28.21	25.35	24.01	20.69	20.56	15.56	11.82	9.738	7.312	5.352	3.020	2.410	.6248	1.681	0.00	0.00
1.3	18.96	16.67	20.64	17.77	24.14	21.03	15.53	15.27	12.00	11.85	10.93	8.299	7.317	3.696	4.099	1.954	.9807	.2816	0.00	0.00
1.5	18.66	20.34	15.61	14.90	12.67	11.75	14.37	10.44	8.436	7.961	6.141	5.408	4.394	2.992	1.869	1.511	1.322	.9889	.3057	0.00
1.7	15.39	7.582	9.168	12.43	12.52	8.989	8.815	7.185	6.278	4.252	5.126	3.955	2.878	2.439	1.183	.3693	.8393	.2526	0.00	0.00
1.9	6.785	5.778	7.259	11.38	6.482	6.629	6.541	7.882	4.831	2.477	2.717	2.745	1.973	.7941	.9975	.7135	0.00	0.00	.3033	0.00
2.1	2.232	5.053	4.082	4.232	4.036	5.947	5.137	3.839	2.327	2.362	1.491	1.128	1.306	.4958	.5267	.9356	.1993	0.00	0.00	0.00
2.3	3.097	4.820	3.517	3.760	3.307	3.212	2.873	3.080	1.670	1.755	1.430	.6230	.5445	0.00	.1921	.1898	0.00	0.00	0.00	0.00
2.5	.6022	1.840	3.584	2.974	1.713	2.309	1.451	.6410	2.646	.8655	.5651	.5037	1.013	.6300	.2140	.2188	.2123	0.00	0.00	0.00
2.7	.5806	.4912	.3580	.5625	.4772	1.399	2.012	1.327	.7206	.4564	.9354	.3873	0.00	0.00	.2353	0.00	0.00	0.00	0.00	0.00
2.9	0.00	.4497	1.742	.9317	1.047	.7160	1.158	.4035	.7420	.3084	.6000	.3774	.4267	.2273	0.00	0.00	0.00	0.00	0.00	0.00
3.1	0.00	0.00	.2834	0.00	.2592	.9321	.2333	.4372	.1999	.1501	0.00	0.00	.2090	0.00	0.00	0.00	0.00	0.00	0.00	0.00
3.3	0.00	.3586	0.00	.3722	1.072	0.00	1.141	.2066	.2040	0.00	.1658	.2022	.2204	0.00	0.00	0.00	0.00	0.00	0.00	0.00
3.5	0.00	0.00	0.00	0.00	0.00	0.00	0.00	0.00	.2312	0.00	0.00	0.00	0.00	0.00	0.00	0.00	0.00	0.00	0.00	0.00
3.7	0.00	0.00	0.00	0.00	.3815	.4257	0.00	.2414	0.00	.1960	0.00	0.00	0.00	0.00	0.00	0.00	0.00	0.00	0.00	0.00
3.9	0.00	0.00	0.00	0.00	0.00	0.00	0.00	0.00	0.00	0.00	0.00	0.00	0.00	0.00	0.00	0.00	0.00	0.00	0.00	0.00

ERROR

	.025	.075	.125	.175	.225	.275	.325	.375	.425	.475	.525	.575	.625	.675	.725	.775	.825	.875	.925	.975
.1	17.32	13.48	11.54	8.398	10.06	10.09	15.72	7.734	6.684	6.624	7.655	4.702	10.23	5.980	4.024	5.902	1.711	5.208	3.546	0.00
.3	11.59	8.831	5.289	5.086	5.077	4.282	3.942	3.970	3.786	3.539	3.982	2.991	3.095	2.842	2.876	2.174	1.879	2.045	2.698	1.516
.5	7.719	6.388	4.742	3.967	3.645	3.410	2.908	2.880	2.709	2.539	2.565	2.319	2.418	2.054	2.022	1.704	1.875	2.218	1.465	1.210
.7	5.659	4.688	4.074	3.289	2.865	2.689	2.463	2.289	2.309	2.006	1.782	1.753	1.766	1.317	1.508	1.204	1.329	.8143	.4875	.7582
.9	4.794	4.330	3.366	2.825	2.656	2.247	2.092	1.979	1.803	1.675	1.520	1.467	1.326	1.246	1.216	1.226	.9081	.7955	.6575	.6316
1.1	4.976	3.004	2.788	2.447	1.997	1.732	1.609	1.494	1.504	1.350	1.206	1.117	.9961	.8926	.7121	.6693	.3610	.6902	0.00	0.00
1.3	3.667	2.439	2.235	1.739	1.751	1.511	1.248	1.235	1.110	1.157	1.146	1.006	.9612	.7254	.8203	.5896	.4392	.2816	0.00	0.00
1.5	3.607	2.793	1.922	1.548	1.221	1.122	1.206	1.015	.9155	.9322	.8518	.8154	.7541	.6697	.5640	.5342	.5401	.4946	.3057	0.00
1.7	3.633	1.686	1.495	1.437	1.260	1.025	.9802	.8655	.8042	.6810	.7731	.7107	.6283	.6099	.4475	.2613	.4200	.2526	0.00	0.00
1.9	2.443	1.564	1.375	1.469	.9676	.9384	.8995	.9567	.7371	.5282	.5668	.5996	.5474	.3551	.4074	.3568	0.00	0.00	.3033	0.00
2.1	1.313	1.361	1.058	.9074	.7922	.9181	.8230	.7013	.5340	.5282	.4213	.3992	.4618	.2864	.3041	.4185	.1993	0.00	0.00	0.00
2.3	1.551	1.463	1.019	.9217	.7602	.7017	.6429	.6573	.4829	.4692	.4316	.3120	.3147	0.00	.1921	.1898	0.00	0.00	0.00	0.00
2.5	.6022	.9227	1.139	.9004	.5722	.6415	.4841	.3205	.6634	.3538	.2826	.2924	.4539	.3640	.2140	.2188	.2123	0.00	0.00	0.00
2.7	.5806	.4912	.3580	.3998	.3377	.5288	.6066	.5019	.3607	.2636	.3822	.2739	0.00	0.00	.2353	0.00	0.00	0.00	0.00	0.00
2.9	0.00	.4497	.8804	.7056	.6347	.4157	.4732	.2853	.3713	.2182	.3006	.2673	.3020	.2273	0.00	0.00	0.00	0.00	0.00	0.00
3.1	0.00	0.00	.2834	0.00	.2592	.5402	.2333	.3107	.1999	.1501	0.00	0.00	.2090	0.00	0.00	0.00	0.00	0.00	0.00	0.00
3.3	0.00	.3586	0.00	.3722	.6366	0.00	.6059	.2066	.2040	0.00	.1658	.2022	.2204	0.00	0.00	0.00	0.00	0.00	0.00	0.00
3.5	0.00	0.00	0.00	0.00	0.00	0.00	0.00	0.00	.2312	0.00	0.00	0.00	0.00	0.00	0.00	0.00	0.00	0.00	0.00	0.00
3.7	0.00	0.00	0.00	0.00	.3815	.4257	0.00	.2414	0.00	.1960	0.00	0.00	0.00	0.00	0.00	0.00	0.00	0.00	0.00	0.00
3.9	0.00	0.00	0.00	0.00	0.00	0.00	0.00	0.00	0.00	0.00	0.00	0.00	0.00	0.00	0.00	0.00	0.00	0.00	0.00	0.00

DIFFERENTIAL CROSS SECTION
NB C**3 / GEV**2 / XF UNIT / NUCLEUS
NEG PION ON TUNGSTEN

$2.7 < M < 3.5$

XF

PT	.025	.075	.125	.175	.225	.275	.325	.375	.425	.475	.525	.575	.625	.675	.725	.775	.825	.875	.925	.975
.1	210.2	188.0	194.5	191.8	198.1	181.4	227.5	160.3	173.4	111.4	104.0	98.51	82.58	75.81	55.27	30.50	18.04	19.47	16.87	5.064
.3	221.1	273.5	168.9	189.2	208.6	202.7	173.9	155.3	145.8	122.1	122.2	86.52	82.68	67.61	50.31	36.82	27.82	13.75	16.36	8.299
.5	195.3	205.2	199.8	169.9	171.8	162.7	161.6	139.6	137.5	110.2	89.80	85.48	72.28	70.00	41.72	34.53	17.61	15.62	3.865	4.337
.7	145.0	161.0	156.2	139.2	157.5	130.0	137.5	120.6	93.04	87.68	71.43	67.42	53.28	39.06	31.01	22.22	17.46	13.82	7.672	.7930
.9	141.1	136.5	133.2	127.1	134.0	112.4	98.84	87.50	84.69	69.18	57.88	47.42	37.51	34.47	24.57	17.33	9.319	5.603	2.539	.6262
1.1	119.4	110.5	97.96	86.33	100.3	80.95	78.29	70.16	54.04	53.56	41.17	33.72	28.18	23.49	14.05	10.42	5.158	2.424	1.006	0.00
1.3	65.06	67.78	82.43	71.87	68.10	63.98	57.33	50.31	40.29	38.87	35.86	22.92	19.24	12.12	8.671	8.833	5.402	1.947	.4536	0.00
1.5	63.89	62.68	51.44	48.40	50.24	39.91	44.34	37.69	28.37	26.33	13.05	19.70	16.43	12.20	7.085	5.382	5.143	.3930	.4533	.4597
1.7	39.53	43.29	34.18	33.70	35.49	35.24	30.64	27.24	21.68	17.12	13.48	11.79	9.436	9.221	3.719	3.594	1.830	2.915	0.00	0.00
1.9	17.81	32.00	27.93	28.45	28.64	21.34	23.05	16.98	12.79	10.99	10.87	8.824	4.537	5.224	1.494	.8026	.2887	1.009	.4496	0.00
2.1	12.89	13.19	21.27	19.56	19.58	16.58	13.93	13.38	9.490	8.996	5.086	4.856	4.637	2.773	2.088	1.699	.6231	.3356	0.00	0.00
2.3	4.610	13.71	11.21	15.42	13.70	12.95	10.18	8.881	5.854	5.703	3.988	4.698	1.287	2.456	2.254	.8958	.6055	0.00	0.00	0.00
2.5	5.262	7.673	10.79	12.15	8.797	9.672	5.670	6.474	5.286	5.017	3.722	2.956	2.303	.3028	.3381	.6351	.3295	0.00	0.00	0.00
2.7	3.080	8.154	4.740	5.653	4.734	8.001	3.575	5.335	3.247	1.564	1.753	.5448	.6526	0.00	.3516	.3464	.3658	0.00	0.00	0.00
2.9	2.263	3.709	3.385	1.710	4.484	3.464	3.316	2.708	3.866	.9270	.8951	.2499	1.328	.3390	.3528	0.00	.3732	0.00	0.00	0.00
3.1	.9527	2.180	2.127	.4459	1.306	1.211	.8749	1.308	1.630	1.939	.4393	.2610	.3387	0.00	0.00	0.00	0.00	0.00	0.00	0.00
3.3	0.00	0.00	.7446	0.00	.9556	.8613	.3787	.6925	1.006	.7633	.4924	.2818	0.00	0.00	0.00	0.00	0.00	0.00	0.00	0.00
3.5	.9179	0.00	1.832	0.00	1.558	0.00	.3252	0.00	.3002	1.342	.2515	0.00	0.00	0.00	0.00	0.00	0.00	0.00	0.00	0.00
3.7	0.00	.4455	0.00	0.00	0.00	0.00	.3645	0.00	.3670	0.00	0.00	0.00	0.00	0.00	0.00	0.00	0.00	0.00	0.00	0.00
3.9	0.00	0.00	0.00	0.00	0.00	0.00	0.00	0.00	0.00	0.00	.3249	0.00	.4088	.4226	0.00	0.00	0.00	0.00	0.00	0.00

ERROR

	.025	.075	.125	.175	.225	.275	.325	.375	.425	.475	.525	.575	.625	.675	.725	.775	.825	.875	.925	.975
.1	39.84	29.27	28.40	24.01	27.36	19.05	43.16	19.34	26.98	14.62	13.74	14.01	11.31	14.49	10.32	8.200	6.695	7.509	7.714	5.064
.3	22.02	19.95	12.20	11.26	11.02	10.00	8.796	8.344	8.206	7.716	7.937	6.755	6.740	6.472	6.040	5.529	5.454	4.230	5.532	3.750
.5	16.82	13.80	10.72	8.512	7.774	7.012	6.699	6.202	6.235	5.706	5.264	5.275	5.075	5.307	4.368	4.346	3.637	3.643	1.934	2.187
.7	12.71	10.52	8.565	6.936	6.597	5.540	5.444	5.067	4.469	4.394	4.041	4.018	3.733	3.463	3.314	3.040	2.926	2.460	2.431	.7930
.9	12.20	9.277	7.383	6.136	5.674	4.743	4.238	3.977	3.931	3.604	3.367	3.135	2.888	2.940	2.642	2.364	1.905	1.622	1.272	.6262
1.1	11.72	8.236	6.187	4.831	4.593	3.779	3.555	3.355	2.977	3.058	2.752	2.543	2.393	2.310	1.862	1.734	1.417	.9444	.7121	0.00
1.3	8.360	6.311	5.444	4.277	3.588	3.219	2.930	2.742	2.491	2.557	2.536	2.042	1.907	1.606	1.446	1.538	1.275	.8722	.4535	0.00
1.5	8.530	6.151	4.256	3.377	2.979	2.531	2.596	2.352	2.054	2.076	1.833	1.904	1.794	1.646	1.340	1.235	1.287	.3930	.4533	.4597
1.7	6.974	5.074	3.505	2.903	2.592	2.476	2.237	2.061	1.833	1.671	1.537	1.498	1.392	1.441	.9608	.9972	.7479	1.031	0.00	0.00
1.9	4.861	4.384	3.281	2.854	2.478	2.046	2.055	1.717	1.468	1.364	1.382	1.331	1.015	1.114	.6103	.4634	.2887	.5825	.4496	0.00
2.1	3.755	2.931	2.989	2.446	2.127	1.867	1.655	1.589	1.317	1.260	.9553	1.014	1.064	.8361	.7388	.6940	.4409	.3356	0.00	0.00
2.3	2.329	3.030	2.296	2.343	1.885	1.733	1.486	1.371	1.088	1.042	.6711	1.027	.5757	.8200	.7975	.5172	.4281	0.00	0.00	0.00
2.5	2.410	2.326	2.423	2.195	1.638	1.593	1.184	1.272	1.130	1.025	.6761	.8551	.8153	.3028	.3381	.4491	.3295	0.00	0.00	0.00
2.7	1.799	2.468	1.683	1.643	1.267	1.541	.9922	1.224	.9387	.5911	.6202	.3869	.4615	0.00	.3516	.3464	.3658	0.00	0.00	0.00
2.9	1.606	1.673	1.391	1.043	1.296	1.097	1.001	.9028	1.034	.4637	.4478	.2499	.6642	.3390	.3528	0.00	.3732	0.00	0.00	0.00
3.1	.9527	1.288	1.229	.4459	.7543	.7009	.5052	.6574	.6658	.6868	.3107	.2610	.3387	0.00	0.00	0.00	0.00	0.00	0.00	0.00
3.3	0.00	0.00	.7446	0.00	.6761	.6116	.3787	.4919	.5916	.4413	.3488	.2818	0.00	0.00	0.00	0.00	0.00	0.00	0.00	0.00
3.5	.9179	0.00	1.163	0.00	1.146	0.00	.3252	0.00	.3002	.6004	.2516	0.00	0.00	0.00	0.00	0.00	0.00	0.00	0.00	0.00
3.7	0.00	.4455	0.00	0.00	0.00	0.00	.3645	0.00	.3670	0.00	0.00	0.00	0.00	0.00	0.00	0.00	0.00	0.00	0.00	0.00
3.9	0.00	0.00	0.00	0.00	0.00	0.00	0.00	0.00	0.00	0.00	.3249	0.00	.4088	.4226	0.00	0.00	0.00	0.00	0.00	0.00

DIFFERENTIAL CROSS SECTION
NB C**3 / GEV**2 / XF UNIT / NUCLEUS
PROTON ON CARBON

2.7 < M < 3.5

PT \ XF	.025	.075	.125	.175	.225	.275	.325	.375	.425	.475	.525	.575	.625	.675	.725	.775	.825	.875	.925	.975
.1	14.31	11.71	11.60	8.981	15.79	6.795	7.627	5.043	4.151	1.516	1.640	.6792	1.040	1.304	0.00	0.00	0.00	0.00	0.00	0.00
.3	12.97	15.93	11.69	10.82	10.74	7.439	6.872	4.018	3.529	2.733	1.359	1.478	.2535	1.078	.1465	0.00	0.00	.3939	0.00	0.00
.5	13.37	12.05	11.38	10.93	9.458	7.029	4.886	4.281	3.820	2.418	1.242	1.110	.3489	.3805	.1259	.1334	.1867	0.00	0.00	0.00
.7	13.67	12.52	9.377	7.813	8.351	5.529	4.067	3.573	1.985	1.564	1.155	.6450	.3884	.3663	.0318	0.00	0.00	0.00	0.00	0.00
.9	8.886	8.420	5.858	5.108	6.003	4.509	3.334	2.074	1.671	1.125	.4671	.5179	.2172	.1817	.0764	.1633	0.00	0.00	0.00	0.00
1.1	5.341	6.500	6.175	5.325	4.345	3.525	2.294	1.991	1.226	.7595	.5042	.3255	.3404	.1100	.1274	0.00	0.00	0.00	0.00	0.00
1.3	5.562	4.153	3.473	3.679	2.927	2.034	1.606	1.295	.9040	.9787	.3928	.3585	.1821	.1059	0.00	.0705	0.00	0.00	0.00	0.00
1.5	2.223	2.986	2.476	2.385	1.643	1.511	1.425	.8489	.6478	.4663	.4298	.1527	.0961	.1072	0.00	0.00	0.00	0.00	0.00	0.00
1.7	2.333	1.770	2.395	1.843	1.462	.9580	1.006	.5453	.3712	.2355	.1240	.0437	.1486	.0549	.0509	0.00	0.00	0.00	0.00	0.00
1.9	.9443	1.207	.8453	1.465	.6955	.7249	.7752	.4383	.0802	.1193	.1656	0.00	0.00	0.00	0.00	0.00	0.00	0.00	0.00	0.00
2.1	.2143	1.552	.6512	.8124	.2681	.2815	.3909	.1691	.1273	0.00	.0446	0.00	0.00	.0574	0.00	0.00	0.00	0.00	0.00	0.00
2.3	0.00	.4439	.6646	.3010	.4609	.3550	.0965	.1447	.1378	.1325	0.00	0.00	0.00	0.00	0.00	0.00	0.00	0.00	0.00	0.00
2.5	.2137	.2791	.1016	.6014	.1950	.0570	.2073	0.00	.1142	.0985	0.00	0.00	0.00	0.00	0.00	0.00	0.00	0.00	0.00	0.00
2.7	0.00	.1745	0.00	.4197	.0785	.1956	.0618	0.00	0.00	.0527	0.00	.0553	0.00	0.00	0.00	0.00	0.00	0.00	0.00	0.00
2.9	.2769	0.00	.2806	0.00	.2531	.0786	.1310	0.00	.0629	0.00	0.00	0.00	0.00	0.00	0.00	0.00	0.00	0.00	0.00	0.00
3.1	0.00	0.00	0.00	0.00	0.00	0.00	0.00	0.00	0.00	.0571	0.00	0.00	0.00	0.00	0.00	0.00	0.00	0.00	0.00	0.00
3.3	0.00	0.00	0.00	0.00	0.00	0.00	0.00	0.00	0.00	0.00	0.00	0.00	0.00	0.00	0.00	0.00	0.00	0.00	0.00	0.00
3.5	0.00	0.00	0.00	.1571	0.00	0.00	0.00	0.00	0.00	0.00	0.00	0.00	0.00	0.00	0.00	0.00	0.00	0.00	0.00	0.00
3.7	0.00	0.00	0.00	0.00	0.00	0.00	0.00	0.00	0.00	0.00	0.00	0.00	0.00	0.00	0.00	0.00	0.00	0.00	0.00	0.00
3.9	0.00	0.00	0.00	0.00	0.00	0.00	0.00	0.00	0.00	0.00	0.00	0.00	0.00	0.00	0.00	0.00	0.00	0.00	0.00	0.00

ERROR

	.025	.075	.125	.175	.225	.275	.325	.375	.425	.475	.525	.575	.625	.675	.725	.775	.825	.875	.925	.975
.1	4.203	2.871	2.562	1.957	4.275	1.464	2.359	1.172	1.129	.6922	.5563	.5219	.6596	.6779	0.00	0.00	0.00	0.00	0.00	0.00
.3	2.624	2.158	1.502	1.260	1.166	.9322	.8576	.6561	.6163	.5536	.3954	.4513	.1874	.4121	.1465	0.00	0.00	.3939	0.00	0.00
.5	2.091	1.517	1.195	1.019	.8827	.6989	.5634	.5338	.5137	.4107	.3031	.2991	.1751	.1905	.1259	.1334	.1867	0.00	0.00	0.00
.7	1.851	1.369	.9729	.7743	.7292	.5547	.4504	.4249	.3185	.2855	.2594	.1949	.1588	.1639	.0818	0.00	0.00	0.00	0.00	0.00
.9	1.492	1.079	.7272	.5707	.5639	.4540	.3776	.2965	.2713	.2251	.2104	.2046	.1085	.1050	.0764	.1156	0.00	0.00	0.00	0.00
1.1	1.190	.9491	.7102	.5515	.4442	.3784	.2964	.2763	.2203	.1741	.1896	.1231	.1289	.0778	.0991	0.00	0.00	0.00	0.00	0.00
1.3	1.177	.7254	.5220	.4485	.3555	.2771	.2394	.2154	.1846	.1999	.1310	.1267	.0911	.0749	0.00	.0705	0.00	0.00	0.00	0.00
1.5	.8004	.6085	.4203	.3535	.2602	.2391	.2254	.1733	.1528	.1347	.1300	.0914	.0681	.0758	0.00	0.00	0.00	0.00	0.00	0.00
1.7	.9127	.5088	.4258	.3175	.2511	.1957	.1937	.1408	.1174	.0902	.0716	.0437	.0859	.0549	.0609	0.00	0.00	0.00	0.00	0.00
1.9	.5719	.4395	.2682	.3003	.1862	.1760	.1779	.1322	.0567	.0684	.0828	0.00	0.00	0.00	0.00	0.00	0.00	0.00	0.00	0.00
2.1	.2143	.5022	.2474	.2259	.1200	.1150	.1304	.0846	.0736	0.00	.0446	0.00	0.00	.0574	0.00	0.00	0.00	0.00	0.00	0.00
2.3	0.00	.2577	.2524	.1513	.1633	.1344	.0682	.0835	.0796	.0765	0.00	0.00	0.00	0.00	0.00	0.00	0.00	0.00	0.00	0.00
2.5	.2137	.1974	.1016	.2267	.1127	.0570	.1037	0.00	.0806	.0695	0.00	0.00	0.00	0.00	0.00	0.00	0.00	0.00	0.00	0.00
2.7	0.00	.1745	0.00	.2104	.0785	.1129	.0618	0.00	0.00	.0527	0.00	.0553	0.00	0.00	0.00	0.00	0.00	0.00	0.00	0.00
2.9	.2769	0.00	.1995	0.00	.1462	.0785	.0928	0.00	.0629	0.00	0.00	0.00	0.00	0.00	0.00	0.00	0.00	0.00	0.00	0.00
3.1	0.00	0.00	0.00	0.00	0.00	0.00	0.00	0.00	0.00	.0571	0.00	0.00	0.00	0.00	0.00	0.00	0.00	0.00	0.00	0.00
3.3	0.00	0.00	0.00	0.00	0.00	0.00	0.00	0.00	0.00	0.00	0.00	0.00	0.00	0.00	0.00	0.00	0.00	0.00	0.00	0.00
3.5	0.00	0.00	0.00	.1571	0.00	0.00	0.00	0.00	0.00	0.00	0.00	0.00	0.00	0.00	0.00	0.00	0.00	0.00	0.00	0.00
3.7	0.00	0.00	0.00	0.00	0.00	0.00	0.00	0.00	0.00	0.00	0.00	0.00	0.00	0.00	0.00	0.00	0.00	0.00	0.00	0.00
3.9	0.00	0.00	0.00	0.00	0.00	0.00	0.00	0.00	0.00	0.00	0.00	0.00	0.00	0.00	0.00	0.00	0.00	0.00	0.00	0.00

DIFFERENTIAL CROSS SECTION
NB C**3 / GEV**2 / XF UNIT / NUCLEUS
POS PION ON CARBON

3.5 < M < 4.0

XF

PT	.025	.075	.125	.175	.225	.275	.325	.375	.425	.475	.525	.575	.625	.675	.725	.775	.825	.875	.925	.975
.1	0.00	0.00	0.00	0.00	0.00	.4992	1.165	0.00	0.00	.5749	0.00	0.00	.5634	.4474	0.00	0.00	0.00	0.00	0.00	0.00
.3	0.00	0.00	.3300	.2829	.8042	0.00	.2320	0.00	.7040	.1927	.2196	0.00	.6300	.2243	.6645	.3539	0.00	.5240	0.00	0.00
.5	0.00	.5018	0.00	.6517	0.00	.5174	0.00	.6801	.2951	.6231	.3267	0.00	0.00	0.00	.4084	0.00	0.00	0.00	0.00	0.00
.7	0.00	.7210	.7055	.5237	.2884	.1277	.3257	.2280	.1981	.3273	.2192	.2146	0.00	.3625	.1599	.1662	0.00	0.00	0.00	0.00
.9	0.00	0.00	.3697	.1591	.2443	.1079	.2690	.1753	.2672	.3731	.2948	.0990	.1093	.1070	.1230	.1373	.1510	0.00	.2071	0.00
1.1	0.00	.2336	.3447	.1311	0.00	.0887	.1649	.0873	.2341	0.00	0.00	.2642	0.00	.0959	0.00	0.00	0.00	0.00	0.00	0.00
1.3	0.00	0.00	0.00	0.00	0.00	0.00	.1533	.0687	.0725	.0736	.0772	0.00	.1696	0.00	.0964	0.00	0.00	0.00	0.00	0.00
1.5	0.00	0.00	.1163	0.00	.0953	.0791	.0730	.1421	0.00	0.00	.0718	.0774	0.00	0.00	0.00	.0967	0.00	0.00	0.00	0.00
1.7	0.00	0.00	.1207	.2169	.0868	.0731	.0689	.0656	.0662	.1345	0.00	.0764	.0820	.0840	0.00	0.00	0.00	0.00	0.00	0.00
1.9	0.00	0.00	0.00	0.00	0.00	.0841	.0684	0.00	0.00	0.00	0.00	0.00	0.00	0.00	0.00	0.00	0.00	0.00	0.00	0.00
2.1	0.00	0.00	0.00	0.00	.0865	.0777	.0720	0.00	.0652	0.00	0.00	0.00	0.00	0.00	0.00	0.00	0.00	0.00	0.00	0.00
2.3	0.00	0.00	0.00	.1408	0.00	0.00	0.00	0.00	0.00	0.00	0.00	0.00	0.00	0.00	0.00	0.00	0.00	0.00	0.00	0.00
2.5	0.00	0.00	0.00	0.00	0.00	0.00	0.00	0.00	0.00	0.00	0.00	0.00	0.00	0.00	0.00	0.00	0.00	0.00	0.00	0.00
2.7	0.00	0.00	0.00	0.00	0.00	0.00	0.00	0.00	0.00	0.00	0.00	0.00	0.00	0.00	0.00	0.00	0.00	0.00	0.00	0.00
2.9	0.00	0.00	0.00	0.00	0.00	0.00	0.00	0.00	0.00	0.00	0.00	0.00	0.00	0.00	0.00	0.00	0.00	0.00	0.00	0.00
3.1	0.00	0.00	0.00	0.00	0.00	0.00	0.00	0.00	0.00	0.00	0.00	0.00	0.00	0.00	0.00	0.00	0.00	0.00	0.00	0.00
3.3	0.00	0.00	0.00	0.00	0.00	0.00	0.00	0.00	0.00	0.00	0.00	0.00	0.00	0.00	0.00	0.00	0.00	0.00	0.00	0.00
3.5	0.00	0.00	0.00	0.00	0.00	0.00	0.00	0.00	0.00	0.00	0.00	0.00	0.00	0.00	0.00	0.00	0.00	0.00	0.00	0.00
3.7	0.00	0.00	0.00	0.00	0.00	.1435	0.00	0.00	0.00	0.00	0.00	0.00	0.00	0.00	0.00	0.00	0.00	0.00	0.00	0.00
3.9	0.00	0.00	0.00	0.00	0.00	0.00	0.00	0.00	0.00	0.00	0.00	0.00	0.00	0.00	0.00	0.00	0.00	0.00	0.00	0.00

ERROR

PT	.025	.075	.125	.175	.225	.275	.325	.375	.425	.475	.525	.575	.625	.675	.725	.775	.825	.875	.925	.975
.1	0.00	0.00	0.00	0.00	0.00	.4992	.8496	0.00	0.00	.5799	0.00	0.00	.5634	.4474	0.00	0.00	0.00	0.00	0.00	0.00
.3	0.00	0.00	.3300	.2829	.4682	0.00	.2320	0.00	.4237	.1927	.2196	0.00	.4482	.2283	.4904	.3539	0.00	.5240	0.00	0.00
.5	0.00	.5018	0.00	.3787	0.00	.3020	0.00	.3052	.2096	.3126	.2316	0.00	0.00	0.00	.2697	0.00	0.00	0.00	0.00	0.00
.7	0.00	.5141	.4092	.3037	.2052	.1277	.1882	.1615	.1402	.1895	.1551	.1519	0.00	.2213	.1599	.1662	0.00	0.00	0.00	0.00
.9	0.00	0.00	.2615	.1591	.1730	.1079	.1553	.1240	.1543	.1865	.1703	.0990	.1093	.1070	.1230	.1373	.1510	0.00	.2071	0.00
1.1	0.00	.2336	.2438	.1311	0.00	.0887	.1170	.0873	.1354	0.00	0.00	.1526	0.00	.0959	0.00	0.00	0.00	0.00	0.00	0.00
1.3	0.00	0.00	0.00	0.00	0.00	0.00	.1085	.0687	.0725	.0735	.0772	0.00	.1199	0.00	.0964	0.00	0.00	0.00	0.00	0.00
1.5	0.00	0.00	.1163	0.00	.0953	.0791	.0730	.1005	0.00	0.00	.0718	.0774	0.00	0.00	0.00	.0957	0.00	0.00	0.00	0.00
1.7	0.00	0.00	.1207	.1535	.0868	.0731	.0689	.0656	.0662	.0986	0.00	.0764	.0820	.0840	0.00	0.00	0.00	0.00	0.00	0.00
1.9	0.00	0.00	0.00	0.00	0.00	.0841	.0684	0.00	0.00	0.00	0.00	0.00	0.00	0.00	0.00	0.00	0.00	0.00	0.00	0.00
2.1	0.00	0.00	0.00	0.00	.0865	.0777	.0720	0.00	.0652	0.00	0.00	0.00	0.00	0.00	0.00	0.00	0.00	0.00	0.00	0.00
2.3	0.00	0.00	0.00	.1408	0.00	0.00	0.00	0.00	0.00	0.00	0.00	0.00	0.00	0.00	0.00	0.00	0.00	0.00	0.00	0.00
2.5	0.00	0.00	0.00	0.00	0.00	0.00	0.00	0.00	0.00	0.00	0.00	0.00	0.00	0.00	0.00	0.00	0.00	0.00	0.00	0.00
2.7	0.00	0.00	0.00	0.00	0.00	0.00	0.00	0.00	0.00	0.00	0.00	0.00	0.00	0.00	0.00	0.00	0.00	0.00	0.00	0.00
2.9	0.00	0.00	0.00	0.00	0.00	0.00	0.00	0.00	0.00	0.00	0.00	0.00	0.00	0.00	0.00	0.00	0.00	0.00	0.00	0.00
3.1	0.00	0.00	0.00	0.00	0.00	0.00	0.00	0.00	0.00	0.00	0.00	0.00	0.00	0.00	0.00	0.00	0.00	0.00	0.00	0.00
3.3	0.00	0.00	0.00	0.00	0.00	0.00	0.00	0.00	0.00	0.00	0.00	0.00	0.00	0.00	0.00	0.00	0.00	0.00	0.00	0.00
3.5	0.00	0.00	0.00	0.00	0.00	0.00	0.00	0.00	0.00	0.00	0.00	0.00	0.00	0.00	0.00	0.00	0.00	0.00	0.00	0.00
3.7	0.00	0.00	0.00	0.00	0.00	.1435	0.00	0.00	0.00	0.00	0.00	0.00	0.00	0.00	0.00	0.00	0.00	0.00	0.00	0.00
3.9	0.00	0.00	0.00	0.00	0.00	0.00	0.00	0.00	0.00	0.00	0.00	0.00	0.00	0.00	0.00	0.00	0.00	0.00	0.00	0.00

DIFFERENTIAL CROSS SECTION
NB C**3 / GEV**2 / XF UNIT / NUCLEUS
NEG PION ON CARBON

3.5 < M < 4.0

XF

PT	.025	.075	.125	.175	.225	.275	.325	.375	.425	.475	.525	.575	.625	.675	.725	.775	.825	.875	.925	.975
.1	1.462	.4102	.2939	.5894	.2138	0.00	0.00	1.119	2.401	.5969	.4971	.6024	0.00	.2374	.2042	.3015	0.00	0.00	0.00	0.00
.3	0.00	.4261	.5402	1.044	.6087	.2880	.3368	.8133	.4597	.4025	.1655	.2171	.6364	.2743	.3610	.1494	.1204	0.00	.3425	0.00
.5	.5094	.5199	1.094	.5397	.7473	.2015	.2694	.2988	.3290	.2477	.7090	.4306	.3999	.0801	.1681	.3657	0.00	.2335	.1465	0.00
.7	0.00	.0993	.2738	.2226	.5438	.3912	.1986	.2268	.2643	.1363	.0920	.1878	.2135	.1243	0.00	0.00	0.00	.1604	0.00	0.00
.9	.2131	0.00	0.00	.2506	.3741	.3049	.3411	.2274	.3444	.1597	.1641	.0413	.2695	.1506	.0987	.1118	0.00	0.00	.0971	0.00
1.1	.1541	.2207	.4685	.1701	.1766	.2263	.1722	.1692	0.00	.2426	.1539	.2327	.0401	0.00	0.00	.0522	0.00	0.00	0.00	0.00
1.3	0.00	0.00	.0835	.3147	.0765	.2434	.1246	.1538	.1491	.0923	.0987	.0695	.1821	.2291	0.00	.0867	.0489	0.00	0.00	0.00
1.5	.1661	0.00	.1053	.0871	.1481	.1006	.0625	.1206	.0589	.1231	.0926	.0960	.0673	.0369	0.00	0.00	.0442	0.00	.0612	0.00
1.7	.5308	0.00	.0711	.0415	.1836	.0673	.0585	.0283	.0848	0.00	.0291	.0639	.0328	.1461	.0402	0.00	0.00	0.00	0.00	0.00
1.9	0.00	0.00	.1314	.0541	.0792	.0668	.0287	0.00	0.00	.0565	.0317	.0325	0.00	0.00	0.00	0.00	.0435	0.00	0.00	0.00
2.1	0.00	.1146	.0829	.1154	0.00	0.00	0.00	0.00	0.00	0.00	0.00	.0307	.0339	0.00	0.00	0.00	0.00	0.00	0.00	0.00
2.3	0.00	0.00	.0674	.1084	0.00	.1131	0.00	0.00	0.00	0.00	0.00	0.00	0.00	0.00	0.00	0.00	0.00	0.00	0.00	0.00
2.5	0.00	0.00	0.00	0.00	0.00	0.00	0.00	0.00	.0313	.0621	0.00	0.00	0.00	0.00	0.00	0.00	0.00	0.00	0.00	0.00
2.7	0.00	0.00	0.00	0.00	0.00	0.00	0.00	0.00	0.00	0.00	.0329	0.00	0.00	0.00	0.00	0.00	0.00	0.00	0.00	0.00
2.9	0.00	0.00	0.00	0.00	0.00	0.00	0.00	0.00	0.00	0.00	0.00	0.00	0.00	0.00	0.00	0.00	0.00	0.00	0.00	0.00
3.1	0.00	0.00	0.00	.0712	0.00	0.00	0.00	0.00	0.00	0.00	0.00	0.00	0.00	0.00	0.00	0.00	0.00	0.00	0.00	0.00
3.3	0.00	0.00	0.00	0.00	0.00	0.00	0.00	0.00	0.00	0.00	0.00	0.00	0.00	0.00	0.00	0.00	0.00	0.00	0.00	0.00
3.5	0.00	0.00	0.00	0.00	0.00	0.00	0.00	0.00	0.00	0.00	0.00	0.00	0.00	0.00	0.00	0.00	0.00	0.00	0.00	0.00
3.7	0.00	0.00	0.00	0.00	0.00	0.00	0.00	0.00	0.00	0.00	0.00	0.00	0.00	0.00	0.00	0.00	0.00	0.00	0.00	0.00
3.9	0.00	0.00	0.00	0.00	0.00	0.00	0.00	0.00	0.00	0.00	0.00	0.00	0.00	0.00	0.00	0.00	0.00	0.00	0.00	0.00

ERROR

PT	.025	.075	.125	.175	.225	.275	.325	.375	.425	.475	.525	.575	.625	.675	.725	.775	.825	.875	.925	.975
.1	1.462	.4102	.2939	.4240	.2138	0.00	0.00	.5148	2.252	.4221	.3675	.3538	0.00	.2374	.2042	.3015	0.00	0.00	0.00	0.00
.3	0.00	.3013	.3192	.3723	.2741	.1668	.1975	.2749	.2097	.2048	.1849	.1557	.2863	.1942	.2110	.1494	.1204	0.00	.3425	0.00
.5	.3614	.3039	.3885	.2210	.2379	.1171	.1350	.1341	.1349	.1243	.2154	.1630	.1792	.0801	.1195	.1837	0.00	.1652	.1465	0.00
.7	0.00	.0993	.1584	.1288	.1815	.1480	.0998	.1016	.1081	.0788	.0651	.0942	.1073	.0880	0.00	0.00	0.00	.1134	0.00	0.00
.9	.2131	0.00	0.00	.1259	.1421	.1156	.1207	.0929	.1149	.0799	.0821	.0413	.1102	.0871	.0699	.0791	0.00	0.00	.0971	0.00
1.1	.1541	.1569	.1914	.0987	.0889	.0925	.0770	.0758	0.00	.0918	.0770	.0951	.0401	0.00	0.00	.0522	0.00	0.00	0.00	0.00
1.3	0.00	0.00	.0835	.1291	.0541	.0921	.0623	.0688	.0667	.0533	.0570	.0492	.0814	.0936	0.00	.0613	.0489	0.00	0.00	0.00
1.5	.1661	0.00	.0745	.0616	.0741	.0581	.0442	.0603	.0417	.0615	.0535	.0555	.0476	.0369	0.00	0.00	.0442	0.00	.0612	0.00
1.7	.3091	0.00	.0711	.0415	.0821	.0476	.0414	.0283	.0490	0.00	.0291	.0452	.0328	.0731	.0402	0.00	0.00	0.00	0.00	0.00
1.9	0.00	0.00	.0931	.0541	.0560	.0472	.0287	0.00	0.00	.0399	.0317	.0325	0.00	0.00	0.00	0.00	.0435	0.00	0.00	0.00
2.1	0.00	.1146	.0829	.0818	0.00	0.00	0.00	0.00	0.00	0.00	0.00	.0307	.0339	0.00	0.00	0.00	0.00	0.00	0.00	0.00
2.3	0.00	0.00	.0674	.0767	0.00	.0653	0.00	0.00	0.00	0.00	0.00	0.00	0.00	0.00	0.00	0.00	0.00	0.00	0.00	0.00
2.5	0.00	0.00	0.00	0.00	0.00	0.00	0.00	0.00	.0313	.0439	0.00	0.00	0.00	0.00	0.00	0.00	0.00	0.00	0.00	0.00
2.7	0.00	0.00	0.00	0.00	0.00	0.00	0.00	0.00	0.00	0.00	.0329	0.00	0.00	0.00	0.00	0.00	0.00	0.00	0.00	0.00
2.9	0.00	0.00	0.00	0.00	0.00	0.00	0.00	0.00	0.00	0.00	0.00	0.00	0.00	0.00	0.00	0.00	0.00	0.00	0.00	0.00
3.1	0.00	0.00	0.00	.0712	0.00	0.00	0.00	0.00	0.00	0.00	0.00	0.00	0.00	0.00	0.00	0.00	0.00	0.00	0.00	0.00
3.3	0.00	0.00	0.00	0.00	0.00	0.00	0.00	0.00	0.00	0.00	0.00	0.00	0.00	0.00	0.00	0.00	0.00	0.00	0.00	0.00
3.5	0.00	0.00	0.00	0.00	0.00	0.00	0.00	0.00	0.00	0.00	0.00	0.00	0.00	0.00	0.00	0.00	0.00	0.00	0.00	0.00
3.7	0.00	0.00	0.00	0.00	0.00	0.00	0.00	0.00	0.00	0.00	0.00	0.00	0.00	0.00	0.00	0.00	0.00	0.00	0.00	0.00
3.9	0.00	0.00	0.00	0.00	0.00	0.00	0.00	0.00	0.00	0.00	0.00	0.00	0.00	0.00	0.00	0.00	0.00	0.00	0.00	0.00

DIFFERENTIAL CROSS SECTION
NB C**3 / GEV**2 / XF UNIT / NUCLEUS
NEG PION ON COPPER

3.5 < M < 4.0

XF

PT	.025	.075	.125	.175	.225	.275	.325	.375	.425	.475	.525	.575	.625	.675	.725	.775	.825	.875	.925	.975
.1	0.00	2.514	5.223	3.275	2.408	2.770	1.121	3.288	3.424	3.413	0.00	5.786	.7890	1.256	4.777	3.279	1.257	3.847	0.00	0.00
.3	5.755	.6151	2.192	.3401	3.700	.8969	1.794	2.165	1.224	.4570	.8704	3.659	.8030	2.024	.4692	1.141	1.559	1.172	.6201	0.00
.5	0.00	1.024	2.822	1.205	1.906	1.775	2.296	1.281	1.492	.7690	1.860	.5790	2.059	.7263	.2567	.8403	.6074	.7063	.8909	0.00
.7	3.504	1.564	1.819	2.119	2.157	1.254	1.993	2.106	3.135	1.994	1.455	1.075	1.287	.6657	.3429	.6461	.4605	0.00	0.00	0.00
.9	.9937	2.369	1.033	2.222	1.818	2.316	1.449	2.910	1.104	1.498	.7743	1.040	.6687	.4305	.3272	0.00	0.00	0.00	0.00	0.00
1.1	.9761	.2913	2.084	.5499	.9789	1.392	.8196	1.179	.6687	.9041	1.270	.8245	.3640	.5175	0.00	.1638	0.00	0.00	.2346	0.00
1.3	0.00	1.057	.2281	1.152	.5567	1.245	.4153	.8661	.4627	.8680	.3059	.4345	.4629	0.00	.1216	0.00	.1598	0.00	0.00	0.00
1.5	.8124	.6340	1.232	.2773	.5102	.5527	.4077	.3928	.4793	.5693	.5825	.3160	.8823	.1208	0.00	0.00	.1420	0.00	0.00	0.00
1.7	0.00	.3371	.1747	.3164	.1286	.1084	0.00	.1942	.3572	.4597	.2894	.2060	.3210	.3576	0.00	.2662	0.00	0.00	0.00	0.00
1.9	.6117	.6005	0.00	0.00	.2731	.3272	.2075	.4532	.1797	.0929	.1000	0.00	.1054	0.00	.1342	0.00	0.00	0.00	0.00	0.00
2.1	0.00	0.00	.2424	.1666	0.00	0.00	.1982	0.00	.0878	.1876	0.00	.1015	.1090	.1122	0.00	0.00	0.00	0.00	0.00	0.00
2.3	0.00	0.00	.7375	0.00	.1432	0.00	.1114	0.00	.1890	0.00	0.00	0.00	0.00	0.00	0.00	0.00	0.00	0.00	0.00	0.00
2.5	0.00	.2955	0.00	0.00	.1799	.3050	.1396	0.00	.1014	.1052	0.00	0.00	.1031	0.00	0.00	0.00	0.00	0.00	0.00	0.00
2.7	0.00	0.00	.2307	0.00	0.00	.1629	0.00	0.00	0.00	0.00	.1029	0.00	0.00	0.00	0.00	0.00	0.00	0.00	0.00	0.00
2.9	0.00	0.00	0.00	0.00	0.00	.1551	0.00	0.00	.1098	0.00	0.00	0.00	0.00	0.00	0.00	0.00	0.00	0.00	0.00	0.00
3.1	0.00	0.00	0.00	0.00	0.00	.1624	0.00	0.00	0.00	0.00	0.00	0.00	0.00	0.00	0.00	0.00	0.00	0.00	0.00	0.00
3.3	0.00	0.00	0.00	0.00	.1942	0.00	.1569	0.00	0.00	0.00	0.00	0.00	0.00	0.00	0.00	0.00	0.00	0.00	0.00	0.00
3.5	0.00	0.00	0.00	0.00	0.00	.1887	0.00	0.00	0.00	.1240	0.00	0.00	.1214	0.00	0.00	0.00	0.00	0.00	0.00	0.00
3.7	0.00	0.00	0.00	0.00	0.00	0.00	.1722	.1530	0.00	0.00	0.00	0.00	0.00	0.00	0.00	0.00	0.00	0.00	0.00	0.00
3.9	0.00	0.00	0.00	0.00	0.00	0.00	0.00	0.00	0.00	0.00	0.00	0.00	0.00	0.00	0.00	0.00	0.00	0.00	0.00	0.00

ERROR

PT	.025	.075	.125	.175	.225	.275	.325	.375	.425	.475	.525	.575	.625	.675	.725	.775	.825	.875	.925	.975
.1	0.00	2.514	2.643	2.008	1.430	1.721	.7928	2.332	2.818	2.946	0.00	5.164	.7890	1.256	3.219	2.631	1.257	3.847	0.00	0.00
.3	2.604	.6151	1.099	.3401	1.179	.6352	.8191	.8348	.5488	.3231	.5056	1.179	.5716	.9164	.4692	.6603	.9381	.8485	.6201	0.00
.5	0.00	.7245	1.071	.6067	.6754	.6291	.6956	.4873	.5303	.3864	.6228	.3356	.5905	.4195	.2567	.4879	.4340	.4998	.6327	0.00
.7	1.583	.7831	.7449	.7105	.6511	.4741	.5764	.5639	.6693	.5340	.4613	.4074	.4566	.3329	.2425	.4233	.3258	0.00	0.00	0.00
.9	.7026	.9037	.5165	.7064	.5757	.5798	.4376	.6074	.3681	.4326	.3162	.3681	.2493	.2465	.2322	0.00	0.00	0.00	0.00	0.00
1.1	.6924	.2913	.7381	.3175	.3704	.4202	.3099	.3560	.2734	.3201	.3834	.3118	.2102	.2588	0.00	.1638	0.00	0.00	.2346	0.00
1.3	0.00	.6191	.2281	.4754	.2784	.3758	.2077	.2888	.2070	.2894	.1766	.2173	.2315	0.00	.1216	0.00	.1598	0.00	0.00	0.00
1.5	.8124	.4491	.5065	.1961	.2554	.2475	.2039	.1965	.2144	.2324	.2379	.1825	.3120	.1208	0.00	0.00	.1420	0.00	0.00	0.00
1.7	0.00	.3371	.1747	.2241	.1286	.1084	0.00	.1373	.1786	.2056	.1672	.1457	.1854	.2064	0.00	.1882	0.00	0.00	0.00	0.00
1.9	.6117	.4276	0.00	0.00	.1933	.1889	.1469	.2028	.1271	.0929	.1000	0.00	.1054	0.00	.1342	0.00	0.00	0.00	0.00	0.00
2.1	0.00	0.00	.2424	.1666	0.00	0.00	.1402	0.00	.0878	.1326	0.00	.1015	.1090	.1122	0.00	0.00	0.00	0.00	0.00	0.00
2.3	0.00	0.00	.4272	0.00	.1432	0.00	.1114	0.00	.1337	0.00	0.00	0.00	0.00	0.00	0.00	0.00	0.00	0.00	0.00	0.00
2.5	0.00	.2955	0.00	0.00	.1799	.2157	.1396	0.00	.1014	.1052	0.00	0.00	.1031	0.00	0.00	0.00	0.00	0.00	0.00	0.00
2.7	0.00	0.00	.2307	0.00	0.00	.1629	0.00	0.00	0.00	0.00	.1029	0.00	0.00	0.00	0.00	0.00	0.00	0.00	0.00	0.00
2.9	0.00	0.00	0.00	0.00	0.00	.1551	0.00	0.00	.1098	0.00	0.00	0.00	0.00	0.00	0.00	0.00	0.00	0.00	0.00	0.00
3.1	0.00	0.00	0.00	0.00	0.00	.1624	0.00	0.00	0.00	0.00	0.00	0.00	0.00	0.00	0.00	0.00	0.00	0.00	0.00	0.00
3.3	0.00	0.00	0.00	0.00	.1942	0.00	.1569	0.00	0.00	0.00	0.00	0.00	0.00	0.00	0.00	0.00	0.00	0.00	0.00	0.00
3.5	0.00	0.00	0.00	0.00	0.00	.1887	0.00	0.00	0.00	.1240	0.00	0.00	.1214	0.00	0.00	0.00	0.00	0.00	0.00	0.00
3.7	0.00	0.00	0.00	0.00	0.00	0.00	.1722	.1530	0.00	0.00	0.00	0.00	0.00	0.00	0.00	0.00	0.00	0.00	0.00	0.00
3.9	0.00	0.00	0.00	0.00	0.00	0.00	0.00	0.00	0.00	0.00	0.00	0.00	0.00	0.00	0.00	0.00	0.00	0.00	0.00	0.00

DIFFERENTIAL CROSS SECTION
NB C**3 / GEV**2 / XF UNIT / NUCLEUS
NEG PION ON TUNGSTEN

3.5 < M < 4.0

PT \ XF	.025	.075	.125	.175	.225	.275	.325	.375	.425	.475	.525	.575	.625	.675	.725	.775	.825	.875	.925	.975
.1	13.22	1.579	4.928	17.30	8.409	13.86	3.432	4.280	4.873	3.038	1.917	3.502	3.262	2.988	2.163	4.051	4.532	12.05	0.00	8.688
.3	10.22	8.127	5.081	7.082	5.294	8.149	8.987	5.873	7.455	7.996	5.591	7.018	4.193	7.389	4.599	0.00	3.743	3.033	.8856	0.00
.5	7.236	3.744	7.853	5.699	6.983	7.568	6.120	5.590	5.812	7.163	4.380	4.562	2.084	7.172	1.828	3.828	2.868	0.00	0.00	.8614
.7	3.464	8.467	5.093	3.338	7.262	5.735	7.511	4.563	4.791	4.108	5.042	6.233	3.875	3.953	3.647	2.821	.3189	2.881	1.607	0.00
.9	3.373	4.577	3.501	5.427	5.676	3.784	4.488	3.590	4.052	4.146	4.816	3.315	1.809	2.816	1.854	2.813	1.430	.3491	.4289	0.00
1.1	5.340	5.053	3.704	2.948	2.457	3.603	2.669	2.951	3.094	1.833	1.599	2.650	1.809	1.730	2.532	.6645	1.057	.5985	.3679	.3929
1.3	4.753	1.144	2.325	3.090	2.920	4.300	1.871	2.148	1.937	3.379	1.981	1.791	1.368	1.609	.3753	.6312	.2430	.2697	0.00	.3300
1.5	4.489	2.871	2.712	1.949	1.858	1.667	1.812	1.585	1.402	1.830	.7313	1.882	.3350	.8699	.1829	.9991	.2283	.5044	0.00	0.00
1.7	1.492	2.843	2.299	.6376	1.167	1.592	.8791	.9657	.9520	.5550	.9954	.6075	.9652	1.042	.3701	.3972	0.00	0.00	0.00	0.00
1.9	0.00	1.642	.9912	1.539	1.184	.4886	.8945	.5375	.7955	.6967	0.00	.1561	.1602	.3488	0.00	.1987	0.00	.2232	0.00	0.00
2.1	0.00	0.00	.7543	0.00	.6105	.5354	.9519	.4286	.3987	.4285	.5862	.1483	.4779	0.00	.1988	.2051	0.00	0.00	0.00	0.00
2.3	0.00	1.396	.3710	.5103	1.161	.3644	.9736	.4562	.2840	.5796	0.00	0.00	.1562	0.00	.3891	0.00	0.00	.4869	0.00	0.00
2.5	.8266	0.00	0.00	.5903	.2378	.4410	.3841	.1693	.1483	.2955	.3023	.1528	.1637	0.00	.2071	0.00	.2283	0.00	.2834	0.00
2.7	0.00	.5448	.3379	.2965	.3064	.2319	.3958	0.00	0.00	.1537	0.00	.1563	.1546	0.00	0.00	0.00	0.00	0.00	0.00	0.00
2.9	.7191	0.00	0.00	0.00	.2951	0.00	0.00	0.00	.4872	.1634	.1593	0.00	0.00	0.00	0.00	0.00	0.00	0.00	0.00	0.00
3.1	.7868	0.00	0.00	.3228	0.00	0.00	0.00	0.00	0.00	0.00	0.00	0.00	.1587	0.00	0.00	0.00	0.00	0.00	0.00	0.00
3.3	0.00	0.00	0.00	0.00	0.00	.2575	0.00	0.00	0.00	0.00	.1648	0.00	0.00	0.00	0.00	0.00	0.00	0.00	0.00	0.00
3.5	0.00	0.00	0.00	0.00	0.00	0.00	0.00	0.00	0.00	0.00	0.00	0.00	0.00	0.00	0.00	0.00	0.00	0.00	0.00	0.00
3.7	0.00	0.00	0.00	0.00	0.00	0.00	0.00	0.00	0.00	0.00	0.00	0.00	0.00	0.00	0.00	0.00	0.00	0.00	0.00	0.00
3.9	0.00	0.00	0.00	0.00	0.00	0.00	.2932	0.00	0.00	0.00	0.00	0.00	0.00	0.00	0.00	0.00	0.00	0.00	0.00	0.00

ERROR

PT \ XF	.025	.075	.125	.175	.225	.275	.325	.375	.425	.475	.525	.575	.625	.675	.725	.775	.825	.875	.925	.975
.1	8.054	1.579	2.884	6.409	5.151	7.933	2.100	2.168	2.608	1.527	1.365	2.089	1.905	2.277	2.163	2.972	3.213	5.775	0.00	6.950
.3	5.190	3.246	2.301	2.317	1.704	2.007	2.111	1.581	1.843	1.975	1.570	1.832	1.494	2.070	1.769	0.00	1.703	1.762	.8856	0.00
.5	2.968	1.682	2.117	1.593	1.607	1.585	1.374	1.256	1.275	1.438	1.135	1.184	.8542	1.574	.8202	1.217	1.181	0.00	0.00	.8614
.7	1.743	2.383	1.473	1.116	1.456	1.225	1.332	.9976	1.001	.9440	1.054	1.203	.9721	1.022	1.012	.9424	.3189	1.095	.9295	0.00
.9	1.715	1.554	1.168	1.321	1.214	.8942	.9372	.8242	.8641	.8841	.9635	.8045	.6034	.7818	.6572	.8497	.6399	.3491	.4289	0.00
1.1	2.228	1.532	1.172	.9359	.7428	.8282	.6680	.6966	.7118	.5535	.5339	.6847	.5723	.5766	.7315	.3838	.5292	.4235	.3679	.3929
1.3	2.152	.8215	.8891	.9011	.7548	.8610	.5403	.5550	.5179	.7047	.5496	.5405	.4839	.5365	.2654	.3650	.2430	.2697	0.00	.3300
1.5	2.040	1.178	.8578	.6500	.5881	.5273	.5231	.4781	.4436	.5076	.3271	.5434	.2369	.3891	.1829	.4469	.2283	.3570	0.00	0.00
1.7	1.055	1.177	.8191	.3690	.4769	.5037	.3590	.3651	.3599	.2775	.3762	.3038	.3941	.4257	.2617	.2809	0.00	0.00	0.00	0.00
1.9	0.00	.8220	.5737	.6315	.4836	.2822	.3654	.2688	.3248	.3116	0.00	.1561	.1602	.2467	0.00	.1987	0.00	.2232	0.00	0.00
2.1	0.00	0.00	.5339	0.00	.3527	.3093	.3892	.2475	.2303	.2474	.2932	.1483	.2759	0.00	.1988	.2051	0.00	0.00	0.00	0.00
2.3	0.00	.8088	.3710	.3612	.5198	.2578	.3982	.2635	.2008	.2898	0.00	0.00	.1562	0.00	.2752	0.00	0.00	.3444	0.00	0.00
2.5	.8266	0.00	0.00	.4176	.2378	.3119	.2716	.1693	.1483	.2089	.2138	.1528	.1637	0.00	.2071	0.00	.2283	0.00	.2834	0.00
2.7	0.00	.5448	.3379	.2965	.3064	.2319	.2801	0.00	0.00	.1537	0.00	.1563	.1546	0.00	0.00	0.00	0.00	0.00	0.00	0.00
2.9	.7191	0.00	0.00	0.00	.2951	0.00	0.00	0.00	.2813	.1634	.1593	0.00	0.00	0.00	0.00	0.00	0.00	0.00	0.00	0.00
3.1	.7868	0.00	0.00	.3228	0.00	0.00	0.00	0.00	0.00	0.00	0.00	0.00	.1587	0.00	0.00	0.00	0.00	0.00	0.00	0.00
3.3	0.00	0.00	0.00	0.00	0.00	.2575	0.00	0.00	0.00	0.00	.1648	0.00	0.00	0.00	0.00	0.00	0.00	0.00	0.00	0.00
3.5	0.00	0.00	0.00	0.00	0.00	0.00	0.00	0.00	0.00	0.00	0.00	0.00	0.00	0.00	0.00	0.00	0.00	0.00	0.00	0.00
3.7	0.00	0.00	0.00	0.00	0.00	0.00	0.00	0.00	0.00	0.00	0.00	0.00	0.00	0.00	0.00	0.00	0.00	0.00	0.00	0.00
3.9	0.00	0.00	0.00	0.00	0.00	0.00	.2932	0.00	0.00	0.00	0.00	0.00	0.00	0.00	0.00	0.00	0.00	0.00	0.00	0.00

DIFFERENTIAL CROSS SECTION
NB C**3 / GEV**2 / XF UNIT / NUCLEUS
PROTON ON CARBON

3.5 < M < 4.0

XF

PT	.025	.075	.125	.175	.225	.275	.325	.375	.425	.475	.525	.575	.625	.675	.725	.775	.825	.875	.925	.975
.1	0.00	.6516	0.00	.3646	.2471	.6954	0.00	0.00	.3491	.2159	0.00	0.00	.6206	0.00	0.00	0.00	0.00	0.00	0.00	0.00
.3	0.00	.2752	.2395	.2700	.3505	.0973	.1032	.0925	.0967	0.00	0.00	0.00	0.00	0.00	0.00	0.00	0.00	0.00	0.00	0.00
.5	0.00	.3339	.5657	.5124	.3417	.3907	.2379	.2138	0.00	0.00	.1507	0.00	.0836	0.00	0.00	0.00	0.00	0.00	0.00	0.00
.7	.4974	.1515	.1058	.1745	.0686	.0656	.1697	.1083	.0948	.1677	0.00	.1166	0.00	0.00	0.00	0.00	0.00	0.00	0.00	0.00
.9	.4455	0.00	0.00	.4454	.0581	.0529	.0504	.1348	.0459	.0912	0.00	0.00	0.00	0.00	0.00	0.00	0.00	0.00	0.00	0.00
1.1	.4855	.1220	.1846	.0658	.0515	.0477	.0814	0.00	0.00	.1301	.1678	.0861	.0471	0.00	0.00	0.00	0.00	0.00	0.00	0.00
1.3	0.00	0.00	.1703	.1329	.0451	.0806	0.00	0.00	.0353	0.00	0.00	0.00	0.00	0.00	0.00	.0540	0.00	0.00	0.00	0.00
1.5	0.00	0.00	0.00	.0995	.0420	.0403	.1086	.0343	0.00	.0356	0.00	0.00	0.00	0.00	0.00	0.00	.0543	0.00	0.00	0.00
1.7	0.00	.1584	0.00	0.00	.0461	.1145	0.00	0.00	0.00	.0347	0.00	0.00	0.00	0.00	.0457	0.00	0.00	0.00	0.00	0.00
1.9	.2258	0.00	.0849	0.00	.0472	.0404	0.00	0.00	0.00	.0342	0.00	.0373	0.00	0.00	0.00	0.00	0.00	0.00	0.00	0.00
2.1	0.00	0.00	.0843	.0575	0.00	0.00	.0349	0.00	0.00	0.00	0.00	0.00	0.00	0.00	0.00	0.00	0.00	0.00	0.00	0.00
2.3	0.00	0.00	0.00	0.00	0.00	0.00	0.00	0.00	0.00	0.00	0.00	0.00	0.00	0.00	0.00	0.00	0.00	0.00	0.00	0.00
2.5	0.00	0.00	0.00	0.00	0.00	0.00	0.00	0.00	0.00	0.00	0.00	0.00	0.00	0.00	0.00	0.00	0.00	0.00	0.00	0.00
2.7	0.00	0.00	0.00	0.00	0.00	0.00	0.00	0.00	0.00	0.00	0.00	0.00	0.00	0.00	0.00	0.00	0.00	0.00	0.00	0.00
2.9	0.00	0.00	0.00	0.00	0.00	0.00	0.00	0.00	0.00	0.00	0.00	0.00	0.00	0.00	0.00	0.00	0.00	0.00	0.00	0.00
3.1	0.00	0.00	0.00	0.00	0.00	0.00	0.00	0.00	0.00	0.00	0.00	0.00	0.00	0.00	0.00	0.00	0.00	0.00	0.00	0.00
3.3	0.00	0.00	0.00	0.00	0.00	0.00	0.00	0.00	0.00	0.00	0.00	0.00	0.00	0.00	0.00	0.00	0.00	0.00	0.00	0.00
3.5	0.00	0.00	0.00	0.00	0.00	0.00	0.00	0.00	0.00	0.00	0.00	0.00	0.00	0.00	0.00	0.00	0.00	0.00	0.00	0.00
3.7	0.00	0.00	0.00	0.00	0.00	0.00	0.00	0.00	0.00	0.00	0.00	0.00	0.00	0.00	0.00	0.00	0.00	0.00	0.00	0.00
3.9	0.00	0.00	0.00	0.00	0.00	0.00	0.00	0.00	0.00	0.00	0.00	0.00	0.00	0.00	0.00	0.00	0.00	0.00	0.00	0.00

ERROR

	.025	.075	.125	.175	.225	.275	.325	.375	.425	.475	.525	.575	.625	.675	.725	.775	.825	.875	.925	.975
.1	0.00	.6516	0.00	.3646	.2471	.6954	0.00	0.00	.2471	.2159	0.00	0.00	.6204	0.00	0.00	0.00	0.00	0.00	0.00	0.00
.3	0.00	.2752	.2395	.1919	.2035	.0973	.1032	.0925	.0967	0.00	0.00	0.00	0.00	0.00	0.00	0.00	0.00	0.00	0.00	0.00
.5	0.00	.2362	.2836	.2305	.1710	.1759	.1379	.1244	0.00	0.00	.1072	0.00	.0836	0.00	0.00	0.00	0.00	0.00	0.00	0.00
.7	.3524	.1515	.1058	.1234	.0686	.0656	.0981	.0767	.0670	.0970	0.00	.0827	0.00	0.00	0.00	0.00	0.00	0.00	0.00	0.00
.9	.3154	0.00	0.00	.1828	.0581	.0529	.0504	.0774	.0459	.0645	0.00	0.00	0.00	0.00	0.00	0.00	0.00	0.00	0.00	0.00
1.1	.3436	.1220	.1316	.0658	.0515	.0477	.0576	0.00	0.00	.0751	.0841	.0609	.0471	0.00	0.00	0.00	0.00	0.00	0.00	0.00
1.3	0.00	0.00	.1211	.0945	.0451	.0570	0.00	0.00	.0353	0.00	0.00	0.00	0.00	0.00	0.00	.0540	0.00	0.00	0.00	0.00
1.5	0.00	0.00	0.00	.0705	.0420	.0403	.0627	.0343	0.00	.0356	0.00	0.00	0.00	0.00	0.00	0.00	.0543	0.00	0.00	0.00
1.7	0.00	.1584	0.00	0.00	.0461	.0661	0.00	0.00	0.00	.0347	0.00	0.00	0.00	0.00	.0457	0.00	0.00	0.00	0.00	0.00
1.9	.2258	0.00	.0849	0.00	.0472	.0404	0.00	0.00	0.00	.0342	0.00	.0373	0.00	0.00	0.00	0.00	0.00	0.00	0.00	0.00
2.1	0.00	0.00	.0843	.0575	0.00	0.00	.0349	0.00	0.00	0.00	0.00	0.00	0.00	0.00	0.00	0.00	0.00	0.00	0.00	0.00
2.3	0.00	0.00	0.00	0.00	0.00	0.00	0.00	0.00	0.00	0.00	0.00	0.00	0.00	0.00	0.00	0.00	0.00	0.00	0.00	0.00
2.5	0.00	0.00	0.00	0.00	0.00	0.00	0.00	0.00	0.00	0.00	0.00	0.00	0.00	0.00	0.00	0.00	0.00	0.00	0.00	0.00
2.7	0.00	0.00	0.00	0.00	0.00	0.00	0.00	0.00	0.00	0.00	0.00	0.00	0.00	0.00	0.00	0.00	0.00	0.00	0.00	0.00
2.9	0.00	0.00	0.00	0.00	0.00	0.00	0.00	0.00	0.00	0.00	0.00	0.00	0.00	0.00	0.00	0.00	0.00	0.00	0.00	0.00
3.1	0.00	0.00	0.00	0.00	0.00	0.00	0.00	0.00	0.00	0.00	0.00	0.00	0.00	0.00	0.00	0.00	0.00	0.00	0.00	0.00
3.3	0.00	0.00	0.00	0.00	0.00	0.00	0.00	0.00	0.00	0.00	0.00	0.00	0.00	0.00	0.00	0.00	0.00	0.00	0.00	0.00
3.5	0.00	0.00	0.00	0.00	0.00	0.00	0.00	0.00	0.00	0.00	0.00	0.00	0.00	0.00	0.00	0.00	0.00	0.00	0.00	0.00
3.7	0.00	0.00	0.00	0.00	0.00	0.00	0.00	0.00	0.00	0.00	0.00	0.00	0.00	0.00	0.00	0.00	0.00	0.00	0.00	0.00
3.9	0.00	0.00	0.00	0.00	0.00	0.00	0.00	0.00	0.00	0.00	0.00	0.00	0.00	0.00	0.00	0.00	0.00	0.00	0.00	0.00

HIGH MASS EVENTS

TARGET	MASS	XF	PT	CROSS SECTION
C	5.01	.458	1.151	6.126
C	4.12	.493	1.506	3.902
C	4.03	.355	1.097	8.529
C	4.86	.400	.632	2.668
C	6.20	.264	.632	4.668
C	5.65	.318	1.237	19.239
C	5.76	.111	.584	9.698
C	4.19	.063	.547	12.319
C	4.08	.436	.791	5.840
C	4.58	.452	.365	10.429
C	4.38	.324	1.839	9.711
C	4.36	.835	.773	5.479
C	4.15	.487	1.097	3.174
C	4.17	.440	.876	2.772
C	4.80	.619	.340	3.442
C	4.02	.174	1.769	13.086
C	4.12	.002	1.524	60.602
C	4.69	.894	.986	6.610
C	4.44	.790	.570	3.016
C	4.24	.259	.321	4.199
C	4.07	.557	1.592	4.009
C	4.53	.696	.521	2.596
C	4.12	-.055	1.184	177.060
C	4.92	.224	.410	5.678
C	6.55	.412	2.166	3.973
C	4.24	.609	.338	2.768
C	5.14	.376	1.371	3.372
C	4.16	.531	.881	3.287
C	4.28	.333	.602	6.470
C	5.30	.426	1.337	2.975
C	4.94	.656	2.263	4.358
C	5.99	.225	.537	6.094
C	5.68	.531	1.984	6.105
C	4.71	.757	.573	2.970
C	4.12	.422	.267	2.427
C	5.01	.417	2.101	4.037
C	4.26	.533	1.681	4.222
C	4.66	.316	1.973	20.086
C	4.13	.134	1.352	26.681
C	5.15	.468	.418	5.139
C	7.03	.367	1.467	7.080
C	4.26	.466	1.032	3.851
C	4.41	.789	1.575	4.094
C	4.37	.463	1.943	5.093
C	5.95	.693	1.105	2.607
C	4.16	.722	1.521	3.609
C	6.17	.231	.550	5.496
C	5.43	-.185	.545	129.511
C	5.02	.632	1.022	2.746

HIGH MASS EVENTS

TARGET	MASS	XF	PT	CROSS SECTION
C	4.96	.668	1.054	2.882
C	4.05	.341	.426	5.699
C	4.62	.816	1.467	6.026
C	4.52	.449	.489	3.463
C	6.26	.552	2.128	4.587
C	5.73	.285	.480	4.242
C	4.34	.277	.368	5.364
C	4.28	.361	.906	6.119
C	4.36	.352	1.147	3.584
C	6.75	.482	.916	5.246
C	4.35	.346	.412	2.950
C	4.26	.404	1.717	12.167
C	4.30	.559	.583	2.675
C	4.83	.470	2.157	5.277
C	4.13	.104	.460	10.122
C	4.50	.832	1.108	5.567
C	6.45	.732	1.561	2.738
C	5.24	.374	1.471	6.131
C	4.18	.459	.177	2.580
C	4.19	.476	1.207	3.263
C	4.12	.058	1.938	37.034
C	4.04	.351	.378	4.196
C	4.39	.456	.286	3.215
C	4.84	.236	.967	5.711
C	4.10	.324	1.340	4.652
C	4.76	.224	1.387	11.226
C	5.67	.584	.870	5.184
C	4.07	.894	.418	5.627
C	6.96	.508	1.419	3.101
C	4.14	.310	.952	5.982
C	4.62	.314	2.078	6.783
C	6.22	.426	2.436	7.657
C	4.05	.363	.069	2.554
C	4.20	.534	.819	2.826
C	6.28	.403	1.106	3.792
C	4.05	.247	1.016	5.151
C	4.11	.656	.950	3.026
C	4.53	.277	.496	12.462
C	4.95	.600	1.652	3.118
C	4.88	.501	.748	3.576
C	4.83	.204	.423	7.522
C	4.23	.549	.822	3.851
C	4.12	.577	.781	3.090
C	7.13	.319	1.151	4.462
C	5.23	.386	1.017	5.713
C	4.55	.166	.766	21.040
C	4.19	.334	1.281	9.488
C	5.64	.618	2.216	3.422
C	4.07	.402	1.504	4.316

HIGH MASS EVENTS

TARGET	MASS	XF	PT	CROSS SECTION
C	5.50	.421	.759	3.293
C	4.80	.416	.900	6.213
C	4.02	.403	1.095	3.239
C	6.23	.306	.859	4.197
C	5.17	.574	2.337	15.644
C	5.81	.350	1.676	4.291
C	5.51	.269	1.091	5.928
C	5.50	.672	.915	2.840
C	5.04	.240	.706	5.346
C	4.43	.249	.679	5.081
C	5.37	.309	1.053	7.778
C	4.60	.258	.292	12.759
C	7.07	.393	1.542	34.553
C	4.45	.642	1.703	3.704
C	4.35	.454	.926	3.245
C	6.43	.124	.282	25.435
C	4.02	.718	.581	3.583
C	5.81	.491	.541	2.569
C	5.07	.625	1.225	6.662
C	9.57	.523	1.044	5.079
C	4.10	.211	.798	9.512
C	5.09	.696	.797	5.123
C	10.19	.097	.698	9.532
C	4.99	.030	.192	11.742
C	4.30	.337	.807	4.547
C	7.78	.519	1.319	6.021
C	4.96	.626	2.689	5.108
C	4.38	.379	.289	4.667
C	4.66	.624	1.051	3.047
C	4.04	.175	1.050	8.586
C	6.35	.333	.592	3.600
C	4.42	.189	1.150	12.509
C	5.83	.077	.522	11.642
C	4.07	.567	.808	3.728
C	4.87	.733	.823	3.300
C	6.44	.619	.791	2.580
C	4.21	.598	.846	3.635
C	5.70	.371	1.344	4.163
C	4.88	.367	.334	6.639
C	4.12	.298	1.554	6.703
C	5.93	.412	.107	3.728
C	4.38	.268	2.112	13.440
C	4.45	.373	.919	3.338
C	4.68	.265	.698	5.343
C	4.77	.863	1.549	8.051
C	6.18	.412	1.848	3.658
C	4.78	.163	1.190	9.431
C	4.41	.682	.782	3.191
C	4.70	.133	.793	10.824

HIGH MASS EVENTS

TARGET	MASS	XF	PT	CROSS SECTION
C	4.05	.160	.671	8.111
C	5.03	.318	1.176	4.885
C	4.70	.470	.177	2.358
C	4.15	.361	1.231	5.171
C	4.20	.366	.096	2.649
C	6.89	-.082	1.144	32.132
C	4.91	.533	.531	2.569
C	4.00	.759	.362	3.876
C	5.32	.512	1.575	3.180
C	4.60	.710	1.197	3.497
C	6.96	.154	.863	35.009
C	4.02	.380	1.105	3.511
C	6.37	.012	.836	15.326
C	4.04	.422	.107	4.840
C	6.47	.589	1.085	13.478
C	8.14	.017	.680	14.655
C	4.63	.386	.730	3.184
C	4.07	.393	.705	3.167
C	4.20	.516	1.087	3.281
C	4.04	.220	.743	12.283
C	6.68	.451	.723	2.803
C	4.04	-.049	1.301	113.749
C	5.44	.261	1.725	13.280
C	6.18	.368	1.936	4.989
C	4.86	.674	.966	3.784
C	4.17	.530	1.466	3.911
C	5.42	.620	.826	3.293
C	4.06	.270	1.053	4.893
C	4.09	.539	.669	2.930
C	4.40	.167	1.192	9.548
C	5.04	.148	2.232	16.934
C	4.38	.402	2.208	8.112
C	5.17	.487	.941	3.209
C	4.36	.463	1.081	3.239
C	4.76	.401	.758	3.000
C	5.16	.454	1.144	5.980
C	4.25	.438	1.605	3.982
C	4.50	.349	1.210	3.765
C	7.43	.710	.423	2.742
C	4.37	.324	.459	5.974
C	4.54	.334	1.060	3.728
C	4.72	.343	.898	5.650
C	4.09	.209	.897	7.104
C	4.02	.434	.501	3.180
C	4.23	.314	.951	3.986
C	4.07	.532	1.953	4.880
C	5.99	.659	.856	7.552
C	4.02	.037	1.452	47.354
C	6.63	.642	1.787	1.463
C	4.70	.543	1.077	12.605

HIGH MASS EVENTS

TARGET	MASS	XF	PT	CROSS SECTION
C	9.69	.356	1.527	5.850
C	4.30	.662	1.081	3.628
C	5.59	.401	1.170	4.493
C	4.15	.237	1.592	17.292
C	4.23	-.037	.960	79.719
C	6.26	.415	1.084	3.973
C	6.03	.171	1.020	8.291
C	4.11	.654	1.282	3.658
C	5.92	.619	.468	2.554
C	4.63	.164	.292	8.916
C	5.14	.612	2.034	13.796
C	4.55	.288	2.013	8.344
C	4.49	.387	.361	3.786
C	4.26	.421	1.279	17.011
C	4.51	.463	1.653	3.973
C	4.25	.462	1.085	3.325
C	4.00	.662	.534	3.350
C	4.77	.514	1.974	6.084
C	5.22	.177	1.977	19.955
C	6.52	.478	1.686	4.028
C	4.53	.261	1.475	8.439
C	4.08	.515	.570	5.939
C	7.75	.648	.919	2.901
C	4.73	.935	.436	6.205
C	4.62	.759	.197	3.058
C	4.61	.428	.881	13.273
C	4.10	.505	1.589	4.935
C	4.16	.384	.645	3.511
C	4.05	.602	.665	3.140
C	4.72	.677	.685	5.277
C	7.29	.173	.423	8.916
C	4.05	.025	1.255	54.168
C	4.93	.018	1.493	31.794
C	5.56	.443	.453	2.539
C	4.00	.269	1.914	8.073
C	5.76	.499	1.071	5.093
C	9.12	.412	.874	22.555
C	5.55	.499	3.030	13.273
C	4.49	.091	.237	9.435
C	4.22	.475	.564	2.886
C	4.18	.056	1.376	28.130
C	4.52	.511	.861	2.854
C	4.03	.843	1.317	8.920
C	4.94	.179	1.143	13.699
C	4.07	.416	.768	2.882
C	5.77	.380	.217	2.927
C	5.40	.427	.377	2.844
C	4.34	.644	1.175	3.331
C	5.38	.356	1.082	6.514
C	4.12	.386	1.066	3.342

HIGH MASS EVENTS

TARGET	MASS	XF	PT	CROSS SECTION
C	4.53	.178	.555	6.189
C	4.63	.127	.895	12.298
C	4.55	.685	.616	3.221
C	4.37	.203	.465	5.424

HIGH MASS EVENTS

TARGET	MASS	XF	PT	CROSS SECTION
CU	4.58	.643	1.029	12.140
CU	4.55	.435	1.222	8.373
CU	4.08	.703	.998	9.407
CU	4.13	.357	.347	9.672
CU	5.46	.665	1.051	7.265
CU	5.45	.048	.115	7.080
CU	4.15	.440	.630	7.716
CU	4.13	.436	.628	12.266
CU	4.17	.344	2.590	24.995
CU	5.30	.679	.509	7.754
CU	6.64	.682	.344	7.871
CU	5.79	.551	1.455	8.681
CU	4.96	.320	1.355	14.751
CU	8.15	.740	.703	20.712
CU	4.00	.267	1.197	14.418
CU	4.64	.098	.817	30.115
CU	4.23	.206	.565	15.570
CU	4.88	-.017	.452	113.113
CU	5.04	.418	.379	9.224
CU	5.01	.502	.122	12.593
CU	5.10	.097	1.450	47.927
CU	5.68	.625	1.131	7.924
CU	5.33	.478	1.502	8.524
CU	4.94	.307	1.546	13.784
CU	5.59	.610	.361	11.217
CU	4.91	.650	.960	7.964
CU	4.66	.723	1.213	9.921
CU	4.46	.262	1.455	37.047
CU	4.12	.604	1.015	9.047
CU	4.73	.826	.511	14.271
CU	4.85	.088	.365	40.673
CU	4.53	.216	.638	15.855
CU	4.34	.056	1.671	86.166
CU	4.10	.140	1.256	34.537
CU	4.21	.536	1.235	10.005
CU	4.10	.761	1.308	13.009
CU	5.24	.718	2.630	29.515
CU	5.22	.438	1.784	10.957
CU	4.11	.651	.220	13.570
CU	4.10	.442	1.231	8.995
CU	4.67	.311	.907	10.507
CU	6.09	.671	.785	7.221
CU	4.49	.313	1.015	10.649
CU	4.39	.243	1.442	22.525
CU	5.08	.267	.546	17.011
CU	5.18	.442	.863	9.618
CU	4.23	.240	1.518	17.649
CU	8.03	.737	1.224	9.777

HIGH MASS EVENTS

TARGET	MASS	XF	PT	CROSS SECTION
CU	4.74	.439	.057	13.265
CU	4.11	.611	1.500	11.490
CU	5.08	.045	1.074	54.236
CU	5.64	.072	1.995	9.521
CU	4.03	.155	1.186	29.372
CU	6.73	.262	2.265	22.057
CU	5.85	.113	1.762	45.865
CU	4.67	.538	1.172	12.763
CU	4.34	.559	.561	10.266
CU	6.31	.563	.331	9.942
CU	5.48	.777	.916	7.780
CU	4.81	.419	1.000	8.524
CU	5.56	.323	1.159	13.476
CU	7.82	.350	.490	14.580
CU	4.95	.258	.121	14.300
CU	4.09	.461	1.123	17.621
CU	6.08	.516	.634	6.955
CU	4.40	.751	.896	9.296
CU	7.37	.652	.887	22.488
CU	4.13	.669	1.019	10.134
CU	4.10	.568	1.311	9.984
CU	6.04	.633	1.399	11.325
CU	4.41	.443	.398	11.034
CU	5.28	.282	.114	18.724
CU	5.50	.764	2.145	10.356
CU	4.72	.414	.900	8.314
CU	4.23	.268	.332	24.376
CU	4.27	.544	.576	14.224
CU	4.74	.588	2.641	13.228
CU	4.52	.782	1.000	9.099
CU	4.30	.309	.551	12.533
CU	4.04	.166	2.309	58.102
CU	5.07	.464	1.488	8.877
CU	4.08	.101	.606	85.123
CU	5.28	.312	2.288	20.632
CU	6.88	.534	1.152	12.493
CU	5.34	.451	1.642	9.483
CU	4.20	.511	.405	8.156
CU	5.27	.224	1.537	34.223
CU	5.58	.366	1.233	31.112
CU	7.44	.475	.666	7.629
CU	5.92	.637	.926	7.460
CU	4.08	.625	1.155	20.054
CU	4.49	.738	.653	45.408
CU	5.55	.597	.223	7.910
CU	5.71	.717	1.006	7.679
CU	7.08	.572	1.519	20.712
CU	4.08	.490	.464	7.629
CU	[illegible]	[illegible]	[illegible]	[illegible]

HIGH MASS EVENTS

TARGET	MASS	XF	PT	CROSS SECTION
CU	4.19	.048	.552	41.845
CU	5.35	.117	.892	33.624
CU	4.23	.167	.871	23.256
CU	4.15	.445	.298	9.659
CU	4.02	.768	.123	13.972
CU	5.31	.224	.595	18.271
CU	6.81	.530	1.813	9.521
CU	4.42	.528	.725	8.373
CU	4.56	.409	.849	8.045
CU	8.10	.557	1.360	9.206
CU	6.01	.494	1.760	23.149
CU	4.14	.241	.740	13.979
CU	5.10	.393	2.302	17.951
CU	5.05	.464	1.327	26.382
CU	5.36	.409	.374	7.048
CU	4.33	.117	.125	32.053
CU	4.06	.877	.693	18.083
CU	4.86	.400	1.688	18.025
CU	7.19	.503	.723	18.740
CU	4.36	.469	.406	14.666
CU	4.07	.075	1.644	76.791
CU	4.06	.237	.811	15.353
CU	4.18	.328	1.765	18.131
CU	4.41	.704	.416	8.827
CU	6.26	.421	.551	13.009
CU	4.86	.151	.490	20.417
CU	6.92	.711	.953	7.144
CU	4.39	.630	.555	7.819
CU	4.19	.835	.329	17.521
CU	4.28	.377	1.839	14.475
CU	5.99	.086	2.254	88.578
CU	4.71	.282	1.219	22.117
CU	5.72	.266	.445	12.836
CU	4.29	.586	2.496	17.426
CU	4.85	.639	2.217	22.924
CU	5.23	.207	.689	15.596
CU	5.05	.810	1.185	16.659
CU	4.07	.585	.688	22.486
CU	4.28	.371	.864	15.842
CU	4.36	.173	.527	23.870
CU	8.06	.564	.249	6.550
CU	4.32	.138	1.225	45.439
CU	4.42	.472	1.732	20.604
CU	4.09	.289	.887	11.915
CU	4.91	.167	.716	27.042
CU	4.51	.255	.986	18.493
CU	4.28	.493	3.177	26.382
CU	4.09	.312	.661	15.548
CU	4.04	[illegible]	[illegible]	[illegible]

HIGH MASS EVENTS

TARGET	MASS	XF	PT	CROSS SECTION
CU	5.16	.307	.054	57.887
CU	4.18	.159	2.912	140.378
CU	4.30	.461	.994	8.242
CU	5.39	.471	1.221	8.961
CU	6.38	.592	1.803	8.358
CU	4.74	.356	2.055	15.057
CU	6.40	.309	.586	14.302
CU	4.65	.304	1.461	29.909
CU	4.91	.325	.919	9.416
CU	4.49	.577	.616	9.188
CU	4.15	.231	1.324	18.748
CU	5.93	.511	1.052	9.370
CU	4.14	.301	1.473	15.052
CU	4.46	-.043	.784	87.851
CU	6.24	.399	.581	14.833
CU	5.68	.422	1.422	9.117
CU	4.36	.346	.827	9.388
CU	5.48	.291	.720	13.239
CU	8.66	.370	1.569	20.788
CU	4.16	.756	.143	8.978
CU	6.16	.560	1.846	16.512
CU	6.27	.336	.561	9.554
CU	5.90	.202	1.493	59.067
CU	5.36	.608	.618	7.858
CU	5.79	.447	1.901	20.622
CU	4.66	.249	.534	14.515
CU	4.24	.699	.620	8.128
CU	6.17	.563	.995	9.963
CU	4.18	.728	1.141	9.657
CU	4.09	.459	1.179	14.055
CU	5.25	.748	1.884	9.389
CU	4.68	.132	.919	27.532
CU	4.41	.472	.587	10.156
CU	6.20	.633	.719	7.144
CU	4.17	.585	.747	9.242
CU	5.76	.367	.553	8.084
CU	4.47	.422	1.422	9.963
CU	4.24	.520	.749	7.937
CU	4.77	.362	.934	8.717
CU	4.60	.140	1.488	43.472
CU	4.51	.247	.113	9.750
CU	4.44	.557	.786	11.669
CU	4.64	.433	1.208	8.170
CU	4.65	.151	.235	14.268
CU	4.51	.380	.076	8.377
CU	4.04	.740	1.482	12.298
CU	5.43	.558	1.101	7.716
CU	5.78	.152	.480	35.248
CU	5.70	.543	1.816	9.242
CU	4.37	.253	.281	11.999

HIGH MASS EVENTS

TARGET	MASS	XF	PT	CROSS SECTION
CU	5.90	.135	1.394	29.951
CU	4.07	.314	1.144	12.812
CU	4.04	.404	1.291	9.370
CU	4.42	.284	1.103	22.643
CU	4.01	.289	.636	9.852
CU	4.22	.183	1.643	32.531
CU	5.63	.690	.596	7.322
CU	5.09	.547	.342	12.763
CU	4.12	.280	1.893	20.798
CU	4.17	.295	1.713	16.128
CU	5.03	.336	1.756	24.105
CU	5.71	.530	.504	17.821
CU	5.45	.249	.764	19.646
CU	4.94	.277	.988	17.631
CU	6.68	.708	.619	7.666
CU	4.43	.332	.622	9.637
CU	4.22	.678	.701	8.778
CU	5.41	.607	.378	15.741
CU	4.25	.375	.552	9.464
CU	6.56	.071	.817	57.026
CU	4.67	.827	1.311	17.377
CU	5.22	.235	1.084	18.067
CU	5.28	.205	2.942	44.705
CU	4.05	.713	.632	12.627
CU	4.98	.507	.467	8.978
CU	4.13	.623	.177	14.486
CU	6.18	.005	1.396	95.067
CU	4.47	.214	2.146	33.008
CU	4.38	.416	.438	17.621
CU	4.35	.469	.476	10.266
CU	4.95	.621	.606	7.367
CU	4.47	.477	1.837	11.086
CU	4.81	.486	.509	8.199
CU	4.09	.262	.777	30.676
CU	4.60	.656	.937	23.972
CU	4.09	.706	.089	8.142
CU	4.62	.614	.467	9.560
CU	4.16	.372	1.878	14.623
CU	5.24	.542	.425	8.018
CU	4.92	.503	.241	6.670
CU	5.46	.403	1.562	11.271
CU	4.83	.035	1.798	112.201
CU	4.12	.385	.608	8.505
CU	4.60	.177	1.273	27.736
CU	4.27	.410	.420	12.078
CU	4.47	.629	1.657	11.060
CU	5.34	.379	.544	9.409
CU	4.47	.682	1.187	9.900
CU	5.28	.612	.989	9.590
CU	4.44	.697	.700	10.448

HIGH MASS EVENTS

TARGET	MASS	XF	PT	CROSS SECTION
CU	4.73	.503	.895	7.819
CU	5.51	.049	1.030	46.453
CU	4.11	.332	.986	11.635
CU	4.75	.653	.928	10.156
CU	5.31	.343	.557	16.194
CU	4.36	.068	.842	36.082
CU	5.08	.395	.399	7.891
CU	4.54	.433	.754	7.937
CU	4.11	.135	.968	27.471
CU	6.32	.439	.314	8.344
CU	7.58	.542	1.322	10.684
CU	4.28	.404	.979	11.462
CU	4.02	.568	.635	9.278
CU	6.53	.568	1.983	12.695
CU	4.29	.284	.338	18.334
CU	5.97	.335	1.195	12.986
CU	4.36	.464	1.194	10.289
CU	4.11	.554	.704	8.433
CU	4.29	.438	2.124	21.369
CU	6.26	.277	.951	13.496
CU	4.62	.413	1.008	11.112
CU	4.45	.625	1.085	16.926
CU	4.30	.832	1.224	19.680
CU	6.31	.422	.768	13.454
CU	6.05	.410	1.277	8.811
CU	4.52	.455	1.880	13.531
CU	6.19	.023	1.080	49.215
CU	5.14	-.005	.374	125.535
CU	6.27	.457	1.388	8.681
CU	4.68	.606	.808	10.379
CU	4.90	.157	.085	32.686
CU	4.54	.391	.485	19.490
CU	5.33	.671	1.395	8.745
CU	4.88	.652	1.857	9.717
CU	4.60	.816	.829	16.243
CU	4.09	.275	.822	12.602
CU	4.13	.370	2.410	20.881
CU	4.34	.506	1.310	9.117
CU	9.02	.567	1.211	10.881
CU	4.41	.676	1.183	34.470
CU	4.47	.324	.474	8.365
CU	6.33	.449	.793	8.827
CU	4.44	.318	1.154	10.845
CU	4.10	.573	.390	11.836
CU	4.84	.525	.439	6.814
CU	4.51	.423	1.954	14.992
CU	8.33	.536	1.725	10.244
CU	6.07	.662	.365	6.824
CU	4.06	.227	1.425	41.696
CU	6.06	.506	.131	6.605

HIGH MASS EVENTS

TARGET	MASS	XF	PT	CROSS SECTION
CU	5.38	.282	1.393	16.302
CU	4.06	.055	.139	97.478
CU	6.40	.361	1.195	15.974
CU	7.62	.473	.885	9.921
CU	5.14	.215	.732	17.074
CU	4.39	.591	.153	8.827
CU	4.74	.231	.922	16.748
CU	4.61	.533	1.291	14.531
CU	4.33	.793	.187	8.403
CU	4.60	.538	.194	26.680
CU	4.13	.393	1.017	8.988
CU	5.71	.285	.697	17.112
CU	7.06	.437	1.654	16.118
CU	4.71	.696	1.073	8.586
CU	4.29	.587	.997	9.540
CU	5.23	.562	.227	8.045
CU	5.49	.765	.806	8.944
CU	5.36	.538	.879	8.156
CU	4.64	.219	1.895	26.250
CU	4.20	.757	.564	8.713
CU	4.48	.446	2.027	11.112
CU	4.07	.543	.186	7.617
CU	4.03	.197	.541	16.570
CU	4.54	.754	2.223	27.943
CU	8.17	.749	.751	6.596
CU	8.09	.718	.986	6.727
CU	4.07	.290	.695	11.341
CU	5.83	.666	1.035	8.018
CU	8.25	.545	1.351	12.627
CU	4.54	.266	1.626	17.329
CU	4.84	.393	.668	10.116
CU	4.37	.381	.982	60.792
CU	6.84	.587	.729	6.661
CU	4.42	.362	2.804	46.658
CU	4.13	.608	.860	16.806
CU	6.27	.649	.686	7.276
CU	4.71	.496	.828	7.496
CU	4.74	.116	2.337	79.302
CU	4.67	.404	.612	7.729
CU	8.29	.574	.872	11.164
CU	4.04	.117	.434	29.528
CU	8.52	.111	.864	27.997
CU	5.42	.727	1.624	12.330
CU	4.91	.366	1.890	11.994
CU	4.47	.383	1.259	9.820
CU	5.30	-.062	.651	115.660
CU	4.53	.110	1.109	82.799
CU	4.43	.495	.310	9.206
CU	[illegible]	[illegible]	[illegible]	[illegible]

HIGH MASS EVENTS

TARGET	MASS	XF	PT	CROSS SECTION
CU	5.01	.560	.923	15.794
CU	4.60	.471	.678	8.761
CU	5.52	.066	.679	35.811
CU	5.62	.388	.821	7.669
CU	4.70	.424	.062	9.370
CU	4.97	.609	.602	14.712
CU	6.62	.397	.392	14.307
CU	4.42	.076	.336	24.949
CU	8.79	.611	.947	6.924
CU	5.00	.436	.807	7.134
CU	5.14	.678	.636	7.617
CU	4.02	.443	.295	7.288
CU	4.64	.466	2.626	17.298
CU	4.60	.433	1.382	9.540
CU	6.58	.234	.633	23.778
CU	4.49	.334	.239	8.206
CU	5.83	.252	.546	16.642
CU	5.55	.195	.722	43.031
CU	4.98	.426	.450	18.094
CU	5.04	.476	.528	6.727
CU	6.99	.467	.728	8.128
CU	4.02	.574	1.725	15.483
CU	5.06	.680	.790	9.942
CU	4.21	.419	1.522	14.097
CU	5.57	.610	.517	7.937
CU	4.37	.366	1.092	14.372
CU	4.11	.611	1.711	16.454
CU	6.94	.456	2.054	21.082
CU	4.10	.536	.433	8.388
CU	5.14	.484	.399	8.761
CU	5.05	.439	.197	8.285
CU	4.78	.067	1.196	98.373
CU	4.38	-.036	.280	110.655
CU	4.48	.618	.790	8.227
CU	4.30	.193	1.061	21.420
CU	4.48	.297	.565	15.302
CU	5.12	.457	.853	8.555
CU	4.36	.697	.488	8.844
CU	5.08	.186	2.462	46.151
CU	4.38	.191	.942	29.667
CU	4.36	.582	.951	8.540
CU	4.43	.143	.580	25.960
CU	4.76	.715	.500	7.532
CU	4.85	.238	1.167	24.901
CU	4.25	.350	.414	16.194
CU	7.25	.637	.889	9.314
CU	5.49	.196	2.982	50.906
CU	4.02	.267	.765	12.764
CU	[illegible]	.171	.778	[illegible]

HIGH MASS EVENTS

TARGET	MASS	XF	PT	CROSS SECTION
CU	5.97	.550	.518	15.689
CU	7.14	.325	1.380	20.610
CU	4.42	.607	.959	31.694
CU	4.05	.097	.669	28.781
CU	5.61	.431	1.205	8.156
CU	4.03	.387	.821	74.239
CU	4.12	.212	.203	14.071
CU	4.34	.389	1.017	15.041
CU	4.74	.328	.374	10.014
CU	4.16	.176	1.290	25.494
CU	4.09	.626	1.646	10.708
CU	4.19	.156	1.683	40.257
CU	4.76	.623	.842	11.490
CU	5.48	.014	.973	52.629
CU	4.20	.286	.901	28.898
CU	4.61	.448	.881	7.666
CU	5.46	.246	1.735	27.919
CU	4.09	.496	.932	8.463
CU	4.42	.242	1.165	16.701
CU	4.23	.691	1.178	10.069
CU	4.31	.366	1.010	9.234
CU	4.50	.701	1.537	29.332
CU	7.80	.688	1.107	11.632
CU	5.34	.320	.714	31.733
CU	5.00	.728	2.132	17.110
CU	4.71	.573	1.895	12.903
CU	7.00	.371	.753	17.180
CU	4.46	.303	.799	10.763
CU	4.55	.012	.532	55.418
CU	4.19	.640	.569	8.745
CU	4.14	.747	1.206	11.379
CU	4.09	.147	.796	29.784
CU	4.61	.254	.207	14.882
CU	4.66	.448	.980	9.880
CU	4.79	.407	.912	9.426
CU	4.12	.874	.201	19.277
CU	5.95	.847	1.460	16.496
CU	7.69	.489	1.834	9.064
CU	4.35	.610	.646	8.128
CU	4.93	.044	.331	32.730
CU	4.06	.270	.470	24.310
CU	4.09	.179	.843	19.715
CU	5.25	.269	.630	15.293
CU	4.32	.335	1.014	11.182
CU	6.40	.614	.367	26.382
CU	4.41	.084	1.589	54.555
CU	4.33	.657	.753	17.173
CU	6.01	.713	1.121	8.031
CU	4.90	.451	1.022	8.524

HIGH MASS EVENTS

TARGET	MASS	XF	PT	CROSS SECTION
CU	4.27	-.079	.423	110.310
CU	5.02	.540	1.096	30.665
CU	5.77	.645	1.661	12.330
CU	4.19	.622	1.057	10.471
CU	5.59	.480	.836	7.288
CU	4.82	.495	1.161	8.227
CU	4.29	.477	1.089	10.588
CU	4.78	.636	2.444	19.842
CU	4.87	.539	.783	11.718
CU	4.40	.332	.880	9.310
CU	5.71	.557	1.024	7.367
CU	4.16	.375	1.091	9.102
CU	4.59	.273	1.896	21.590
CU	4.30	.320	1.226	18.900
CU	4.20	.468	.378	8.199
CU	4.24	.221	.604	16.734
CU	5.61	.264	2.839	41.784
CU	4.02	.149	1.487	37.414
CU	4.00	.231	.943	16.911
CU	5.71	.725	.994	8.270
CU	4.59	.578	.756	7.754
CU	4.05	.305	.740	18.904
CU	4.05	.094	.163	27.430
CU	4.24	.122	1.304	38.481
CU	4.13	.308	.244	11.655
CU	5.71	.518	1.107	7.592
CU	4.88	.229	1.328	18.550
CU	5.01	.345	1.149	15.140
CU	5.66	.522	.561	15.333
CU	4.64	.439	.529	12.560
CU	4.38	.099	2.289	80.694
CU	5.73	.746	1.553	8.761
CU	4.36	.408	.699	9.082
CU	5.50	.329	.117	12.600
CU	7.33	.700	.988	6.996
CU	5.06	.312	.236	10.229
CU	4.10	.589	1.628	11.034
CU	4.12	.367	.244	10.151
CU	4.70	.556	.437	6.924
CU	5.29	.439	.750	9.838
CU	4.16	.360	.931	15.960
CU	4.14	.149	1.117	28.948
CU	4.36	.646	1.570	10.612
CU	4.05	.229	.535	14.905
CU	4.90	.468	.560	7.520
CU	4.75	.158	1.341	34.123
CU	4.61	.725	.524	8.199
CU	4.50	.524	2.060	11.379
CU	4.61	.365	.174	9.287
CU	4.61	.298	2.570	24.794

HIGH MASS EVENTS

TARGET	MASS	XF	PT	CROSS SECTION
CU	4.25	.559	.256	13.191
CU	5.31	-.037	.917	85.734
CU	4.93	.208	1.492	33.745
CU	6.46	.799	1.175	7.402
CU	4.54	.294	1.000	11.941
CU	4.11	.172	.706	35.947
CU	4.54	.194	.885	17.279
CU	4.01	.265	.849	32.636
CU	4.24	.324	.957	10.522
CU	6.13	.479	1.336	18.025
CU	4.03	.412	1.064	19.595
CU	5.14	.401	1.242	8.745
CU	4.81	.456	.518	6.894
CU	5.58	.486	.622	6.795
CU	5.72	.741	1.132	8.433
CU	4.93	.496	.432	8.388
CU	5.71	.701	2.628	10.757
CU	5.15	.791	.891	8.844
CU	5.30	.391	.146	23.624
CU	5.48	.395	1.203	10.262

HIGH MASS EVENTS

TARGET	MASS	XF	PT	CROSS SECTION
W	4.04	.522	.863	17.264
W	6.02	.414	1.193	15.300
W	4.09	.501	1.251	16.592
W	4.53	.204	2.200	91.476
W	4.83	.244	.755	29.739
W	4.29	.514	.765	12.053
W	4.05	.384	.288	12.995
W	4.33	.380	1.842	19.643
W	4.69	.655	.555	17.785
W	4.30	.140	.909	42.442
W	5.18	.446	.220	15.270
W	4.03	.055	.646	66.771
W	5.34	.184	2.873	85.378
W	4.80	.624	1.069	14.972
W	4.00	.393	1.590	18.875
W	5.96	.095	.503	98.459
W	4.27	.402	1.433	17.303
W	4.33	.380	1.518	20.450
W	4.00	.670	.957	16.344
W	5.27	.700	.774	24.030
W	4.52	.445	1.626	16.070
W	4.44	.113	.378	81.727
W	4.53	.412	.388	22.027
W	4.17	.531	.185	14.913
W	4.97	.280	2.419	37.749
W	4.15	.457	1.121	21.293
W	4.31	.311	.405	49.232
W	4.12	.132	.722	45.153
W	4.48	.507	1.296	21.532
W	4.60	.244	2.223	51.790
W	4.23	.246	.617	25.515
W	4.54	.424	.648	12.129
W	5.13	.700	.229	12.167
W	4.96	.578	1.371	13.887
W	4.99	.112	2.043	124.923
W	4.06	.461	.797	13.148
W	6.63	.426	1.416	14.770
W	5.43	.725	1.020	12.970
W	4.01	.539	2.500	33.620
W	4.14	.626	1.784	19.859
W	4.52	.581	.434	12.304
W	4.17	.237	.940	28.906
W	5.52	.591	.632	23.732
W	6.79	.171	.247	31.184
W	4.07	.442	1.055	15.392
W	4.86	.246	.498	21.552
W	4.41	.405	1.655	37.211
W	7.50	.507	1.594	16.206
W	5.61	.392	.774	19.563

HIGH MASS EVENTS

TARGET	MASS	XF	PT	CROSS SECTION
W	5.20	.819	.517	22.593
W	5.16	.255	.874	41.916
W	4.14	.438	.827	12.566
W	5.52	.535	3.622	42.586
W	10.88	.492	1.619	17.110
W	4.35	.742	1.350	13.448
W	4.49	.181	1.162	35.312
W	4.47	.480	1.909	19.655
W	5.23	.067	1.688	97.782
W	5.29	.329	1.588	21.217
W	4.81	.418	.546	16.104
W	4.30	-.068	.401	250.518
W	6.19	.705	.787	11.458
W	4.46	.255	.285	23.237
W	4.62	.184	.294	34.644
W	5.60	.264	1.711	33.201
W	4.21	.720	.671	15.209
W	4.14	.504	.634	12.053
W	5.45	.597	.779	11.977
W	4.94	.585	1.622	13.354
W	4.26	.507	.310	11.579
W	5.20	.383	.638	15.938
W	4.05	.773	.760	14.248
W	6.09	.675	.665	19.406
W	5.87	.201	.720	32.429
W	5.52	.647	1.341	13.193
W	4.25	.382	1.156	19.276
W	4.73	.310	2.160	29.210
W	4.82	.565	1.413	33.473
W	4.15	.416	1.551	16.485
W	4.01	.337	1.722	37.652
W	5.79	.105	1.609	99.126
W	4.98	.764	.520	12.649
W	4.24	.692	.626	12.840
W	4.45	.716	.375	16.138
W	5.18	.648	1.513	23.019
W	4.21	.641	.571	12.649
W	4.16	.577	1.540	19.212
W	4.08	.546	.939	13.216
W	4.85	.472	1.302	14.972
W	4.25	.496	1.618	16.773
W	4.05	.205	.979	41.801
W	4.67	.614	1.481	13.036
W	4.14	.612	.236	19.555
W	5.77	.389	.863	36.818
W	4.27	.450	1.301	15.676
W	5.31	.553	1.607	36.158
W	4.24	.403	.873	14.770
W	5.21	.026	1.200	112.164

HIGH MASS EVENTS

TARGET	MASS	XF	PT	CROSS SECTION
W	7.13	-.170	1.113	326.260
W	7.01	.393	.753	14.159
W	6.00	.506	1.662	32.619
W	4.35	.372	1.283	15.148
W	4.36	.322	1.254	18.000
W	4.36	.272	.562	24.868
W	6.48	.584	.455	11.093
W	4.01	.394	.954	24.898
W	4.17	.819	1.140	27.863
W	4.05	.625	.861	19.116
W	4.03	.752	.170	11.510
W	7.06	.480	.297	16.485
W	4.02	.374	.722	14.842
W	4.76	.514	.137	12.670
W	4.84	.532	1.038	16.700
W	4.16	.239	.383	23.567
W	4.28	.480	.688	15.708
W	4.34	.327	.657	16.299
W	4.84	.381	.402	53.161
W	5.37	.399	.957	24.450
W	4.21	.454	.526	11.109
W	5.86	.295	1.429	23.505
W	4.76	.809	1.525	26.621
W	4.90	.328	1.162	17.596
W	5.30	.447	1.239	13.308
W	6.42	.392	1.640	27.267
W	5.46	.767	1.251	12.404
W	4.78	.759	.192	10.888
W	5.04	.663	2.274	16.104
W	4.06	.495	.991	37.761
W	5.04	.655	.884	17.303
W	4.25	.608	.314	19.260
W	4.61	.101	.725	50.003
W	4.89	.231	1.243	83.997
W	4.98	.625	.482	12.053
W	6.14	.367	.281	25.983
W	9.86	.397	.926	16.105
W	5.78	.796	1.477	12.284
W	4.48	.398	1.292	17.163
W	4.21	.372	.899	14.249
W	5.06	.304	3.547	67.143
W	5.78	.407	.667	13.519
W	4.47	.893	.815	26.016
W	4.05	.210	1.286	29.890
W	4.90	.319	1.810	24.139
W	5.33	.286	.660	19.068
W	5.09	.180	1.119	41.800
W	6.08	.805	.578	18.999
W	5.98	.317	1.335	30.528

HIGH MASS EVENTS

TARGET	MASS	XF	PT	CROSS SECTION
W	4.11	.409	4.285	107.501
W	4.30	.244	.493	31.635
W	4.82	.380	1.103	13.483
W	6.76	.497	.697	22.545
W	4.06	.236	.519	25.663
W	4.82	.497	1.449	27.279
W	5.39	.494	.898	15.362
W	4.13	.274	.536	31.413
W	4.42	.063	.803	62.706
W	4.00	.222	.645	50.185
W	5.62	.701	.575	11.289
W	7.63	.555	.352	10.317
W	7.09	.199	2.502	84.748
W	4.08	.473	2.059	17.744
W	4.45	.610	1.092	14.436
W	5.24	-.005	.634	145.726
W	4.85	.740	.979	13.519
W	5.67	.394	.795	13.162
W	5.09	.594	.893	11.977
W	4.72	.115	.135	34.492
W	5.02	.904	1.143	24.184
W	4.61	.410	.357	10.617
W	4.85	.386	.772	12.333
W	4.30	.623	1.213	13.378
W	6.41	.629	1.654	14.169
W	5.28	.524	3.947	52.146
W	6.09	.628	.701	15.644
W	4.10	.362	.698	12.739
W	5.96	.351	1.156	27.609
W	7.31	.507	.375	13.737
W	4.62	.304	.628	17.295
W	4.18	.580	1.591	29.482
W	4.23	.327	.854	14.953
W	4.13	.553	1.562	23.229
W	8.39	.520	1.275	16.628
W	4.47	.193	2.432	74.426
W	4.17	.194	.660	27.971
W	7.21	.436	.801	13.495
W	4.73	.220	.698	51.181
W	4.07	.672	1.746	38.327
W	4.10	.283	3.276	96.252
W	5.51	.788	.495	11.475
W	4.08	.378	.312	11.439
W	4.88	.203	1.185	108.991
W	5.26	.676	.891	18.605
W	5.27	.281	2.203	36.235
W	5.84	.617	1.283	15.740
W	4.05	.736	.495	12.344
W	9.94	.274	.631	31.351
W	4.77	.403	2.759	24.888

HIGH MASS EVENTS

TARGET	MASS	XF	PT	CROSS SECTION
W	4.46	.786	1.669	19.260
W	4.15	.388	.596	19.741
W	6.97	.580	2.186	13.216
W	4.53	.362	1.646	20.714
W	4.07	.634	.194	11.441
W	4.89	.038	.934	76.669
W	4.74	.331	.720	18.411
W	4.28	.255	.290	20.533
W	7.35	.210	1.642	54.299
W	4.05	.549	1.685	17.226
W	5.95	.443	.349	30.060
W	7.98	.574	1.272	14.463
W	4.52	.265	.944	37.809
W	5.23	.012	.235	61.992
W	4.52	.568	1.330	13.472
W	4.33	.313	.730	14.621
W	4.05	.451	.533	19.962
W	4.10	.686	1.983	19.505
W	4.01	.747	.729	13.103
W	4.18	.381	1.318	21.742
W	5.50	.397	1.179	22.538
W	4.08	.435	.397	11.775
W	4.22	.066	.581	80.885
W	6.39	.707	2.031	13.425
W	5.77	.675	.235	14.855
W	5.22	.376	2.123	19.733
W	7.13	.224	.879	26.930
W	5.20	.674	.749	11.667
W	9.80	.411	.958	32.619
W	4.38	.615	1.168	13.148
W	7.03	-.171	.443	356.297
W	4.32	.635	.990	17.662
W	4.64	.696	2.428	70.325
W	5.77	.441	1.675	13.472
W	4.58	.272	1.028	20.695
W	5.88	.080	.448	45.968
W	4.92	.297	.446	19.975
W	8.83	.386	1.379	19.132
W	4.08	.648	1.315	14.798
W	5.46	-.112	.816	310.229
W	4.93	.501	1.009	15.392
W	4.19	.607	.866	13.036
W	4.09	.611	1.723	26.709
W	10.36	.545	1.023	94.456
W	7.59	.437	.822	159.679
W	5.50	.438	1.337	23.158
W	4.35	.161	.821	51.088
W	5.27	.399	.574	11.340
W	5.68	.625	1.619	16.138
W	4.14	.480	.433	12.187

HIGH MASS EVENTS

TARGET	MASS	XF	PT	CROSS SECTION
W	4.49	.236	1.831	42.418
W	4.35	.529	1.304	13.787
W	5.08	.101	2.807	180.322
W	4.82	-.087	.640	185.503
W	4.07	.335	.710	37.472
W	6.23	.633	.825	20.387
W	4.33	.558	.381	11.424
W	5.23	.273	.684	52.746
W	4.10	.386	1.859	179.840
W	4.33	.439	.320	27.182
W	4.42	.382	2.084	20.426
W	10.71	.190	1.992	43.930
W	4.91	.592	2.324	66.656
W	4.63	.637	2.358	20.119
W	8.43	.172	1.541	72.328
W	5.12	.745	.301	10.935
W	4.87	.742	.828	16.240
W	4.92	.559	.307	10.588
W	5.63	.694	1.399	12.628
W	4.62	.556	.427	11.125
W	7.02	.029	.603	95.608
W	4.84	.551	.628	11.373
W	4.03	.207	1.407	57.427
W	5.58	.735	.875	11.793
W	4.80	.233	1.345	29.443
W	4.53	.425	.317	37.948
W	5.41	.373	1.962	19.334
W	4.12	.666	.093	11.597
W	4.10	.492	.216	10.873
W	4.03	.501	1.469	14.884
W	5.39	.269	1.559	24.749
W	8.11	.505	1.257	15.708
W	5.43	.072	.706	63.475
W	6.44	.189	1.957	50.317
W	4.10	.452	.500	19.505
W	6.11	.754	.778	11.323
W	4.69	.221	.974	106.302
W	4.09	.379	1.594	33.086
W	4.33	.159	1.344	47.670
W	4.06	.447	.192	15.970
W	5.38	.290	1.629	29.240
W	4.20	.346	.743	24.545
W	7.33	.034	.578	116.105
W	5.21	.188	.820	35.441
W	4.85	.413	.457	10.387
W	4.17	.466	.719	11.174
W	4.35	.559	1.010	12.444
W	4.57	.631	.461	11.721
W	7.95	.179	.443	34.179
W	4.44	.599	.483	11.492

HIGH MASS EVENTS

TARGET	MASS	XF	PT	CROSS SECTION
W	5.05	.133	.704	50.044
W	4.20	.118	1.336	70.574
W	4.26	.063	2.587	188.087
W	7.51	.611	.770	10.721
W	4.25	.500	1.139	13.239
W	4.35	.750	.914	12.970
W	4.08	.113	.799	48.701
W	6.85	.449	.804	13.148
W	7.30	.389	.919	20.193
W	6.46	.560	.951	77.576
W	4.02	.275	.816	19.540
W	4.34	.029	2.118	251.503
W	4.12	.361	.831	12.969
W	4.29	.021	2.922	27.773
W	6.96	.423	.546	22.348
W	5.22	.743	.264	11.061
W	5.27	.494	.110	14.601
W	5.46	.532	2.342	21.412
W	4.53	.850	1.043	24.486
W	5.22	.627	.562	14.409
W	4.01	.250	.490	25.904
W	7.55	.433	.977	33.620
W	6.29	.204	1.302	39.112
W	4.17	.181	.521	28.027
W	4.87	.511	.744	13.495
W	4.98	.513	.898	16.309
W	4.76	.377	2.109	60.415
W	5.65	.654	1.019	15.676
W	4.29	.364	.895	40.998
W	5.58	.348	1.209	46.042
W	4.83	.699	.180	12.505
W	4.94	.381	.845	49.472
W	6.32	.549	1.288	12.948
W	6.94	.705	1.839	17.187
W	4.93	.469	1.233	17.952
W	5.47	.103	1.223	77.471
W	4.22	-.037	.846	439.320
W	4.00	.579	.979	12.265
W	6.10	.421	1.321	14.328
W	5.05	.177	.555	39.499
W	5.98	.417	1.313	32.758
W	4.97	.629	.679	20.551
W	4.41	.691	1.525	17.581
W	4.46	.766	.747	12.840
W	4.09	.364	1.225	15.412
W	4.11	.141	1.311	57.528
W	4.67	.315	.597	15.314
W	4.28	.674	.660	12.628
W	4.5[illegible]	.777	1.714	16.076

HIGH MASS EVENTS

TARGET	MASS	XF	PT	CROSS SECTION
W	4.47	.472	1.293	13.425
W	4.68	.696	.767	12.992
W	5.03	.143	1.064	73.885
W	4.59	.791	.556	13.059
W	5.69	.537	1.731	25.132
W	6.09	.319	1.262	21.015
W	5.87	.217	1.333	33.346
W	5.05	.384	1.026	19.605
W	5.73	.856	.856	21.430
W	4.26	.414	.249	24.335
W	5.33	.610	.576	11.158
W	4.48	.485	1.301	27.773
W	4.82	.037	.711	63.985
W	4.57	.587	1.265	13.126
W	4.97	.707	.608	11.757
W	5.40	.531	2.052	22.219
W	4.70	.317	2.147	27.258
W	5.51	.388	1.008	15.212
W	4.94	.558	1.463	14.195
W	5.22	.347	1.154	17.071
W	4.04	.294	1.364	36.783
W	4.16	.417	1.638	18.515
W	4.94	.390	1.787	21.527
W	5.14	.458	.735	16.206
W	4.54	.365	2.374	28.882
W	6.50	.871	.958	20.502
W	4.00	.638	1.210	14.039
W	6.06	.689	.502	11.866
W	5.25	.276	.641	24.920
W	5.34	.301	1.394	32.246
W	5.16	.084	.796	54.010
W	5.40	.370	1.277	15.680
W	4.79	.307	1.227	20.324
W	5.75	.458	2.062	15.580
W	6.48	.369	1.389	16.465
W	4.30	.337	.738	17.846
W	4.33	.449	1.033	12.992
W	5.67	.005	.696	15.300
W	4.01	.636	.395	12.505
W	5.75	.263	.279	26.654
W	5.75	.558	.612	10.501
W	6.31	.229	1.591	42.634
W	4.12	.351	.211	33.635
W	4.44	.549	1.106	12.905
W	8.76	.663	.613	26.432
W	4.03	.076	.958	150.440
W	4.10	.573	1.460	14.713
W	5.24	.246	2.480	91.045
W	6.24	.331	1.019	17.375

HIGH MASS EVENTS

TARGET	MASS	XF	PT	CROSS SECTION
W	4.33	.502	1.171	12.587
W	5.96	.271	.804	133.087
W	7.16	.236	1.485	35.762
W	5.34	.293	1.725	38.719
W	4.35	.666	.912	14.884
W	4.88	.353	1.605	21.469
W	4.20	.245	2.015	41.041
W	4.24	.663	1.820	16.810
W	4.50	.591	1.169	12.883
W	4.85	.595	1.745	14.436
W	8.94	.664	1.674	13.664
W	4.77	.278	.937	21.757
W	4.81	.625	1.051	18.471
W	4.59	.641	1.329	13.448
W	4.13	.500	1.091	25.132
W	4.97	.450	.425	10.736
W	4.18	.192	.177	30.320
W	4.29	.636	.726	14.629
W	4.98	.480	.219	16.036
W	4.24	.610	.680	22.091
W	5.19	.440	3.598	92.155
W	5.65	.313	.962	21.888
W	4.32	.449	.046	14.685
W	6.22	.331	1.756	23.878
W	4.90	.446	.925	93.382
W	5.35	.009	1.896	222.738
W	4.00	.421	.493	13.126
W	5.72	.365	1.078	28.255
W	5.26	.652	.811	15.119
W	5.95	.308	1.952	27.102
W	6.51	.341	1.366	26.755
W	5.22	.705	.799	23.659
W	4.07	.625	.291	12.424
W	4.18	.657	.959	13.737
W	4.64	.369	1.768	32.994
W	4.22	.370	.386	11.279
W	4.33	.747	.686	19.859
W	4.97	.598	1.560	20.944
W	5.55	.460	1.436	18.927
W	7.06	.241	.464	22.024
W	4.38	.736	1.553	20.067
W	4.84	.612	1.453	13.615
W	4.09	.311	1.413	20.179
W	6.60	.475	1.067	16.700
W	4.15	.353	.961	14.531
W	5.99	.363	1.271	17.011
W	4.66	.161	.675	43.360
W	5.19	.141	.983	40.087
W	8.40	.550	1.000	13.615

HIGH MASS EVENTS

TARGET	MASS	XF	PT	CROSS SECTION
W	4.00	.448	.842	27.279
W	4.65	.444	.676	10.951
W	6.49	.453	2.778	28.817
W	4.40	.108	.759	71.059
W	4.49	.340	1.508	19.923
W	5.53	.771	.720	11.456
W	5.19	.752	1.372	14.382
W	4.37	.506	.918	12.883
W	5.61	-.068	.771	166.460
W	4.32	.220	.996	30.134
W	4.51	.422	.541	11.739
W	6.29	.414	.122	39.924
W	4.01	.392	1.428	27.564
W	4.27	.249	1.885	64.385
W	4.47	.430	.524	17.910
W	5.30	.564	.803	16.628
W	4.46	.399	1.063	20.477
W	5.25	.194	.799	28.640
W	4.34	.494	.436	11.109
W	6.01	.448	1.332	13.737
W	4.28	.366	.904	22.557
W	4.30	.423	1.259	37.948
W	5.28	.294	2.887	57.419
W	4.81	.526	1.000	14.328
W	5.27	.122	1.985	91.945
W	4.79	.589	1.622	13.787
W	4.12	.713	.651	12.926
W	6.32	.213	1.536	34.679
W	4.25	.486	.967	13.239
W	4.17	.317	1.767	23.882
W	7.27	.412	.985	262.732
W	4.33	.841	1.557	29.164
W	4.80	.318	1.049	23.980
W	4.57	.504	.048	10.982
W	4.91	.044	.366	118.358
W	4.39	.827	.135	21.839
W	4.85	.352	.595	14.890
W	4.14	.928	.551	28.091
W	6.66	.303	.982	39.002
W	5.55	.268	.310	21.519
W	4.90	.429	1.776	15.486
W	5.11	.719	.831	11.527
W	4.13	.669	.464	12.324
W	4.16	.313	.945	32.592
W	4.05	.658	.747	13.401
W	7.22	.481	.520	11.339
W	5.21	.439	.645	20.172
W	4.39	.597	1.196	16.520
W	4.79	.365	2.067	23.140
W	5.14	.451	1.963	16.628

HIGH MASS EVENTS

TARGET	MASS	XF	PT	CROSS SECTION
W	4.48	.369	.817	13.049
W	5.33	.407	.127	10.207
W	4.21	.313	.499	24.779
W	4.66	.256	.841	21.709
W	6.44	.469	.650	14.657
W	4.38	.587	1.137	18.079
W	5.50	.339	.352	40.166
W	4.29	.364	.774	25.783
W	4.12	.426	1.471	15.239
W	8.07	.704	.931	16.515
W	4.07	.347	.868	14.561
W	4.33	.349	1.762	92.199
W	7.22	.247	.938	27.938
W	4.78	.550	1.170	12.265
W	4.17	.259	.813	20.081
W	4.36	.438	.492	36.853
W	5.57	.595	.853	24.969
W	4.64	.420	1.914	29.711
W	5.37	.769	1.793	13.014
W	4.11	.195	.277	25.289
W	6.68	.444	1.177	15.838
W	4.74	.560	.948	21.715
W	5.80	.288	.214	21.785
W	4.07	.239	.521	21.125
W	4.53	.738	.901	13.567
W	7.47	.254	1.032	27.602
W	4.08	.423	.681	13.591
W	4.09	.820	1.738	38.370
W	4.21	.288	1.586	41.722
W	4.37	.221	2.664	74.196
W	5.07	.749	.585	11.273
W	4.45	.741	1.282	14.091
W	4.31	.615	1.355	14.169
W	5.94	.255	.649	35.873
W	4.27	.419	1.409	19.807
W	4.68	.380	.887	12.704
W	4.26	.159	1.091	42.768
W	6.98	.126	.945	43.049
W	6.97	.378	1.425	16.637
W	6.10	.190	.705	28.456
W	8.14	.465	.911	16.810
W	4.97	.508	.826	13.014
W	4.37	.525	.622	29.596
W	4.07	.420	.341	147.784
W	4.02	.764	1.415	52.865
W	9.05	.431	.620	18.295
W	5.62	.244	1.140	45.141
W	4.81	.821	1.039	24.184
W	4.22	.317	.713	16.154
W	4.24	.367	.842	14.936

HIGH MASS EVENTS

TARGET	MASS	XF	PT	CROSS SECTION
W	5.05	.289	.962	23.073
W	6.37	.577	.999	16.003
W	4.13	.456	1.289	32.481
W	4.61	.454	.803	13.862
W	5.60	.441	1.126	13.239
W	4.93	.091	1.297	82.544
W	4.01	.563	2.245	26.802
W	9.84	.294	1.798	32.627
W	4.29	.412	1.624	17.994
W	4.03	.762	.510	12.384
W	5.22	.467	1.105	16.275
W	4.92	.503	.832	11.109
W	4.26	.489	.176	12.424
W	10.44	.640	.978	34.843
W	5.41	.239	.561	22.212
W	4.68	.368	.769	12.568
W	4.38	.528	1.909	19.859
W	4.34	.124	1.814	97.860
W	4.33	-.034	.552	119.274
W	4.19	.407	.563	12.424
W	4.05	.339	.295	12.708
W	4.13	.706	.217	17.187
W	5.64	.453	1.414	23.659
W	6.69	.290	.692	37.991
W	4.53	.503	.799	11.884
W	4.50	.393	.712	166.149
W	4.11	.348	.627	18.719
W	5.42	.770	2.346	26.162
W	4.90	.505	.643	16.664
W	4.31	.553	1.145	13.448
W	5.73	.437	.790	11.174
W	4.08	.071	.319	85.001
W	5.69	.149	1.340	60.711
W	4.55	.431	.580	10.873
W	4.11	.229	1.231	31.693
W	4.20	.763	.516	12.505
W	5.15	.207	.215	24.696
W	4.18	.598	1.139	14.601
W	4.66	-.005	.641	207.715
W	4.09	.414	1.611	16.628
W	4.41	.519	.905	12.505
W	4.03	.299	.716	17.963
W	4.73	.589	.462	28.926
W	4.17	.366	1.446	24.563
W	4.32	.144	2.488	126.440
W	4.34	.239	1.077	44.154
W	4.89	.781	.750	13.193
W	4.97	.695	2.148	16.592
W	4.60	.348	1.856	28.705
W	7.03	.614	.197	9.955

HIGH MASS EVENTS

TARGET	MASS	XF	PT	CROSS SECTION
W	5.41	.242	.307	25.877
W	4.42	.051	.898	73.495
W	5.48	.246	.368	20.983
W	4.69	.416	.829	11.775
W	5.44	.528	.335	10.317
W	4.97	.427	.631	10.486
W	5.75	.468	.660	10.827
W	4.06	.402	.939	13.014
W	4.70	.327	.355	17.829
W	4.53	.489	.542	13.713
W	5.52	-.091	1.037	249.384
W	7.33	.551	.678	75.151
W	4.39	.633	1.685	24.181
W	4.61	.350	1.130	21.693
W	5.04	.607	1.459	24.490
W	4.42	.366	1.576	18.451
W	4.13	.659	.190	11.940
W	4.71	.185	.491	43.443
W	4.60	.573	1.635	16.449
W	4.69	.427	.542	17.785
W	6.19	.471	1.436	16.070
W	4.30	.228	.344	25.742
W	4.75	.754	.661	12.072
W	4.05	.771	.759	12.861
W	4.03	.053	1.010	91.560
W	4.77	.237	.371	23.825
W	5.34	.557	1.568	12.840
W	4.08	.531	.783	29.596
W	5.47	.674	1.769	29.711
W	4.31	.215	1.493	121.308
W	4.44	-.051	.434	209.709
W	5.22	-.077	1.130	248.505
W	5.53	.819	.248	19.595
W	4.85	.563	.823	11.632
W	6.00	.484	1.087	11.373
W	7.69	.742	1.115	10.812
W	8.43	.528	1.580	13.887
W	5.63	.209	.573	25.500
W	4.12	.686	.539	15.644
W	4.42	.480	.960	34.843
W	4.92	.188	1.204	35.668
W	4.33	.514	.304	23.299
W	7.89	.609	1.141	12.691
W	7.13	.361	1.335	20.974
W	4.78	.202	1.075	119.212
W	4.19	.528	.440	10.951
W	4.27	.015	1.023	13.148
W	4.24	.011	.789	90.282
W	6.03	-.003	1.074	102.920

HIGH MASS EVENTS

TARGET	MASS	XF	PT	CROSS SECTION
W	4.47	.286	1.593	23.938
W	4.79	.771	1.124	22.348
W	6.82	.447	1.962	21.715
W	4.35	.277	1.750	29.090
W	4.11	.379	.392	24.288
W	6.21	.442	.743	16.773
W	4.08	.017	.956	116.989
W	4.04	.146	.214	29.917
W	7.29	.342	1.890	23.613
W	4.30	.523	1.141	15.805
W	6.86	.684	.548	10.234
W	5.47	.238	.832	44.470
W	5.80	-.053	1.402	239.299
W	4.37	.295	2.073	29.454
W	6.40	.267	.180	21.928
W	4.47	.691	.937	12.649
W	5.96	.207	1.018	27.300
W	6.49	.453	.825	16.414
W	4.20	.235	2.377	51.421
W	6.22	.721	.443	10.529
W	5.96	.501	1.086	12.015
W	5.02	.217	.386	44.446
W	5.16	.494	.080	15.870
W	4.10	.345	.548	11.727
W	7.03	.206	1.781	42.707
W	8.93	.687	1.159	12.110
W	4.74	.365	.809	15.101
W	4.86	.632	1.357	14.143
W	4.90	.754	.529	11.597
W	6.73	.782	.614	10.998
W	4.10	.409	.620	12.206
W	8.48	.741	.970	15.708
W	8.52	.424	.840	21.472
W	4.50	.186	1.118	33.490
W	4.06	.716	1.179	37.031
W	5.66	.429	1.102	21.412
W	4.70	.671	2.777	25.050
W	5.45	.749	.204	11.223
W	5.06	.577	1.427	13.615
W	4.32	.250	.816	29.432
W	5.72	.376	1.076	15.938
W	5.01	.797	.221	11.306
W	5.25	.653	.898	24.258
W	5.38	.784	1.431	22.882
W	4.07	.281	1.994	107.095
W	5.67	.394	1.045	35.535
W	4.18	.343	.224	17.309
W	4.61	.419	.725	13.216
W	4.77	.493	.585	12.015

HIGH MASS EVENTS

TARGET	MASS	XF	PT	CROSS SECTION
W	4.94	.411	.632	17.662
W	4.54	.548	.305	10.966
W	4.52	.399	.672	13.013
W	4.28	.562	.962	12.992
W	4.66	.291	1.531	33.885
W	5.04	.258	1.115	29.493
W	4.37	.164	.367	28.611
W	4.22	.611	.384	15.517
W	4.61	.430	1.186	13.713
W	7.60	.319	.355	25.604
W	4.23	.836	.183	22.482
W	4.79	.492	.831	11.306
W	4.31	.459	1.095	29.257
W	4.35	.637	.556	11.614
W	5.25	.169	.753	34.434
W	4.16	.665	1.483	15.001
W	5.73	.308	.588	35.561
W	5.91	.032	1.076	117.400
W	6.31	.301	.683	27.545
W	6.21	.264	1.390	77.608
W	4.04	.571	1.021	13.495
W	4.16	.291	1.056	18.817
W	5.50	.705	1.116	12.206
W	6.13	.124	.548	41.702
W	7.22	.479	1.377	24.181
W	4.27	.338	.594	12.636
W	4.46	.637	.948	12.776
W	4.20	.595	2.174	48.210
W	5.52	.200	.988	30.822
W	6.16	.190	.254	31.540
W	4.24	.700	.667	13.081
W	5.20	.280	2.036	33.731
W	8.75	.404	2.227	22.679
W	4.00	.445	1.173	13.615
W	5.69	.507	1.044	13.448
W	4.65	.518	.223	23.229
W	4.49	.595	.675	15.001
W	4.70	.191	1.084	36.153
W	4.76	.252	1.033	32.048
W	4.44	.688	.860	16.036
W	5.93	.537	1.150	25.215
W	4.04	.106	.535	44.824
W	4.14	.795	1.100	15.001
W	6.56	.769	.873	10.721
W	5.18	.774	1.470	17.034
W	4.55	.424	1.953	15.676
W	4.44	.711	.212	11.475
W	4.34	.559	1.429	19.605
W	5.99	.369	.942	24.569

HIGH MASS EVENTS

TARGET	MASS	XF	PT	CROSS SECTION
W	6.11	.887	.760	21.330
W	4.15	.337	1.262	23.293
W	5.04	.579	1.274	12.712
W	5.73	.656	.376	11.142
W	4.14	.539	.382	27.376
W	4.80	.486	1.339	13.308
W	4.39	.527	.427	17.744
W	4.08	.191	1.957	60.922
W	5.01	.283	1.933	31.654
W	4.82	.528	2.934	32.619
W	4.40	.705	1.924	25.984
W	4.07	.113	1.051	55.575
W	8.44	.160	1.964	47.964
W	5.23	.163	.047	53.581
W	4.33	.333	2.072	27.326
W	4.81	.239	.459	22.814
W	5.04	.835	.617	22.263
W	4.54	.607	.161	10.982
W	4.23	.222	.359	36.039
W	8.02	.307	.997	21.537
W	7.62	.207	.449	29.923
W	5.93	.241	1.010	26.063
W	4.26	.016	1.112	255.490
W	6.26	.384	1.198	20.204
W	4.73	.494	.427	16.996
W	4.59	.568	.384	11.650
W	4.28	.404	.225	10.706
W	4.32	.756	.840	13.962
W	5.80	.561	.920	17.662
W	7.29	.786	.683	10.706
W	4.75	.485	2.579	33.328
W	5.23	.772	.814	11.940
W	4.01	.809	.207	23.243
W	4.16	.165	.672	37.050
W	4.81	.413	.808	137.963
W	6.89	.456	.274	14.518
W	5.04	.469	.288	10.706
W	5.58	.490	1.055	11.158
W	5.20	.223	.831	42.476
W	4.90	.493	1.125	17.226
W	4.40	.252	1.241	83.952
W	4.19	.393	1.303	16.477
W	4.96	.380	.314	11.713
W	5.87	.209	.594	24.802
W	4.12	.064	.812	69.603
W	4.42	.506	.562	22.413
W	4.76	.259	1.451	51.611
W	4.10	.500	.778	15.209
W	4.03	.493	.242	20.830
W	4.35	.186	1.397	41.553

HIGH MASS EVENTS

TARGET	MASS	XF	PT	CROSS SECTION
W	4.07	.727	1.099	28.926
W	4.70	.319	1.468	18.986
W	4.62	.654	1.199	12.970
W	4.09	.247	.471	20.087
W	4.97	.542	.512	12.926
W	4.07	.651	1.574	16.275
W	4.20	.212	1.646	52.990
W	5.03	.626	1.844	15.089
W	5.05	.273	1.188	28.664
W	5.03	.654	1.971	15.676
W	4.03	.334	.334	17.668
W	4.30	.104	1.540	113.493
W	4.79	.180	1.321	41.334
W	6.01	.459	.817	10.812
W	4.50	.411	.385	11.289
W	4.42	.143	.256	32.415
W	4.47	.282	.973	32.466
W	4.18	.106	1.238	65.840
W	5.18	.395	1.908	17.806
W	4.00	.622	.819	15.549
W	4.07	.442	1.824	23.089
W	4.33	.373	.702	18.934
W	4.01	.214	1.943	84.796
W	5.90	.365	.571	54.647
W	6.81	.422	.321	19.406
W	4.45	.606	.400	11.527
W	5.41	.533	1.956	16.520
W	4.01	.354	.989	17.290
W	4.43	.414	1.099	13.354
W	4.51	.574	1.611	15.060
W	4.36	.751	1.136	23.158
W	4.99	.491	.804	38.714
W	4.60	.625	1.049	12.797
W	6.96	.549	1.509	87.166
W	4.06	.355	.738	14.377
W	6.37	.195	1.839	42.724
W	4.13	.071	1.354	97.444
W	7.21	.094	2.433	127.646
W	4.05	.481	1.608	16.172
W	4.23	.614	1.506	22.814
W	4.10	.789	1.269	25.897
W	4.94	.908	.462	21.430
W	4.14	.668	.303	14.657
W	4.37	.584	.815	16.737
W	5.78	-.185	1.605	2403.316
W	4.02	.572	.441	39.310
W	5.47	.022	.755	82.356
W	4.61	.690	1.027	13.331
W	4.21	.177	.443	27.295
W	7.92	.513	2.040	15.423

HIGH MASS EVENTS

TARGET	MASS	XF	PT	CROSS SECTION
W	8.25	.641	1.764	26.251
W	4.02	.469	1.307	16.172
W	4.27	.796	2.062	42.586
W	4.64	.009	1.120	205.711
W	4.19	.474	2.107	18.696
W	9.62	.455	.429	17.501
W	6.31	.558	.702	11.125
W	4.28	.481	1.338	17.622
W	4.08	.629	1.589	24.888
W	5.37	.387	.206	27.573
W	7.39	.772	1.158	34.529
W	10.65	.413	.871	19.555
W	4.75	.449	.856	14.248
W	4.78	.297	.771	18.529
W	7.32	.470	1.850	25.298
W	6.02	.200	.964	29.917
W	7.11	-.114	1.027	218.705
W	4.23	.181	.561	39.164
W	4.31	.323	1.553	20.883
W	5.11	.206	1.398	43.624
W	4.47	.301	1.655	23.024
W	6.66	.295	.696	39.067
W	6.07	.325	1.903	29.683
W	4.01	.660	.056	11.903
W	4.09	.419	2.162	22.283
W	5.01	.362	1.955	50.503
W	4.79	.077	1.269	104.353
W	5.66	.608	1.908	33.620
W	4.00	.396	1.422	21.373
W	5.33	.133	.682	43.051
W	4.13	.354	1.299	85.787
W	5.51	.269	.171	34.908
W	5.06	.429	.356	29.369
W	6.36	.493	1.425	25.466
W	4.11	.494	.472	13.887
W	6.29	.343	2.262	27.216
W	4.41	.690	.412	11.579
W	6.05	.492	.517	10.736
W	5.67	.620	1.020	27.976
W	4.54	.055	.625	109.259
W	4.88	.327	.443	31.212
W	4.72	.046	1.510	123.278
W	4.18	.301	.326	14.298
W	5.14	.402	1.321	14.117
W	6.22	.472	.652	20.279
W	4.26	.231	.713	29.762
W	5.07	.712	.576	11.579
W	5.33	.726	3.048	69.686
W	4.63	.625	.326	11.959
W	7.88	.480	.053	21.001

HIGH MASS EVENTS

TARGET	MASS	XF	PT	CROSS SECTION
W	6.00	.650	2.170	22.479
W	4.73	.351	.553	54.544
W	4.11	.591	1.026	13.354
W	4.26	.493	.901	16.172
W	4.02	.443	.287	13.713
W	4.25	.839	.400	22.894
W	4.36	.424	1.225	15.209
W	5.65	.452	.341	10.602
W	4.38	.210	.583	47.602
W	5.99	.105	.655	60.856
W	5.28	.803	.584	21.632
W	4.57	.470	.836	21.293
W	4.05	.720	.732	12.970
W	4.01	.823	.502	23.931
W	4.66	.390	.830	13.480
W	6.05	.420	.550	85.248
W	8.39	.748	.773	11.174
W	4.03	.186	.423	30.324
W	6.51	.210	.975	30.217
W	4.77	.457	.763	12.992
W	4.16	.227	1.057	51.974
W	4.17	.485	1.643	14.913
W	4.22	.249	1.765	56.487
W	4.28	.535	.623	11.739
W	7.54	.738	1.379	44.827
W	5.35	.620	.854	12.053
W	4.75	.495	1.529	13.664
W	4.05	.564	1.539	14.657
W	4.90	.526	1.229	15.119
W	5.40	.530	1.301	18.251
W	8.30	.683	.476	10.207
W	5.51	.470	1.507	30.662
W	4.51	.346	1.365	32.349
W	4.50	.691	.873	21.175
W	10.00	.217	.503	43.495
W	5.76	.725	1.871	22.679
W	4.14	.267	.991	26.546
W	4.77	.722	1.075	12.948
W	5.94	.464	1.099	11.424
W	5.49	.384	.692	12.836
W	4.43	.430	1.044	17.662
W	4.74	.434	1.029	12.444
W	4.35	.505	2.053	39.717
W	4.98	.447	1.009	26.991
W	5.32	.887	.773	23.086
W	4.76	.388	.619	21.476
W	4.38	.286	1.418	41.316
W	4.41	.690	1.315	24.807
W	6.11	.267	1.196	18.010

HIGH MASS EVENTS

TARGET	MASS	XF	PT	CROSS SECTION
W	4.64	.626	1.268	21.839
W	4.85	.610	1.685	19.555
W	4.11	.414	1.253	26.991
W	5.04	.500	1.724	15.517
W	4.38	.339	.598	17.864
W	5.00	.729	1.528	12.970
W	5.63	.013	.383	64.795
W	8.46	.197	1.560	48.683
W	4.07	.504	.844	13.887
W	4.14	.571	1.124	14.169
W	4.08	-.005	.958	143.395
W	4.39	.135	.370	32.340
W	4.51	.230	1.227	36.100
W	5.88	.320	.325	20.887
W	4.56	.762	.820	12.733
W	4.84	.599	2.820	25.050
W	5.88	.303	.784	19.750
W	5.28	.683	.719	11.424
W	5.21	.763	1.152	13.567
W	4.51	.301	1.935	26.749
W	5.59	.370	1.054	28.519
W	5.09	.372	.540	22.152
W	9.85	.504	1.097	20.172
W	4.48	.293	.143	26.850
W	4.89	.355	.767	16.728
W	4.32	.496	1.618	15.970
W	4.12	.287	1.255	26.522
W	4.03	.488	.513	11.848
W	5.98	.139	1.767	59.928
W	5.32	.653	2.526	24.727
W	4.02	.588	.854	13.148
W	4.23	.833	.842	24.930
W	4.06	.553	1.369	14.490
W	7.33	.393	1.431	85.374
W	4.23	-.002	.833	235.035
W	4.70	.242	1.000	45.303
W	4.83	.466	.365	10.842
W	5.17	.685	.987	15.676
W	5.39	.426	.996	21.234
W	5.37	.442	.376	10.429
W	4.71	.429	2.123	49.454
W	5.49	.239	1.300	27.558
W	4.20	.523	1.013	16.104
W	4.58	.391	.736	13.455
W	5.79	.788	2.223	16.206
W	4.95	.163	.766	111.201
W	4.12	.439	.642	11.721
W	4.13	.262	.376	18.438
W	4.21	.555	.408	11.458

HIGH MASS EVENTS

TARGET	MASS	XF	PT	CROSS SECTION
W	5.72	.488	.895	13.171
W	5.22	.705	.947	15.772
W	4.96	.088	.362	48.695
W	4.50	.214	1.198	108.295
W	4.95	.690	.445	11.793
W	4.21	.099	1.530	88.904
W	6.52	.516	.524	13.615
W	4.16	.413	1.064	23.806
W	4.49	.366	.436	14.757
W	4.05	.394	1.659	18.320
W	8.43	.506	.871	24.181
W	4.70	.524	3.169	46.740
W	5.12	.739	.193	19.655
W	4.72	.600	.823	12.364
W	5.03	.904	.285	21.430
W	4.92	.381	.398	12.400
W	4.18	.127	.341	34.343
W	4.46	.744	.361	12.818
W	4.57	.328	1.306	16.069
W	4.00	.210	1.373	42.421
W	4.13	.082	.737	65.772
W	4.10	.475	.244	18.560
W	7.09	.492	.206	10.661
W	4.28	-.021	1.017	163.043
W	5.36	.593	1.008	17.703
W	4.90	.039	.591	68.390
W	4.99	.770	2.514	35.162
W	4.36	.086	1.815	109.934
W	9.44	.587	1.171	14.855
W	4.32	.769	.936	13.988
W	6.39	.240	.871	75.277
W	4.73	.466	1.031	14.169
W	5.36	.498	.358	9.904
W	4.91	.462	.949	50.101
W	4.27	.045	.421	71.327
W	4.26	.481	.732	24.258
W	4.72	.425	1.044	13.962
W	5.57	.220	.024	28.911
W	5.31	.374	1.510	16.869
W	5.28	.432	.938	31.416
W	8.96	.223	.965	28.816
W	6.10	.358	1.073	15.616
W	4.13	.150	.968	53.943
W	5.25	.674	1.177	12.284
W	4.15	.498	.507	14.328
W	4.07	.073	2.315	173.404
W	4.39	.435	.920	13.912
W	6.50	.741	.827	11.142
W	4.59	.669	.438	11.597

HIGH MASS EVENTS

TARGET	MASS	XF	PT	CROSS SECTION
W	4.06	.381	.532	20.401
W	4.22	.327	.645	26.379
W	4.15	.172	1.071	40.472
W	4.17	.255	.971	39.273
W	4.32	.759	.632	12.444
W	4.51	.707	.644	16.996
W	5.71	.312	1.025	18.171
W	4.45	.345	1.011	31.085
W	5.48	.556	1.146	14.091
W	6.26	.244	1.534	31.994
W	5.00	.535	1.135	20.279
W	4.07	.257	1.635	39.893
W	5.16	.677	.331	11.356
W	5.49	.263	.851	30.117
W	6.14	-.032	.626	82.558
W	5.14	.647	.549	10.781
W	4.72	.275	.174	26.530
W	5.87	.438	.732	11.921
W	7.74	.612	1.030	13.126
W	5.70	.366	1.320	17.389
W	4.97	.856	1.661	25.918
W	5.82	.325	.381	35.949
W	6.74	.312	2.092	54.532
W	4.99	.352	1.642	27.384
W	8.41	.470	.797	14.275
W	4.03	.271	1.631	34.652
W	10.12	.510	.384	22.679
W	4.99	.620	.518	16.036
W	5.43	.462	1.190	28.496
W	6.53	.576	1.564	14.770
W	7.50	.097	.198	49.927
W	4.91	.490	1.310	16.036
W	4.17	.455	1.093	13.171
W	4.95	.237	1.627	34.158
W	5.14	.481	.907	26.991
W	4.08	.678	1.618	18.880
W	4.08	.622	.977	13.567
W	8.35	.520	.522	11.273
W	5.49	.439	2.244	17.868
W	5.60	.668	1.114	19.406
W	7.88	.079	.891	77.161
W	7.36	.476	1.990	15.708
W	7.51	.063	.535	47.288
W	4.83	.208	1.956	69.817
W	4.82	.734	1.473	14.573
W	4.09	.144	.156	43.494
W	4.43	.349	1.131	15.071
W	5.07	.274	1.229	44.804
W	4.36	.213	.441	25.799
W	5.20	.573	1.461	13.495

HIGH MASS EVENTS

TARGET	MASS	XF	PT	CROSS SECTION
W	9.05	-.031	.607	91.925
W	6.19	.365	2.333	25.098
W	4.21	.457	1.722	16.003
W	8.98	.641	1.391	13.862
W	4.13	.687	1.221	15.300
W	4.17	.120	.414	44.750
W	9.34	.615	1.309	12.424
W	4.12	.625	.636	12.970
W	5.01	.324	.600	14.603
W	4.25	.694	.839	17.622
W	4.91	.397	2.638	23.862
W	4.96	.346	1.056	15.559
W	4.46	.214	1.278	46.382
W	4.13	-.043	.439	177.046
W	4.47	.207	.494	34.001
W	5.35	.335	.543	14.352
W	5.33	.029	2.400	163.277
W	4.97	.108	1.087	81.816
W	7.26	.579	1.579	12.072
W	4.16	.133	1.825	80.172
W	4.91	.301	.824	19.770
W	4.71	.504	1.642	22.814
W	4.09	.486	.790	31.287
W	4.17	.280	.703	26.496
W	4.24	.503	1.348	14.490
W	4.40	.390	.495	14.268
W	4.40	.263	1.240	80.282
W	5.72	.550	.541	11.174
W	5.43	.371	1.076	18.511
W	5.78	.366	2.464	25.307
W	6.30	.618	.363	22.612
W	9.30	.504	.875	24.105
W	4.34	.413	1.410	16.070
W	4.02	.299	1.522	30.932
W	4.01	.591	.462	28.286
W	5.33	.812	.960	22.445
W	4.35	.408	1.205	22.545
W	4.86	.281	2.298	36.792
W	4.29	.719	.753	19.212
W	4.84	.414	.843	31.545
W	8.16	.557	.457	20.333
W	4.52	.534	.690	11.475
W	4.03	.104	1.260	67.097
W	5.93	.202	2.968	79.914
W	6.13	.301	2.968	38.027
W	4.73	.450	1.171	13.285
W	5.10	.713	.576	11.597
W	4.27	.536	1.151	13.787
W	6.30	.271	.691	37.636
W	4.29	.630	1.306	21.293

HIGH MASS EVENTS

TARGET	MASS	XF	PT	CROSS SECTION
W	4.83	.557	.528	10.951
W	5.26	.179	2.029	51.821
W	4.65	.518	1.296	43.553
W	4.58	.237	.886	39.097
W	5.67	.320	2.690	36.250
W	4.25	.367	.879	19.092
W	5.33	.532	.961	34.374
W	5.38	.512	1.061	12.883
W	4.38	.774	.828	13.036
W	6.67	.658	.635	21.654
W	5.47	.513	1.655	13.285
W	9.19	.388	1.388	22.051
W	9.37	.356	1.312	21.253
W	4.71	.209	.579	24.493
W	6.38	.327	2.425	42.258
W	4.28	.122	.444	49.544
W	6.06	.462	1.275	12.226
W	6.85	.365	.551	32.164
W	4.10	.459	1.237	25.382
W	8.78	.159	.757	70.053
W	4.74	.039	.231	49.024
W	4.78	.493	.837	16.414
W	5.64	.063	1.068	66.109
W	4.66	.476	1.433	26.896
W	4.52	.654	1.369	21.839
W	4.35	.470	.913	12.818
W	6.06	.266	.187	18.005
W	4.79	.386	1.028	15.806
W	4.59	.386	1.110	26.891
W	4.75	.466	.888	12.566
W	4.47	.613	.811	13.126
W	5.32	.492	.418	10.262
W	4.83	.632	.779	11.632
W	4.84	.460	.549	10.602
W	5.27	.352	.130	15.680
W	4.42	.525	.910	12.053
W	4.90	.304	.753	42.772
W	7.82	.163	2.338	64.897
W	4.77	.445	1.028	12.754
W	4.18	.431	.962	12.797
W	4.52	.479	2.534	30.298
W	4.24	.415	.411	10.588
W	10.99	.081	.691	54.377
W	4.20	.370	1.225	15.281
W	4.40	.166	.347	49.277
W	7.46	.421	2.195	25.132
W	7.74	.677	1.172	11.407
W	4.53	.789	1.724	24.105
W	5.93	.319	.605	17.845
W	4.53	.456	1.974	38.911

HIGH MASS EVENTS

TARGET	MASS	XF	PT	CROSS SECTION
W	5.45	.392	.977	13.428
W	4.46	.463	1.144	13.988
W	4.56	.688	.222	11.793
W	4.95	.401	.819	11.597
W	4.26	.404	.745	12.245
W	4.53	.280	1.318	21.354
W	5.00	.716	.722	12.091
W	4.02	.506	.517	11.848
W	4.87	.316	.863	24.584
W	4.10	.132	.372	31.159
W	5.25	.634	1.055	11.903
W	7.54	.515	1.561	14.855
W	4.14	.345	.777	23.231
W	4.45	.366	.367	21.657
W	4.20	.505	1.264	33.918
W	4.87	.761	.857	13.262
W	4.58	.852	.244	22.120
W	5.89	.166	1.281	48.270
W	4.13	.687	.985	14.143
W	5.09	.364	.664	17.240
W	4.13	.337	.887	38.003
W	5.86	.194	.490	40.022
W	4.03	.368	2.034	22.010
W	7.00	.211	.925	48.102
W	6.21	.712	.394	11.061
W	4.22	.057	.732	62.148
W	5.57	.681	1.422	26.432
W	4.24	.529	.791	13.543
W	5.64	.567	1.101	14.169
W	4.13	.564	1.895	16.810
W	4.16	.535	1.229	14.195
W	4.03	.790	.379	37.031
W	5.39	.573	.406	11.407
W	4.44	.411	1.837	17.501
W	5.98	.623	1.156	11.441
W	5.18	.530	.882	12.015
W	4.18	.653	1.301	14.827
W	4.03	.696	.393	12.566
W	5.53	.306	1.331	21.481
W	4.20	.075	3.178	242.739
W	5.09	.781	.621	12.110
W	9.36	.075	1.183	62.830
W	4.28	.117	.466	63.563
W	4.62	.133	.766	60.115
W	4.24	.653	1.070	13.425
W	9.25	.474	1.245	15.549
W	5.40	.447	1.491	13.285
W	6.31	.297	1.337	23.756
W	[illegible]	[illegible]	[illegible]	[illegible]

HIGH MASS EVENTS

TARGET	MASS	XF	PT	CROSS SECTION
W	4.30	.277	.622	23.233
W	4.79	.673	.533	12.245
W	4.22	.684	.346	12.265
W	4.95	.329	.949	15.661
W	9.30	.219	1.770	39.322
W	4.93	.203	2.056	52.155
W	5.08	.642	1.326	12.525
W	4.99	.491	.812	17.662
W	4.34	.288	.403	16.336
W	5.51	.314	.581	72.961
W	5.30	.434	1.273	12.566
W	4.61	.351	1.574	18.727
W	4.03	.343	1.849	38.080
W	5.85	.332	1.143	31.268
W	5.70	.543	.812	11.014
W	4.52	.242	.475	28.136
W	4.15	.387	1.167	15.229
W	4.43	.470	1.375	18.696
W	4.11	.425	1.562	15.392
W	7.41	.280	1.153	35.745
W	4.86	.535	.759	11.829
W	4.22	.539	1.699	15.549

References

1. C. de Vries *et al.*, Phys. Rev. Lett. 8, 381, 466(E) (1962).

2. E. D. Bloom *et al.*, Report to the Fourteenth International Conference on High Energy Physics, Vienna, 1968;

   E. D. Bloom *et al.*, Phys. Rev. Lett. 23, 930 (1969);

   M. Breindenback *et al.*, Phys. Rev. Lett. 23, 935 (1969).

3. M. Gell-Mann and Y. Ne'eman, *The Eightfold Way*, Benjamin, New York, 1964.

4. S. Herb *et al.*, Phys. Rev. Lett. 39, 252 (1977);

   W. Innes *et al.*, Phys. Rev. Lett. 39, 1240, 1640(E) (1977);

   D. Kaplan *et al.*, Phys. Rev. Lett. 40, 435 (1978);

   J. Yoh *et al.*, Phys. Rev. Lett. 44, 684 (1978).

5. S. D. Drell and T.-M. Yan, Phys. Rev. Lett. 25, 316, 902(E) (1970) and Ann. Phys. 66, 578 (1971).

6. K. J. Anderson et al., Phys. Rev. Lett. 36, 237 (1976);

K. J. Anderson et al., Phys. Rev. Lett. 37, 799 (1976);

K. J. Anderson et al., Phys. Rev. Lett. 37, 803 (1976);

J. G. Branson et al., Phys. Rev. Lett. 38, 580 (1977);

J. G. Branson et al., Phys. Rev. Lett. 38, 1331 (1977);

J. G. Branson et al., Phys. Rev. Lett. 38, 1334 (1977);

J. G. Branson, Ph. D. thesis, Princeton University, 1977, (unpublished);

G. G. Henry, Ph. D. thesis, University Of Chicago, 1978, (unpublished);

K. J. Anderson et al., to be published in Phys. Rev.

7. R. Bouclier et al., Nucl. Instr. and Meth. 115, 235 (1974);

Vera Luth, CERN NP internal report 74-4, (Jan., 1974).

8. W. A. Loomis et al., Phys. Rev. Lett. 35, 1983 (1975).

9. B. Aubert et al., Fermilab-Conf-75/31-exp., April, 1975.

10. K. B. Burns et al., Nucl. Instr. and Meth. 106, 171 (1973).

11. H. Cunitz et al., Nucl. Instr. and Meth. 91, 211 (1971).

12. T. A. Nunamaker, Nucl. Instr. and Meth. 106, 557 (1973).

13. T. A. Nunamaker and David B. Turner, Nucl. Instr. and Meth. 113, 445 (1975).

14. Dennis Theriot, Fermilab-TM-229, March, 1970.

15. B. Rossi, High Energy Particles, Prentice Hall, (1952), P. 71.

16. a) J. J. Aubert et al., Phys. Rev. Lett. 33, 1404 (1974);

b) Y. M. Antipov et al., Phys. Lett. 60B, 309 (1976);

c) H. D. Snyder et al., Phys. Rev. Lett. 36, 1415 (1976);

d) F. W. Busser et al., Phys. Lett. 56B, 482 (1975).

17. F. C. Winkelmann et al., Phys. Lett. 56B, 101 (1975).

18. Yu. M. Antipov et al., Phys. Lett. 76B, 235 (1978).

19. J. W. Cronin et al., Phys. Rev. D11, 3105 (1975), and the references contained therein;

U. Becker et al., Phys. Rev. Lett. 37, 1931 (1977);

L. Kluberg et al., Phys. Rev. Lett. 38, 670 (1977).

20. L. M. Lederman, XIX International Conference on High Energy Physics, Tokyo, Japan, 1978 (unpublished).

21. J. C. Collins and D. E. Soper, Phys. Rev. D16, 2219 (1977).

22. C. Bricman *et al.*, *Review of Particle Properties*, LBL-100, April, 1978, p. 136.

23. A. J. Buras and K. J. F. Gaemers, Nucl. Phys. B132, 249 (1978).

24. G. C. Fox, Nucl. Phys. B131, 107 (1977);
I. Hinchliffe and C. H. Llewellyn-Smith, Nucl. Phys. B128, 93 (1977);

25. M. Gluck and E. Reya, Nucl. Phys. B130, 76 (1977).

26. Many of the predictions use the Drell-Yan-West relation (S. D. Drell and T.-M. Yan, Phys. Rev. Lett. 24, 181 (1970); G. B. West, Phys. Rev. Lett. 24, 1206 (1970)) which states that if the elastic form factor (F_{el}) behaves like $(1/q^2)^p$ at large q^2, then νW_2 will go as $(1-x)^{2p-1}$ as x approaches 1. Brodsky and Farrar (Phys. Rev. Lett. 31, 1153 (1973)) used quark counting rules to conclude that $F_{el}(q^2) \sim (q^2)^{1-n}$ where n is the number of quarks. Recent measurments of C. J. Bebek *et al.*, (Phys. Rev. D17, 1693 (1978)) indicate that $F^{pi}_{el}(q^2) \sim 1/q^2$ in agreement with Brodsky and Farrar. Then the Drell-Yan-West relation would predict $\nu W^{pi}_2 \sim (1-x)^1$.

27. G. R. Farrar, Nucl. Phys. B77, 429 (1974);

G. Alterelli et al., Nucl. Phys. B92, 413 (1975);

A. Donnachie and P. V. Landshoff, Nucl. Phys. B112, 233 (1676);

R. D. Field and R. P. Feynman, Phys. Rev. D15, 2590 (1977);

G. R. Farrar and D. R. Jackson, Phys. Rev. Lett. 35, 1416 (1975).

28. P. V. Landshoff and J. C. Polkinghorne, Nucl. Phys. B19, 432 (1970);

J. Kuti and W. F. Weisskopf, Phys. Rev. D4, 3418 (1971).

29. For a good review of the possible QCD sources for p_T along with other implications QCD has for the Drell-Yan model, see E. L. Berger, "Massive Lepton Pair Production In Hadronic Collisions," in New Results in High Energy Physics - 1978, Vanderbilt Conference (AIP Conference Proceedings, No. 45, 1978).

30. G. R. Farrar, Nucl. Phys. B77, 429 (1974);

R. D. Field and R. P. Feynamn, Phy. Rev. D15, 2590 (1977).

31. For circuit details, see the MECL data sheets from Motorola Semiconductor Products Inc., P. O. Box 20924,

Phoenix, Arizona 85036.

32. Augat Inc., 33 Perry Avenue, P. O. Box 799, Attleboro, Massachusetts 02703.

33. Denison et al., Nucl. Phys. B61, 62 (1973).

34. K. J. Anderson, R. N. Coleman, G. E. Hogan, K. P. Karhi, K. T. McDonald, C. B. Newman, J. E. Pilcher, E. I. Rosenberg, G. H. Sanders, A. J. S. Smith, and J. J. Thaler, Phys. Rev. Lett. 42, 944 (1979);
G. E. Hogan et al., Phys. Rev. Lett. 42, 948 (1979);
C. B. Newman et al., Phys. Rev. Lett. 42, 951 (1979);
C. B. Newman, Ph. D. thesis, University Of Chicago, 1979, (unpublished).

ACKNOWLEDGEMENTS

The author would first like to thank his collaborators[34] for making this experiment such an enjoyable success. In particular, I would like to thank K. T. McDonald and C. B. Newman for their time spent discussing the analysis of this experiment.

I would also like to thank Howard Edwards of the Elementary Particles Laboratory at Princeton University and the techincal staff who work with him. I especially want to thank Marius Isaila, Carl Bopp, and Richard Rabberman who all helped me in the design and construction of the mass logic.

Finally, I would like to thank my advisor, A. J. S. Smith, for his guidance throughout the past three years.

At Princeton, funding for the experiment came from the U. S. Department of Energy, and personally, from the National Science Foundation Predoctral Fellowship program.